Imperial College of Science, Technology and Medicine
Department of Chemistry

Structural Behaviour Of Ionic Liquids

Andrew Dolan

Submitted in part fulfilment of the requirements for the award of
Doctor of Philosophy in Chemistry of Imperial College London
28.2.13

Declarations

I, Andrew Dolan, declare that all the work contained in this document is my own, other than that which has been referenced for external attribution.

The copyright of this thesis rests with the author and is made available under a Creative Commons Attribution Non-Commercial No Derivatives licence. Researchers are free to copy, distribute or transmit the thesis on the condition that they attribute it, that they do not use it for commercial purposes and that they do not alter, transform or build upon it. For any reuse or redistribution, researchers must make clear to others the licence terms of this work.

Abstract

The ring flipping behaviour of some pyrrolidinium based ionic liquids has been examined using variable temperature NMR spectroscopy, which allows the calculation of the Gibb's free energy of activation of the ring flip. As it was impossible to examine the neat ionic liquids, the work was carried out in solution. The role of the solvent was investigated and its effect on the ring flip activation energy of N-methylpyrrolidinium *bis*(trifluoromethylsulfonyl)imide was found to be accurately described by the Kamlet-Taft parameters of the solvent. A range of ionic liquids were examined in dimethylsulfoxide solutions. For a range of N-methylpyrrolidinium ionic liquids there was no correlation found between any property of the system and the ring flip activation energy. For a range of N-alkylpyrrolidinium hydrogensulfate ionic liquids there was a positive correlation between the ring flip activation energy and the free volume of the solution. While the free volume term correlates well, it is believed to be indicative of some underlying entropic effect.

A range of 1-alkyl-3-methylimidazolium and 1,3-dialkylimidazolium ionic liquids were examined using small angle X-Ray diffractometry. It was found that 1-alkyl-3-methylimidazolium thiocyanates have a unique pre-peak in their diffraction patterns, the structural origin of this peak is a repeating structure that is about twice the length of the cation. Ionic liquids with other anions reported to date, and those studied here, all have a pre-peak originating from a repeating structure that is about the length of the cation. This strongly suggests 1-alkyl-3-methylimidazolium thiocyanates have a different liquid structure than other ionic liquids. A pre-peak was found in 1-butyl-3-methylimidazolium thiocyanate, which is the first report of a pre-peak in an imidazolium based IL with such a short alkyl chain. It was also found that 1,3-dihexylimidazolium ionic liquids have two peaks in the very small angle regime. It was not possible to precisely determined the structural origin of these peaks, however there are two possible explanations. Either first and second order diffraction peaks of a repeating structure about twice the length of cation are being seen, or there are two different structures being formed in the liquid, one of which repeats on the length scale of one cation, the other of which repeats on the length scale of two cations.

Acknowledgements

I have had the good fortune to work with so many people around Imperial, that I'm afraid it is hard to adequately thank people without this section getting rather too long!

First and foremost, I must thank Tom. Tom has let me follow my own path through my studies, letting me pursue my own interests and always being on hand to put me back on track. Tom is an excellent teacher and has a manner of explaining complicated things in simple ways without making the audience feel like they are getting the 'dumbed down' version; a talent of his that I have been thankful for.

What I have learned from Jason is that thermodynamics are cruel and unusual and to be avoided at all costs, I'll leave the maths to him. Jason has always been there as a sounding board for my profoundly stupid questions, and while he never forgets to tell me they are stupid questions, he has not yet banned me from asking them.

The Welton group has been my home for 4 years. There are too many people to list here individually, however I must thank Lorna, Tom Wells and Agi; during my formative years as a hopeless undergrad and 1st year PhD they patiently helped me. Georgina, while you and I rarely seemed to be in the office at the same time, we shared three years PhD 'fun' and gripes and you never failed to brighten my day with a funny story. To all of the Welton Group, past and present, thanks for making my time so much fun.

While the Welton group has been my home, my thesis wouldn't have been complete without the help and advice of many other people around the chemistry department.

Tricia's boundless enthusiasm for computational chemistry is part of what inspired me to do my own computational work; she has been a great help in teaching me. Richard from Tricia's group has proof read my thesis as well as being the brains behind dispersion interactions in ILs, Thanks!

Nick has been an immense help with all of the X-Ray Diffraction work I did; he has literally taught me everything I know about the subject. Nick, I hope I wasn't

too much of a pain in the ass. Sowmiah and Arwen were both very helpful when I couldn't find Nick to annoy, so thank you all.

Peter, thanks for running all of the NMRs; I know this year has extra busy for you, which makes your time all the more valuable.

I am fortunate to have the support of a loving family who haven't given up on me, even during my dark days of thesis writing. I can only blame my relentless need to ask questions on my parents. They always patiently answered my questions when I was young, and always encouraged me to keep learning and keep asking questions; to anyone of whom I have asked too many questions, blame my parents! My brother and sister taught me the value of conflict and conflict resolution. While Phil and I tended to resolve our conflicts with physical violence, Louise taught me that that was not cool, at least once I out grew her...

Finally, Trang. We've shared our journey through our PhDs, through the good and bad bits, and even on the worst days you have my things easier just by being there. If we can share the rest of our life like that, I'll be happy!

Contents

Abstract **3**

Acknowledgements **3**

List of Tables **11**

List of Figures **14**

Abbreviations **15**

1 Introduction **19**

1.1 Ionic Liquids 19

1.2 Outline of Work 24

2 Synthesis **26**

2.1 Introduction 26

2.2 Synthesis And Characterisation 27

2.2.1 Imidazolium based ILs 28

2.2.2 Pyrrolidinium based ILs 54

2.2.3 Discussion 63

3 Site Exchange In Pyrrolidinium Ionic Liquids 64

3.1 Aims . . . 64

3.2 Introduction . . . 65

3.2.1 Dynamic Effects in NMR Spectroscopy . . . 65

3.2.2 NMR features of Ionic Liquids . . . 70

3.2.3 Computational Chemistry . . . 73

3.2.4 Calculating Volumes . . . 79

3.2.5 Hole theory in Ionic Liquids . . . 82

3.3 Results of Variable Temperature NMR Spectra of Ionic Liquids . . . 83

3.3.1 Ring Flip Activation Energies of ILs . . . 83

3.3.2 The Role of the Solvent . . . 88

3.3.3 Density Measurements . . . 92

3.3.4 Free Volumes . . . 93

3.4 Results of study of ring flip activation energy of $[C_1Hpyrr]^+$ cation in $[C_1Hpyrr][HSO_4]$ and $[C_4C_1im][NTf_2]$ mixtures . . . 97

3.5 Conclusions . . . 99

4 X-Ray Diffractometry of Imidazolium Ionic Liquids 101

4.1 Aims . . . 101

4.2 Introduction . . . 102

4.2.1 Ionic Liquids as self-assembly media . . . 102

4.2.2 Structuring in neat long chain Ionic Liquids: Thermotropic Liquid Crystals . . . 106

4.2.2.1 Thermotropic Liquid Crystal Phases . . . 106

4.2.2.2 Thermotropic Behaviour of long chain Ammonium compounds . . . 108

4.2.2.3 Thermotropic Behaviour of long chain Pyridinium compounds . . . 110

4.2.2.4 Thermotropic Behaviour of long chain Imidazolium compounds . . . 112

4.2.3 Structuring in neat short chain Ionic Liquids . . . 114

4.3 Introduction to X-Ray Diffraction . . . 121

4.3.1 Generating X-Rays . . . 122

4.3.2 Beam Conditioning . . . 124

4.3.3 Sample Diffraction . . . 125

4.3.4 The Phase Shift . . . 126

4.3.5 Transmission Profile . . . 127

4.3.6 Data Fitting Methods . . . 128

4.4 Results and Discussion . . . 130

4.4.1 Single Crystal Structures . . . 131

4.4.2 Synchotron X-Ray Diffraction Results . . . 135

4.4.3 SAXS Diffraction Results, grouped by Anion . . . 137

4.4.3.1 Bis(trifluoromethylsufonyl)imide Ionic Liquids . . . 140

4.4.3.2 Chloride Ionic Liquids . . . 142

4.4.3.3 Bromide Ionic Liquids . . . 144

4.4.3.4 Nitrate Ionic Liquids . . . 146

4.4.3.5 Thiocyanate Ionic Liquids . . . 148

4.4.4 X-Ray Diffraction Results, Grouped by Cation 151

4.4.4.1 The origin of the pre-peak 151

4.4.4.2 The effect of the Anion 153

4.4.4.3 Unique Feature in the XRD patterns of $[C_6C_6im]^+$ ILs 156

4.4.4.4 The origin of Peak 1 159

4.5 Conclusions and Further Work 162

4.5.1 Conclusions 162

4.5.2 Further Work 163

5 Conclusion **165**

Bibliography **167**

A Crystal Structures **180**

A.1 $[C_4C_4im]Cl$ 180

A.2 $[C_4C_1im][NO_3]$ 184

List of Tables

3.1 Activation Energies Of Ring Flips Of ILs 85

3.2 Table of IL Densities and Ring Flip Activation Energies 94

3.3 Calculated Ionic Volumes 95

3.4 Ionic Liquid Volumes, Density, Free Volumes 95

3.5 Free Volume of Solutions of Ionic Liquds (40% in DMSO), and Ring Flip Activation Energies 96

4.1 Different Fitted Peak Maxima for $[C_6C_6im][SCN]$ 130

4.2 Table Compaing XRD data from Diamond Advanced Light Source (D) and the laboratory beamline (B) 136

4.3 Peak Table of $[X][NTf_2]$ ILs 141

4.4 Peak Table of [X]Cl ILs 143

4.5 Peak Table of [X]Br ILs 145

4.6 Peak Table of $[X][NO_3]$ ILs 147

4.7 Peak Table of [X][SCN] ILs 148

4.8 Table of pre-peak Positions of $[C_8C_1im]^+$ ILs 151

4.9 Peak Table of $[C_6C_6im][Y]$ ILs 156

A.1 Details of $[C_4C_4im]Cl$ Crystal Structure Determination 181

A.2 Selected Bond Lengths of $[C_4C_4im]Cl$ Crystal 182

A.3 Selected Bond Angles of $[C_4C_4im]Cl$ Crystal 183

A.4 Details of $[C_4C_1im][NO_3]$ Crystal Structure Determination 184

A.5 Selected Bond Lengths of $[C_4C_1im][NO_3]$ Crystal 185

A.6 Selected Bond Angles of $[C_4C_1im][NO_3]$ Crystal 186

List of Figures

1.1 Some common IL cations 21

1.2 Some common IL anions 21

3.1 Resonance Structures of DMF 66

3.2 Labelled ^{1}H-NMR spectrum of $[C_1Hpyrr][HSO_4]$ 70

3.3 Equatorial and Axial Conformers of the *N*-methylpyrrolidinium Cation 71

3.4 Schematics of Solvent Accessible Surface and Molecular Surface[84] . . 81

3.5 Variable temperature ^{1}H-NMR of 40mol% $[C_1Hpyrr][HSO_4]$ in DMSO, 293 (bottom) to 373K (top) in 10K Steps 84

3.6 Chemical Shift of NH δ(ppm) vs. Activation energy of ring flip $\Delta G^{\ddagger}$. 87

3.7 β Value of Solvent vs. Ring Flip Activation Energy of $[C_1Hpyrr][NTf_2]$ ($\Delta G^{\ddagger}$) 89

3.8 LSER showing Experimental (Exp.) and Predicted (Pred.) Ring Flip Activation Energies ($\Delta G^{\ddagger}$) 90

3.9 LSER showing Experimental (Exp.) and Predicted (Pred.) Ring Flip Activation Energies ($\Delta G^{\ddagger}$) exluding water 91

3.10 Density Measurement Of Mixture Of $[C_1Hpyrr][OTf]$ And Acetonitrile 92

3.11 Density Measurement Of Mixture Of $[C_1Hpyrr]Cl$ And Acetonitrile . 93

3.12 Density Measurement Of Mixture Of $[C_1Hpyrr][NTf_2]$ And Acetonitrile 93

3.13 Activation energy of ring flip $\Delta G^{\ddagger}(kJmol^{-1})$ vs. Density(gcm^{-3}) . . . 94

3.14 Ring Flip Activation Energy vs Free Volume 96

3.15 Activation Energy of Ring Flip vs Free Volume of mixture of $[C_1Hpyrr][HSO_4]$ and $[C_4C_1im][NTf_2]$ 98

3.16 Activation Energy of Ring Flip vs Free Volume of mixture of $[C_1Hpyrr][HSO_4]$ and $[C_4C_1im][NTf_2]$ 99

4.1 *N*-(4-methoxybenzylidene)-4-butylaniline 107

4.2 Sketch of the nematic phase[118] 107

4.3 Sketch of the smectic A and smectic C phases[118] 108

4.4 Sketch of Copper X-Ray emission profile 123

4.5 Example Diffraction Pattern Image 126

4.6 Phase Shift of Two Light Waves 127

4.7 Radial Integration of Diffraction Pattern of Blank Capillary 129

4.8 Crystal Structure of $[C_4C_1im][NO_3]$ 132

4.9 Packing Structure of $[C_4C_1im][NO_3]$ 132

4.10 Crystal Structure of $[C_4C_4im]Cl$ 134

4.11 Packing Structure of $[C_4C_4im]Cl$ 134

4.12 SAXS Data Collected on Synchotron 135

4.13 WAXS Data Collected on Synchotron 136

4.14 Trace of X-Ray Diffraction patterns of $[C_8C_1im][NO_3]$ 138

4.15 Stack plot of Integrations of X-Ray Diffraction patterns of $[X][NTf_2]$ ILs 141

4.16 Stack plot of 1D scattering patterns of [X]Cl ILs 143

4.17 Stack plot of 1D scattering patterns of [X]Br ILs 145

4.18 Stack plot of 1D scattering patterns of [X][NO_3] ILs 147

4.19 Stack plot of 1D scattering patterns of [X][SCN] ILs 149

4.20 Sketch of the molecular structure giving rise to the pre-peak in ILs . . 152

4.21 Sketch of the molecular structures giving rise to the pre-peak in $[SCN]^-$ ILs 152

4.22 Stack of Integrations of X-Ray Diffraction patterns of [C_8C_1im][Y] ILs 155

4.23 Stack of Integrations of X-Ray Diffraction patterns of [C_6C_6im][Y] ILs 155

4.24 'V'-Shaped conformer of $[C_6C_6im]^+$ Cation 158

4.25 Linear conformer of $[C_6C_6im]^+$ Cation 158

4.26 'L'-Shaped conformer of $[C_6C_6im]^+$ Cation 158

4.27 Possible repeating Structure of $[C_6C_6im]^+$ ILs in 'V'-Shaped Conformer 160

4.28 Repeating Structure of $[C_6C_6im]^+$ ILs 161

List Of Abbreviations

This list is, hopefully, comprehensive. Should any ILs be missing, hopefully the systematic abbreviations used will prove coherent enough to make positive identification possible.

This list has been separated into groups each of which run alphabetically. The groups are, in this order, ionic liquid cations, ionic liquid anions and abbreviations by chapter.

Cations

- 1-alkyl-3-methylimidazolium $[C_xC_1im]^+$, where x is the number of carbons in the alkyl chain
- 1-alkyl-3-methylpyrrolidinium $[C_xC_1pyrr]^+$, where x is the number of carbons in the alkyl chain
- 1-alkylpyridinium $[C_xpy]^+$, where x is the number of carbons in the alkyl chain
- 1-alkylpyrrolidinium $[C_xHpyrr]^{++}$, where x is the number of carbons in the alkyl chain
- 1,3-dialkylimidazodium $[C_xC_xim]^+$, where x is the number of carbons in the alkyl chain
- tetralkylammonium $[N_{x,x,x,x,}]^+$, where x is the number of carbons in the alkyl chain
- tetraalkylphosphonium $[P_{x,x,x,x,}]^+$, where x is the number of carbons in the alkyl chain
- 1-butyl-3-methylimidazolium $[C_4C_1im]^+$
- 1-ethyl-3-methylimidazolium $[C_2C_1im]^+$
- 1,3-dibutylimidazodium $[C_4C_4im]^+$
- 1,3-dihexylimidazodium $[C_6C_6im]^+$

- 1-dodecyl-3-methylimidazolium $[C_{12}C_1im]^+$
- 1-hexadecyl-3-methylimidazolium $[C_{16}C_1im]^+$
- 1-hexyl-3-ethylimidazolium $[C_6C_2im]^+$
- 1-hexyl-3-methylimidazolium $[C_6C_1im]^+$
- 1-octyl-3-methylimidazolium $[C_8C_1im]^+$
- N-ethylpyrrolidinium $[C_2Hpyrr]^+$
- N-butyl-N-methylpyrrolidinium $[C_4C_1pyrr]^+$
- N-butylpyrrolidinium $[C_4Hpyrr]^+$
- N-hexylpyrrolidinium $[C_6Hpyrr]^+$
- N-methylpyrrolidinium $[C_1Hpyrr]^+$
- N-penylpyrrolidinium $[C_5Hpyrr]^+$
- N-propylpyrrolidinium $[C_3Hpyrr]^+$

Anions

- dicyanamide $[N(CN)_2]^-$
- bis(trifluoromethylsulphonyl)imide $[NTf_2]^-$
- hexfluorophosphate $[PF_6]^-$
- hydrogen sulphate $[HSO_4]^-$
- methyl carbonate $[MeCO_3]^-$
- methyl sulphate $[MeSO_4]^-$
- monomethylethylether sulfate $[C_1OC_2OC_2OC_2SO_3]^-$
- nitrate $[NO_3]^-$
- tetrafluoroborate $[BF_4]^-$

- thiocyanate $[SCN]^-$
- trifluoromethylsulphonate $[OTf]^-$
- halide ions are expressed by their elemental symbol

Chapter 1

- Ionic Liquid, IL
- Nuclear Magnetic Resonance Spectroscopy, NMR
- Room Temperature Ionic Liquid, RTIL

Chapter 2

- acetonitrile, MeCN
- dichloromethane, DCM
- dimethylsulfoxide, DMSO
- Elemental Analysis, EA
- ElectroSpray Ionization, ESI
- ethyl acetate, EtOAc
- tetrahydrofuran, THF
- InfraRed, IR
- Liquid Secondary Ionization Mass Spectrometry, LSIMS

Chapter 3

- Becke's three parameter functional, B3LYP
- density functional theory, DFT

- dimethylformamide, DMF
- generalised gradient approximation, GGA
- Hartree-Fock, HF
- linear solvation energy relationship, LSER
- local spin-density approximation, LSDA
- Møller-Plesset perturbation, MP

Chapter 4

- critical micelle concentration, CMC
- critical packing parameter, CPP
- differential scanning calorimetry, DSC
- dynamic light scattering, DLS
- ethylammoniumnitrate, EAN
- energy dispersive X-Ray diffraction, EDXD
- hexadecyltrimethylammonium bromide, CTAB
- molecular dynamics, MD
- small angle neutron scattering, SANS
- small angle X-Ray diffraction, SAXS
- wide angle X-Ray diffraction, WAXS
- X-Ray diffraction, XRD

Chapter 1

Introduction

1.1 Ionic Liquids

Ionic Liquids (ILs) are certainly not new, with the first reports of room temperature molten salts occurring nearly 100 years ago.[1] Until recently they have been considered something of a curiosity rather than an important class of liquid or solvent in their own right. Until the late '90s what work there was fell under the umbrella of molten salts. The limitation of this is that molten salts are traditionally high temperature engineering fluids and are particularly utilized in handling and processing of very heavy metals. They are costly and certainly unsuitable for 'traditional' laboratory based chemistry. One of the earliest breakthroughs towards room temperature ionic liquids (RTILs) came with the synthesis of 1-ethyl-3-methylimidazolium methylcarbonate and 1-ethyl-3-methylimidazolium tetrafluoroborate ($[C_2C_1im][MeCO_3]$ and $[C_2C_1im][BF_4]$)[2] which is often credited with sparking a broader interest in the field. However it was only with the development of truly air and water stable molten salts (the two above are prone to hydrolyse slowly), such as the bis(trifluoromethylsulfonyl)imide and trifluoromethylsulfate salts ($[NTf_2]^-$ and $[OTf]^-$), that ILs really broke off into their own research area. This is partly because ILs becoming both air stable and molten at room temperature allowed a wider group of researchers to begin investigations. Since then the area has exploded in size in such a way that a complete summary of the field is the purview of books.[3–5] There

are a series of comprehensive reviews that have covered most areas of the field. In the area of physical chemistry of ILs there are reviews of physical properties, such as surface tension,[6] physicochemical properties,[7–9] electrochemical applications[10] and there is an online database of physical & physicochemical properties.[11] In the areas of organic and inorganic chemistry there have been reviews regarding ILs as reaction media,[12] catalysts[13] and biocatalysts.[14] Of particular interest to this thesis, the structural behaviour of ILs[15] has been reviewed recently. There have also been reviews on subsets of ILs, such as protic ILs[16] and task specific ILs.[17] Finally, there have been a number of ILs used in industrial processes,[18] including a number of patents for uses as diverse as azeotrope breaking[19] and polymer dissolution and processing.[20] These patents and the fully developed industrial uses have proven the economic viability to what had been a skeptical audience.

One property of ILs that makes them attractive, particularly from an industrial and processing perspective, is their extremely low volatility. This makes them mostly non-flammable and eliminates evaporative losses, which contribute to ILs 'being green', a concept which has recently entered the zeitgeist in a significant way. ILs also have the potential of lowering solvent costs in the long term due to lower attrition rates. The low volatility also makes them attractive to electrochemists as conductive media; they are safe to confine and won't suffer long term evaporative or diffusive losses. With traditional electrolytes such losses can limit device lifetimes by causing salt deposits on electrode surfaces.

While the upper temperature limit of what is an IL is not at all defined there is evidence to suggest that even the most thermally stable ILs such as 1-butyl-3-methylimidazolium *bis*(trifluoromethylsulfonyl)imide ($[C_4C_1im][NTf_2]$) begin to decompose above 400^oC. This means viable process operating temperatures are somewhat below this,[21] although this still represents an extremely wide range of viable temperatures when compared to molecular solvents. A number of differential scanning calorimetry studies have now produced high quality decomposition data for a range of ILs,[22–24] which can elucidate the decomposition route as well as the onset temperature.

It has been suggested that there are about than 10^6 combinations of ions that would

create ILs[18] and therefore an estimated 10^{18} ternary mixtures. It is semantic as to whether or not that figure is remotely accurate, as the majority of research is limited to a relatively small range of cations and anions, the most common of which are shown in Figures 1.1 & 1.2 respectively. As there are a variety of cation and anion combinations it is possible to select an IL with suitable properties for a particular process which has led to ILs being dubbed 'designer solvents' or 'task specific' solvents. This began with relatively broad selection criteria such as water miscible/immiscible anions and mutually immiscible ILs.[25] Recently there has been a trend toward more subtle tuning criteria such as functionalising alkyl chains. There are now examples of nitrile,[26] alcohol & polyether,[27] ester[28] and siloxane[29] functional groups on the cation alkyl chains. There are a small number of examples of modified or functionalised anions, such as alkylsulfates[28] and diethylenegylcol monomethylethere sulphate ($[C_1OC_2OC_2OSO_3]^-$).[30] There are also a range of examples of 'task specific' ILs for catalyst immobilisation,[31,32] which are designed to coordinate strongly to metal centres to fix them in the IL phase while allowing products to be separated.

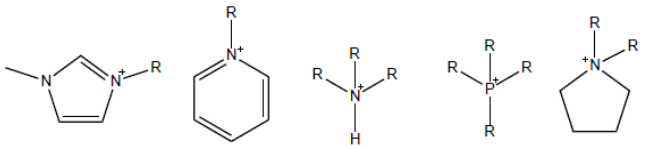


Figure 1.1: Some common IL cations

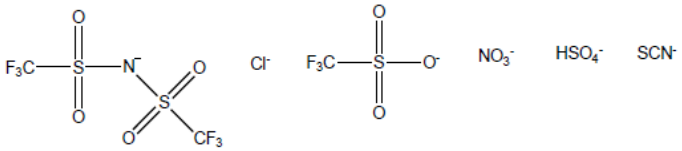


Figure 1.2: Some common IL anions

The iterative modification of IL properties by switching ions is important to achieve the best results in a given process. For example biomass processing seems to be best performed by ILs with planar cations and hydrogen bonding anions, while solar cell research requires low viscosity ILs in order to facilitate rapid electron/hole separation.[33,34]

As it stands, an exhaustive list of named and known reactions have been attempted using ILs as the solvent and it is now clear that reactions in ILs generally behave similarly to reactions in other media, giving the usual products and following typical kinetics. Welton & Hallett dedicated a significant portion of their review to this area recently.[12] Of course interesting exceptions exist, such as nucleophilic substitutions of ionic substrates in ILs which proceed *via* unconventional kinetics,[35] however the nature of such exceptions are beyond the scope of this work.

There is a large body of work concerning mixtures of ILs with other solvents, which is broadly split into three categories. Firstly, a range of physicochemical studies on thermodynamics and phase behaviour of mixtures, particularly water and alcohols[36–39] (Non-aqueous mixtures of ILs have been reviewed by Heintz[40]). Secondly, a large number of studies have begun focusing on ILs as biomass processing fluids, which has recently been reviewed.[41] It should be noted that the majority of work thus far has been on the properties of single ILs and biomass, but this will develop into a multicomponent procedure as the various separation problems are solved. Finally, all of the work to date on self assembly and surfactants is multicomponent work and is summarised by Greaves & Drummond.[42] The nature of 'amphilic' ILs and any structures they may form in the pure state is currently of much academic interest and will be discussed in detail in Chapter 4.

Mixtures of ILs are also being explored, however the relatively small amount of current work on this has been reviewed elsewhere.[43] Mixing further widens the possibilities of tuning properties to specific functions. Thus far there has been interesting work done using mixtures of ILs in solar cells,[34] where they are ideal as nonvolatile solvents that are unlikely to diffuse across an organic electronic component. Further to this the active redox couple involved in light capture was incorporated into the anion of one component of the mixture, which was an interesting application.

Some expectations for what will occur in IL mixtures have already been shown by Lui *et al.*. It was shown that the extinction coefficient of Kosower's complex (a salt) in ILs was directly proportional to its concentration.[44] This is evidence that there are no preferential interactions between the Kosower's complex pyridinium based cation and iodide anion and equally that the solvent IL ions have no higher affinity for each

other than for the Kosower's complex ions; the mixture is thermodynamically ideal. This is supported by theoretical work by Lynden-Bell[45] on charge screening of ion pairs dissolved in ILs and more recent work on excess thermodynamic measurements of mixtures which shows they have very small enthalpies of mixing.[46]

That certain ILs mix ideally, or very close to ideally, is not in itself surprising. Indeed it would be expected that all 'common' ILs would mix in a way that is close to ideal, given the relatively small amount of variation in ions. As yet there is little work concerning mixtures of ILs where there are significant differences in the ILs. One study that touched on this area used lithium tetrafluoroborate in $[C_4C_1im][BF_4]$, and showed that there were large scale domains enriched in lithium content.[47] Lithium salt addition to ILs has been particularly well studied because of its potential for use in electrochemical devices.

The language used to describe ILs varies depending on the application being discussed, but it is convenient to use certain descriptors consistently. While the relative permitivity, or dielectric constant, is often an adequate predictor of how a typical molecular solvent may affect a solute property or reaction, it often fails in the presence of specific interactions, which are important in ILs. The Kamlet-Taft parameter system offers a useful way to describe some of the different properties of ILs that affect the way they behave as solvents.

Kamlet and Taft developed a series of Linear Solvation Energy Relationships which classify solvents on three of their properties. First is hydrogen bond acidity, or α, which is the ability of the solvent to donate a proton into a hydrogen bond.[48] Second is hydrogen bond basicity, or β, which is the ability of the solvent to accept a hydrogen bond.[49] Third is the dipolarity and dipolarisability of the solvent, or π^*; this parameter accounts for the remaining non-specific interactions which can affect the properties or behaviour of a solute (while numerical order has been given for grammatical purposes, there is no *order condescendi*). The parameters are measured against the solvato-chromic shift of various sets of dyes, but they are then normalised to give a value between 0 and 1, although it is possible to have values beyond this range. The α scale is normalised such that cyclohexane is 0 and methanol is 1. The β scale is normalised such that cyclohexane is 0 and hexamethylphosphoric acid

triamide is 1 The π^* scale is normalised such that cyclohexane is 0 and DMSO is 1.

The determination of a solvent's Kamlet-Taft parameters is typically performed by measuring the peak maxima of a series of solvato-chromic dyes in the solvent in question. The π^* and β or a solvent can be determined using a dye pair, a common pair is 4-nitroaniline and N,N-diethyl-4-nitroaniline. The α value can be determined using Reichardt's Dye and the π^* value. There are numerous other dyes available to measure a given parameter, and the literature values for molecular solvents are average values from multiple dyes.

The Kamlet-Taft parameters are useful descriptors of ILs because ILs can be made up of many cations and anions with a wide variety of properties. The α parameter of an ionic liquid is most strongly dependent on the cation. The β parameter of an ionic liquid is strongly dependent on the anion of the IL, and generally have a wider range of values than the cations. The π^* value of ILs are generally around 0.8. As the π^* values are relatively unchanging for ILs, they rarely enter discussion as a variable, despite some reactions being strongly dependent on them.[50]

While Kamlet-Taft parameters are not being examined in this thesis, they will be used where appropriate as a way to describe the properties of ILs and solvents being used in this study. In particular the Kamlet-Taft system will be used in Chapter 3.

This section has been short and rather general, the specific background and pertinent literature will be discussed in detail in the introduction of the appropriate chapter.

1.2 Outline of Work

Chapter 2 in this Thesis details the synthesis of all ILs used. While this section is largely experimental *minutae*, a number of novel ILs were made and there are some synthetic steps of interest which merit the inclusion of a small discussion.

Chapter 3 is a study on the ring-flip of some N-alkylpyrrolidinium ($[C_xHpyrr]^+$) based ILs. A broadly accepted feature of ILs is that a given N,N-dialkylpyrrolidinium salt is likely to melt at a significantly lower temperature than the similar N,N'-

dialkylimidazolium salt. There is a large body of melting point data to support this, however little investigation of the root cause; it is often explained as a direct result of the additional freedom of the pyrrolidinium ring. An observation of the ^{1}H-NMR of [C_1Hpyrr][HSO_4] synthesised within the group showed that the ring protons were being individually resolved at room temperature provided an opportunity to investigate this phenomenon. A range of ILs were made in order to attempt to find some fundamental relationship governing the properties of the IL and the ring flip activation energy.

Chapter 4 is an investigation of the structure of the liquid state of room temperature ionic liquids (RTILS) using X-ray diffraction. In order to limit the scope of the work, imidazolium based ILs will be the focus, with a variety of alkyl substituents and anions. Although imidazolium ILs are the most widely studied in the literature, the role of the anions and their potential for dispersion interaction has not been examined.

Chapter 2

Synthesis

2.1 Introduction

The synthesis of the 'common' ILs are now well established and details are now well summarised in books,[3] additionally local procedures[51] exist to efficiently produce N-N'-dialkylimidazolium chlorides and bromides and their subsequent metathesis products.[52] While the longer chain imidazolium salts are uncommon, their syntheses are similar to their shorter homologues.[53] The literature synthesis of ILs with the thiocyanate anion[54] was inadequate, as both silver thiocyanate and silver halides are insoluble in water which leaves little thermodynamic driving force. A solubility study was undertaken and acetonitrile proved suitable. Two syntheses of ILs with the nitrate anion were investigated; direct alkylation as has been recently investigated,[55] and silver nitrate metathesis using methods developed by Wilkes and Zaworotko.[2] Direct alkylation is preferred, however alkyl nitrates are not widely available and they are sensitive reagents due to the oxidising power of the nitrate group. Silver nitrate metathesis is a suitable alternative and opens up a much wider range of possible products.

The chlorides ILs synthesised here are all common intermediates for subsequent metathesis and are all known in the literature,[3,56] with the exception of $[C_6C_2im]Cl$ and $[C_6C_6im]Cl$, which the author believes are novel. Similarly bromide ILs are also common intermediates,[3] the symmetric 1,3-dialkylimidazolium bromides were

used as intermediates in the synthesis of their bis(trifluoromethylsulfonyl)imide salts by Xiao *et al.*[57], although the author does not believe there are any reports of $[C_6C_2im]Br$ and $[C_6C_6im]Br$ in the literature. The synthesis used here is similar to those in the above literature.

The bis(trifluoromethylsulfonyl)imide ILs are all known in the literature[57,58] with the exception of $[C_6C_2im][NTf_2]$ and $[C_6C_6im][NTf_2]$. The 1-alkyl-3-methylimidazolium bis(trifluoromethylsulfonyl)imide ILs are all well studied in the literature.[8] The symmetric 1,3-dialkylimidazolium bis(trifluoromethylsulfonyl)imide ILs up to dipentyl were synthesised by Xiao *et al.*[57] The synthetic methods used here are the same as those in the above literature.

The thiocyanate ILs presented here are believed by the author to be novel, with the exception of $[C_4C_1im][SCN]$, which is reported in the literature.[54,59,60] Other thiocyanate based ILs are reported in the literature,[54,59,60] including $[C_2C_1im][SCN]$.[60] Additionally pyrrolidinium,[60] ammonium,[60], pyridinium[59] and piperidinium[59] thiocyanate ILs are reported in the literature. The above literature synthesised the thiocyanate ILs *via* silver thiocyanate metathesis in water, in this study barium thiocyanate and acetonitrile were used.

The 1-alkyl-3-methylimidazolium nitrate ILs have been reported in the literature by Seddon *et al.*,[61] additionally direct alkylation has been demonstrated as a viable synthetic method.[55] It is believed by the author that the other nitrate ILs synthesised here are novel. $[C_4C_1im][NO_3]$ was prepared *via* direct alkylation using a similar procedure to that of Smith *et al.*,[55] the other were prepared by silver nitrate metathesis using literature methods.[61]

2.2 Synthesis And Characterisation

Reagents and analytical methods

All reagents, unless otherwise stated here, were purchased from Sigma-Aldrich and were purified using standard techniques, except silver nitrate which was used as received. N-butylnitrate was purchased from Chemos GMBH and was used as re-

ceived. Barium thiocyanate trihydrate was purchased from ICI and was used as received.

Mass spectrometry was carried out on either a Micromass AutoSpec Premier (LSIMS) or a Micromass LCT Premier (ESI). For LSIMS samples acetonitrile was used as solvent, which often leads to a strong cyanide peak at 26 a.u., as was the case in some spectra. NMR spectroscopy was carried out on a Bruker 400MHz Spectrometer at 400Mhz for ^{1}H spectra and 100MHz for ^{13}C. Additionally ^{13}C are routinely ^{1}H decoupled, thus all signals are singlets unless explicitly stated. IR was performed using a Perkin-Elmer Spectrum 100 Spectrophotometer. Density measurements were taken on an Anton-Parr DMA38 vibrating tube densitometer. The instrumentation of the X-Ray line will be discussed in Chapter 4.

NMR Assignments

Abbreviations describing the multiplicities of the NMR signals have been used. 's' refers to a singlet, 'd' to a doublet and 't' to a triplet. Other multiplicities are written in full. Where protons couple to protons on multiple different carbons, the multiplicity is labelled as it appears on the spectrum, for example a proton coupling to two different methylene groups, with a coupling constant of 7.5Hz, would appear on the spectrum as a quintet, although in truth it is a triplet of triplets. Similarly a multiplicity that appears as a sextet is in truth a triplet of quartets.

2.2.1 Imidazolium based ILs

1-ethyl-3-methylimidazolium bromide

Ethyl acetate (400mL) and 1-methylimidazole (303g, 3.7mol, 1eq) were mixed under nitrogen. Ethyl bromide (454g, 4.25mol, 1.15eq) was cooled to minus 10^{o}C in the freezer and added dropwise over 15 minutes. The mixture was allowed to warm to room temperature and was stirred under nitrogen overnight. Due to rapid precipitation, yielding well packed crystals, the usual ethyl acetate wash was ineffective. Acetonitrile (150mL) was added and the mixture was heated gently until homogeneous. The solution was then extracted with ethyl acetate (3x150mL) and the

solution was placed in a freezer to allow crystallisation, after which the remaining solvent was decanted. NMR spectroscopy showed the product to be of insufficient quality. The mixture was recrystallised from acetonitrile and ethyl acetate (6:1 v/v) and dried *in vacuo* overnight. Isolated white crystals of $[C_2C_1im]Br$ (860g, 2.9mol, 81% yield, m.p 64-65^{o}C).*m/z* (LSIMS$^+$) $[C_2C_1im]^+$ 111, 100%, (LSIMS$^-$) $^{79}Br^-$, 79, 100%, $^{81}Br^-$, 81, 97%. EA: (calc. C 37.72, H 5.80, N 14.66) found C 37.51, H 5.77, N 14.71. ^{1}H-NMR (400MHz, d_6-DMSO): $\delta = 9.22$ppm (s, 1H, C(2)H), $\delta = 7.83$ppm (s, 1H, C(4)H), $\delta = 7.74$ppm (s, 1H, C(5)H), $\delta = 4.20$ppm (quartet $^3J_{HH} = 7.2$Hz, 2H, NC$\mathbf{H}_2$CH$_3$), $\delta = 3.86$ppm (s, 3H, NCH$_3$), $\delta = 1.42$ppm (t, $^3J_{HH} = 7.2$Hz, 3H, NCH$_2$C$\mathbf{H}_3$). ^{13}C-NMR (100MHz d_6-DMSO): $\delta = 136.7$ppm, (C(2)), $\delta = 124.0$ppm (C(4)), $\delta = 122.5$ppm (C(5)), $\delta = 44.6$ppm (N$\mathbf{C}$H$_2$CH$_3$), $\delta = 36.2$ppm (NCH$_3$), $\delta = 15.6$ppm (NCH$_2\mathbf{C}$H$_3$). IR (cm^{-1}): 3132 symmetric ring C-H stretch & 3064 asymmetric ring C-H stretch, 2971 & 2939 asymmetric chain C-H stretch, 2872 symmetric chain C-H stretch, 1572 inplane ring bend, 1374 CH_2 asymmetric wag, 1339 CH_2 twist, 1274 full chain CH_2 symmetric wag, 1259 full chain CH_2 asymmetric wag, 1256 full chain CH_2twist, 1170 asymmetric ring C-H in plane bend, 1112 symmetric ring C-H in plane bend, 1021 asymmetric C-C stretch, 858 symmetric C-H ring out of plane bend, 751 asymmetric C-H ring out of plane bend, 680 C-N in plane bend, 668 out of plane C-N bend.

1-ethyl-3-methylimidazolium bis(trifluoromethylsulfonyl)imide

1-ethyl-3-methylimidazolium bromide (66.492g, 0.348mol, 1eq) in dichloromethane (400mL) was added to lithium bis(trifluoromethylsulfonyl)imide (99.780g, 0.348mol, 1eq) and the slurry stirred vigorously for 2 days. Water was added until two colourless phases were seen (75mL). The organic phase was collected and washed with water (2x20mL). The solvent was evaporated and the liquid residue dried under vacuum for 2 days. Collected colourless liquid 1-ethyl-3-methylimidazolium bis(trifluoromethylsulfonyl)imide (136.16g, 0.338mol, 97% yield). *m/z* (LSIMS$^+$) $[C_2C_1im]^+$ 111, 100%, (LSIMS$^-$) $[NTf_2]^-$, 280, 100%. EA: (calc. C 24.55, H 2.83, N 10.74) found C 24.28, H 2.94, C 10.61. ^{1}H-NMR (400MHz, d_6-DMSO): $\delta = 9.11$ppm (s, 1H, C(2)H), $\delta = 7.75$ppm (s, 1H, C(4)H), $\delta = 7.67$ppm (s, 1H, C(5)H), $\delta = 4.20$ppm (quartet $^3J_{HH} = 7.2$Hz, 2H, NC$\mathbf{H}_2$CH$_3$), $\delta = 3.86$ppm (s,

3H, NCH_3), δ = 1.44ppm (t, $^3J_{HH}$ = 7.2Hz, 3H, $NCH_2C\mathbf{H}_3$). ^{13}C-NMR (100MHz, d_6-DMSO): δ = 136.7ppm (C(2)), δ = 123.99ppm (C(4)), δ = 122.32ppm (C(5)), δ = 119.93ppm (q, $^1J_{CF}$ = 320Hz, $\mathbf{C}F_3$), δ = 44.58ppm ($N\mathbf{C}H_2CH_3$), δ = 35.99ppm (NCH_3), δ = 15.29ppm ($NCH_2\mathbf{C}H_3$). IR (cm^{-1}): 3153 symmetric ring C-H stretch & 3112 asymmetric ring C-H stretch, 2955 & 2932 asymmetric chain C-H stretches, 2879 symmetric chain C-H stretch, 1564 in plane ring bend, 1464 CH_3 & CH_2 symmetric wags, 1347 SO_2 asymmetric stretch, 1334 CH_2 twist, 1278 full chain CH_2 symmetric wag, 1261 full chain CH_2 asymmetric wag, 1227 full chain CH_2 twist, 1178 C-S stretch, 1133 CF_3 stretch, 1052 S-N stretch, 949 asymmetric chain twist, 848 symmetric C-H ring out of plane bend, 788 asymmetric C-H ring out of plane bend, 762 C-N in plane bend, 750 out of plane C-N bend.

1-butyl-3-methylimidazolium chloride

1-methylimidazole (295.4g, 3.6mol, 1eq) was mixed with ethyl acetate (400mL). 1-chlorobutane (366.6g, 3.9mol, 1.1eq) was added drop wise over 15 minutes. The solution was heated to 50^{o}C and stirred under a reflux condenser and nitrogen for 2 weeks. White crystals precipitated. The ethyl acetate was removed and the crystals were dried *in vacuo* for 1 hour, then washed with ethyl acetate (3x100mL). The crystals were dried *in vacuo* overnight. Collected white crystals of $[C_4C_1im]Cl$ (594.75g, 3.4mol, 94% yield, m.p. 60-61^{o}C). *m/z* (ESI$^+$) $[C_4C_1im]^+$ 139, 100%, (LSIMS$^-$) $^{35}Cl^-$ 35, 100%, $^{37}Cl^-$ 37, 35%. EA: (calc. C 55.01, H 8.66, N 16.04) found C 54.86, H 8.77, N 15.95. ^{1}H-NMR (400MHz, d_6-DMSO): δ = 9.30ppm (s 1H, C(2)H), δ = 7.82ppm (s 1H, C(4)H), δ = 7.75ppm (s 1H, C(5)H), δ = 4.19ppm (t $^3J_{HH}$ = 7.2Hz 2H, $NC\mathbf{H}_2CH_2CH_2CH_3$), δ = 3.87ppm (s 3H, NCH_3), δ = 1.77ppm (quintet, $^3J_{HH}$ = 7.2Hz 2H, $NCH_2C\mathbf{H}_2CH_2CH_3$), δ = 1.27ppm (sextet $^3J_{HH}$ = 7.2Hz 2H, $N(CH_2)_2C\mathbf{H}_2CH_3$), δ = 0.90ppm (t, $^3J_{HH}$ = 7.2Hz 3H, $N(CH_2)_3C\mathbf{H}_3$). ^{13}C-NMR (100MHz, d_6-DMSO): δ = 136.76ppm (C(2)H), δ = 123.42ppm (C(4)H), δ = 122.20ppm (C(5)H), δ = 48.20ppm ($N\mathbf{C}H_2(CH_2)_2CH_3$), δ = 35.57ppm (NCH_3), δ = 31.33ppm ($NCH_2\mathbf{C}H_2CH_2CH_3$), δ = 18.63ppm ($N(CH_2)_2\mathbf{C}H_2CH_3$), δ = 13.15ppm ($N(CH_2)_3\mathbf{C}H_3$). IR (cm^{-1}): 3123 symmetric ring C-H stretch & 3059 asymmetric ring C-H stretch, 2965 & 2933 asymmetric chain C-H stretches, 2874 symmetric chain C-H stretch, 1564 inplane ring bend, 1378 CH_2 asymmetric

wag, 1333 CH_2 twist, 1274 full chain CH_2 symmetric wag, 1260 full chain CH_2 asymmetric wag, 1226 full chain CH_2twist, 1163 asymmetric ring C-H in plane bend, 1116 symmetric ring C-H in plane bend, 1023 asymmetric C-C stretch, 859 symmetric C-H ring out of plane bend, 750 asymmetric C-H ring out of plane bend, 680 C-N in plane bend, 668 out of plane C-N bend.

1-butyl-3-methylimidazolium bis(trifluoromethylsulfonyl)imide

1-butyl-3-methylimiazolium chloride (172.75g, 0.989mol, 1eq) in dichloromethane (800mL) was added to lithium bis(trifluoromethylsulfonyl)imide (284.2g, 0.989mol, 1eq) and the slurry stirred vigiorously for 2 days. Water was added until two colourless phases were seen (75mL). The organic phase was collected and washed with water (2x20mL). The solvent was evaporated and the liquid residue dried under vacuum for 2 days. Collected colourless liquid 1-butyl-3-methylimidazolium bis(trifluoromethylsulfonyl)imide (394.0g, 95% yield). *m/z* (LSIMS$^+$) $[C_4C_1im]^+$ 139, 100%, (LSIMS$^-$) $[NTf_2]^-$, 280, 100%. EA (calc. C 28.64, H 3.61, N 10.02) found C 28.52, H 3.74, N 9.92, ^{1}H-NMR (400MHz, d_6-DMSO): $\delta = 9.30$ppm (s, 1H, C(2)H), $\delta = 7.82$ppm (s, 1H, C(4)H), $\delta = 7.75$ppm (s, 1H, C(5)H), $\delta = 4.19$ppm (t, $^3J_{HH} = 7.2$Hz, 2H, NC$\mathbf{H}_2$$CH_2CH_2CH_3$), $\delta = 3.87$ppm (s, 3H, NCH_3), $\delta = 1.77$ppm (quintet, $^3J_{HH} = 7.2$Hz, 2H, NCH_2C$\mathbf{H}_2$$CH_2CH_3$), $\delta = 1.27$ppm (sextet, $^3J_{HH} = 7.2$Hz, 2H, $N(CH_2)_2$C$\mathbf{H}_2$$CH_3$), $\delta = 0.914$ppm (t, $^3J_{HH} = 7.2$Hz, 3H, $N(CH_2)_3$C$\mathbf{H}_3$). ^{13}C-NMR (100MHz, d_6-DMSO): $\delta = 136.94$ppm (C(2)H), $\delta = 124.00$ppm (C(4)H), $\delta = 122.64$ppm (C(5)H), $\delta = 119.94$ppm (q, $^1J_{CF} = 320$Hz, $\mathbf{C}F_3$), $\delta = 48.99$ppm ($N\mathbf{C}H_2(CH_2)_2CH_3$), $\delta = 36.06$ppm (NCH_3), $\delta = 31.78$ppm ($NCH_2\mathbf{C}H_2CH_2CH_3$), $\delta = 19.16$ppm ($N(CH_2)_2\mathbf{C}H_2CH_3$), $\delta = 13.48$ppm ($N(CH_2)_3\mathbf{C}H_3$). IR (cm^{-1}): 3149 symmetric ring C-H stretch & 3115 asymmetric ring C-H stretch, 2967 & 2939 asymmetric chain C-H stretch, 2879 symmetric chain C-H stretch, 1564 inplane ring bend, 1464 CH_3 & CH_2 symmetric wags, 1347 SO_2 asymmetric stretch, 1329 CH_2 twist, 1275 full chain CH_2 symmetric wag, 1260 full chain CH_2 asymmetric wag, 1226 full chain CH_2 twist, 1178 C-S stretch, 1133 CF_3 stretch, 1052 S-N stretch, 949 asymmetric chain twist, 848 symmetric C-H ring out of plane bend, 788 asymmetric C-H ring out of plane bend, 762 C-N in plane bend, 750 out of plane C-N bend.

1-butyl-3-methylimidazolium nitrate

Due to the fact that alkylnitrates are reactive and have a propensity to form explosive mixtures, extreme caution should be exercised when undertaking this reaction. Butylnitrate (10.26g, 86mmol, 1.5eq) was mixed with ethylacetate (5mL). To this mixture a solution of ethylacetate (5mL) and methylimidazole (4.6mL, 57mmol, 1eq) was added dropwise with vigorous stirring. The solution was then refluxed for 24 hours, during which time a second liquid phase appeared. The mixture was cooled to -20^{o}C and white crystals of 1-butyl-3-methylimidazolium nitrate (15.5g, 77mmol, 89% Yield, m.p. 30-31^{o}C) were collected. *m/z* (LSIMS$^+$) $[C_4C_1im]^+$ 139, 100%, (LSIMS$^-$) NO_3^- 62, 30%. EA (calc. C 47.75, H 7.51, N 20.88) found C 47.63, H 7.39. N 20.83. ^{1}H-NMR (400MHz d_6-DMSO): δ = 9.27ppm (s, 1H, C(2)H), δ = 7.55ppm (s, 1H, C(4)H), δ = 7.49ppm (s, 1H, C(5)H), δ = 4.33ppm (t, $^3J_{HH}$ = 7.2Hz, 2H, NC$\mathbf{H}_2$CH$_2$CH$_2$CH$_3$), δ = 4.12ppm (s, 3H, NCH$_3$), δ = 1.92ppm (quintet, $^3J_{HH}$ = 7.2Hz, 2H, NCH$_2$C$\mathbf{H}_2$CH$_2$CH$_3$), δ = 1.39ppm (sextet, $^3J_{HH}$ = 7.2Hz, 2H, N(CH$_2$)$_2$C$\mathbf{H}_2$CH$_3$), δ = 0.96ppm (t, $^3J_{HH}$ = 7.2Hz, 3H, N(CH$_2$)$_3$C$\mathbf{H}_3$). ^{13}C-NMR (100MHz d_6-DMSO): δ = 137.10ppm (C(2)H), δ = 124.08ppm (C(4)H), δ = 122.75ppm (C(5)H), δ = 48.95ppm (N$\mathbf{C}$H$_2$(CH$_2$)$_2$CH$_3$), δ = 36.13ppm (NCH$_3$), δ = 31.83ppm (NCH$_2$$\mathbf{C}H_2CH_2CH_3$), δ = 19.22ppm (N(CH$_2$)$_2$$\mathbf{C}H_2CH_3$), δ = 13.71ppm (N(CH$_2$)$_3$$\mathbf{C}H_3$). IR (cm^{-1}): 3150 symmetric ring C-H stretch, 3093 NO_3^- overtone, 2963 & 2936 asymmetric chain C-H stretch, 2877 symmetric chain C-H stretch, 1575 inplane ring bend, 1461 NCH$_3$ umbrella, 1331 NO Stretch, 1169 asymmetric ring C-H in plane bend, 1132 symmetric ring C-H in plane bend, 1041 asymmetric C-C stretch, 829 symmetric C-H ring out of plane bend (shoulder), 777 asymmetric C-H ring out of plane bend, 696 C-N in plane bend, 668 out of plane C-N bend.

1-butyl-3-methylimidazolium thiocyanate

1-butyl-3-methylimidazolium chloride (2.09g, 11.96mmol, 1eq) in acetonitrile (15mL) was mixed with barium thiocyanate (1.84g, 5.98mmol, 0.5eq) in acetonitrile (15mL) and the solution was stirred for 4 hours. A white precipitate was formed. The suspension was centrifuged and the liquor decanted. The solvent was removed yielding a slightly pink liquid 1-butyl-3-methylimidazolium thiocyanate (1.86g, 9.43mmol, 79%). *m/z* (LSIMS$^+$) $[C_4C_1im]^+$ 139, 100%, (LSIMS$^-$) CN^- 26, 95%, S^- 32, 94%,

SCN^- 58, 100%. EA (calc. C 54.79 H 7.66, N 21.3) found C 54.72, H 7.60, N 21.3. ^{1}H-NMR (400MHz d_6-DMSO): δ = 9.30ppm (s, 1H, C(2)H), δ = 7.82ppm (s, 1H, C(4)H), δ = 7.75ppm (s. 1H, C(5)H), δ = 4.19ppm (t, $^3J_{HH}$ = 7.2Hz, 2H, NC**H**$_2$CH$_2$CH$_2$CH$_3$), δ = 3.87ppm (s, 3H, NCH_3), δ = 1.77ppm (quintet, $^3J_{HH}$ = 7.2Hz, 2H, $NCH_2C\mathbf{H}_2CH_2CH_3$), δ = 1.27ppm (sextet, $^3J_{HH}$ = 7.2Hz, 2H, $N(CH_2)_2C\mathbf{H}_2CH_3$), δ = 0.90ppm (t, $^3J_{HH}$ = 7.2Hz, 3H, $N(CH_2)_3C\mathbf{H}_3$). ^{13}C-NMR (100MHz $CDCl_3$): δ = 136.67ppm (C(2)H). δ = 131.66ppm (SCN), δ = 123.85ppm (C(4)H), δ = 122.30ppm (C(5)H), δ = 50.11ppm ($N\mathbf{C}H_2(CH_2)_2CH_3$), δ = 36.78ppm (NCH_3), δ = 32.09ppm ($NCH_2\mathbf{C}H_2CH_2CH_3$), δ = 19.52ppm ($N(CH_2)_2\mathbf{C}H_2CH_3$), δ = 13.48ppm ($N(CH_2)_3\mathbf{C}H_3$). IR (cm^{-1}): 3149 symmetric ring C-H stretch & 3103 asymmetric ring C-H stretch, 2960 & 2935 asymmetric chain C-H stretch, 2873 symmetric chain C-H stretch, 2048 (S)C-N stretch, 1571 inplane ring bend, 1463 R-CH_3 umbrella, 1380 CH_2 asymmetric wag, 1333 CH_2 twist, 1275 full chain CH_2 symmetric wag, 1260 full chain CH_2 asymmetric wag, 1226 full chain CH_2 twist, 1162 asymmetric ring C-H in plane bend, 1115 symmetric ring C-H in plane bend, 1025 asymmetric C-C stretch, 947 asymmetric chain twist, 840 symmetric C-H ring out of plane bend, 751 asymmetric C-H ring out of plane bend, 648 C-N in plane bend, 619 out of plane C-N bend.

1-hexyl-3-methylimidazolium chloride

Chlorohexane (78.11g, 0.61mol, 1.3eq) and acetonitrile (100mL) were mixed and 1-methylimidazole (40mL, 0.48mol, 1eq) was added dropwise. The solution was refluxed for 3 days, during which time two phases developed. The acetonitrile was decanted and the residual liquid was washed with ethyl acetate (2x100mL), and dried at 35^{o}C under vacuum for 3 days. Collected viscous slightly yellow liquid, 1-hexyl-3-methylimidazolium chloride (90.15g, 0.43mol, 90% yield). *m/z* (LSIMS$^+$) $[C_6C_1im]^+$ 167, 100%, (LSIMS$^-$) $^{35}Cl^-$ 35, 100%, $^{37}Cl^-$ 37, 30%. EA (calc. C 59.25 H 9.45, N 13.82) found C 59.21, H 9.39, N 13.77. ^{1}H-NMR (400MHz d_6-DMSO): δ = 9.64ppm (s, 1H, C(2)H), δ = 7.94ppm (s, 1H, C(4)H), δ = 7.86ppm (s, 1H, C(5)H), δ = 4.21ppm (t, $^3J_{HH}$ = 7.2Hz, 2H, $NC\mathbf{H}_2(CH_2)_4CH_3$), δ = 3.89ppm (s, 3H, NCH_3), δ = 1.77ppm (broad s, 2H, $NCH_2C\mathbf{H}_2(CH_2)_3CH_3$), δ = 1.23ppm (broad s, 6H, $N(CH_2)_2(C\mathbf{H}_2)_3CH_3$), δ = 0.86ppm (t, $^3J_{HH}$ = 7.2Hz, 3H, $N(CH_2)_5C\mathbf{H}_3$).

^{13}C-NMR (100MHz d_6-DMSO): δ = 137.21ppm (C(2)H), δ = 124.00ppm (C(4)H), δ = 122.73ppm (C(5)H), δ = 49.08ppm (N**C**$H_2(CH_2)_5CH_3$), δ = 36.14ppm (NCH_3), δ = 31.02ppm (NCH_2**C**$H_2(CH_2)_3CH_3$), δ = 29.87ppm ($N(CH_2)_2$**C**$H_2(CH_2)_2CH_3$), δ = 25.59ppm ($N(CH_2)_3$**C**$H_2CH_2CH_3$), δ = 22.34ppm ($N(CH_2)_4$**C**H_2CH_3), δ = 14.27ppm ($N(CH_2)_5$**C**H_3). IR (cm^{-1}): 3122 symmetric ring C-H stretch & 3058 asymmetric ring C-H stretch, 2965 & 2933 asymmetric chain C-H stretch, 2874 symmetric chain C-H stretch, 1568 inplane ring bend, 1469 NCH_3 umbrella, 1381 CH_2 asymmetric wag, 1335 CH_2 twist, 1274 full chain CH_2 symmetric wag, 1260 full chain CH_2 asymmetric wag, 1226 full chain CH_2 twist, 1163 asymmetric ring C-H in plane bend, 1116 symmetric ring C-H in plane bend, 1023 asymmetric C-C stretch, 859 symmetric C-H ring out of plane bend, 750 asymmetric C-H ring out of plane bend, 680 C-N in plane bend, 668 out of plane C-N bend.

1-hexyl-3-methylimidazolium bromide

1-methylimidazole (42.21g, 0.51mol, 1eq) and ethyl acetate (100mL) were mixed and bromohexane (85mL, 0.62mol, 1.2eq) was added dropwise. The solution was refluxed overnight during which time two phases appeared. The solvent was decanted, and the residual liquid was washed with ethyl acetate (2x100mL), and dried at 35^{o}C under vacuum for 3 days. 1-hexyl-3-methylimidazolium bromide was collected as a colourless liquid (94.22g, 0.43mol, 85% yield). *m/z* (LSIMS$^+$) $[C_6C_1im]^+$ 167, 100%, (LSIMS$^-$) CN^- 26, 100% $^{79}Br^-$ 79, 30%, $^{81}Br^-$ 81, 31%. EA (calc. C 48.59 H 7.75, N 11.33) found C 48.12, H 7.41, N 11.05. ^{1}H-NMR (400MHz d_6-DMSO): δ = 9.47ppm (s, 1H, C(2)H), δ = 7.93ppm (s, 1H, C(4)H), δ = 7.84ppm (s, 1H, C(5)H), δ = 4.21ppm (t, $^3J_{HH}$ = 7.2Hz, 2H, NC**H**$_2(CH_2)_4CH_3$), δ = 3.89ppm (s, 3H, NCH_3), δ = 1.76ppm (broad s, 2H, NCH_2C**H**$_2(CH_2)_3CH_3$), δ = 1.22ppm (broad s, 6H, $N(CH_2)_2$(C**H**$_2)_3CH_3$), δ = 0.81ppm (t, $^3J_{HH}$ = 6.6Hz, 3H, $N(CH_2)_5$C**H**$_3$). ^{13}C-NMR (100MHz d_6-DMSO): δ = 137.00ppm (C(2)H), δ = 123.96ppm (C(4)H), δ = 122.71ppm (C(5)H), δ = 49.11ppm (N**C**$H_2(CH_2)_5CH_3$), δ = 36.26ppm (NCH_3), δ = 31.00ppm (NCH_2**C**$H_2(CH_2)_3CH_3$), δ = 29.87ppm ($N(CH_2)_2$**C**$H_2(CH_2)_2CH_3$), δ = 25.57ppm ($N(CH_2)_3$**C**$H_2CH_2CH_3$), δ = 22.33ppm ($N(CH_2)_4$**C**H_2CH_3), δ = 14.27ppm ($N(CH_2)_5$**C**H_3). IR (cm^{-1}): 3137 symmetric ring C-H stretch & 3057 asymmetric ring C-H stretch, 2954 & 2929 asymmetric chain C-H stretch,

2857 symmetric chain C-H stretch, 1568 in plane ring bend, 1458 NCH_3 umbrella, 1427 R-CH_3 umbrella (shoulder), 1379 CH_2 asymmetric wag, 1337 CH_2 twist, 1275 full chain CH_2 symmetric wag, 1260 full chain CH_2 asymmetric wag, 1226 full chain CH_2twist, 1167 asymmetric ring C-H in plane bend, 1120 symmetric ring C-H in plane bend, 1020 asymmetric C-C stretch, 825 symmetric C-H ring out of plane bend (shoulder), 763 asymmetric C-H ring out of plane bend, 696 C-N in plane bend, 668 out of plane C-N bend.

1-hexyl-3-methylimidazolium bis(trifluoromethylsulfonyl)imide

1-hexyl-3-methylimiazolium bromide (2.7191g, 11mmol, 1eq) in dichloromethane (25mL) was added to lithium bis(trifluoromethylsulfonyl)imide (3.2787g, 11.4mol, 1eq) and the slurry stirred vigorously overnight. Water was added until two colourless phases were seen (15mL). The organic phase was collected and washed with water (2x20mL). The solvent was evaporated and the liquid residue dried under vacuum for 2 days. Collected colourless liquid 1-butyl-3-methylimidazolium bis(trifluoromethylsulfonyl)imide (4.92g, 11mmol, 100% yield). *m/z* (LSIMS$^+$) $[C_6C_1im]^+$ 167, 100%, (LSIMS$^-$) $[NTf_2]^-$, 280, 100%. EA (calc. C 32.21 H 4.28, N 9.39) found C 32.01, H 3.13, N 9.22. ^{1}H-NMR (400MHz d_6-DMSO): $\delta = 9.10$ppm (s, 1H, C(2)H), $\delta = 7.74$ppm (s, 1H, C(4)H), $\delta = 7.68$ppm (s, 1H, C(5)H), $\delta = 4.16$ppm (t, $^3J_{HH} = 7.2$Hz, 2H, $NC\mathbf{H}_2(CH_2)_4CH_3$), $\delta = 3.86$ppm (s, 3H, NCH_3), $\delta = 1.79$ppm (broad s, 2H, $NCH_2C\mathbf{H}_2(CH_2)_3CH_3$), $\delta = 1.28$ppm (broad s, 6H, $N(CH_2)_2(C\mathbf{H}_2)_3CH_3$), $\delta = 0.87$ppm (t, $^3J_{HH} = 6.6$Hz, 3H, $N(CH_2)_5C\mathbf{H}_3$). ^{13}C-NMR (100MHz d_6-DMSO): $\delta = 136.91$ppm (C(2)H), $\delta = 124.99$ppm (C(4)H), $\delta = 122.64$ppm (C(5)H), $\delta = 119.93$ppm (q, $^1J_{CF} = 320$Hz, $\mathbf{C}F_3$), $\delta = 49.25$ppm ($N\mathbf{C}H_2(CH_2)_5CH_3$), $\delta = 36.08$ppm (NCH_3), $\delta = 30.96$ppm ($NCH_2\mathbf{C}H_2(CH_2)_3CH_3$), $\delta = 29.77$ppm ($N(CH_2)_2\mathbf{C}H_2(CH_2)_2CH_3$), $\delta = 25.56$ppm ($N(CH_2)_3\mathbf{C}H_2CH_2CH_3$), $\delta = 22.27$ppm ($N(CH_2)_4\mathbf{C}H_2CH_3$), $\delta = 14.08$ppm ($N(CH_2)_5\mathbf{C}H_3$). IR (cm^{-1}): 3156 symmetric ring C-H stretch & 3121 asymmetric ring C-H stretch, 2961 & 2935 asymmetric chain C-H stretch, 2864 symmetric chain C-H stretch, 1573 in plane ring bend, 1469 CH_3 & CH_2 symmetric wags, 1347 SO_2 asymmetric stretch, 1330 CH_2 twist, 1275 full chain CH_2 symmetric wag, 1260 full chain CH_2 asymmetric wag, 1226 full chain CH_2 twist, 1178 C-S stretch, 1133 CF_3 stretch, 1052 S-N stretch, 948

asymmetric chain twist, 848 symmetric C-H ring out of plane bend, 788 asymmetric C-H ring out of plane bend, 762 C-N in plane bend, 750 out of plane C-N bend.

1-hexyl-3-methylimidazolium nitrate

1-butyl-3-methylimidazolium chloride (1.92g, 9.5mmol, 1eq) was dissolved in water (10mL) and silver nitrate solution (31.7mL, 0.3M, 1eq) was added dropwise. The suspension was filtered and dried on a freeze drier. Collected 1-butyl-3-methylimidazolium nitrate as a viscous liquid (1.68g, 7.3mmol, 77% yield). *m/z* (LSIMS$^+$) $[C_6C_1im]^+$ 167, 100%, (LSIMS$^-$) NO_3^- 62, 100%. EA (calc. C 52.39, H 8.35, N 18.33) found C 52.22, H 8.25, N 18.16. ^{1}H-NMR (400MHz d_6-DMSO): δ = 9.13ppm (s, 1H, C(2)H), δ = 7.78ppm (s, 1H, C(4)H), δ = 7.71ppm (s, 1H, C(5)H), δ = 4.15ppm (t, $^3J_{HH}$ = 7.2Hz, 2H, NC$\mathbf{H}_2$(CH$_2$)$_4$CH$_3$), δ = 3.85ppm (s, 3H, NCH$_3$), δ = 1.77ppm (broad s, 2H, NCH$_2$C$\mathbf{H}_2$(CH$_2$)$_3$CH$_3$), δ = 1.26ppm (broad s, 6H, N(CH$_2$)$_2$(C$\mathbf{H}_2$)$_3$CH$_3$), δ = 0.86ppm (t, $^3J_{HH}$ = 6.6Hz, 3H, N(CH$_2$)$_5$C$\mathbf{H}_3$). ^{13}C-NMR (100MHz d_6-DMSO): δ = 137.00ppm (C(2)H), δ = 124.01ppm (C(4)H), δ = 122.74ppm (C(5)H), δ = 49.22ppm (N$\mathbf{C}$H$_2$(CH$_2$)$_5$CH$_3$), δ = 36.19ppm (NCH$_3$), δ = 31.00ppm (NCH$_2$$\mathbf{C}H_2$(CH$_2$)$_3CH_3$), δ = 29.79ppm (N(CH$_2$)$_2$$\mathbf{C}H_2$(CH$_2$)$_2CH_3$), δ = 25.60ppm (N(CH$_2$)$_3$$\mathbf{C}H_2CH_2CH_3$), δ = 22.33ppm (N(CH$_2$)$_4$$\mathbf{C}H_2CH_3$), δ = 14.30ppm (N(CH$_2$)$_5$$\mathbf{C}H_3$). IR (cm^{-1}): 3146 symmetric ring C-H stretch, 3097 NO_3 overtone, 2956 asymmetric chain C-H stretch, 2860 symmetric chain C-H stretch, 1571 in plane ring bend, 1464 NCH_3 umbrella, 1328 NO Stretch, 1166 asymmetric ring C-H in plane bend, 1117 symmetric ring C-H in plane bend, 1039 asymmetric C-C stretch, 829 symmetric C-H ring out of plane bend (shoulder), 762 asymmetric C-H ring out of plane bend, 680 C-N in plane bend, 668 out of plane C-N bend.

1-hexyl-3-methylimidazolium thiocyanate

1-hexyl-3-methylimidazolium chloride (1.62g, 7.17mmol, 1eq) in acetonitrile (15mL) was mixed with barium thiocyanate (1.11g, 3.58mmol, 0.5eq) in acetonitrile (15mL) and the solution was stirred for 4 hours. A white precipitate was formed. The suspension was centrifuged and the liquor decanted. The solvent was removed yielding a slightly pink liquid 1-hexyl-3-methylimidazolium thiocyanate (1.86g, 6.43mmol, 90%). *m/z* (LSIMS$^+$) $[C_6C_1im]^+$ 167, 100%, (LSIMS$^-$) CN^- 26, 100%, $^{32}S^-$ 32, 95%, SCN^- 58, 30%. EA (calc. C 54.79, H 7.66, N 21.3) found C 54.85, H 7.74, N 21.30. ^{1}H-NMR (400MHz d_6-DMSO): δ = 9.11ppm (s, 1H, C(2)H), δ = 7.77ppm

(s, 1H, C(4)H), δ = 7.70ppm (s, 1H, C(5)H), δ = 4.16ppm (t, $^3J_{HH}$ = 7.2Hz, 2H, NC$\mathbf{H}_2$(CH$_2$)$_4$CH$_3$), δ = 3.86ppm (s, 3H, NCH$_3$), δ = 1.78ppm (broad s, 2H, NCH$_2$C$\mathbf{H}_2$(CH$_2$)$_3$CH$_3$), δ = 1.26ppm (broad s, 6H, N(CH$_2$)$_2$(C$\mathbf{H}_2$)$_3$CH$_3$), δ = 0.85ppm (t, $^3J_{HH}$ = 6.6Hz, 3H, N(CH$_2$)$_5$C$\mathbf{H}_3$). ^{13}C-NMR (100MHz d$_6$-DMSO): δ = 136.95ppm (C(2)H), δ = 130.04ppm (SCN), δ = 124.07ppm (C(4)H), δ = 122.72ppm (C(5)H), δ = 49.26ppm (N$\mathbf{C}$H$_2$(CH$_2$)$_4$CH$_3$), δ = 36.23ppm (NCH$_3$), δ = 31.00ppm (NCH$_2$$\mathbf{C}H_2$(CH$_2$)$_3CH_3$), δ = 29.80ppm (N(CH$_2$)$_2$$\mathbf{C}H_2$(CH$_2$)$_2CH_3$), δ = 25.60ppm (N(CH$_2$)$_3$$\mathbf{C}H_2CH_2CH_3$), δ = 22.33ppm (N(CH$_2$)$_4$$\mathbf{C}H_2CH_3$), δ = 14.30ppm (N(CH$_2$)$_5$$\mathbf{C}H_3$). IR (cm^{-1}): 3149 symmetric ring C-H stretch & 3104 asymmetric ring C-H stretch, 2956 & 2930 asymmetric chain C-H stretch, 2859 symmetric chain C-H stretch, 2047 SC-N stretch, 1563 in plane ring bend, 1460 NCH$_3$ umbrella, 1427 R-CH$_3$ umbrella, 1379 CH$_2$ asymmetric wag, 1338 CH$_2$ twist, 1275 full chain CH$_2$ symmetric wag, 1260 full chain CH$_2$ asymmetric wag, 1226 full chain CH$_2$ twist, 1164 asymmetric ring C-H in plane bend, 1120 symmetric ring C-H in plane bend, 1030 asymmetric C-C stretch, 949 asymmetric chain twist, 841 symmetric C-H ring out of plane bend, 750 asymmetric C-H ring out of plane bend, 680 C-N in plane bend, 668 out of plane C-N bend.

1-octyl-3-methylimidazolium chloride

Chlorooctane (13.55g, 91.12mmol, 1.1eq) and acetonitrile (75mL) were mixed and 1-methylimidazole (7mL, 82mmol, 1eq) was added dropwise. The solution was refluxed for 10 days. The acetonitrile was removed under vacuum and the residual liquid was washed with ethyl acetate (2x100mL) then dried at 35^{o}C under vacuum for 3 days. Collected slightly viscous yellow liquid, 1-octyl-3-methylimidazolium chloride (17.91g, 72mmol, 88% yield). *m/z* (LSIMS$^+$) [C$_8$C$_1$im]$^+$ 195, 100%, (LSIMS$^-$) ^{35}Cl$^-$ 35, 100%, ^{37}Cl$^-$ 37, 30%. EA (calc. C 62.45, H 10.05, N 12.14) found C 62.41, H 10.00, N 12.07. ^{1}H-NMR (400MHz d$_6$-DMSO): δ = 9.30ppm (s, 1H, C(2)H), δ = 7.82ppm (s, 1H, C(4)H), δ = 7.75ppm (s, 1H, C(5)H), δ = 4.17ppm (t, $^3J_{HH}$ = 7.2Hz, NC$\mathbf{H}_2$(CH$_2$)$_5$CH$_3$), δ = 3.87ppm (s, 3H, NCH$_3$), δ = 1.78ppm (quintet, $^3J_{HH}$ = 7.2Hz, 2H, NCH$_2$C$\mathbf{H}_2$(CH$_2$)$_5$CH$_3$), δ = 1.13ppm (broad s, 10H, N(CH$_2$)$_2$(C$\mathbf{H}_2$)$_5$CH$_3$), δ = 0.84ppm (t, $^3J_{HH}$ = 7.08Hz, 3H, N(CH$_2$)$_7$C$\mathbf{H}_3$). ^{13}C-NMR (100MHz d$_6$-DMSO): δ = 137.20ppm (C(2)H), δ = 124.02ppm (C(4)H),

$\delta = 122.73$ppm (C(5)H), $\delta = 49.12$ppm ($\mathrm{N}\mathbf{C}\mathrm{H}_2(\mathrm{CH}_2)_6\mathrm{CH}_3$), $\delta = 36.15$ppm (NCH_3), $\delta = 31.63$ppm ($\mathrm{NCH}_2\mathbf{C}\mathrm{H}_2(\mathrm{CH}_2)_5\mathrm{CH}_3$), $\delta = 29.90$ppm ($\mathrm{N}(\mathrm{CH}_2)_2\mathbf{C}\mathrm{H}_2(\mathrm{CH}_2)_4\mathrm{CH}_3$), $\delta = 28.95$ppm ($\mathrm{N}(\mathrm{CH}_2)_3\mathbf{C}\mathrm{H}_2(\mathrm{CH}_2)_3\mathrm{CH}_3$), $\delta = 28.82$ppm ($\mathrm{N}(\mathrm{CH}_2)_4\mathbf{C}\mathrm{H}_2(\mathrm{CH}_2)_2\mathrm{CH}_3$), $\delta = 25.96$ppm ($\mathrm{N}(\mathrm{CH}_2)_5\mathbf{C}\mathrm{H}_2\mathrm{CH}_2\mathrm{CH}_3$), $\delta = 22.51$ppm ($\mathrm{N}(\mathrm{CH}_2)_6\mathbf{C}\mathrm{H}_2\mathrm{CH}_3$), $\delta = 14.38$ppm ($\mathrm{N}(\mathrm{CH}_2)_7\mathbf{C}\mathrm{H}_3$). IR ($\mathrm{cm}^{-1}$): 3127 symmetric ring C-H stretch & 3051 asymmetric ring C-H stretch, 2955 & 2924 asymmetric chain C-H stretch, 2855 symmetric chain C-H stretch, 1569 in plane ring bend, 1464 NCH_3 umbrella, 1427 R-CH_3 umbrella (shoulder), 1378 CH_2 asymmetric wag, 1337 CH_2 twist, 1275 full chain CH_2 symmetric wag, 1260 full chain CH_2 asymmetric wag, 1226 full chain CH_2 twist, 1168 asymmetric ring C-H in plane bend, 1120 symmetric ring C-H in plane bend, 1019 asymmetric C-C stretch, 841 symmetric C-H ring out of plane bend (shoulder), 750 asymmetric C-H ring out of plane bend, 680 C-N in plane bend, 668 out of plane C-N bend.

1-octyl-3-methylimidazolium bromide

Bromooctane (31.06g, 0.161mol, 1.5eq) and acetonitrile (100mL) were mixed and 1-methylimidazole (8.55mL, 0.107mol, 1eq) was added dropwise. The solution was refluxed for 2 days. The was acetonitrile decanted and the residual liquid was washed with ethyl acetate (2x100mL) then dried at 35^{o}C under vacuum for 3 days. Collected viscous colourless liquid, 1-octyl-3-methylimidazolium bromide (26.70g, 0.097mol, 91% yield). *m/z* (LSIMS$^+$) $[\mathrm{C}_8\mathrm{C}_1\mathrm{im}]^+$ 195, 100%, (LSIMS$^-$) $^{79}\mathrm{Br}^-$ 79, 100%, $^{81}\mathrm{Br}^-$ 81, 90%. EA (calc. C 52.37, H 8.42, N 29.03) found C 52.40, H 8.50, N 29.08. ^{1}H-NMR (400MHz d_6-DMSO): $\delta = 9.33$ppm (s, 1H, C(2)H), $\delta = 7.85$ppm (s, 1H, C(4)H), $\delta = 7.78$ppm (s, 1H, C(5)H), $\delta = 4.18$ppm (t, $^3\mathrm{J}_{HH} = 7.2$Hz, 2H, $\mathrm{NC}\mathbf{H}_2(\mathrm{CH}_2)_6\mathrm{CH}_3$), $\delta = 3.87$ppm (s, 3H, NCH_3), $\delta = 1.77$ppm (quintet, $^3\mathrm{J}_{HH} = 7$Hz, 2H, $\mathrm{NCH}_2\mathrm{C}\mathbf{H}_2(\mathrm{CH}_2)_5\mathrm{CH}_3$), $\delta = 1.23$ppm (s, 10H, $\mathrm{N}(\mathrm{CH}_2)_2(\mathrm{C}\mathbf{H}_2)_5\mathrm{CH}_3$), $\delta = 0.84$ppm (t, 3H, $^3\mathrm{J}_{HH} = 6.68$Hz). ^{13}C-NMR (100MHz d_6-DMSO): $\delta = 137.01$ppm (C(2)), $\delta = 123.96$ppm (C(4)), $\delta = 122.71$ppm (C(5)), $\delta = 49.10$ppm ($\mathrm{N}\mathbf{C}\mathrm{H}_2(\mathrm{CH}_2)_6\mathrm{CH}_3$), $\delta = 36.26$ppm ($\mathrm{N}\mathbf{C}\mathrm{H}_2(\mathrm{CH}_2)_6\mathrm{CH}_3$), $\delta = 31.63$ppm ($\mathrm{NCH}_2\mathbf{C}\mathrm{H}_2(\mathrm{CH}_2)_5\mathrm{CH}_3$), $\delta = 29.90$ppm ($\mathrm{N}(\mathrm{CH}_2)_2\mathbf{C}\mathrm{H}_2(\mathrm{CH}_2)_4\mathrm{CH}_3$), $\delta = 28.94$ppm ($\mathrm{N}(\mathrm{CH}_2)_3\mathbf{C}\mathrm{H}_2(\mathrm{CH}_2)_3\mathrm{CH}_3$), $\delta = 28.82$ppm ($\mathrm{N}(\mathrm{CH}_2)_4\mathbf{C}\mathrm{H}_2(\mathrm{CH}_2)_2\mathrm{CH}_3$), $\delta = 25.96$ppm ($\mathrm{N}(\mathrm{CH}_2)_5\mathbf{C}\mathrm{H}_2\mathrm{CH}_2\mathrm{CH}_3$), $\delta = 22.51$ppm ($\mathrm{N}(\mathrm{CH}_2)_6\mathbf{C}\mathrm{H}_2\mathrm{CH}_3$), $\delta = 14.38$ppm (RCH_3).

IR (cm^{-1}): 3137 symmetric ring C-H stretch & 3055 asymmetric ring C-H stretch, 2955 & 2925 asymmetric chain C-H stretch, 2855 symmetric chain C-H stretch, 1569 in plane ring bend, 1464 NCH_3 umbrella, 1427 R-CH_3 umbrella (shoulder), 1378 CH_2 asymmetric wag, 1337 CH_2 twist, 1275 full chain CH_2 symmetric wag, 1260 full chain CH_2 asymmetric wag, 1226 full chain CH_2 twist, 1167 asymmetric ring C-H in plane bend, 1120 symmetric ring C-H in plane bend, 1019 asymmetric C-C stretch, 825 symmetric C-H ring out of plane bend (shoulder), 749 asymmetric C-H ring out of plane bend, 696 C-N in plane bend, 668 out of plane C-N bend.

1-octyl-3-methylimidazolium bis(trifluoromethylsulfonyl)imide

1-octyl-3-methylimidazolium chloride (1.9258g, 8.3mmol, 1eq) in dichloromethane (25mL) was added to lithium bis(trifluoromethylsulfonyl)imide (2.381g, 8.3mmol, 1eq) and the slurry stirred vigorously overnight. Water was added until two colourless phases were seen (15mL). The organic phase was collected and washed with water (2x20mL). The solvent was evaporated and the liquid residue dried under vacuum for 2 days. Collected colourless liquid 1-octyl-3-methylimidazolium bis(trifluoromethylsulfonyl)imide (4.21g, 8.2mmol, 98% yield). *m/z* ($LSIMS^+$) $[C_8C_1im]^+$ 195, 100%, ($LSIMS^-$) $[NTf_2]^-$ 281, 100%. EA: (calc. C 35.36, H 4.88, N 8.84) found C 35.25, H 4.81, N 8.77. ^{1}H-NMR (400MHz d_6-DMSO): $\delta = 9.11$ppm (s, 1H, C(2)H), $\delta = 7.74$ppm (s, 1H, C(4)H), $\delta = 7.67$ppm (s, 1H, C(5)H), $\delta = 4.17$ppm (t, $^3J_{HH} = 7.2$Hz, $NC\mathbf{H}_2(CH_2)_6CH_3$), $\delta = 3.87$ppm (s, 3H, NCH_3), $\delta = 1.81$ppm (quintet, $^3J_{HH} = 7.2$Hz, 2H, $NCH_2C\mathbf{H}_2(CH_2)_5CH_3$), $\delta = 1.26$ppm (broad s, 10H, $N(CH_2)_2(C\mathbf{H}_2)_5CH_3$), $\delta = 0.87$ppm (t, $^3J_{HH} = 7.08$Hz, 3H, $N(CH_2)_7C\mathbf{H}_3$). ^{13}C-NMR (100MHz d_6-DMSO): $\delta = 136.92$ppm (C(2)H), $\delta = 123.96$ppm (C(4)H), $\delta = 122.61$ppm (C(5)H), $\delta = 119.94$ppm (quartet, $^1J_{CF} = 319$Hz, $\mathbf{C}F_3$), $\delta = 49.27$ppm ($N\mathbf{C}H_2(CH_2)_6CH_3$), $\delta = 36.02$ppm (NCH_3), $\delta = 31.59$ppm ($NCH_2\mathbf{C}H_2(CH_2)_5CH_3$), $\delta = 29.83$ppm ($N(CH_2)_2\mathbf{C}H_2(CH_2)_4CH_3$), $\delta = 28.89$ppm ($N(CH_2)_3\mathbf{C}H_2(CH_2)_3CH_3$), $\delta = 28.76$ppm ($N(CH_2)_4\mathbf{C}H_2(CH_2)_2CH_3$), $\delta = 25.91$ppm ($N(CH_2)_5\mathbf{C}H_2CH_2CH_3$), $\delta = 22.45$ppm ($N(CH_2)_6\mathbf{C}H_2CH_3$), $\delta = 14.08$ppm ($N(CH_2)_3\mathbf{C}H_3$). IR (cm^{-1}): 3148 symmetric ring C-H stretch & 3116 asymmetric ring C-H stretch, 2961 & 2935 asymmetric chain C-H stretch, 2864 symmetric chain C-H stretch, 1565 in plane ring bend, 1469 CH_3 & CH_2 sym-

metric wags, 1347 SO_2 asymmetric stretch, 1330 CH_2 twist, 1275 full chain CH_2 symmetric wag, 1260 full chain CH_2 asymmetric wag, 1226 full chain CH_2twist, 1178 C-S stretch, 1133 CF_3 stretch, 1052 S-N stretch, 960 asymmetric chain twist, 848 symmetric C-H ring out of plane bend, 788 asymmetric C-H ring out of plane bend, 762 C-N in plane bend, 750 out of plane C-N bend.

1-octyl-3-methylimidazolium nitrate

1-octyl-3-methylimidazolium chloride (1.93g, 8.3mmol, 1eq) was dissolved in water (10mL) and silver nitrate solution (36.7mL, 0.3M, 1eq) was added dropwise. The solution was filtered and dried on a freezedrier. Collected 1-octyl-3-methylimidazolium nitrate as a viscous liquid (1.52g, 6.2mmol, 70% yield). *m/z* (LSIMS$^+$) $[C_8C_1im]^+$ 195, 100%, (LSIMS$^-$) NO_3^- 62, 30%. EA: (calc. C 56.01, H 9.01, N 16.33) found C 55.78, H 8.85, N 16.17. ^{1}H-NMR (400MHz, d_6-DMSO): δ = 9.19ppm (s, 1H, C(2)H), δ = 7.80ppm (s, 1H, C(4)H), δ = 7.73ppm (s, 1H, C(5)H), δ = 4.16ppm (t, $^3J_{HH}$ = 7.2Hz, NC$\mathbf{H}_2$(CH$_2$)$_5$CH$_3$), δ = 3.86ppm (s, 3H, NCH$_3$), δ = 1.78ppm (quintet, $^3J_{HH}$ = 7.2Hz, 2H, NCH$_2$C$\mathbf{H}_2$(CH$_2$)$_5$CH$_3$), δ = 1.24ppm (broad s, 10H, N(CH$_2$)$_2$(C$\mathbf{H}_2$)$_5$CH$_3$), δ = 0.85ppm (t, $^3J_{HH}$ = 7.2Hz 3H, N(CH$_2$)$_7$C$\mathbf{H}_3$). ^{13}C-NMR (100MHz, d_6-DMSO): δ = 137.08ppm (C(2)H), δ = 124.07ppm (C(4)H), δ = 122.74ppm (C(5)H), δ = 49.23ppm (N$\mathbf{C}$H$_2$(CH$_2$)$_6$CH$_3$), δ = 36.14ppm (NCH$_3$), δ = 31.64ppm (NCH$_2$$\mathbf{C}H_2$(CH$_2$)$_5CH_3$), δ = 29.87ppm (N(CH$_2$)$_2$$\mathbf{C}H_2$(CH$_2$)$_4CH_3$), δ = 28.95ppm (N(CH$_2$)$_3$$\mathbf{C}H_2$(CH$_2$)$_3CH_3$), δ = 28.81ppm (N(CH$_2$)$_4$$\mathbf{C}H_2$(CH$_2$)$_2CH_3$), δ = 25.97ppm (N(CH$_2$)$_5$$\mathbf{C}H_2CH_2CH_3$), δ = 22.53ppm (N(CH$_2$)$_6$$\mathbf{C}H_2CH_3$), δ = 14.38ppm (N(CH$_2$)$_3$$\mathbf{C}H_3$). IR (cm^{-1}): 3150 symmetric ring C-H stretch & 3107 asymmetric ring C-H stretch, 2953 & 2929 asymmetric chain C-H stretch, 2857 symmetric chain C-H stretch, 2051 SC-N stretch, 1564 in plane ring bend, 1462 NCH_3 umbrella, 1429 R-CH_3 umbrella, 1372 CH_2 asymmetric wag, 1333 CH_2 twist, 1270 full chain CH_2 symmetric wag, 1263 full chain CH_2 asymmetric wag, 1226 full chain CH_2 twist, 1165 asymmetric ring C-H in plane bend, 1120 symmetric ring C-H in plane bend, 1020 asymmetric C-C stretch, 950 asymmetric chain twist, 849 symmetric C-H ring out of plane bend, 739 asymmetric C-H ring out of plane bend, 677 C-N in plane bend, 662 out of plane C-N bend.

1-octyl-3-methylimidazolium thiocyanate

1-octyl-3-methylimidazolium chloride (1.16g, 4.58mmol, 1eq) in acetonitrile (15mL) was mixed with barium thiocyanate (0.71g, 2.29mmol, 0.5eq) in acetonitrile (15mL) and the solution was stirred for 4 hours. A white precipitate was formed. The suspension was centrifuged and the liquor decanted. The solvent was removed yielding a slightly pink liquid 1-octyl-3-methylimidazolium thiocyanate (0.96g, 3.80mmol, 83% Yield). *m/z* (LSIMS$^+$) $[C_8C_1im]^+$ 195, 100%, (LSIMS$^-$) CN^- 26, 100%, S^- 32, 85%, SCN^- 58, 85%. EA: (calc. C 61.62, H 9.15, N 6.58) found C 61.26, H 9.09, N 16.62. ^{1}H-NMR (400MHz, d_6-DMSO): δ = 9.13ppm (s, 1H, C(2)H), δ = 7.79ppm (s, 1H, C(4)H), δ = 7.72ppm (s, 1H, C(5)H), δ = 4.18ppm (t, $^3J_{HH}$ = 7.2Hz, $NC\mathbf{H}_2(CH_2)_5CH_3$), δ = 3.88ppm (s, 3H, NCH_3), δ = 1.79ppm (quintet, $^3J_{HH}$ = 7.2Hz, 2H, $NCH_2C\mathbf{H}_2(CH_2)_5CH_3$), δ = 1.23ppm (broad s, 10H, $N(CH_2)_2(C\mathbf{H}_2)_5CH_3$), δ = 0.83ppm (t, $^3J_{HH}$ = 7.08Hz, 3H, $N(CH_2)_7C\mathbf{H}_3$). ^{13}C-NMR (100MHz, d_6-DMSO): δ = 136.97ppm C(2)H. δ = 130.34ppm, SCN. δ = 124.03ppm, C(4)H. δ = 122.71ppm, C(5)H. δ = 49.33ppm $N\mathbf{C}H_2(CH_2)_6CH_3$, δ = 36.26ppm NCH_3, δ = 31.64ppm $NCH_2\mathbf{C}H_2(CH_2)_5CH_3$, δ = 29.92ppm $N(CH_2)_2\mathbf{C}H_2(CH_2)_4CH_3$, δ = 28.95ppm $N(CH_2)_3\mathbf{C}H_2(CH_2)_3CH_3$, δ = 28.82ppm $N(CH_2)_4\mathbf{C}H_2(CH_2)_2CH_3$, δ = 25.99ppm $N(CH_2)_5\mathbf{C}H_2CH_2CH_3$, δ = 22.53ppm $N(CH_2)_6\mathbf{C}H_2CH_3$, δ = 14.38ppm $N(CH_2)_3\mathbf{C}H_3$. IR (cm^{-1}): 3144 symmetric ring C-H stretch & 3095 asymmetric ring C-H stretch, 2955 & 2925 asymmetric chain C-H stretch, 2855 symmetric chain C-H stretch, 2048 (S)C-N stretch, 1569 in plane ring bend, 1460 R-CH_3 umbrella, 1379 CH_2 asymmetric wag, 1338 CH_2 twist, 1275 full chain CH_2 symmetric wag, 1260 full chain CH_2 asymmetric wag, 1226 full chain CH_2 twist, 1164 asymmetric ring C-H in plane bend, 1120 symmetric ring C-H in plane bend, 1030 asymmetric C-C stretch, 949 asymmetric chain twist, 841 symmetric C-H ring out of plane bend, 750 asymmetric C-H ring out of plane bend, 680 C-N in plane bend, 668 out of plane C-N bend.

1-hexyl-3-ethylimidazolium chloride

1-ethylimidazole (9.13g, 95mmol, 1eq) and acetonitrile (75mL) were mixed and chlorohexane (14.4mL, 105mmol, 1.1eq) was added dropwise. The solution was refluxed for 5 days. The acetonitrile removed under vacuum and the residual liq-

uid was washed with ethyl acetate (2x100mL) then dried at 35^{o}C under vacuum for 3 days. Collected viscous liquid, 1-hexyl-3-ethylimidazolium chloride (17.1g, 78.9mmol, 83% yield). *m/z* (LSIMS$^+$) $[C_6C_2im]^+$ 181, 100%, (LSIMS$^-$) $^{35}Cl^-$ 35, 100%, $^{37}Cl^-$ 37, 30%. EA: (calc. C 60.95, H 9.77, N 12.92) found C 60.86, H 9.58, N 12.84. ^{1}H-NMR (400MHz, d_6-DMSO): δ = 9.67ppm (s, 1H, C(2)H), δ = 7.94ppm (s, 1H, C(4)H), δ = 7.92ppm (s, 1H, C(5)H), δ = 4.26ppm (m, 4H, NC$\mathbf{H}_2$CH$_3$ and NC$\mathbf{H}_2$(CH$_2$)$_4$CH$_3$), δ = 1.81ppm (quintet, $^3J_{HH}$ = 7.2Hz, 2H, NCH$_2$C$\mathbf{H}_2$(CH$_2$)$_3$CH$_3$), δ = 1.43ppm (t, $^3J_{HH}$ = 7.6Hz, NCH$_2$C$\mathbf{H}_3$), δ = 1.27ppm (broad s, 6H, N(CH$_2$)$_2$(C$\mathbf{H}_2$)$_3$CH$_3$), δ = 0.82ppm (t, $^3J_{HH}$ = 6.8Hz, 3H, N(CH$_2$)$_5$C$\mathbf{H}_3$). ^{13}C-NMR (100MHz, d_6-DMSO): δ = 136.45ppm C(2)H, δ = 122.87ppm C(4)H, δ = 122.62ppm C(5)H, δ = 49.20ppm N$\mathbf{C}$H$_2$(CH$_2$)$_5$CH$_3$, δ = 44.59ppm N$\mathbf{C}$H$_2$CH$_2$, δ = 31.01ppm NCH$_2\mathbf{C}$H$_2$(CH$_2$)$_3$CH$_3$, δ = 29.81ppm N(CH$_2$)$_2\mathbf{C}$H$_2$(CH$_2$)$_2$CH$_3$, δ = 25.65ppm N(CH$_2$)$_3\mathbf{C}$H$_2$CH$_2$CH$_3$, δ = 22.34ppm N(CH$_2$)$_4\mathbf{C}$H$_2$CH$_3$, δ = 15.61ppm NCH$_2\mathbf{C}$H$_3$, δ = 14.30ppm N(CH$_2$)$_5\mathbf{C}$H$_3$. IR (cm^{-1}): 3121 symmetric ring C-H stretch & 3055 asymmetric ring C-H stretch, 2961 & 2932 asymmetric chain C-H stretch, 2872 symmetric chain C-H stretch, 1561 in plane ring bend, 1472 NCH$_3$ umbrella, 1374 CH$_2$ asymmetric wag, 1334 CH$_2$ twist, 1275 full chain CH$_2$ symmetric wag, 1260 full chain CH$_2$ asymmetric wag, 1226 full chain CH$_2$ twist, 1163 asymmetric ring C-H in plane bend, 1116 symmetric ring C-H in plane bend, 1023 asymmetric C-C stretch, 859 symmetric C-H ring out of plane bend, 747 asymmetric C-H ring out of plane bend, 683 C-N in plane bend, 664 out of plane C-N bend.

1-hexyl-3-ethylimidazolium bromide

1-ethylimidazole (12.24g, 0.13mol, 1eq) and EtOAc (35mL) were mixed and bromohexane (20mL, 0.15mol, 1.1eq) was added dropwise. The solution was refluxed overnight, during which time two phases appeared. The solvent was decanted and residual liquid was washed with ethyl acetate (2x100mL) then dried at 35^{o}C under vacuum for 3 days. Collected colourless liquid, 1-hexyl-3-ethylimidazolium bromide (29.54g, 0.11mol, 87% yield). *m/z* (LSIMS$^+$) $[C_6C_2im]^+$ 181, 100%, (LSIMS$^-$) CN$^-$ 26, 100% Br$^-$ 79, 35%, Br$^-$ 81, 35%. EA: (calc. C 50.58, H 8.10, N 10.72) found C 50.38, H 7.89, N 10.65. ^{1}H-NMR (400MHz, d_6-DMSO): δ = 9.53ppm (s, 1H, C(2)H),

δ = 7.95ppm (s, 1H, C(4)H), δ = 7.93ppm (s, 1H, C(5)H), δ = 4.24ppm (m, 4H, NC$\mathbf{H}_2$$CH_3$ and NC$\mathbf{H}_2$$(CH_2)_4CH_3$), δ = 1.79ppm (broad s, 2H, $NCH_2C\mathbf{H}_2(CH_2)_3CH_3$), δ = 1.42ppm (t, $^3J_{HH}$ = 7.32Hz, $NCH_2C\mathbf{H}_3$), δ = 1.24ppm (broad s, 6H, $N(CH_2)_2(C\mathbf{H}_2)_3CH_3$), δ = 0.82ppm (t, $^3J_{HH}$ = 6.6Hz 3H, $N(CH_2)_5C\mathbf{H}_3$). ^{13}C-NMR (100MHz, d_6-DMSO): δ = 136.24ppm C(2)H, δ = 122.85ppm C(4)H, δ = 122.58ppm C(5)H, δ = 49.18ppm $N\mathbf{C}H_2(CH_2)_5CH_3$, δ = 44.61ppm $N\mathbf{C}H_2CH_2$, δ = 30.99ppm $NCH_2\mathbf{C}H_2(CH_2)_3CH_3$, δ = 29.81ppm $N(CH_2)_2\mathbf{C}H_2(CH_2)_2CH_3$, δ = 25.60ppm $N(CH_2)_3\mathbf{C}H_2CH_2CH_3$, δ = 22.33ppm $N(CH_2)_4\mathbf{C}H_2CH_3$, δ = 15.63ppm $NCH_2\mathbf{C}H_3$, δ = 14.27ppm $N(CH_2)_5\mathbf{C}H_3$. IR (cm^{-1}): 3131 symmetric ring C-H stretch & 3073 asymmetric ring C-H stretch, 2956 & 29234 asymmetric chain C-H stretch, 2875 symmetric chain C-H stretch, 1562 in plane ring bend, 1463 R-CH_3 umbrella, 1379 CH_2 asymmetric wag, 1334 CH_2 twist, 1261 full chain CH_2 asymmetric wag, 1222 full chain CH_2 twist, 1163 asymmetric ring C-H in plane bend, 1116 symmetric ring C-H in plane bend, 1023 asymmetric C-C stretch, 825 symmetric C-H ring out of plane bend (shoulder), 762 asymmetric C-H ring out of plane bend, 696 C-N in plane bend, 652 out of plane C-N bend.

1-hexyl-3-ethylimidazolium bis(trifluoromethylsulfonyl)imide

1-hexyl-3-ethylimidazolium chloride (3.25g, 15.0mmol, 1eq) was dissolved in DCM (100mL) and slurried over lithium bis(trifluoromethylsulfonyl)imide (4.48g, 15.6mmol, 1.04eq) for 4 hours. Water (40mL) was added and the organic phase collected. The solvent was removed and 1-hexyl-3-ethylimidazolium bis(trifluoromethylsulfonyl)imide was collected as a colourless liquid (6.59g, 14.3mmol, 95%). *m/z* (LSIMS$^+$) $[C_6C_2im]^+$ 181, 100%, (LSIMS$^-$) $[NTf_2]^-$ 280, 100%. EA: (calc. C 33.84, H 4.59, N 9.11) found C 33.72, H 4.44, N 9.97. ^{1}H-NMR (400MHz, d_6-DMSO): δ = 9.20ppm (s, 1H, C(2)H), δ = 7.79ppm (s, 1H, C(4)H), δ = 7.78ppm (s, 1H, C(5)H), δ = 4.20ppm (m, 4H, NC$\mathbf{H}_2$$CH_3$ and NC$\mathbf{H}_2$$(CH_2)_4CH_3$), δ = 1.81ppm (broad s, 2H, $NCH_2C\mathbf{H}_2(CH_2)_3CH_3$), δ = 1.44ppm (t, $^3J_{HH}$ = 7.32Hz, 3H, $NCH_2C\mathbf{H}_3$), δ = 1.28ppm (broad s, 6H, $N(CH_2)_2(C\mathbf{H}_2)_3CH_3$), δ = 0.87ppm (t $^3J_{HH}$ = 6.6Hz 3H, $N(CH_2)_5C\mathbf{H}_3$). ^{13}C-NMR (100MHz, d_6-DMSO): δ = 136.06ppm C(2)H, δ = 122.81ppm C(4)H, δ = 122.54ppm C(5)H, δ = 119.94ppm, q, $^1J_{CF}$ = 320Hz, $\mathbf{C}F_3$, δ = 49.34ppm $N\mathbf{C}H_2(CH_2)_5CH_3$, δ = 44.67ppm $N\mathbf{C}H_2CH_2$, δ = 30.97ppm

$NCH_2\mathbf{C}H_2(CH_2)_3CH_3$, δ = 29.75ppm $N(CH_2)_2\mathbf{C}H_2(CH_2)_2CH_3$, δ = 25.61ppm $N(CH_2)_3\mathbf{C}H_2CH_2CH_3$, δ = 22.29ppm $N(CH_2)_4\mathbf{C}H_2CH_3$, δ = 15.34ppm $NCH_2\mathbf{C}H_3$, δ = 14.10ppm $N(CH_2)_5\mathbf{C}H_3$. IR (cm^{-1}): 3151 symmetric ring C-H stretch & 3116 asymmetric ring C-H stretch, 2961 & 2935 asymmetric chain C-H stretch, 2864 symmetrich chain C-H stretch, 1565 in plane ring bend, 1469 CH_3 & CH_2 symmetric wags, 1347 SO_2 asymmetric stretch, 1330 CH_2 twist, 1275 full chain CH_2 symmetric wag, 1260 full chain CH_2 asymmetric wag, 1226 full chain CH_2 twist, 1178 C-S stretch, 1133 CF_3 stretch, 1052 S-N stretch, 960 asymmetric chain twist, 848 symmetric C-H ring out of plane bend, 788 asymmetric C-H ring out of plane bend, 762 C-N in plane bend, 750 out of plane C-N bend.

1-hexyl-3-ethylimidazolium nitrate

1-hexyl-3-ethylimidazolium bromide (2.36g, 9.0mmol, 1eq) was dissolved in water (10mL) and silver nitrate solution (30.0mL, 0.3M, 1eq) was added dropwise. The solution was filtered and dried on a freezedrier. Collected 1-hexyl-3-ethylimidazolium nitrate as a viscous liquid (1.61g, 6.6mmol, 70% yield). *m/z* (LSIMS$^+$) $[C_6C_2im]^+$ 181, 100%, (LSIMS$^-$) CN^- 26, 100%, $NO_3{}^-$ 62, 40%. EA: (calc. C 54.30, H 8.70, N 17.27) found C 54.19, H 8.66, N 17.35. ^{1}H-NMR (400MHz, d_6-DMSO): δ = 9.26ppm (s, 1H, C(2)H), δ = 7.83ppm (s, 1H, C(4)H), δ = 7.81ppm (s, 1H, C(5)H), δ = 4.19ppm (m, 4H, $NC\mathbf{H}_2CH_3$ and $NC\mathbf{H}_2(CH_2)_4CH_3$), δ = 1.79ppm (broad s, 2H, $NCH_2C\mathbf{H}_2(CH_2)_3CH_3$), δ = 1.42ppm (t, $^3J_{HH}$ = 7.32Hz, $NCH_2C\mathbf{H}_3$), δ = 1.26ppm (broad s, 6H, $N(CH_2)_2(C\mathbf{H}_2)_3CH_3$), δ = 0.85ppm (t, $^3J_{HH}$ = 6.6Hz, 3H, $N(CH_2)_5C\mathbf{H}_3$). ^{13}C-NMR (100MHz, d_6-DMSO): δ = 136.22ppm C(2)H, δ = 122.88ppm C(4)H, δ = 122.62ppm C(5)H, δ = 49.29ppm $N\mathbf{C}H_2(CH_2)_5CH_3$, δ = 44.67ppm $N\mathbf{C}H_2CH_2$, δ = 30.99ppm $NCH_2\mathbf{C}H_2(CH_2)_3CH_3$, δ = 29.75ppm $N(CH_2)_2\mathbf{C}H_2(CH_2)_2CH_3$, δ = 25.63ppm $N(CH_2)_3\mathbf{C}H_2CH_2CH_3$, δ = 22.32ppm $N(CH_2)_4\mathbf{C}H_2CH_3$, δ = 15.49ppm $NCH_2\mathbf{C}H_3$, δ = 14.27ppm $N(CH_2)_5\mathbf{C}H_3$. IR (cm^{-1}): 3138 symmetric ring C-H stretch, 3092 NO_3 overtone, 2957 & 2929 asymmetric chain C-H stretches, 2860 symmetric chain C-H stretch, 1565 in plane ring bend, 1453 NCH_2CH_3 umbrella, 1329 NO Stretch, 1164 asymmetric ring C-H in plane bend, 1120 symmetric ring C-H in plane bend, 1039 asymmetric C-C stretch, 829 symmetric C-H ring out of plane bend (shoulder), 766 asymmetric C-H ring out

of plane bend, 680 C-N in plane bend, 668 out of plane C-N bend.

1-hexyl-3-ethylimidazolium thiocyanate

1-hexyl-3-ethylimidazolium chloride (1.24g, 6.12mmol, 1eq) in acetonitrile (15mL) was mixed with barium thiocyanate (0.85g, 3.06mmol, 0.5eq) in acetonitrile (15mL) and the solution was stirred for 4 hours. A white precipitate was formed. The suspension was centrifuged and the liquor decanted. The solvent was removed yielding a slightly pink liquid 1-hexyl-3-ethylimidazolium thiocyanate (1.35g, 5.69mmol, 93%). *m/z* (LSIMS$^+$) $[C_6C_2im]^+$ 181, 100%, (LSIMS$^-$) CN^- 26, 100%, S^- 32, 80%, SCN^- 62, 80%. EA: (calc. C 60.21, H 8.84, N 17.55) found C 59.72, H 8.48, N 17.04. ^{1}H-NMR (400MHz, d_6-DMSO): δ = 9.21ppm (s, 1H, C(2)H), δ = 7.81ppm (s, 1H, C(4)H), δ = 7.80ppm (s, 1H, C(5)H), δ = 4.21ppm (m, 4H, $NC\mathbf{H}_2CH_3$ and $NC\mathbf{H}_2(CH_2)_4CH_3$), δ = 1.79ppm (broad s, 2H, $NCH_2C\mathbf{H}_2(CH_2)_3CH_3$), δ = 1.42ppm (t, $^3J_{HH}$ = 7.32Hz, 3H, $NCH_2C\mathbf{H}_3$), δ = 1.23ppm (broad s, 6H, $N(CH_2)_2(C\mathbf{H}_2)_3CH_3$), δ = 0.81ppm (t, $^3J_{HH}$ = 6.6Hz 3H, $N(CH_2)_5C\mathbf{H}_3$). ^{13}C-NMR (100MHz, d_6-DMSO): δ = 136.10ppm C(2)H, δ = 130.29ppm SCN, δ = 122.83ppm C(4)H, δ = 122.55ppm C(5)H, δ = 49.39ppm $N\mathbf{C}H_2(CH_2)_5CH_3$, δ = 44.77ppm $N\mathbf{C}H_2CH_2$, δ = 30.99ppm $NCH_2\mathbf{C}H_2(CH_2)_3CH_3$, δ = 29.80ppm $N(CH_2)_2\mathbf{C}H_2(CH_2)_2CH_3$, δ = 25.64ppm $N(CH_2)_3\mathbf{C}H_2CH_2CH_3$, δ = 22.32ppm $N(CH_2)_4\mathbf{C}H_2CH_3$, δ = 15.52ppm $NCH_2\mathbf{C}H_3$, δ = 14.24ppm $N(CH_2)_5\mathbf{C}H_3$. IR (cm^{-1}): 3138 symmetric ring C-H stretch & 3093 asymmetric ring C-H stretch, 2956 & 2930 asymmetric chain C-H stretch, 2859 symmetric chain C-H stretch, 2047 (S)C-N stretch, 1563 in plane ring bend, 1460 R-CH_3 umbrella, 1379 CH_2 asymmetric wag, 1338 CH_2 twist, 1275 full chain CH_2 symmetric wag, 1260 full chain CH_2 asymmetric wag, 1226 full chain CH_2 twist, 1164 asymmetric ring C-H in plane bend, 1120 symmetric ring C-H in plane bend, 1030 asymmetric C-C stretch, 949 asymmetric chain twist, 841 symmetric C-H ring out of plane bend, 750 asymmetric C-H ring out of plane bend, 680 C-N in plane bend, 668 out of plane C-N bend.

1,3-dibutylimidazolium chloride

Chlorobutane (36mL, 0.35mol, 1.2eq) was added to a mixture of N-butylimidazole (36mLg, 0.29mol, 1eq) and EtOAc (100mL). The mixture was refluxed for 5 days, in which time two phases appeared. The ethyl acetate was decanted, and the IL

washed with EtOAc (2x50mL) and dried under vacuum for 1 hour and recrystallised from MeCN/EtOAc (4:1). Collected white crystals of 1,3-dibutylimidazolium chloride (52.39g, 0.24mol, 83% Yield, m.p. 48-50^{o}C). *m/z* (LSIMS$^+$) $[C_4C_4im]^+$ 181, 100%, (LSIMS$^-$) $^{35}Cl^-$ 35, 100%, $^{37}Cl^-$ 37, 30%. EA: (calc. C 60.95, H 9.77, N 12.92) found C 60.91, H 9.72, N 12.89. ^{1}H-NMR (400MHz, d_6-DMSO): $\delta = 9.30$ppm (s, 1H, C(2)H), $\delta = 7.88$ppm (d, $^3J_{HH} = 1.56$Hz, 2H, C(4&5)H), $\delta = 4.19$ppm (t, $^3J_{HH} = 7.2$Hz, 4H, NC$\mathbf{H}_2$CH$_2$CH$_2$CH$_3$), $\delta = 1.77$ppm (quintet, $^3J_{HH} = 7.2$Hz, 4H, NCH$_2$C$\mathbf{H}_2$CH$_2$CH$_3$), $\delta = 1.27$ppm (sextet, $^3J_{HH} = 7.2$Hz, 4H, N(CH$_2$)$_2$C$\mathbf{H}_2$CH$_3$), $\delta = 0.90$ppm (t, $^3J_{HH} = 7.2$Hz, 6H, N(CH$_2$)$_3$C$\mathbf{H}_3$). ^{13}C-NMR (100MHz, d_6-DMSO): $\delta = 136.76$ppm C(2)H, $\delta = 123.42$ppm C(4)H, $\delta = 122.20$ppm C(5)H, $\delta = 48.20$ppm N$\mathbf{C}$H$_2$(CH$_2$)$_2$CH$_3$, $\delta = 31.33$ppm NCH$_2\mathbf{C}$H$_2$CH$_2$CH$_3$, $\delta = 18.63$ppm N(CH$_2$)$_2\mathbf{C}$H$_2$CH$_3$, $\delta = 13.15$ppm N(CH$_2$)$_3\mathbf{C}$H$_3$. IR (cm^{-1}): 3120 symmetric ring C-H stretch & 3055 asymmetric ring C-H stretch, 2961 & 2932 asymmetric chain C-H stretch, 2872 symmetric chain C-H stretch, 1561 in plane ring bend, 1466 NCH$_3$ umbrella, 1378 CH$_2$ asymmetric wag, 1334 CH$_2$ twist, 1275 full chain CH$_2$ symmetric wag, 1260 full chain CH$_2$ asymmetric wag, 1226 full chain CH$_2$ twist, 1163 asymmetric ring C-H in plane bend, 1116 symmetric ring C-H in plane bend, 1023 asymmetric C-C stretch, 859 symmetric C-H ring out of plane bend, 750 asymmetric C-H ring out of plane bend, 680 C-N in plane bend, 668 out of plane C-N bend.

1,3-dibutylimidazolium bromide

Bromobutane (54mL, 0.5mol, 1.2eq) was added to a mixture of N-butylimidazole (33mL, 0.41mol, 1eq) and EtOAc (100mL). The mixture was refluxed at 70^{o}C for 3 days, in which time two phases appeared. The ethyl acetate was decanted, and the IL washed with EtOAc (2x50mL) and dried under vacuum for 1 hour and washed with MeCN/EtOAc (1:1). Collected colourless IL 1,3-dibutylimidazolium bromide (79.96g, 0.36mol, 89% Yield). *m/z* (LSIMS$^+$) $[C_4C_4im]^+$ 181, 100%, (LSIMS$^-$) CN$^-$ 26, 100%, $^{79}Br^-$ 79, 45%, $^{81}Br^-$ 81, 45%. EA: (calc. C 50.58, H 8.10, N 10.72) found C 50.41, H 7.86, N 10.61. ^{1}H-NMR (400MHz, d_6-DMSO): $\delta = 9.72$ppm (s, 1H, C(2)H), $\delta = 8.02$ppm (d, $^3J_{HH} = 1.56$Hz, 2H, C(4&5)H), $\delta = 4.25$ppm (t, $^3J_{HH} = 7.2$Hz, 4H, NC$\mathbf{H}_2$CH$_2$CH$_2$CH$_3$), $\delta = 1.78$ppm (quintet, $^3J_{HH} = 7.2$Hz, 4H, NCH$_2$C$\mathbf{H}_2$CH$_2$CH$_3$), $\delta = 1.17$ppm (sextet, $^3J_{HH} = 7.2$Hz, 4H, N(CH$_2$)$_2$C$\mathbf{H}_2$CH$_3$),

$\delta = 0.82$ppm (t, $^3J_{HH} = 7.2$Hz, 6H, $N(CH_2)_3C\mathbf{H}_3$). ^{13}C-NMR (100MHz, d_6-DMSO): $\delta = 140.16$ppm C(2)H, $\delta = 124.14$ppm C(4)H, $\delta = 123.42$ppm C(5)H, $\delta = 48.71$ppm $N\mathbf{C}H_2(CH_2)_2CH_3$, $\delta = 31.23$ppm $NCH_2\mathbf{C}H_2CH_2CH_3$, $\delta = 16.91$ppm $N(CH_2)_2\mathbf{C}H_2CH_3$, $\delta = 12.32$ppm $N(CH_2)_3\mathbf{C}H_3$. IR (cm^{-1}): 3135 symmetric ring C-H stretch & 3073 asymmetric ring C-H stretch, 2956 & 29234 asymmetric chain C-H stretch, 2873 symmetric chain C-H stretch, 1562 in plane ring bend, 1463 R-CH_3 umbrella, 1379 CH_2 asymmetric wag, 1334 CH_2 twist, 1260 full chain CH_2 asymmetric wag, 1226 full chain CH_2 twist, 1163 asymmetric ring C-H in plane bend, 1116 symmetric ring C-H in plane bend, 1023 asymmetric C-C stretch, 825 symmetric C-H ring out of plane bend (shoulder), 764 asymmetric C-H ring out of plane bend, 696 C-N in plane bend, 657 out of plane C-N bend.

1,3-dibutylimidazolium bis(trifluoromethylsulfonyl)imide

1,3-dibutylimidazolium chloride (2.3188g, 10.7mmol, 1eq) was dissolved in DCM (50mL) slurried over lithium bis(trifluoromethylsulfonyl)imide (3.21g, 11.2mmol, 1.04eq) for 4 hours. Water (20mL) was added and the organic phase collected. The solvent was removed and 1,3-dibutylimidazolium bis(trifluoromethylsulfonyl)imide was collected as a colourless liquid (5.313g, 11.5mmol, 98%). *m/z* ($LSIMS^+$) $[C_4C_4im]^+$ 181, 100%, ($LSIMS^-$) $[NTf_2]^-$ 280, 100%. EA: (calc. C 33.84, H 4.59, N 9.11) found C 33.73, H 4.51, N 9.15. ^{1}H-NMR (400MHz, d_6-DMSO): $\delta = 9.21$ppm (s, 1H, C(2)H), $\delta = 7.81$ppm (d, $^3J_{HH} = 1.56$Hz, 2H, C(4&5)H), $\delta = 4.17$ppm (t, $^3J_{HH} = 7.2$Hz, 4H, $NC\mathbf{H}_2CH_2CH_2CH_3$), $\delta = 1.79$ppm (quintet, $^3J_{HH} = 7.2$Hz, 4H, $NCH_2C\mathbf{H}_2CH_2CH_3$), $\delta = 1.25$ppm (sextet, $^3J_{HH} = 7.2$Hz, 4H, $N(CH_2)_2C\mathbf{H}_2CH_3$), $\delta = 0.91$ppm (t, $^3J_{HH} = 7.2$Hz, 6H, $N(CH_2)_3C\mathbf{H}_3$). ^{13}C-NMR (100MHz, d_6-DMSO): $\delta = 136.4$ppm C(2)H, $\delta = 122.93$ppm C(4)H and C(5)H, $\delta = 119.95$ppm (quartet, $^1J_{CF} = 320$Hz, $\mathbf{C}F_3$), $\delta = 49.05$ppm $N\mathbf{C}H_2(CH_2)_2CH_3$, $\delta = 31.73$ppm $NCH_2\mathbf{C}H_2CH_2CH_3$, $\delta = 19.25$ppm $N(CH_2)_2\mathbf{C}H_2CH_3$, $\delta = 13.69$ppm $N(CH_2)_3\mathbf{C}H_3$. IR (cm^{-1}): 3149 symmetric ring C-H stretch & 3115 asymmetric ring C-H stretch, 2967 & 2939 asymmetric chain C-H stretch, 2879 symmetric chain C-H stretch, 1564 in plane ring bend, 1464 CH_3 & CH_2 symmetric wags, 1347 SO_2 asymmetric stretch, 1329 CH_2 twist, 1275 full chain CH_2 symmetric wag, 1260 full chain CH_2 asymmetric wag, 1226 full chain CH_2 twist, 1178 C-S stretch, 1133 CF_3

stretch, 1052 S-N stretch, 949 asymmetric chain twist, 848 symmetric C-H ring out of plane bend, 788 asymmetric C-H ring out of plane bend, 762 C-N in plane bend, 750 out of plane C-N bend.

1,3-dibutylimidazolium nitrate

1,3-dibutylimidazolium bromide (2.36g, 10.9mmol, 1eq) was dissolved in water (10mL) and silver nitrate solution (36.3mL, 0.3M, 1eq) was added dropwise. The solution was filtered and dried on a freezedrier. Collected 1,3-dibutylimidazolium nitrate as a viscous liquid (2.09g, 8.61mmol, 79% yield). *m/z* (LSIMS$^+$) $BuNO_3{}^+$ 118, 100%, $[C_4C_4im]^+$ 181, 10%. (LSIMS$^-$) $NO_3{}^-$ 62, 100%. EA: (calc. C 54.30, H 8.70. N 17.27) found C 54.19, H 8.66, N 17.36. ^{1}H-NMR (400MHz, d_6-DMSO): δ = 9.26ppm (s, 1H, C(2)H), δ = 7.61ppm (d, $^3J_{HH}$ = 1.52Hz, 2H, C(4&5)H), δ = 4.33ppm (t, $^3J_{HH}$ = 7.2Hz, 4H, NC$\mathbf{H}_2$CH$_2$CH$_2$CH$_3$), δ = 1.91ppm (quintet, $^3J_{HH}$ = 7.2Hz, 4H, NCH$_2$C$\mathbf{H}_2$CH$_2$CH$_3$), δ = 1.38ppm (sextet, $^3J_{HH}$ = 7.2Hz, 4H, N(CH$_2$)$_2$C$\mathbf{H}_2$CH$_3$), δ = 0.95ppm (t, $^3J_{HH}$ = 7.2Hz, 6H, N(CH$_2$)$_3$C$\mathbf{H}_3$). ^{13}C-NMR (100MHz, d_6-DMSO): δ = 137.05ppm C(2)H, δ = 124.00ppm C(4)H and C(5)H, δ = 49.01ppm N$\mathbf{C}$H$_2$(CH$_2$)$_2$CH$_3$, δ = 31.79ppm NCH$_2\mathbf{C}$H$_2$CH$_2$CH$_3$, δ = 19.24ppm N(CH$_2$)$_2\mathbf{C}$H$_2$CH$_3$, δ = 13.70ppm N(CH$_2$)$_3\mathbf{C}$H$_3$. IR (cm^{-1}): 3150 symmetric ring C-H stretch, 3093 NO_3 overtone, 2963 & 2936 asymmetric chain C-H stretch, 2877 symmetric chain C-H stretch, 1575 in plane ring bend, 1461 NCH_3 umbrella, 1331 NO Stretch, 1169 asymmetric ring C-H in plane bend, 1132 symmetric ring C-H in plane bend, 1041 asymmetric C-C stretch, 829 symmetric C-H ring out of plane bend (shoulder), 777 asymmetric C-H ring out of plane bend, 696 C-N in plane bend, 668 out of plane C-N bend.

1,3-dibutylimidazolium thiocyanate

1,3-dibutylimidazolium chloride (2.80g, 11.70mmol, 1eq) in acetonitrile (15mL) was mixed with barium thiocyanate (1.80g, 5.85mmol, 0.5eq) in acetonitrile (15mL) and the solution was stirred for 4 hours. A white precipitate formed as a suspension. The suspension was centrifuged and the liquor decanted. The solvent was removed yielding a slightly pink liquid 1,3-dibutylimidazolium thiocyanate (2.34g, 9.77mmol, 84%). *m/z* (LSIMS$^+$) $[C_4C_4im]^+$ 181, 100%, (LSIMS$^-$) CN^- 26, 100%, S^- 32, 70%, SCN^- 58, 60%. ^{1}H-NMR (400MHz, d_6-DMSO): δ = 9.22ppm (s, 1H, C(2)H),

$\delta = 7.81$ppm (d, $^3J_{HH} = 1.56$Hz, 2H, C(4&5)H), $\delta = 4.18$ppm (t, $^3J_{HH} = 7.2$Hz, 4H, $NC\mathbf{H}_2CH_2CH_2CH_3$), $\delta = 1.78$ppm (quintet, $^3J_{HH} = 7.2$Hz, 4H, $NCH_2C\mathbf{H}_2CH_2CH_3$), $\delta = 1.25$ppm (sextet, $^3J_{HH} = 7.2$Hz, 4H, $N(CH_2)_2C\mathbf{H}_2CH_3$), $\delta = 0.89$ppm (t, $^3J_{HH} = 7.2$Hz, 6H, $N(CH_2)_3C\mathbf{H}_3$). ^{13}C-NMR (100MHz, d_6-DMSO): $\delta = 136.39$ppm C(2)H, $\delta = 122.91$ppm C(4)H and C(5)H, $\delta = 49.10$ppm $N\mathbf{C}H_2(CH_2)_2CH_3$, $\delta = 31.76$ppm $NCH_2\mathbf{C}H_2CH_2CH_3$, $\delta = 19.27$ppm $N(CH_2)_2\mathbf{C}H_2CH_3$, $\delta = 13.72$ppm $N(CH_2)_3\mathbf{C}H_3$. IR (cm^{-1}): 3138 symmetric ring C-H stretch & 3095 asymmetric ring C-H stretch, 2960 & 2935 asymmetric chain C-H stretch, 2873 symmetric chain C-H stretch, 2048 (S)C-N stretch, 1563 in plane ring bend, 1463 R-CH_3 umbrella, 1380 CH_2 asymmetric wag, 1333 CH_2 twist, 1275 full chain CH_2 symmetric wag, 1260 full chain CH_2 asymmetric wag, 1226 full chain CH_2 twist, 1162 asymmetric ring C-H in plane bend, 1115 symmetric ring C-H in plane bend, 1025 asymmetric C-C stretch, 947 asymmetric chain twist, 840 symmetric C-H ring out of plane bend, 751 asymmetric C-H ring out of plane bend, 648 C-N in plane bend, 619 out of plane C-N bend.

1,3-dihexylimidazolium chloride

Chlorohexane (48.74g, 0.4mol, 2eq) and ethylacetate (40mL) were mixed and 1-hexylimidazole (33mL, 0.2mol, 1eq) was added dropwise. The solution was refluxed for 24 hours then placed in the freezer. The ethylacetate was decanted, and the residual liquid was washed with ethyl acetate (2x20mL), and dried at 35^{o}C under vacuum for 3 days. Collected viscous colourless liquid, 1,3-dihexylimidazolium chloride (50.57g, 0.16mmol, 83% yield). *m/z* (LSIMS$^+$) $[C_6C_6im]^+$ 237, 100%, (LSIMS$^-$) $^{35}Cl^-$ 35, 100%, $^{37}Cl^-$ 37, 30%. EA: (calc. C 65.22, H 10.16, N 10.87) found C 65.10, H 10.24, N 10.94. ^{1}H-NMR (400MHz, d_6-DMSO): $\delta = 9.68$ppm (s, 1H, C(2)H), $\delta = 7.94$ppm (d, $^3J_{HH} = 1.52$Hz, 2H, C(4&5)H), $\delta = 4.18$ppm (t, $^3J_{HH} = 7.12$Hz, 4H, $NC\mathbf{H}_2CH_2CH_2CH_3$), $\delta = 1.80$ppm (quintet, $^3J_{HH} = 7.16$Hz, 4H, $NCH_2C\mathbf{H}_2CH_2CH_3$), $\delta = 1.26$ppm (broad s, 12H, $N(CH_2)_2C\mathbf{H}_2CH_3$), $\delta = 0.87$ppm (t, $^3J_{HH} = 7.2$Hz, 6H, $N(CH_2)_3C\mathbf{H}_3$). ^{13}C-NMR (100MHz, d_6-DMSO): $\delta = 136.74$ppm C(2)H, $\delta = 122.64$ppm C(4)H and C(5)H, $\delta = 49.20$ppm, $N\mathbf{C}H_2(CH_2)_2CH_3$. $\delta = 30.98$ppm, $NCH_2\mathbf{C}H_2(CH_2)_3CH_3$. $\delta = 29.75$ppm, $N(CH_2)_2\mathbf{C}H_2(CH_2)_2CH_3$. $\delta = 25.59$ppm, $N(CH_2)_3\mathbf{C}H_2CH_2CH_3$. $\delta = 22.36$ppm,

$N(CH_2)_4\mathbf{C}H_2CH_3$. δ = 14.26ppm, $N(CH_2)_5\mathbf{C}H_3$. IR (cm^{-1}): 3130 symmetric ring C-H stretch & 3043 asymmetric ring C-H stretch, 2955 & 2928 asymmetric chain C-H stretch, 2858 symmetric chain C-H stretch, 1562 in plane ring bend, 1460 NCH_3 umbrella, 1379 CH_2 asymmetric wag, 1334 CH_2 twist, 1276 full chain CH_2 symmetric wag, 1275 full chain CH_2 asymmetric wag, 1226 full chain CH_2 twist, 1165 asymmetric ring C-H in plane bend, 1116 symmetric ring C-H in plane bend, 1023 asymmetric C-C stretch, 890 symmetric C-H ring out of plane bend, 729 asymmetric C-H ring out of plane bend, 680 C-N in plane bend, 668 out of plane C-N bend.

1,3-dihexylimidazolium bromide

Bromohexane (9.49g, 57.5mmol, 1eq) and ethylacetate (50mL) were mixed and 1-hexylimidazole (8.76g, 57.5mmol, 1eq) was added dropwise. The solution was refluxed for 6 hours, and cooled in the freezer. The ethylacetate was decanted, and the residual liquid was washed with ethyl acetate (2x50mL), and dried at 35^oC under vacuum for 3 days. Collected viscous colourless liquid, 1,3-dihexylimidazolium bromide (18.37g, 52.07mmol, 89% yield). *m/z* (LSIMS$^+$) $[C_6C_6im]^+$ 237, 100%, (LSIMS$^-$) CN^- 26, 100%, $^{79}Br^-$ 79, 50%, $^{81}Br^-$ 81, 50%. EA: (calc. C 56.78, H 9.21, N 8.83) found C 53.94, H 8.75, N 8.39. ^{1}H-NMR (400MHz, d_6-DMSO): δ = 9.58ppm (s, 1H, C(2)H), δ = 7.94ppm (d, $^3J_{HH}$ = 1.48Hz, 2H, C(4&5)H), δ = 4.22ppm (t, $^3J_{HH}$ = 7.12Hz, 4H, $NC\mathbf{H}_2CH_2CH_2CH_3$), δ = 1.79ppm (quintet, $^3J_{HH}$ = 7.16Hz, 4H, $NCH_2C\mathbf{H}_2CH_2CH_3$), δ = 1.22ppm (broad s, 12H, $N(CH_2)_2C\mathbf{H}_2CH_3$), δ = 0.82ppm (t, $^3J_{HH}$ = 7.2Hz, 6H, $N(CH_2)_3C\mathbf{H}_3$). ^{13}C-NMR (100MHz, d_6-DMSO): δ = 136.53ppm C(2)H, δ = 122.91ppm C(4)H and C(5)H, δ = 49.19ppm, $N\mathbf{C}H_2(CH_2)_2CH_3$. δ = 30.97ppm, $NCH_2\mathbf{C}H_2(CH_2)_3CH_3$. δ = 29.77ppm, $N(CH_2)_2\mathbf{C}H_2(CH_2)_2CH_3$. δ = 25.55ppm, $N(CH_2)_3\mathbf{C}H_2CH_2CH_3$. δ = 22.34ppm, $N(CH_2)_4\mathbf{C}H_2CH_3$. δ = 14.21ppm, $N(CH_2)_5\mathbf{C}H_3$. IR (cm^{-1}): 3129 symmetric ring C-H stretch & 3059 asymmetric ring C-H stretch, 2956 & 2928 asymmetric chain C-H stretch, 2858 symmetric chain C-H stretch, 1562 in plane ring bend, 1458 R-CH_3 umbrella, 1378 CH_2 asymmetric wag, 1334 CH_2 twist, 1260 full chain CH_2 asymmetric wag, 1226 full chain CH_2 twist, 1167 asymmetric ring C-H in plane bend, 1108 symmetric ring C-H in plane bend, 1026 asymmetric C-C stretch, 825 symmetric C-H ring out of plane bend (shoulder), 764 asymmetric C-H ring out of plane bend,

696 C-N in plane bend, 657 out of plane C-N bend.

1,3-dihexylimidazolium bis(trifluoromethylsulfonyl)imide

1,3-dihexylimiazolium chloride (1.18g, 4.3mmol, 1eq) in dichloromethane (75mL) was added to lithium bis(trifluoromethylsulfonyl)imide (1.27g, 4.4mmol, 1.02eq) and the slurry stirred vigorously for 4 hours. Water was added until two colourless phases were seen (25mL). The organic phase was collected and washed with water (2x20mL). The solvent was evaporated and the liquid residue dried under vacuum for 2 days. Collected colourless liquid 1,3-dihexylimidazolium bis(trifluoromethylsulfonyl)imide (2.21g, 4.2mmol 98% yield). *m/z* (LSIMS$^+$) $[C_6C_6im]^+$ 237, 100%, (LSIMS$^-$) $[NTf_2]^-$ 280, 100%. EA: (calc. C 39.45, H 5.65, N 8.12) found C 38.27 H 5.48, N 7.87. ^{1}H-NMR (400MHz, d_6-DMSO): $\delta = 9.21$ppm (s, 1H, C(2)H), $\delta = 7.78$ppm (s, 2H, C(4,5)H), $\delta = 4.18$ppm (t, $^3J_{HH} = 7.04$Hz 4H, $NC\mathbf{H}_2(CH_2)_5CH_3$), $\delta = 1.81$ppm (quintet, 4H, $NCH_2C\mathbf{H}_2(CH_2)_3CH_3$), $\delta = 1.25$ppm (broad s, 12H, $N(CH_2)_2(C\mathbf{H}_2)_3CH_3$), $\delta = 0.85$ppm (t, $^3J_{HH} = 7.04$Hz, 6H, $N(CH_2)_5C\mathbf{H}_3$). ^{13}C-NMR (100MHz, d_6-DMSO): $\delta = 136.35$ppm C(2)H, $\delta = 122.83$ppm C(4 and 5)H, $\delta = 119.96$ppm (quartet, $^1J_{CF} = 320$Hz, $\mathbf{C}F_3$), $\delta = 49.34$ppm, $N\mathbf{C}H_2(CH_2)_2CH_3$, $\delta = 30.93$ppm $NCH_2\mathbf{C}H_2(CH_2)_3CH_3$, $\delta = 29.69$ppm $N(CH_2)_2\mathbf{C}H_2(CH_2)_2CH_3$, $\delta = 25.55$ppm $N(CH_2)_3\mathbf{C}H_2CH_2CH_3$, $\delta = 22.23$ppm $N(CH_2)_4\mathbf{C}H_2CH_3$, $\delta = 13.97$ppm, $N(CH_2)_5\mathbf{C}H_3$. IR (cm^{-1}): 3148 symmetric ring C-H stretch & 3116 asymmetric ring C-H stretch, 2961 & 2935 asymmetric chain C-H stretch, 2864 symmetric chain C-H stretch, 1565 in plane ring bend, 1469 CH_3 & CH_2 symmetric wags, 1347 SO_2 asymmetric stretch, 1330 CH_2 twist, 1275 full chain CH_2 symmetric wag, 1260 full chain CH_2 asymmetric wag, 1226 full chain CH_2 twist, 1178 C-S stretch, 1133 CF_3 stretch, 1052 S-N stretch, 960 asymmetric chain twist, 848 symmetric C-H ring out of plane bend, 788 asymmetric C-H ring out of plane bend, 762 C-N in plane bend, 750 out of plane C-N bend.

1,3-dihexylimidazolium nitrate

1,3-dihexylimidazolium chloride (1.28g, 4.7mmol, 1eq) was dissolved in water (10mL) and silver nitrate solution (15.7mL, 0.3M, 1eq) was added dropwise. The solution was filtered and dried on a freezedrier. Collected 1,3-dihexylimidazolium nitrate as a viscous liquid (0.96g, 3.2mmol, 69% yield). *m/z* (LSIMS$^+$) $[C_6C_6im]^+$ 237,

100%, (LSIMS$^-$) CN^- 26, 100%, NO_3^- 62, 40%. EA: (calc. C 60.17, H 9.76, N 14.03) found C 60.08, H 9.75, N 13.96. NMR ^{1}H-NMR (400MHz, d_6-DMSO): δ = 9.15ppm (s, 1H, C(2)H), δ = 7.78ppm (s, 2H, C(4,5)H), δ = 4.17ppm (t, $^3J_{HH}$ = 7.20Hz, 4H, $NC\mathbf{H}_2(CH_2)_4CH_3$), δ = 1.78ppm (quintet, $^3J_{HH}$ = 7.20Hz, 4H, $NCH_2C\mathbf{H}_2(CH_2)_3CH_3$), δ = 1.26ppm (broad s, 12H, $N(CH_2)_2(C\mathbf{H}_2)_3CH_3$), δ = 0.89ppm (t, $^3J_{HH}$ = 7.20Hz, 6H, $N(CH_2)_5C\mathbf{H}_3$). ^{13}C-NMR (100MHz, d_6-DMSO): δ = 136.999ppm C(2)H, δ = 124.03ppm C(4/5)H, δ = 49.24ppm, $N\mathbf{C}H_2(CH_2)_4CH_3$, δ = 31.10ppm $NCH_2\mathbf{C}H_2(CH_2)_3CH_3$, δ = 29.75ppm $N(CH_2)_2\mathbf{C}H_2(CH_2)_2CH_3$, δ = 25.59ppm $N(CH_2)_3\mathbf{C}H_2CH_2CH_3$, δ = 22.27ppm $N(CH_2)_4\mathbf{C}H_2CH_3$, δ = 14.21ppm, $N(CH_2)_5\mathbf{C}H_3$. IR (cm^{-1}): 3135 symmetric ring C-H stretch, 3090 NO_3 overtone, 2956 & 2929 asymmetric chain C-H stretch, 2860 symmetric chain C-H stretch, 1564 in plane ring bend, 1453 NCH_2CH_3 umbrella, 1331 NO Stretch, 1163 asymmetric ring C-H in plane bend, 1120 symmetric ring C-H in plane bend, 1039 asymmetric C-C stretch, 829 symmetric C-H ring out of plane bend (shoulder), 766 asymmetric C-H ring out of plane bend, 680 C-N in plane bend, 668 out of plane C-N bend.

1,3-dihexylimidazolium thiocyanate

1,3-dihexylimidazolium chloride (7.98g, 29.25mmol, 1eq) in acetonitrile (30mL) was mixed with barium thiocyanate (4.50g, 14.63mmol, 0.5eq) in acetonitrile (30mL) and the solution was stirred for 4 hours. A white precipitate was formed. The suspension was centrifuged and the liquor decanted. The solvent was removed yielding a slightly pink liquid 1,3-dihexylimidazolium thiocyanate (9.00g, 29.25mmol, 93%). *m/z* (LSIMS$^+$) $[C_6C_6im]^+$ 237, 100%, (LSIMS$^-$) CN^- 26, 100%, S^- 32, 80%, SCN^- 58, 50%. EA: (calc. C 65.04, H 9.89, N 14.22) found C 63.74, H 9.69, N 13.94. ^{1}H-NMR (400MHz, d_6-DMSO): δ = 9.22ppm (s, 1H, C(2)H), δ = 7.81ppm (s, 2H, C(4,5)H), δ = 4.17ppm (t, $^3J_{HH}$ = 7.04Hz, 4H, $NC\mathbf{H}_2(CH_2)_5CH_3$), δ = 1.79ppm (quintet, $^3J_{HH}$ = 7.16Hz, 4H, $NCH_2C\mathbf{H}_2(CH_2)_3CH_3$), δ = 1.25ppm (broad s, 12H, $N(CH_2)_2(C\mathbf{H}_2)_3CH_3$), δ = 0.85ppm (t, $^3J_{HH}$ = 7.2Hz 6H, $N(CH_2)_5C\mathbf{H}_3$). ^{13}C-NMR (100MHz, d_6-DMSO): δ = 136.40ppm C(2)H, δ = 130.03ppm SCN, δ = 122.93ppm C(4 and 5)H, δ = 49.34ppm, $N\mathbf{C}H_2(CH_2)_2CH_3$, δ = 30.95ppm $NCH_2\mathbf{C}H_2(CH_2)_3CH_3$, δ = 29.69ppm $N(CH_2)_2\mathbf{C}H_2(CH_2)_2CH_3$, δ = 25.58ppm $N(CH_2)_3\mathbf{C}H_2CH_2CH_3$,

δ = 22.34ppm $N(CH_2)_4\mathbf{C}H_2CH_3$, δ = 14.25ppm, $N(CH_2)_5\mathbf{C}H_3$. IR (cm^{-1}): 3135 symmetric ring C-H stretch & 3086 asymmetric ring C-H stretch, 2956 & 2929 asymmetric chain C-H stretch, 2858 symmetric chain C-H stretch, 2047 (S)C-N stretch, 1562 in plane ring bend, 1460 R-CH_3 umbrella, 1379 CH_2 asymmetric wag, 1338 CH_2 twist, 1275 full chain CH_2 symmetric wag, 1260 full chain CH_2 asymmetric wag, 1226 full chain CH_2 twist, 1164 asymmetric ring C-H in plane bend, 1120 symmetric ring C-H in plane bend, 1030 asymmetric C-C stretch, 949 asymmetric chain twist, 841 symmetric C-H ring out of plane bend, 750 asymmetric C-H ring out of plane bend, 680 C-N in plane bend, 668 out of plane C-N bend.

2.2.2 Pyrrolidinium based ILs

N-methylpyrrolidinium hydrogensulfate

Sulfuric acid (5M, 7.9mL, 10.19g, 0.0393mol) was added dropwise with vigorous stirring to N-methylpyrrolidine (4.09mL, 3.35g, 0.0393 mol), with cooling. Water was removed from the resultant solution at 40^{o}C under vacuum, during which the solution went from colourless to slightly orange. Collected the viscous liquid N-methyl-pyrrolidinium hydrogensulfate (7.65g, 0.0388mol, 94% Yield). *m/z* ($LSIMS^+$):
$[C_1Hpyrr]^+$ 86, 100%, ($LSIMS^-$): $[HSO_4]^-$ 97, 100%. EA: (calc. C 32.78, H 7.15, N 7.64) found C 32.60, H 6.98, N 7.74. ^{1}H-NMR (400 MHz, DMSO-d6) δ = 7.83ppm (s, 1H, HSO_4), δ = 9.46ppm (s, 1H, NH), δ = 3.47ppm (s, 2H, CαH_{ax}), δ = 2.94ppm (s, 2H, CαH_{eq}), δ = 2.78ppm (t, 3H, CH_3), δ = 2.00ppm (s, 2H, CβH_{ax}), δ = 1.83ppm (s, 2H, CβH_{eq}). ^{13}C-NMR (100 MHz, DMSO-d6): δ = 55.28ppm Cα, δ = 40.53ppm CH_3, δ = 23.16ppm Cβ. IR (cm^{-1}): 2945, asymmetric CH stretches, 2905 symmetric CH stretches, 1462 CH_3 umbrella, 1401 symmetric CH bend, 1358 CH_2 symmetric wag, 1333 asymmetric wag, 1232 ring twist, 1229 asymmetric S=O stretch, 1180 asymmetric S=O stretch, 1042 C-C stretch, 1008 symmetric S=O stretch, 962 ring C-C stretch, 888 ring bend.

N-ethylpyrrolidinium hydrogensulfate

Sulfuric acid (5M, 8.2mL, 10.58g, 0.0411mol) was added dropwise with vigorous stir-

ring to N-ethylpyrrolidine (5.00mL, 4.08g, 0.0411 mol), with cooling. Water was removed from the resultant solution at 40^{o}C under vacuum, during which the solution went from colourless to slightly dark red. The viscous liquid N-ethyl-pyrrolidinium hydrogensulfate (7.65g, 0.0388mol, 94% Yield). *m/z* (LSIMS$^+$): $[C_2Hpyrr]^+$ 100, 100%, (LSIMS$^-$): $[HSO_4]^-$ 97, 100%. EA: (calc. C 36.53, H 7.66, N 7.10) found C 36.75, H 7.48, N 7.29. ^{1}H-NMR (400 MHz, DMSO-d6) δ = 10.02ppm (s, 1H, HSO_4), δ = 9.46ppm (s, 1H, NH), δ = 3.48ppm (s, 2H, CαH_{ax}), δ = 3.14ppm (t, $^3J_{HH}$ = 8Hz, 2H, CH_2, δ = 2.99ppm (s, 2H, CβH_{eq}), δ = 1.98ppm (s, 2H, CβH_{ax}), δ = 1.83ppm (s, 2H, CβH_{eq}), δ = 1.19ppm (t, $^3J_{HH}$ = 8Hz, 3H, CH_3). ^{13}C-NMR (100 MHz, DMSO-d6): δ = 53.1ppm Cα, δ = 49.5ppm $\mathbf{C}H_2CH_3$, δ = 23.0ppm Cβ, δ = 11.2ppm CH_3. IR (cm^{-1}): 2942, asymmetric CH stretches, 2899 symmetric CH stretches, 1462 CH_3 umbrella, 1401 symmetric CH bend, 1358 CH_2 symmetric wag, 1333 CH_2 asymmetric wag, 1232 ring twist, 1225 asymmetric S=O stretch, 1170 asymmetric S=O stretch, 1042 C-C stretch, 1002 symmetric S=O stretch, 965 ring C-C stretch, 882 ring bend.

N-propylpyrrolidinium hydrogensulfate

N-(propan-1-one)pyrrolidine

To propionyl chloride (10.517g, 0.115mol, 1.1eq) in chloroform (50mL) at 0^{o}C, pyrrolidine (7.35g, 0.103mol, 1.0eq) in chloroform (50mL) was added drop wise. After complete addition the solution was stirred overnight. The solution was washed with concentrated sodium hydroxide solution (20mL) then washed by 10% sodium hydroxide solution (100mL). The organic layer was evaporated to dryness. Collected colourless liquid, N-(propan-1-one)pyrrolidine (12.67g, 0.1mmol, 96% yield). *m/z* (ESI$^+$): $[C_2H_5C(O)pyrr]^+$ 127, 100%. EA: (calc. C 66.10, H 10.30, N 11.01) found C 66.11, H 10.34, N 10.96. ^{1}H-NMR ($CDCl_3$): δ = 3.37ppm (t, $^3J_{HH}$ = 6.88Hz, 2H, CαH_{ax}), δ = 3.26ppm (t, $^3J_{HH}$ = 6.88Hz, 2H, CαH_{eq}), δ = 2.03ppm (quartet, $^3J_{HH}$ = 7.44Hz, 2H, $CH_3C\mathbf{H}_2C$(O)R. δ = 1.86ppm (quintet, $^3J_{HH}$ = 6.52Hz, 2H, CβH_{ax}), δ = 1.75ppm (quintet, $^3J_{HH}$ = 6.52Hz, 2H, CβH_{eq}), δ = 0.97ppm (t, $^3J_{HH}$ = 7.52Hz, 2H, $C\mathbf{H}_3CH_2$C(O)R). ^{13}C-NMR ($CDCl_3$): δ = 171.47ppm, C=O, δ = 46.17ppm & δ = 45.66ppm, Cα, δ = 27.35ppm, $\mathbf{C}H_2$C=O, δ = 26.07ppm & δ = 24.41ppm Cβ, δ = 9.34ppm $CH_2\mathbf{C}H_3$. IR (cm^{-1}): 2975, asymmetric CH

stretches, 2877 symmetric CH stretches, 1605 CO stretch, 1443 CH_3 umbrella, 1378 symmetric CH bend, 1343 CH_2 symmetric wag, 1318 asymmetric wag, 1254 & 1229 ring twist, 1037 C-C stretch, 914 ring C-C stretch, 810 ring bend.

N-propyl pyrrolidine

Lithium aluminium hydride (2.85g, 75mmol, 0.8eq) was slurried in dry diethylether (50mL). To this N-(propan-1-one)pyrrolidine (11.93g, 93.8mmol, 1eq) in diethylether (50mL) was added dropwise allowing the mixture to reflux under its own heat. After addition was complete the reaction was refluxed for 8 hours. The remaining lithium aluminium hydride was quenched by adding water (2.9mL), 10% sodium hydroxide solution (5.7mL) and water (8.5mL). The mixture was filtered, washing the residue with ether (2x25mL), and the solvent removed under vacuum. The crude product was then distilled under vacuum to collect the colourless liquid N-propylpyrrolidine (b.p 44^{o}C at 38mBar, 5.74g, 50mmol, 54% Yield). *m/z* (ESI$^+$): $[C_3H_7pyrr]^+$ 113, 100%. EA: (calc. C 74.27, H 13.36, N 12.37) found C 72.04, H 12.96, N 12.00. ^{1}H-NMR ($CDCl_3$): δ = 2.47ppm (s, 4H, CαH_2), δ = 2.37ppm (t, $^3J_{HH}$ = 7.44Hz, 2H, NC$\mathbf{H}_2CH_2CH_3$). δ = 1.76ppm (s, 4H, CβH_2), δ = 1.53ppm (sextet, $^3J_{HH}$ = 7.88Hz, 2H, $CH_2C\mathbf{H}_2CH_3$), δ = 0.90ppm (t, $^3J_{HH}$ = 7.4Hz, 3H, R-CH_3). ^{13}C-NMR (100 MHz, DMSO-d6): δ = 58.67ppm, N-$\mathbf{C}H_2CH_2CH_3$, 54.21ppm, Cα, δ = 23.35ppm, Cβ, δ = 22.28ppm $NCH_2\mathbf{C}H_2CH_3$, δ = 12.12ppm $CH_2CH_2\mathbf{C}H_3$. IR (cm^{-1}): 2966, asymmetric CH stretches, 2880 symmetric CH stretches, 1450 CH_3 umbrella, 1417 symmetric CH bend, 1352 CH_2 symmetric wag, 1334 asymmetric wag, 1243 & 1221 ring twist, 1041 C-C stretch, 965 ring C-C stretch, 875 ring bend.

N-propylpyrrolidinium hydrogensulfate

N-propylpyrrolidine (5.26g, 46.5mmol, 1eq) was added dropwise to a solution of 96% sulfuric acid (4.75g, 46.5mmol, 1eq) and water (5mL). The solution was dried under vacuum at 30^{o}C for 3 days. Collected colourless liquid N-propylpyrrolidinium hydrogensulfate (9.82g, 46.5mmol, 100% yield). *m/z* (ESI$^+$): $[C_3Hpyrr]^+$ 112, 100%. (ESI$^-$): $[HSO_4]^-$ 97, 100%. EA: (calc. C 39.79, H 8.11, N 6.63), C 39.75, H 8.10, N 6.72. ^{1}H-NMR (400 MHz, DMSO-d6) δ = 10.02ppm (s, 1H, HSO_4), δ = 9.38ppm (s, 1H, NH), δ = 3.46ppm (s, 2H, CαH_{ax}), δ = 3.02ppm (m, 4H, CαH_{eq} & NC$\mathbf{H}_2CH_2CH_3$, δ = 1.95ppm (s, 2H, CβH_{ax}), δ = 1.82ppm (s, 2H, CβH_{eq}),

$\delta = 1.58$ppm (broad s, 2H, RC$\mathbf{H}_2$CH$_3$), $\delta = 0.83$ppm (t, $^3J_{HH} = 7.32$Hz, 3H, RCH$_3$). ^{13}C-NMR (100 MHz, DMSO-d6): $\delta = 55.85$ppm N$\mathbf{C}$H$_2$CH$_2$CH$_3$, $\delta = 53.54$ppm Cα, $\delta = 22.91$ppm Cβ, $\delta = 19.2$ppm R$\mathbf{C}$H$_2$CH$_3$, $\delta = 11.18$ppm RCH$_3$. IR (cm^{-1}): 2954, asymmetric CH stretches, 2902 symmetric CH stretches, 1463 CH$_3$ umbrella, 1410 symmetric CH bend, 1356 CH$_2$ symmetric wag, 1337 asymmetric wag, 1234 ring twist, 1215 asymmetric S=O stretch, 1162 asymmetric S=O stretch, 1045 C-C stretch, 1013 symmetric S=O stretch, 968 ring C-C stretch, 880 ring bend.

N-butylpyrrolidinium hydrogensulfate

Sulfuric acid (5M, 7.9mL, 10.19g, 0.0393mol) was added dropwise with vigorous stirring to N-butylpyrrolidine (5.8mL, 5.00g, 0.0393mol), with cooling. Water was removed from the resultant solution at 40^{o}C under vacuum, during which the solution went from colourless to red. The viscous liquid N-butyl-pyrrolidinium hydrogensulfate (8.5g, 0.0377mol, 96% Yield). m/z (ESI$^+$): [C$_4$Hpyrr]$^+$ 128, 100%. (ESI$^-$): [HSO$_4$]$^-$ 97, 100%. EA: (calc. C 42.65, H 8.50, N 6.22), C 41.99, H 8.31, N 6.22. ^{1}H-NMR (400 MHz, DMSO-d6): $\delta = 9.46$ppm (s, 1H, NH), $\delta = 3.52$ppm (s, 2H, CαH$_{ax}$), $\delta = 3.08$ppm (t, $^3J_{HH} = 8$Hz, 2H, NCH$_2{}^n$Pr), $\delta = 2.99$ppm (s, 2H, CβH$_{eq}$), $\delta = 1.98$ppm (s, 2H, CβH$_{ax}$), $\delta = 1.86$ppm (s, 2H, CβH$_{eq}$), $\delta = 1.59$ppm (quintet, 2H, NCH$_2$C$\mathbf{H}_2$Et), $\delta = 1.29$ppm (sextet, $^3J_{HH} = 8$Hz, 2H, NCH$_2$CH$_2$C$\mathbf{H}_2$CH$_3$), $\delta = 0.88$ppm (t, $^3J_{HH} = 8$Hz, 3H, CH$_3$). ^{13}C-NMR (100 MHz, DMSO-d6): $\delta = 53.1$ppm C(α), $\delta = 49.5$ppm N$\mathbf{C}$H$_2$(CH$_2$)$_2$CH$_3$, $\delta = 23.0$ppm C(β), $\delta = 18.8$ppm, NCH$_2$$\mathbf{C}H_2CH_2CH_3$, $\delta = 14.4$ppm N(CH$_2$)$_2$$\mathbf{C}H_2CH_3$, $\delta = 11.2$ppm RCH$_3$. IR (cm^{-1}): 2948, asymmetric CH stretches, 2895 symmetric CH stretches, 1460 CH$_3$ umbrella, 1399 symmetric CH bend, 1356 CH$_2$ symmetric wag, 1337 asymmetric wag, 1234 ring twist, 1221 asymmetric S=O stretch, 1169 asymmetric S=O stretch, 1042 C-C stretch, 1012 symmetric S=O stretch, 965 ring C-C stretch, 882 ring bend.

N-hexylpyrrolidinium hydrogensulfate

N-(hexan-1-one) pyrrolidine

To caprioyl chloride (8.8499g, 65.7mmol, 1.1eq) in chloroform (50mL) at 0^{o}C, pyrrolidine (5.0mL, 60mmol, 1.0eq) in chloroform (50mL) was added dropwise. After

complete addition the solution was stirred overnight. The solution was washed with concentrated sodium hydroxide solution (20mL) then washed by 10% sodium hydroxide solution (100mL). The organic layer was evaporated to dryness. Collected colourless liquid, N-(hexan-1-one)pyrrolidine (8.95g, 56.2mmol, 94% yield). *m/z* (ESI^+): N-(propan-1-one-2,3-ene)pyrrolidine$^+$ 125, 100%, N-(butan-1-one-2,3-ene)pyrrolidine$^+$ 139, 60%, $[C_5H_{11}C(O)pyrr]^+$ 169, 100%. EA: (calc. C 70.96, H 11.31, N 8.28), C 70.89, H 11.30, N 8.26. ^{1}H-NMR (400MHz, $CDCl_3$): $\delta = 3.47$ppm (t, $^3J_{HH} = 6.88$Hz, 2H, CαH_{ax}), $\delta = 3.42$ppm (t, $^3J_{HH} = 6.88$Hz, 2H, CαH_{eq}), $\delta = 2.26$ppm (t $^3J_{HH} = 7.52$Hz, 2H, RC(O)C$\mathbf{H}_2(CH_2)_3CH_3$). $\delta = 1.96$ppm (s, 2H, CβH_{ax}), $\delta = 1.86$ppm (s, 2H, CβH_{eq}), $\delta = 1.65$ppm (quintet, $^3J_{HH} = 7.6$Hz, 2H, $RC(O)CH_2C\mathbf{H}_2(CH_2)_2CH_3$), $\delta = 1.33$ppm (broad s, 4H, $RC(O)(CH_2)_2(C\mathbf{H}_2)_2CH_3$), $\delta = 0.91$ppm (t, $^3J_{HH}$=6.92Hz, 3H, RCH_3). ^{13}C-NMR (100MHz, $CDCl_3$): $\delta = 171.90$ppm, C=O, $\delta = 46.62$ppm & $\delta = 45.57$ppm, Cα, $\delta = 27.35$ppm, $\mathbf{C}H_2C{=}O$, $\delta = 26.07$ppm & $\delta = 24.41$ppm Cβ, $\delta = 9.34$ppm CH_2CH_3. IR (cm^{-1}): 2973, asymmetric CH stretches, 2876 symmetric CH stretches, 1605 CO stretch, 1443 CH_3 umbrella, 1378 symmetric CH bend, 1343 CH_2 symmetric wag, 1318 asymmetric wag, 1251 & 1231 ring twist, 1039 C-C stretch, 912 ring C-C stretch, 851 ring bend.

N-hexyl pyrrolidine

Lithium aluminium hydride (1.01g, 26.6mmol, 2eq) was slurried in dry THF (50mL). To this N-(hexan-1-one)pyrrolidine (4.23g, 26.6mmol, 1eq) in THF (50mL) was added dropwise allowing the mixture to reflux under its own heat. After addition was complete the reaction was refluxed for 8 hours. The remaining lithium aluminium hydride was quenched by adding water (1mL), 10% sodium hydroxide solution (2mL) and water (3mL). The mixture was filtered, washing the residue with THF (2x25mL), and the solvent removed under vacuum. The crude product was then distilled under vacuum to collect the colourless liquid N-hexylpyrrolidine (b.p 36^{o}C at 2.1mBar, 1.33g, 8.6mmol, 32% Yield). *m/z* (ESI^+): $[C_6Hpyrr]^+$ 155, %100. EA: (calc. C 77.35, H 13.63, N 9.02), C 77.28, H 13.60, N 8.97. ^{1}H-NMR (400MHz, $CDCl_3$): $\delta = 2.48$ppm (broad s, 4H, CαH_2), $\delta = 2.41$ppm (t, $^3J_{HH} = 7.76$Hz, 2H, $NC\mathbf{H}_2(CH_2)_4CH_3$), $\delta = 1.77$ppm (broad s, 4H, CβH_2), $\delta = 1.51$ppm (quintet, $^3J_{HH} = 7.56$Hz, 2H, $NCH_2C\mathbf{H}_2(CH_2)_3CH_3$), $\delta = 1.29$ppm

(broad s, 6H, $N(CH_2)_2(C\mathbf{H}_2)_3CH_3$), δ = 0.88ppm (t, $^3J_{HH}$ = 6.92Hz, 3H, $N(CH_2)_5CH_3$). ^{13}C-NMR (100Mhz, $CDCl_3$): δ = 48.67ppm N-$\mathbf{C}H_2(CH_2)_4CH_3$, 46.30ppm C(1), 45.62ppm C(4), δ = 34.17ppm $NCH_2\mathbf{C}H_2(CH_2)_3CH_3$, δ = 31.55ppm $N(CH_2)_2\mathbf{C}H_2(CH_2)_2CH_3$, δ = 26.12ppm $N(CH_2)_3\mathbf{C}H_2CH_2CH_3$, δ = 24.51ppm, C(2), δ = 24.42ppm, C(3), δ = 22.49ppm $N(CH_2)_4\mathbf{C}H_2CH_3$, δ = 14.33ppm $N(CH_2)_5\mathbf{C}H_3$. IR (cm^{-1}): 2962, asymmetric CH stretches, 2882 symmetric CH stretches, 1453 CH_3 umbrella, 1412 symmetric CH bend, 1351 CH_2 symmetric wag, 1334 asymmetric wag, 1244 & 1220 ring twist, 1042 C-C stretch, 965 ring C-C stretch, 875 ring bend.

N-hexylpyrrolidinium hydrogensulfate

N-hexylpyrrolidine (1.23g, 7.95mmol, 1eq) was added to a solution of 96% sulfuric acid (0.812g, 7.95mmol, 1eq) and water (5mL) and stirred for 2 hours. The solution was dried under reduced pressure at 30^o for 3 days, collected N-hexylpyrrolidinium hydrogensulfate (2.04g, 7.95mmol, 100% yield). *m/z* (ESI^+): $[C_6Hpyrr]^+$ 156, %100. (ESI^-): $[HSO_4]^-$ 97, 100%. EA: (calc. C 47.41, H 9.15, N 5.53) found C 47.29, H 8.99, N 5.71. ^{1}H-NMR (400 MHz, d_6-DMSO): δ = 9.84ppm (s, 1H, HSO_4), δ = 9.43ppm (s, 1H, R_3NH), δ = 3.52ppm (broad s, 2H, CαH_{ax}), δ = 3.11ppm (t, $^3J_{HH}$ = 5.76Hz, 2H, $NCH_2(CH_2)_4CH_3$, δ = 2.99ppm (broad s, 2H, CαH_{eq}), δ = 1.99ppm (broad s, 2H, CβH_{ax}), δ = 1.85ppm (broad s, 2H, CβH_{eq}), δ = 1.61ppm (quintet, $^3J_{HH}$ = 6.44Hz, 2H, $NCH_2C\mathbf{H}_2C_4H_9$), δ = 1.28ppm (s, 6H, $N(CH_2)_2(C\mathbf{H}_2)_3CH_3$), δ = 0.87ppm (t, $^3J_{HH}$ = 6.44Hz, 2H, $N(CH_2)_5CH_3$). ^{13}C-NMR (100 MHz, d_6-DMSO): δ = 54.43ppm, $N\mathbf{C}H_2(CH_2)_4CH_3$, δ = 53.64ppm, Cα, δ = 31.15ppm, $NCH_2\mathbf{C}H_2(CH_2)_3CH_3$, δ = 26.08ppm, $N(CH_2)_2\mathbf{C}H_2(CH_2)_2CH_3$, δ = 25.61ppm, $N(CH_2)_3\mathbf{C}H_2CH_2CH_3$, δ = 22.99ppm, Cβ, δ = 22.34ppm, $N(CH_2)_4\mathbf{C}H_2CH_3$, δ = 14.32ppm, $N(CH_2)_5\mathbf{C}H_3$. IR (cm^{-1}): 2962, asymmetric CH stretches, 2882 symmetric CH stretches, 1453 CH_3 umbrella, 1412 symmetric CH bend, 1351 CH_2 symmetric wag, 1334 asymmetric wag, 1244 ring twist, 1221 asymmetric S=O stretch, 1169 asymmetric S=O stretch, 1042 C-C stretch, 1007 symmetric S=O stretch, 965 ring C-C stretch, 875 ring bend.

N-methylpyrrolidinium chloride

Hydrochloric acid (37% w/w, 2.738g, 0.0294mol, 1eq) was diluted with water (30mL)

and added dropwise to a solution of *N*-methylpyrrolidine (2.50g, 0.0294mol, 1eq) and water (10mL) with cooling (0^oC). The solvent was removed under vacuum, leaving an off white solid residue, N-methylpyrrolidinium chloride (3.538g, 0.0291mol, 99% Yield, mp 147-150^oC). *m/z* (LSIMS$^+$): $[C_1Hpyrr]^+$ 86, %100. (LSIMS$^-$): $^{35}Cl^-$ 35, 100%, $^{37}Cl^-$ 37, 75%. EA: (calc. C 49.38, H 9.95, N 11.52) found C 49.29, H 9.80, N 11.45. ^{1}H-NMR (400 MHz, d_6-DMSO): δ = 11.19ppm (s, 1H, NH), δ = 3.48ppm (s, 2H, CαH_{ax}), δ = 3.19ppm (s, 2H, CαH_{eq}), δ = 2.75ppm (s, 3H, CH_3), δ = 1.93ppm (s, 4H, CβH_2). ^{13}C-NMR (100 MHz, d_6-DMSO): δ = 54.71ppm Cα, δ = 40.16ppm, CH_3, δ = 23.42ppm, Cβ. IR (cm^{-1}): 2955, asymmetric CH stretches, 2875 symmetric CH stretches, 1454 CH_3 umbrella, 1420 symmetric CH bend, 1366 CH_2 symmetric wag, 1331 asymmetric wag, 1244 ring twist, 1052 C-C stretch, 978 ring C-C stretch, 871 ring bend.

N-methylpyrrolidinium trifluoromethanesulfonate

N-methylpyrrolidine (2.50g, 29.4mmol, 1eq) was dissolved in water (10mL). The stirred solution was cooled in an ice bath and trifluoromethanesulfonic acid (4.413g, 29.4mmol, 1eq) was added dropwise. The IL was dried *in vacuo* at 50^{o}C. Collected slightly orange solid, *N*-methylpyrrolidinium trifluoromethanesulfonate (6.84g, 29.1mmol, 99% yield, mp 79-80^{o}C) *m/z* (LSIMS$^+$): $[C_1Hpyrr]^+$ 86, %100. (LSIMS$^-$): $[OTf]^-$ 149, 100%, EA: (calc. C 30.64, H 5.15, N 5.95) found C 30.58, H 5.11, N 5.84. ^{1}H-NMR (400 MHz, d_6-DMSO): δ = 9.44ppm (s, 1H, NH), δ = 3.49ppm (s, 2H, CαH_{ax}), δ = 2.95ppm (s, 2H, CαH_{eq}), δ = 2.81ppm (s, 3H, CH_3), δ = 2.01ppm (s, 2H, CβH_{ax}), δ = 1.85ppm (s, 2H, CβH_{eq}). ^{13}C-NMR (100 MHz, d_6-DMSO): δ = 120.38ppm (quartet, $^3J_{CF}$ = 320.1Hz, CF_3), δ = 54.71ppm Cα, δ = 40.16ppm, CH_3, δ = 23.42ppm, Cβ. IR (cm^{-1}): 2955, asymmetric CH stretches, 2875 symmetric CH stretches, 1454 CH_3 umbrella, 1420 symmetric CH bend, 1366 CH_2 symmetric wag, 1331 asymmetric wag, 1269 asymmetric S-O stretch, 1244 ring twist, 1225 C-S stretch, 1182 symmetric S-O stretch, 1034 symmetric C-F stretch, 978 ring C-C stretch, 871 ring bend.

N-methylpyrrolidinium bis(trifluoromethylsulfonyl)imide

An solution of bis(trifluoromethylsulfonyl)imidic acid (6.53g, 0.0232 mol, 1eq) in water(30mL) was added to a solution of N-methylpyrrolidine (1.99 g, 0.0232 mol, 1eq)

in water (10mL) dropwise under ice-bath cooling and stirring to precipitate white crystals from the colourless solution. Concentrated *in vacuo* which yielded white solid, N-methylpyrrolidinium bis(trifluoromethylsulfonyl)imide (7.2208g, 0.0215 mol, 93% Yield, mp 72-74^{o}C). *m/z* (LSIMS$^+$): $[C_1Hpyrr]^+$ 86, %100. (LSIMS$^-$): $[NTf_2]^-$ 280, 100%. EA: (calc. C 22.95, H 3.30, N 7.65) found C 22.87, H 3.16, N 7.59. ^{1}H-NMR (400 MHz, d_6-DMSO): $\delta = 9.44$ppm (s, 1H, NH), $\delta = 3.34$ppm (s, 2H, CαH_{ax}), $\delta = 3.07$ppm (s, 2H, CαH_{eq}), $\delta = 2.81$ppm (s, 3H, CH_3), $\delta = 1.94$ppm (s, 4H, CβH_2). ^{13}C-NMR (100 MHz, d_6-DMSO): $\delta = 120.38$ppm quartet, $^3J_{CF} = 320.1$Hz, CF_3, $\delta = 54.71$ppm Cα, $\delta = 40.16$ppm, CH_3, $\delta = 23.42$ppm, Cβ. IR (cm^{-1}): 2969 asymmetric C-H stretch, 2881 symmetric C-H stretch, 1467 CH_3 umbrella, 1433 CH_2 bend, 1348 asymmetric S-O stretch, 1183, S-O symmetric stretch, 1034 symmetric C-F stretch, 977 ring C-C stretch, 870 ring bend.

N-butyl-N-methylpyrrolidinium chloride

Several batches of $[C_4C_1pyrr]Cl$ were prepared. Crystallisation was slow and low yielding in every case, with an average first crop yield of 27%, however the mother liquors of all reactions were collected and combined, which slowly yielded a large additional batch of crystals (739.5g, 4.2mol). The total yield of $[C_4C_1pyrr]Cl$ crops was 67%.

Example procedure: Cold (from fridge) chlorobutane (300mL, 2.85mol, 1.2eq) was added dropwise to a solution of N-methylpyrrolidine (220g, 250mL, 2.4mol, 1eq) and ethyl acetate (300mL). The mixture was allowed to come to room temperature and was then heated to 55^{o}C for 2 weeks under nitrogen. The mixture was allowed to cool and the solvent was decanted. The solid was dried *in vacuo* for 1 hour. The crystals were washed with 200mL of ethyl acetate and dried *in vacuo* overnight. Collected white crystals of $[C_4C_1pyrr]Cl$ (186.2g, 1.05mol, 40% Yield). A second crop of crystals was collected from the reaction liquor. The liquor was reduced in volume on the rotary evaporator and stored in the freezer, collected white needle crystals of $[C_4C_1pyrr]Cl$ (144.3g, 0.81mol, 31% Yield). m/z (ESI$^+$) $[C_4C_1pyrr]^+$ 142, (ESI$^-$) $^{35}Cl^-$ 35, 100%, $^{37}Cl^-$ 37, 33%. EA: (Calculated C 60.83, H 11.34, N 7.88) found C 60.65, H 11.21, N 7.77. ^{1}H-NMR (400 MHz, d_6-DMSO): $\delta = 3.50$ppm (broad s, 4H, CαH_2), $\delta = 3.35$ppm (t, $^3J_{HH} =$

7.4Hz, 2H, NC**H**$_2$CH$_2$CH$_2$CH$_3$), δ = 3.01ppm (s, 3H, NCH$_3$), δ = 2.08ppm (broad s, 4H, CβH$_2$), δ = 1.68ppm (quintet, $^3J_{HH}$ = 7.4Hz, 2H, NCH$_2$C**H**$_2$CH$_2$CH$_3$), δ = 1.33 ppm (sextet, $^3J_{HH}$ = 7.4Hz, 2H, N(CH$_2$)$_2$C**H**$_2$CH$_3$), δ = 0.93ppm (t, $^3J_{HH}$ = 7.4Hz, 3H, N(CH$_2$)$_3$C**H**$_3$). ^{13}C-NMR (100 MHz, d$_6$-DMSO): δ = 62.83ppm CαH$_2$, δ = 62.11ppm CβH$_2$, δ = 46.97ppm NCH$_3$, δ = 24.85ppm N**C**H$_2$(CH$_2$)$_2$CH$_3$, δ = 20.82 ppm NCH$_2$**C**H$_2$CH$_2$CH$_3$, δ = 19.19ppm N(CH$_2$)$_2$**C**H$_2$CH$_3$, δ = 13.39ppm N(CH$_2$)$_3$CH$_3$. IR (cm^{-1}): 2966 asymmetric C-H stretch, 2880 symmetric C-H stretch, 1461 CH$_3$ umbrella, 1452 CH$_2$ bend, 1153 asymmetric CH$_2$ wag, 1041 symmetric CH$_2$ wag, 875 ring C-C stretch.

N-butyl-N-methylpyrrolidinium bis(trifluoromethylsufonyl)imide

Three batches of N-butyl-N-methylpyrrolidinium bis(trifluoromethylsufonyl)imide, ([C$_4$C$_1$pyrr][NTf$_2$]) were prepared. Yields for this metathesis are high; the average of the three batches was 94%.

[C$_4$C$_1$pyrr]Cl (39.4g, 0.22mol, 1.05eq) was dissolved in dry DCM (500mL), this solution was added to lithium bis(trifluoromethylsufonyl)imide (54.9g, 0.21mol, 1eq) and stirred at room temperature for 2 days. The solution was decanted from the solid white precipitate, which was then washed with dry DCM and the washings combined with the solution. The solution was washed with water portions (2x250mL) until both aqueous and organic phases showed a negative silver nitrate result. The DCM was then removed, and the residual IL dried *in vacuo* overnight at 50^{o}C. Collected colourless viscous liquid [C$_4$C$_1$pyrr][NTf$_2$] (76.6g, 0.18mol, 90% Yield). m/z (ESI$^+$) [C$_4$C$_1$pyrr-H]$^+$ 141, 100%, (ESI$^-$) [NTf$_2$]$^-$ 280, 100%. EA: (Calculated C 31.28, H 4.77, N 6.63) C 31.41, H 4.63, N 6.61. ^{1}H-NMR (400MHz DMSO): δ = 3.66ppm (broad s, 4H, C(α)**H**$_2$), δ = 3.47ppm (t, $^3J_{HH}$= 8.2Hz, 2H, NC**H**$_2$(CH$_2$)$_2$CH$_3$), δ = 2.98ppm (s, 3H, NC**H**$_3$), δ = 2.33ppm (s, 4H, C(β)**H**$_2$), δ = 1.89ppm (quintet, $^3J_{HH}$= 8.1Hz, 2H, NCH$_2$C**H**$_2$CH$_2$CH$_3$), δ = 1.32ppm (sextet, 2H, $^3J_{HH}$= 7.3Hz, NCH$_2$CH$_2$C**H**$_2$CH$_3$), δ = 0.94ppm (t, 3H, $^3J_{HH}$= 7.3Hz, N(CH2)3C**H**$_3$). ^{13}C-NMR (DMSO): δ = 119.96ppm q, $^1J_{CF}$= 319Hz, CF$_3$. δ = 63.87ppm C(α)H$_2$, δ = 63.39ppm C(β)H$_2$, δ = 47.91ppm NCH$_3$, δ = 25.38ppm N**C**H$_2$(CH$_2$)$_2$CH$_3$, δ = 21.50ppm NCH$_2$**C**H$_2$CH$_2$CH$_3$, δ = 19.74ppm N(CH$_2$)$_2$**C**H$_2$CH$_3$, δ = 13.85ppm N(CH$_2$)$_3$CH$_3$. IR (cm^{-1}): 2969 asymmetric C-H stretch, 2881 symmetric C-H

stretch, 1467 CH_3 umbrella, 1433 CH_2 bend, 1348 asymmetric S-O stretch, 1183, S-O symmetric stretch, 1034 symmetric C-F stretch, 977 ring C-C stretch, 870 ring bend.

2.2.3 Discussion

In general the synthesis of ILs here has produced ILs of excellent quality, particularly the well established procedures. The acid base neutralisation reactions to make some the pyrrolidinium ILs are exothermic and fast, but produce almost quantitative yields very rapidly. Metathesis reactions are generally high yielding, so they typically given near quantitative yields too.

The yields of the nitrates are lower than expected, as metathesis reactions are expected to produce near quantitative yields and silver nitrate is no exception. The low yields come from mechanical loses; the nitrate ILs were found to be extremely surface active and foam badly under drying, additionally they appeared to have a high affinity for glass, so any transfer between vessels leads to losses.

The direct alkylation reaction to produce 1-butyl-3-methylimidazolium nitrate worked well and gave an exceptionally high product purity.

Chapter 3

Site Exchange In Pyrrolidinium Ionic Liquids

3.1 Aims

It was discovered that the ring proton signals in the ^{1}H-NMR Spectrum of $[C_1Hpyrr][HSO_4]$ were fully resolved at room temperature. The protons on each carbon are in a unique chemical environment, which provides a unique opportunity to examine the ring behaviour in more detail. There is an assumption that pyrrolidinium based ILs have lower melting points than similar imidazolium ILs because of the vibrational and rotational freedom of the pyrrolidinium ring.

The resolution of the axial and equatorial ring protons' signals, when an average signal would be expected, allows the activation energy of the ring flip of the pyrrolidinium ring to be calculated using information collected from variable temperature NMR spectroscopy.

In order to investigate this fully a range of protonated pyrrolidinium based ILs were synthesised and variable temperature NMR spectra were collected, before being examined for some correlation between the activation energy of the ring flip of the pyrrolidinium and some property or properties of the IL.

3.2 Introduction

3.2.1 Dynamic Effects in NMR Spectroscopy

Initial theoretical estimates for spin-lattice relaxation times of nuclear spins at room temperature in an external magnetic field were long, ranging from 100s of seconds to years.[62] With the development of experimental methods to probe nuclear spins it was quickly realised that even slowly relaxing samples were relaxing much faster than this. For example early measurements on solid paraffin wax[63] showed a relaxation time for protons of less than one minute. Further investigations discovered that nuclear relaxation was occurring in the range of 10^{-4} to 100 seconds. Protons in particular have relaxation times shorter than 1 second. Early studies on ammonia and water[64] looked at the temperature dependence of relaxation signals and the rate of chemical exchange of protons. It was found that if the rate of chemical exchange is faster than the relaxation of the proton, an average signal of all the protons is seen. If the chemical exchange is slower than the relaxation of the proton then the protons are resolved individually in their different environments. While this relationship is true for all nuclei in principle, it has only been significantly investigated with respect to protons because the timescales are appropriate; protons relax rapidly, their nuclear relaxation is on a similar timescale to some chemical dynamics. Other common NMR nuclei (such as ^{13}C and ^{31}P) have longer relaxation times, while conversely quadrupolar nuclei often relax too fast to be resolved at all, due to an additional relaxation mechanism that is only inhibited in highly symmetric environments. For a complete summary of dynamic effects in NMR there are books available.[65]

In order to further introduce dynamic NMR, an example will be used. Hindered rotation around the N-C(O) bond in N,N-dimethylformamide (DMF) is simple, well researched and one of the first dynamic processes investigated using NMR spectroscopy.[66] Fig. 3.1 shows the structure of DMF and its resonance forms. As can be seen from the resonance structure, there is a certain amount of double bond character to the carbon nitrogen bond. This inhibits rotation, which affects the chemical shifts of the N-methyl groups, when observed by NMR. Because of the dipole mo-

ment of the molecule and through space shielding and deshielding effects, the methyl group 'cis' to the carbonyl is slightly shielded relative to the 'trans' methyl. What this leads to is the appearance of two distinct chemical and magnetic environments, which, in turn, gives rise to two distinct NMR signals at room temperature. As the temperature of the sample is increased, what at first appears as a broadening of the two *N*-methyl group NMR signals eventually leads to their peak maxima converging. A special criterion is introduced, at the temperature at which a single flat topped peak is seen; this is called the coalescence temperature. The importance of this will be discussed later. Above the coalescence temperature a single peak is seen, which is the average of the two low temperature peaks.

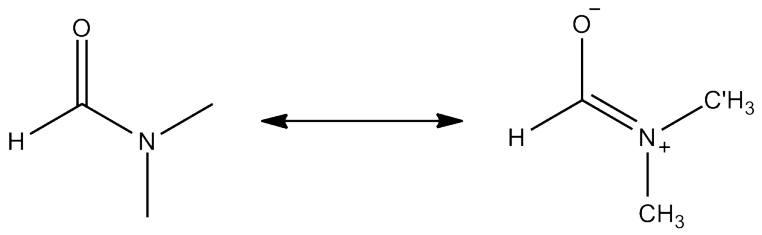


Figure 3.1: Resonance Structures of DMF

Other than being diagrammatically interesting, information about the kinetics and thermodynamics of the system can be extracted from the spectra collected across a temperature range, the mathematics of which will be introduced now. Eqn. 3.1 shows an equilibrium between two proton positions.

$$H_a \overset{k}{\rightleftharpoons} H_e \tag{3.1}$$

This represents the (relatively) simple case of a two site exchange. In this case the sites are labelled 'a' for axial and 'e' for equatorial to describe the proton positions in a pyrrolidinium ring. In simple two site examples it is possible to use the work of Gutowsky and Saika[67] to derive the coalesence temperature mathematically. They determined the equation for local magnetisation (M_a) at H_a (Eqn. 3.2), where ω is the applied radio pulse, M_o is the static magnetisation, $\alpha_a = (1/T_2 - i(\Delta\omega + \delta\omega/2)$, $2/T_2$ is the linewidth at half maximum intensity, τ_a is the lifetime of the proton in position a (and similar for e) and $\delta\omega$ is the separation of the two peaks.

$$M_a = \frac{i.\omega.M_o[(\tau_a + \tau_e) + \tau_a.\tau e(\alpha_a[H]_e + \alpha_e[H]_a)]}{(1 + \alpha_a\tau_a)(1 + \alpha_e\tau b) - 1} \tag{3.2}$$

If you expand Eqn. 3.2 and retain the imaginary components (using $M = \mu + i\nu$), we generate the spectrum line shape relationship Eqn. 3.3:

$$\nu = \frac{\omega.M_o[1 + \tau/T_2)P + QR]}{P^2 + R^2} \tag{3.3}$$

where

$$\begin{aligned} P &= \tau[(1/T_2^2) - (\Delta\omega)^2 + (\delta\omega/2)^2] + 1/T_2 \\ Q &= \tau[\Delta\omega - (\delta\omega/2)([H]_a - [H]_e)] \\ R &= \Delta\omega[1 + (2\tau/T_2)] + (\delta\omega/2)([H]_a - [H]_e) \\ \tau &= \frac{\tau_a.\tau_e}{\tau_a + \tau_e} \end{aligned}$$

This is the complete equation, which can be applied to any dynamic two site system. A number of simplifications can be made to internal rotation systems, as opposed to proton exchange systems, because the following relationships are true: The populations of the axial and equatorial protons are equal and the residence lifetimes in both positions are equal. This can be expressed mathematically as:

$$[H]_a = [H]_e$$

$$\tau_a = \tau_e$$

$$\Rightarrow \tau = \frac{\tau_a^2}{2\tau_a}$$

Which leads to the removal of a number of terms:

$$\begin{aligned} P &= \tau[(1/T_2^2) - (\Delta\omega)^2 + (\delta\omega/2)^2] + 1/T_2 \\ Q &= \tau\Delta\omega \\ R &= \Delta\omega[1 + (2\tau/T_2)] \end{aligned}$$

The peak positions and their dependence on τ are given by the maxima of Eqn. 3.3, and can be located by solving the 5^{th} order equation generated by differentiating ν with respect to $\Delta\omega$:

$$\left(\frac{\tau^4}{T_2}\right)(\Delta\omega)^5 + 2\tau^2 S\left(1 + \frac{\tau}{T_2}\right)\Delta\omega^3 + \left[\left(1 + \frac{\tau}{T_2}\right)\left(1 + \frac{2\tau}{T_2}\right)^2 - \tau.S\left(2 + \frac{3\tau}{T_2}\right)\right] S\Delta\omega = 0 \tag{3.4}$$

Where S is

$$S = \frac{1}{T_2} + \frac{\tau}{T_2^3} + \tau\left(\frac{\delta\omega}{2}^2\right)$$

If the linewidth ($2/T_2$) is much smaller than the peak separation $\delta\omega$ (i.e. the peaks are fully resolved), all terms with T_2 can be ignored, as they govern the behaviour in the overlap region.

$$2\tau^3\Delta\omega^3\left(\frac{\delta\omega}{2}^2\right) + \tau\Delta\omega\left(\frac{\delta\omega}{2}^2\right) - 2\tau^3\left(\frac{\delta\omega}{2}^4\right)\Delta\omega = 0 \tag{3.5}$$

This then leads to the two remarkably simple results, that the experimentally observed separation $\delta\omega_e$ is:

$$\delta\omega_e \equiv 2\Delta\omega = 2\left(\frac{\delta\omega}{2} - \left(\frac{1}{2\tau^2}\right)^{1/2}\right) \tag{3.6}$$

This can be expressed in a different manner to illustrate the behaviour of the system:

$$\delta\omega_e \equiv 2\Delta\omega = \delta\omega\left(1 - \left(\frac{2}{\tau^2\delta\omega^2}\right)^{1/2}\right) \quad \text{if} \quad \tau\delta\omega > \sqrt{2}$$

and

$$\delta\omega_e = 0 \quad if \quad \tau\delta\omega \leq \sqrt{2}$$

At this stage we can mathematically introduce the coalescence temperature; when the experimentally observed peak separation is 0, the following is true:

$$\tau\delta\omega = \sqrt{2} \tag{3.7}$$

Given that the lifetime is the reciprocal of the exchange rate, and converting ω from a radial frequency to a normal frequency, the rate of site exchange (k) at the coalescence temperature is:

$$k = \frac{\pi\Delta\nu}{\sqrt{2}}\ (s^{-1}) \tag{3.8}$$

Where $\Delta\nu$ is the peak separation (in Hz) at low temperature (i.e. in the absence of site exchange). This simple result from a rather complicated set of mathematics can then be combined with Eyring equation[68?] used in transition state theory:

$$k = K\left(\frac{k_b T}{h}\right)e^{\left(\frac{-\Delta G^{\ddagger}}{RT}\right)} \tag{3.9}$$

Where k is the reaction rate (in this case exchange), K is a scaling factor (typically 1 for molecules), k_b is Boltzmann's constant, h is Plank's constant, R is the ideal

gas constant and $\Delta G^{\ddagger}$ is the Gibb's activation energy. Eqns. 3.8 and 3.9 can be combined to give:

$$\frac{\pi\Delta\nu}{\sqrt{2}} = K\left(\frac{k_b T}{h}\right) e^{\left(\frac{-\Delta G^{\ddagger}}{RT}\right)} \tag{3.10}$$

This equation can be worked through to give an expression for $\Delta G^{\ddagger}$ in terms of T_c and $\Delta\nu$, where T_c is the temperature at which a single flat topped peak is seen, or coalescence temperature and the pre-exponential factor K is assumed to be 1.

$$\begin{aligned} e^{\left(\frac{-\Delta G^{\ddagger}}{RT_c}\right)} &= \left(\frac{h\pi\Delta\nu}{k_b T_c\sqrt{2}}\right) \\ \frac{-\Delta G^{\ddagger}}{RT_c} &= ln\left(\frac{h\pi\Delta\nu}{k_b T_c\sqrt{2}}\right) \\ -\Delta G^{\ddagger} &= RT_c\left[ln\left(\frac{h\pi}{\sqrt{2}k_b}\right) + ln\Delta\nu - lnT_C\right] \end{aligned}$$

Which is commonly expressed as

$$\Delta G^{\ddagger} = 8.314T_c(22.96 + lnT_c - ln\Delta\nu) \tag{3.11}$$

The same relationship is often expressed using base-10 logarithms and using Calories rather than Joules. Whatever the form of the relationship, it allows for rapid determination of the activation energies of exchange processes.

While the mathematics governing the behaviour are precise, the precision of the $\Delta G^{\ddagger}$ figure generated is relatively low. If simple visual inspection is employed to determine the T_c there is some small margin for error, unless multiple spectra at minutely different, but precisely determined temperatures are collected. Full line-shape analysis can be performed, allowing for mathematical analysis of the peak, which can determine whether any inflection points are present in the line, however the increase in accuracy is marginal compared to the time required for such analysis. The other aspect affecting the precision of the result is the peak separation, which should ideally be determined "well below" the coalescence temperature. This is a vague criterion, given that all NMR peaks move with temperature, although it is true that thermal drift in peaks is low and coalescing peaks will tend to drift in the same direction at the same rate until site exchange begins to broaden the peaks. On the whole the errors in determining the peak separation are small unless it is impossible to collect a spectrum significantly below the coalescence temperature.

3.2.2 NMR features of Ionic Liquids

The spectroscopic feature that is to be the focus of this chapter appears in the spectra of pyrrolidinium based ILs, and was first observed in the spectrum of $[C_1Hpyrr][HSO_4]$, which is shown in Fig. 3.2. As can be seen from the assignment, the ring protons, which would typically be assumed to be equivalent at the α and β positions, in fact appear as pairs. It was decided that the best way to investigate this phenomenon would be to make a range of pyrrolidinium ILs and salts, and examine the activation energy of the ring flip using variable temperature ^{1}H NMR.

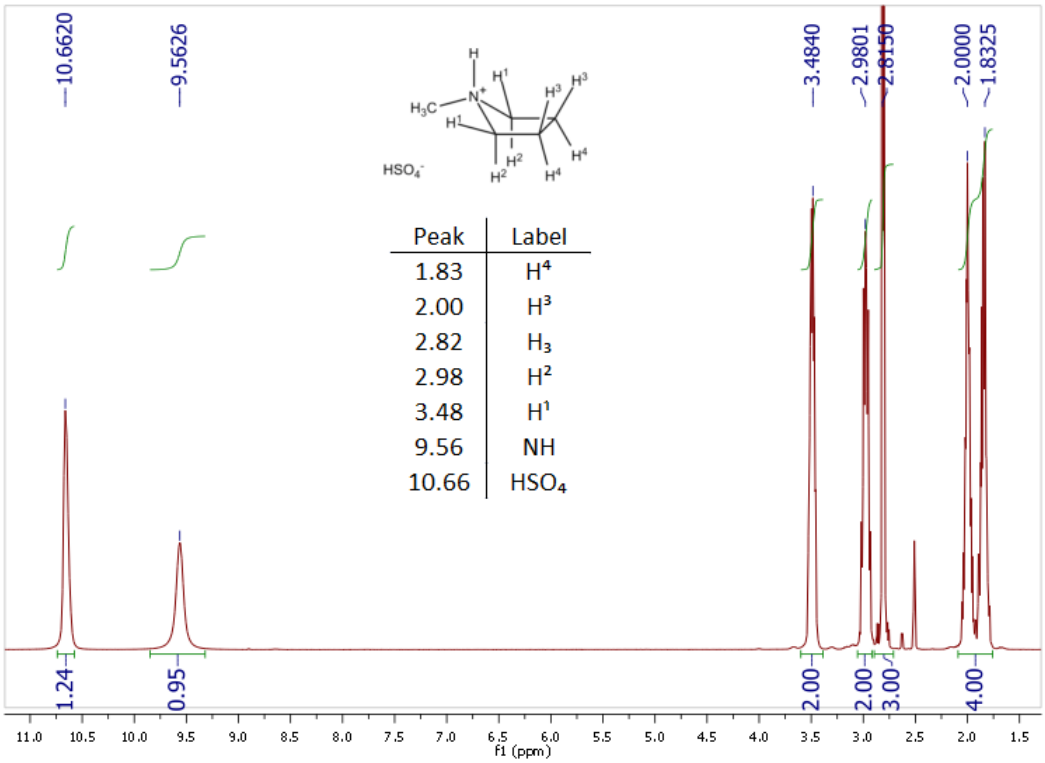


Figure 3.2: Labelled ^{1}H-NMR spectrum of $[C_1Hpyrr][HSO_4]$

The lowest energy conformation of a 5-membered ring is often called the 'envelope' conformer. For cyclopentane the 5 envelope conformers are degenerate, however for pyrrolidine or pyrrolidinium rings the nitrogen being 'out of plane' represents the global minimum. For a *N*-methylpyrrolidinium cation there are two nitrogen 'out of plane' conformers, which are shown in Fig. 3.3.

A similar example was studied by Umebayashi *et al.*[69] using DFT and Raman Spec-



Figure 3.3: Equatorial and Axial Conformers of the *N*-methylpyrrolidinium Cation

troscopy. They found that for $[C_4C_1pyrr][NTf_2]$ the conformer with the nitrogen out of plane and the butyl chain equatorial* represents the global free energy minimum and the butyl chain being axial is about 2.8kJmol^{-1} higher in energy.

It is noteworthy that a number of other envelope conformers, with the nitrogen in plane and a carbon out of plane, were of similar energy to the nitrogen out of plane and butyl chain axial conformer. Of these other conformers the highest in energy is only 5kJmol^{-1} higher in energy than the global minimum, that is the nitrogen out of plane and the butyl chain equatorial. This shows that for relatively small systems like this the ring conformer stabilities are relatively unhindered by internal steric interactions. Umebayashi *et al.* do not discuss the energy barriers between the conformers; it is this energy barrier that will be examined in this chapter.

It is informative to calculate the population differences of the ring conformers of $[C_4C_1pyrr][NTf_2]$, using the information from Umebayashi *et al.*, and consider it in reference to the mathematics governing the ring flip of the similar *N*-methylpyrrolidinium based ILs. The population difference of the axial and equatorial conformers can be estimated (assuming the other ring conformers are not populated for simplicity), using the Boltzmann equation as is shown in Eqn. 3.12.

$$\begin{aligned} \frac{N_a}{N_e} &= e^{\frac{-\Delta E}{RT}} \\ \frac{N_a}{N_e} &= e^{\frac{-2400}{8.314*298.15}} \\ \frac{N_a}{N_e} &= 0.38 \end{aligned} \tag{3.12}$$

Where N_a represents the axial conformer and N_e is the equatorial, ΔE is take from the computational study of Umebayashi *et al.*[69] and T is arbitrarily taken as

*In this case equatorial refers to groups approximately in the same plane as the four carbons of the ring and axial represents groups approximately perpendicular to the plane of the four carbons.

room temperature for this example. As can be seen from the result, about 30% percent of the population exists in the axial conformer and 70% in the equatorial conformer, when limiting it to a two level system. The imbalance of conformer populations would not affect the calculated activation energy of the ring flip because the system is never perturbed from equilibrium. At equilibrium the rates of forward and backward reaction (site exchange in this case) are equal in order to maintain the thermodynamic status quo. Increasing the temperature of the system increases the rate of reaction in both directions but for simple conformational changes it does not alter the equilibrium position nor does it perturb the system from equilibrium.

It is also fortunate that in $[C_x\text{Hpyrr}]^+$ based systems the axial protons of the axial conformer occur at the exact chemical shift as the axial protons from the equatorial conformer, if this were not true the spectrum would be more complicated to analyse, although the fundamental mathematics governing the ring flip wouldn't be affected. It is likely that the reason the two conformers produce identical spectra is the mediating influence of the nitrogen. The nitrogen suppresses potential ^{3}J coupling to the NH proton, which would be expected to be present in the equatorial conformer. When the NH is axial it is almost anti-periplanar to the axial alpha protons. This is not true when the NH is equatorial, as it is gauche to both axial and equatorial alpha protons. The nitrogen also mediates any inductive effect that would be seen when changing the length of the alkyl chain.

In order to investigate this phenomenon further, a range of ILs were synthesised, varying the nature of the anion and the length of the alkyl group on the pyrrolidinium cation. These ILs are $[C_1\text{Hpyrr}][HSO_4]$, $[C_1\text{Hpyrr}][\text{OTf},]$ $[C_1\text{Hpyrr}][NTf_2]$, $[C_1\text{Hpyrr}]\text{Cl}$, $[C_2\text{Hpyrr}][HSO_4]$, $[C_3\text{Hpyrr}][HSO_4]$, $[C_4\text{Hpyrr}][HSO_4]$ and $[C_6\text{Hpyrr}][HSO_4]$. Complete synthetic details are given in Chapter 2. These ILs were then characterised using variable temperature ^{1}H-NMR spectroscopy, the results of which follow in Section 3.3.

3.2.3 Computational Chemistry

Over the course of the investigation it became apparent that some computational assistance was required. What follows is a short overview of computational chemistry as it was used in this study.

Ab initio computational chemistry is essentially a method for calculating the electronic wave function of a system as accurately as is affordable. Afford ability in this sense refers to computation time, rather than a fixed cost. Once the wave function of a molecule or system is available, it is possible to calculate most properties of the molecule and use the optimised structure in molecular dynamics of larger systems.[70]

In order to calculate the wave function of a molecule the Schrödinger equation (Eqn. 3.13) for the system must be solved.

$$\hat{H}\Psi(\mathbf{q},t) = -\frac{\hbar\partial\Psi(\mathbf{q},t)}{i\partial t} \tag{3.13}$$

This equation governs how the wave function (Ψ) varies with time (t) and space- & spin-coordinate ($\mathbf{q}$), and fully describes the system. A common simplification to the equation is given in Eqn. 3.14 and is time independent.

$$\hat{H}\Psi(\mathbf{q}) \;=\; E\Psi(\mathbf{q}) \tag{3.14}$$

The Hamiltonian operator ($\hat{H}$) describes the total energy of the system, both kinetic and potential. In order to simplify the equation the Born-Oppenheimer approximation is used. The Born-Oppenheimer approximation states that energy (kinetic and potential) of the nucleus is independent of the energy of the electrons. In essence the motion of the electrons doesn't affect the motion of the nuclei. The approximation is possible because of the great difference in mass, which results in very different timescales of motion. A second approximation, which follows from the Born-Oppenheimer approximation, is called the clamped nucleus approximation. This states that from the reference frame on the electrons the nuclei are stationary over short time intervals. These approximations allow the calculation of the electronic wave function including parameters of nuclear charge and position and the removal of the nuclear motions from the Hamiltonian operator. Thus the Hamiltonian can be written as shown in Eqn. 3.15 where $\hat{h}_1$ is the energy of the electron

and the interaction of the electron with the nuclei and $\hat{h}_2$ is the electron-electron interactions, ∇ is a position vector matrix, Z_A is the charge of the nucleus and $r_{x,j}$ is the separation of the particles. All of these quantities are typically expressed in atomic units.

$$\begin{aligned} \hat{H}_{elec} &= \hat{h}_1 + \hat{h}_2 \\ \hat{h}_1 &= -\sum_{i}^{N} \frac{1}{2}\nabla_i^2 + \sum_{i}^{N}\sum_{A}^{M} \frac{Z_A}{r_{i,A}} \\ \hat{h}_2 &= \sum_{i}^{N}\sum_{j>i}^{N} \frac{1}{r_{i,j}} \end{aligned} \tag{3.15}$$

While $\hat{h}_2$ describes in interaction of two electrons, it doesn't stop them disobeying the Pauli exclusion principle. In order to resolve this a matrix is generated and the wave function is the determinant of this matrix, which contains the combinations of electron wave functions (χ) and positions ($\mathbf{q}$) and is shown in Eqn. 3.16.

$$\Psi = \frac{1}{\sqrt{N!}} \begin{vmatrix} \chi_1\mathbf{q}_1 & \chi_2\mathbf{q}_1 & \cdots & \chi_N\mathbf{q}_1 \\ \chi_1\mathbf{q}_2 & \chi_2\mathbf{q}_2 & \cdots & \chi_M\mathbf{q}_2 \\ \vdots & \vdots & \ddots & \vdots \\ \chi_1\mathbf{q}_N & \chi_2\mathbf{q}_N & \cdots & \chi_N\mathbf{q}_N \end{vmatrix} \tag{3.16}$$

While it is not apparent immediately, within this matrix it can be shown that electrons with the same spin cannot exist in the same space, while electrons of different spin have a small probability of occupying the same space, so while the Hamiltonian operator doesn't preclude electrons from overlapping, the wave function does. In order to calculate the wave function it is necessary to apply one more approximation, which states that the calculated energy of the system will always be higher than (or equal to if a perfect calculation were performed) the real energy of the system, this is called a variational calculation.

$$E\Phi_{real} \leq E\Phi_{calc}$$

This approximation allows the calculation to become a minimisation problem which can be iteratively solved, rather than requiring an analytical solution; the calculation just needs an initial guess of the Hamiltonian operator as a starting point. However one of the limitations of a variational calculation is that the accuracy of a result is

dependent on the quality of the guess. A bad guess will converge, however it will converge significantly above the 'real' value, conversely an extremely good guess can approach the Hartree-Fock (HF) limit which is as close to the real value as the basis set allows.

A basis set is part of the initial guess, and while it can take a number of forms, many basis sets are a linear combination of atomic orbital functions. The basis set is used to reduce the scale of the calculation by providing accurate initial guess values to 'core' orbitals, which are extremely important in determining the total energy of the system, but are relatively unchanging from one chemical environment to another. The 6-311G basis set is an example of this. Thus a large part of the basis set is a effectively a set of pre-optimised values to rapidly minimise and converge the energies and wave functions of core electrons of a system. Valence electrons are described using additional functions that can include polarisation (such as '(d,p)') and diffusivity (such as '+'). The polarisation term (d,p) adds a 'p' orbital function to the hydrogen basis set and a 'd' type orbital function to the 2nd row elements which allow for more distortion and asymmetry in the molecular orbitals (and electron density) of these elements. This term is important for very polar bonds, such as the N^+-H bond in $[C_xHpyrr]^+$. The diffusivity term adds accuracy to the calculations of the edges of the orbitals far from the nucleus, which is important for heavy atoms and anions which have more diffuse orbitals than the corresponding neutral atom or molecule. This is important for large anions where the charge is delocalised over many atoms, such as the $[NTf_2]^-$ where the charge is spread over 7 atoms. So an example of a full basis set using these functions is '6-311G+(d,p)'.

This provides the basic framework for *ab-initio* calculation, however because the Hartree-Fock method models an independent electron moving through an average static field, no electron correlations are included. The electron correlations are split into two categories; dynamic and static. Dynamic correlations refer to how one electron can instantaneously influence the position of a second electron. Static correlations refer to a system in which there are two nearly degenerate states which cannot be adequately described by a single Slater Determinant. There are a range of methods available to account for electron correlations which can be applied after

the initial Hartree-Fock optimisation. As always there is a compromise between the quality of calculation and the economy of calculation which is particularly acutely felt by post Hartree-Fock methods. In post HF methods computation time scales to the 5^{th} (or greater) power of the size of the calculation, compared to a HF calculation where computation time scales to the 4^{th} power of the size. That is a HF-calculation that is doubled in size takes 16 times as long to solve.

Density-Functional Theory (DFT)[71] is an improvement on typical HF methods. DFT is based on two theorems by Hoenberg and Kohn, the first of which states that the Hamiltonian operator depends on the distribution of electron density, thus the energy can be expressed as a function of electron density.

$$E \;=\; \hat{E}(\rho)$$

The second is similar to variational theory, in that it states that the electron density with the lowest total energy is the electron density of the ground state. Thus the energy of the ground state, as a function of electron density, can be expressed as a sum of contributions, shown in Eqn. 3.17.

$$\hat{E_0}(\rho_0) \;=\; \int \rho_0(\mathbf{r}) V_{N,e}\, \mathrm{d}\mathbf{r} + J(\rho_0) + T(\rho_o) + E_{ncl}(\rho_o) \tag{3.17}$$

The first term ($\rho_0(\mathbf{r})\mathrm{V}_{N,e}\, \mathrm{d}\mathbf{r}$) is the interaction of the electrons with the nuclei, which can be known exactly. The second ($\mathrm{J}(\rho_0)$) is the electron-electron interactions. The third term ($\mathrm{T}(\rho_o)$) is the kinetic energy. The final term ($\mathrm{E}_{ncl}(\rho_o)$) is a non-classical energy term, which encompasses features not included in the other terms and a correction applied to the electron-electron interaction and kinetic energy due to Coulombic correlations.

Kohn and Sham developed a method for calculating a correct kinetic energy term by introducing a non-interacting reference state system that has the same electron density as the real, interacting system. It is described by a Slater determinant analogous to that in Eqn. 3.16 where the determinant is the kinetic energy, rather than a wave function. This allows for the calculation of exact kinetic energies of electrons in a non-interacting reference state. Eqn 3.18 shows the Kohn-Sham operator.

$$\hat{f}^{KS}\chi_i = \; -\sum_{A}^{M} \frac{Z_A}{r_{1,A}} \;+\; \int \frac{\rho(\mathbf{r}_2)}{r_{1,2}}\, \mathrm{d}\mathbf{r}_2 \;-\; \frac{1}{2}\nabla^2 \;+\; V_{XC}(\mathbf{r}_1) \tag{3.18}$$

The terms of this equation are the same as those in Eqn. 3.17, however the kinetic energy term is exact, but refers to the non-interacting reference system. Most of the kinetic energy is accounted for by this term; the remainder, plus other correlations (E_{nuc} in Eqn. 3.16) are included in the exchange-correlation potential V_{XC}. In principle the Kohn-Sham DFT solution is exact, within the limitations of the basis set, however there are very few examples for which the correct values for the exchange-correlation potential are known. Therefore the key feature of DFT is the use of different approximations and expressions for V_{XC}.

A common method of determining the exchange-correlation potential is the use of a local density approximation, which depend on the electron density at a given position in space. The quality of these calculations can be improved upon by including the spin-distribution of the system, which gives the 'local spin-density approximation' (LSDA) functional.

The exchange-correlation potential is usually split into an exchange-correlation functional and an independent-correlation functional, examples of which are the Slater exchange functional[72] and the Vosko, Wilk and Nusair local correlation functional.[73] This LSDA functional performs well for solid state systems, however doesn't return accurate results for gas phase and molecular chemistry.

A method to improve this is the generalised gradient approximation (GGA), which includes additional terms describing the gradient of the electron density at a given point. There are two broad classes of GGA, one of which uses a first principles approach and the other uses an empirical approach. Each has its own merits and areas of application. The empirical methods tend to work better for gas phase behaviour and chemical reactions and will be used in this study.

Empirical GGAs have some physical restrictions included and the remaining parameters are found by fitting to known data series, such as exchange energies of noble gases.[74] An example of an empirical GGA is the Beck88 (B88) exchange function, where the GGA is included as a correction to the LSDA term.

$$
\begin{aligned}
E_X^{B88}(\rho_\alpha, \rho_\beta) &= E_X^{LSDA} - \beta \sum_{\sigma=\alpha,\beta} \int \rho_\sigma^{\frac{4}{3}} \frac{x_\sigma^2}{1 + 6\beta x_\sigma sinh^{-1} x_\sigma} \, \mathrm{d}\mathbf{r} \qquad (3.19) \\
x_\sigma &= \frac{|\nabla \rho_\sigma|}{\rho_\sigma^{4/3}} \\
\beta &= 0.0042
\end{aligned}
$$

Hybrid functionals allow for mixing for the Hartree-Fock exchange correlation potential with the DFT exchange correlation potential to again improve upon the result, the most common hybrid functional is Becke's three parameter functional, the familiar B3LYP,[75] Eqn. 3.20, which mixes, in order, the local Slater exchange, the exact Hartree-Fock exchange, the Beck88 GGA correction, the Vosko, Wilk & Nusair local correlation functional and the LYP GGA correlation functional.

$$
\begin{aligned}
E_{XC}^{B3LYP}(\rho_\alpha, \rho_\beta) &= (1-a) E_X^S(\rho_\alpha, \rho_\beta) + a\, E_X^{HF} + b\, \Delta E_X^{B88}(\rho_\alpha, \rho_{beta}) \qquad (3.20) \\
&\quad + (1-c)\, E_C^{VWN}(\rho_\alpha, \rho_\beta) + c\, E_C^{LYP}(\rho_\alpha, \rho_\beta) \\
a &= 0.20 \\
b &= 0.72 \\
c &= 0.81
\end{aligned}
$$

B3LYP is an extremely popular density functional in computational chemistry because it performs well in a wide range of areas. This has lead to it being favoured because there is a wealth of data to which computations can be directly compared without questions about variations caused by the choice of functional. It is for this reason that the B3LYP functional was used in this study.

It is worth noting here that DFT doesn't completely account for Van der Waals interactions and dispersion interactions; further modifications need to be applied to the theory to incorporate such interactions. Van der Waals interactions are generally only important in intermolecular calculations of specific systems; a simple example would be a model of noble gases. Dispersion interactions are weak interactions between electrons that are insignificant for individual molecules but are extremely important for large systems and are possibly of interest for small clusters of ions.

DFT is by no means the only option for post Hartree-Fock methods available; there are others that take different approaches to calculating electron correlations, for example Møller-Plesset perturbation (MP) theory. MP theory is based on a mathematical approximation for multiple electron correlations that far predates computational chemistry.[76] This theory relies on adding small perturbations to Hamiltonians describing known systems, in order to approximate more complex systems. A simple example of this is applying a small electrical potential perturbation to a hydrogen, which leads to the Stark effect, when spectral lines are shifted in an electric field. Also B3LYP is by no means the last step in development of this type of functional. A range of more specialised functionals have been developed for certain tasks[77,78] and a series of more complex functionals (meta-hybrid GGAs and double hybrid GGAs) have also been developed that build on the work of simpler DFT methods. Despite more comprehensive DFT methods being available B3LYP remains extremely popular and accounts for about 80% of ISI Web Of Knowledge references to DFT between 1990 and 2006.[72] This is because it is robust and reliable, is now extremely well understood and there exists a large body of comparative data in the literature that eliminates any possible ambiguity about whether results differ because of substance or method.

With these computational methods in place it is possible to now perform a calculation on a molecule and receive reliable output. The methodology for this involves performing an optimisation calculation, followed by subsequent calculations of specific properties. All calculations were performed using the Gaussian '09 Software Package. A B3LYP functional with a 6-311+G(d,p) basis set was used for all elements. The 'ultrafine' integration grid was used and electron density convergence criterion of 10^{-9} (SCF=conver=9) was used for the DFT calculations. These add sample points to the integration surface and tighter convergence criteria respectively, to optimisation calculations.

3.2.4 Calculating Volumes

The use of computational chemistry was required because, as part of the analysis it was necessary to calculate ionic volumes, in order to calculate the free volumes of the

solutions. The free volume is the effective ionic volumes minus the theoretical ionic volumes, where the effective ionic volume is taken from the density and molecular weight and the theoretical ionic volumes are computationally determined.

Unfortunately defining the volume of a molecule is somewhat ambiguous; much like a balloon, a molecule appears to have an obvious 'surface', however upon closer inspection the surface is found to be malleable. In this way it is controversial as to what a 'true' volume is, because a volume is affected by the medium in which it is contained. Thus the methods of calculation must be understood in order to use the appropriate calculation for this investigation.

The first way (traditional, perhaps) to calculate volumes is by using crystal structures. This works well enough for spherical ions, particularly if you can pair up extremely dissimilarly sized ions, in which case a cubic lattice unit is found, where the lattice parameter corresponds to twice the ionic radius of the larger ion,[79] and the smaller anions sit in the interstitial spaces. There is also the soft sphere method,[80] which gives a remarkably good prediction of inter-ionic distances in simple systems and good predictions of the ionic radii. The various models have been compared and critiqued by Lang and Smith recently.[81]

Measuring volumes for non-spherical ions and molecules becomes increasingly difficult, because the models for calculating volumes rely on close packing of atoms and molecules and bisecting the distance between two atoms. Large molecules are unlikely to be close packed, thus simply bisecting internuclear vectors is not appropriate. An extensive list of Van der Waals volumes and radii of small organic groups were published by Bondi.[82] The values were arrived at by collating a wide range of available data and are now commonly used as standard values. There are methods for using these simple atom and molecule fragments to literally build larger molecules from them like puzzles. This method is commonly used in modern crystallography, with computational assessment of the fitting.

Modern crystallographic methods typically generate a (mathematically) smooth molecular surface. The method for this involves several steps. The first step is to generate a molecular surface, this can either be achieved by using an electron probability surface, typically the 95% surface (this can be calculated from X-ray

scattering data), or by calculating the nuclear centres and applying Van der Waals spheres of fixed radius. The second step is to trace a small probe sphere of a fixed radius over this surface.[83] This can then generate two surfaces. The first is the solvent accessible surface, which is the surface drawn by the position of the center of the probe molecule as it traces the rough molecular surface. The second is the molecular surface, which is the surface drawn by the point of contact of the probe and the rough surface, plus the arcs, geodesic triangles and geodesic polygons generated by the probe when it is in contact with the rough surface at two, three or more points. This is more simply represented visually, as shown in Fig. 3.4.[84]

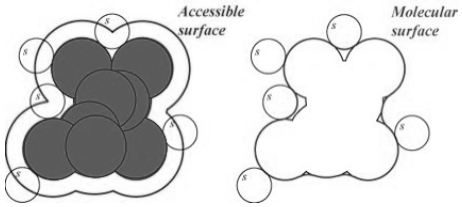


Figure 3.4: Schematics of Solvent Accessible Surface and Molecular Surface[84]

Computational chemistry is another method of determining molecular volumes. Once an optimised molecular (or ionic) structure has been determined, the volume can be calculated rapidly. Volume calculations in computational chemistry are subject to some of the same problems as the methods outlined above. There is no hard surface at which to compute a volume; most volume calculations are done within the 0.001eBohr^{-3} envelope. The calculation of volumes using computational chemistry was developed by Bader *et al.*,[85] who examined the electron density cut off and selected the 0.001eBohr^{-3} envelope over other values, as the volumes agree with van der Waals radii of non-polar molecules and contains about 96% of the electron density of the molecule. A study by Mitchell and Speckman[86] shows how the calculated volume varies with electron density cut off in various models. As electron density is a probability function, it only asymptotically approaches zero, so at very low electron densities a small change in threshold value can lead to huge changes in calculated volume. Computational representations of molecular orbitals, for example, are often drawn where the surface represents the 90% probability surface, because a 100% surface is infinitely large.

Since a molecular volume is not fixed is it important to maintain internal consistency,

that way reliable correlations can be determined. However it is difficult to make comparisons between results relying on different volume calculations. Because of this, the application of some of these methods is situational; the solvent accessible surface was functionally designed to calculate the volume of proteins in water, while computational chemistry volumes are outputted with an effective spherical radius (Stokes' radius) designed for use in Stokes-Einsteinian systems (i.e. dilute, rapidly correlating and much larger than the medium).

3.2.5 Hole theory in Ionic Liquids

While the work in this thesis is not directly related to other work which uses hole theory to investigate viscosity, surface tension and conductivity in ILs, there are common features. Hole theory is a statistical thermodynamics method used to calculated various liquid properties by considering the size and distribution of holes in the medium.[87]. Both hole theory and the treatment here require ionic volumes to be calculated for some measurement of free volume or hole sizes. One of the questions still raised in the field of ILs is the exact nature of the diffusing species in IL (in an external electric field). Abbott applied hole theory[87] to study viscosity,[88] conductivity,[89] density and surface tension.[90] Larriba also applied a similar treatment to surface tension.[91] The correlations and calculations of these bulk transport properties are based upon a relationship between surface tension and hole volume that is not fundamental; there is a constant required, however it appears to be invariant for the ILs studied thus far. However it functions well to calculate viscosity for ILs. The same relationship doesn't work for salt solutions, where the constant is very different. This is presumably because strong specific interactions such as hydration spheres affect the partial molar volumes of the water and salt.

The above calculations by Abbott and Larriba used a volume based on spherical IL ions, the radius of which is calculated for use in self-consistent reaction field calculations, in which the solute is much larger than the solvent and is modeled (in its simplest form) by a dielectric field. While in ILs the solvent and solute are one and the same it is not clear what, if any, effect this has on the quality of the calculations.

3.3 Results of Variable Temperature NMR Spectra of Ionic Liquids

The temperature controller of the spectrometer was calibrated against methanol for the temperature range 180K-300K and against ethylene glycol for the temperature range 300K-423K. The spectrometer temperature range is 173K-423K Spectra collected above room temperature were sampled on the heating cycle and samples collected below room temperature were collected on the cooling cycle. All samples were equilibrated for 5 minutes before collecting the spectrum.

3.3.1 Ring Flip Activation Energies of ILs

An example of a stack plot of NMR spectra collected at varying temperatures is shown in Fig. 3.5. Spectrum 1 in Fig. 3.5 was collected at 293K, each consecutive spectrum was collected 10K higher in temperature. Spectrum 9 was collected at 373K. As the temperature increases a number of changes in the spectral features can be seen. The most important features, for the purposes of this study, are the temperature dependent chemical shifts, and the line width of the signals of the ring protons, which are pairs of peaks at 1.8ppm and 3.0ppm. As the temperature increases first line broadening occurs, then the peaks begin to converge. As can also be seen in the spectra, as the peaks of the ring protons converge the signal no longer drops completely to the baseline in between the peaks. As temperature continues to rise the coalescence temperature is reached and a single flat topped peak is seen. This can be seen occurring for the alpha protons (around 3ppm) in Fig. 3.5 in spectrum number 7, which is at 353K. Above the coalescence temperature peaks collapse into relatively sharp singlets, as the thermal energy is the system renders the molecule completely vibrationally free. The other feature to notice in the spectra is the thermal dependence of the $N^{+}\mathbf{H}$ and $[\mathbf{H}SO_4]^{-}$ proton peaks. These protons are in potential hydrogen bonding and proton exchanging environments, both of which show strong temperature dependence, but this is of relatively passing interest here.

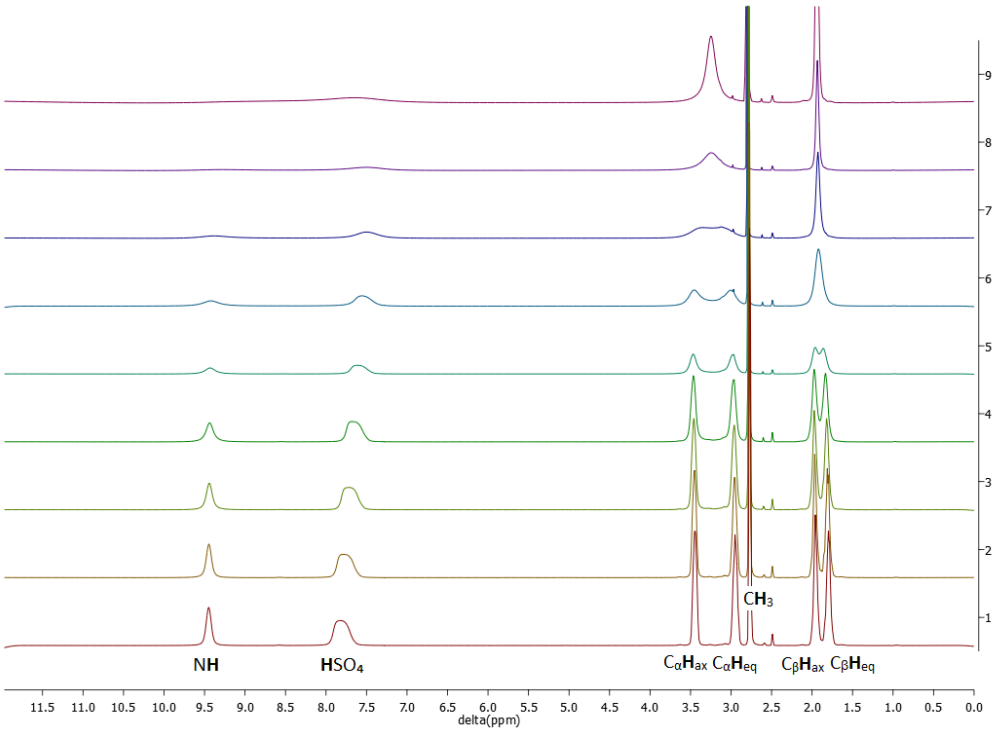


Figure 3.5: Variable temperature ^{1}H-NMR of 40mol% [C_1Hpyrr][HSO_4] in DMSO, 293 (bottom) to 373K (top) in 10K Steps

Shown in Table 3.1 is a summary of the NMR results. It is worth stating here some of the difficulties of obtaining this data. The only IL in which is was possible to collect a spectrum of the pure liquid was [C_2Hpyrr][HSO_4]. For the other [C_xHpyrr][HSO_4] (x=1, 3, 4 or 6) ILs the coalescence temperature of the ring protons in the pure liquid was above the maximum temperature accessible to the spectrometer which was 150^{o}C or 428K. For the other [C_1Hpyrr][Y] ([Y]=[NTf_2]$^-$, Cl^- or [OTf]$^-$) salts, which are all solid at room temperature, the coalescence temperature of the ring protons had been passed upon melting the salt.

This made it necessary to undertake the study in solution. The ILs being used can be separated into two sets, each of which have different solvent requirements.

The [C_xHpyrr][HSO_4] (x=1, 2, 3, 4, 6) ILs, are all liquid at room temperature, but the coalescence temperature of the ring protons in the neat liquids is high. Thus a solvent must be found in which the coalescence temperatures of the ring protons occur within the temperature range of the spectrometer. Few solvents proved suitable for collecting spectra at elevated temperatures, because even in solution high

temperatures were needed to observe coalescence of the ring protons. The chlorinated solvents, benzene, acetonitrile and water were all tried and ruled out. This left only high boiling solvents, such as DMF and DMSO. DMSO was available and preliminary work showed it was suitable for the [C_xHpyrr][HSO_4] ILs.

The other ILs in the study, [C_1Hpyrr]Cl, [C_1Hpyrr][NTf_2] and [C_1Hpyrr][OTf] are all solid at room temperature and in all three the coalescence temperature of the ring protons had been passed upon melting. These ILs require a solvent in which the coalescence temperature of the ring protons can be observed. DMSO also proved to be a suitable solvent for these ILs, although the freezing point of the solvent was approached. Coalescence of the proton signals was observed above the freezing temperature of the solvent, although only the alpha proton signals were above their coalescence temperature for [C_1Hpyrr]Cl and [C_1Hpyrr][NTf_2]. The beta protons had a coalescence temperature below the freezing point of the solvent. The fact the these are only slightly above the freezing point of the solvent does affect the precision of the $\Delta\nu$ term, as it was impossible to get far below the coalescence temperature, however $\Delta G^{\ddagger}$ is much more strongly dependent on coalescence temperature of the protons, than it is on the peak separation.

		α protons			β protons		
Ionic Liquid	Solvent	T_c(K)	$\Delta\nu$(Hz)	$\Delta G^{\ddagger}$(kJmol^{-1})	T_c(K)	$\Delta\nu$(Hz)	$\Delta G^{\ddagger}$(kJmol^{-1})
[C_1Hpyrr][HSO_4]	DMSO	342	49.50	73	353	195.61	71
[C_2Hpyrr][HSO_4]	Neat	425	59.56	91	-	-	-
	DMSO	328	54.24	70	348	198.43	70
[C_3Hpyrr][HSO_4]	DMSO	383	57.72	82	408	181.88	83
[C_4Hpyrr][HSO_4]	DMSO	371	51.32	79	393	205.62	80
[C_6Hpyrr][HSO_4]	DMSO	388	50	84	413	185.56	84
[C_1Hpyrr]Cl(s)	DMSO	<293	-	-	313	200	63
[C_1Hpyrr][NTf_2](s)	DMSO	<293	-	-	309	184	62
[C_1Hpyrr][OTf](s)	DMSO	363	65.60	77	380	218.61	77
[C_4C_1pyrr][NTf_2]	MeCN	228	50	48	-	-	-

Table 3.1: Activation Energies Of Ring Flips Of ILs

The coalescence temperatures are accurate to the nearest degree. A change of one Kelvin in coalescence temperature represents a change of 0.25kJmol^{-1} in activation energy of the ring flip. The $\Delta\nu$ is accurate to 0.04Hz, which represents a

change of 0.002kJmol^{-1} in the activation energy of the ring flip. Thus the physical measurements are more precise than the results displayed. The ring flip activation energies are shown to the nearest kJmol^{-1}, as it would be inappropriate to attach two figures of significance (the precision of the physical measurement) to the ring flip activation energies when the α and β position ring flip activation energies within the same molecule do not agree to that level of significance. The peak separation of values [C_1Hpyrr]Cl, [C_1Hpyrr][NTf_2] and [C_4C_1pyrr][NTf_2] are given less significance because it was not possible to get far below the coalescence temperature. [C_4C_1pyrr][NTf_2] is included here to illustrate how stark the difference of ring flip activation energy is when the NH is replaced with a NMe; [C_1Hpyrr][NTf_2] has a ring flip activation energy of 62kJmol^{-1} which is 14kJmol^{-1} (slight over 25%) higher than the ring flip activation energy of [C_4C_1pyrr][NTf_2], which is only 48kJmol^{-1}. Also for consideration, the activation energy of the ring flip of the parent molecule, N-methylpyrrolidine, is 32kJmol^{-1}.[92]

It is not clear at first glance that there is a particular trend to the data; particularly given that [C_2Hpyrr][HSO_4] has a lower ring flip activation energy than [C_1Hpyrr][HSO_4]. In order to elucidate the behaviour it is necessary to find some property of the IL or system to correlate with the ring flip activation energy. An obvious starting point is to examine the role of any possible hydrogen bonding interaction along the N-H bond, as there are a range of coordinating and non-coordinating anions represented. As can be seen from Fig. 3.6 no such correlation is found, because, with the exception of [C_1Hpyrr]Cl, the NH protons in all of the ILs in the study have a chemical shift of 9.45ppm.

The appearance of the NH proton at 9.45ppm in all of the ILs except the chloride could be indicative of two things. The chloride could be capable of a closer approach to the nitrogen than the other anions based on its small size. The other possibility is that the DMSO is interacting with the NH proton in all cases except the chloride. This is not unreasonable given that the chloride is the only anion that is capable of stronger specific interactions than DMSO, although the triflate and hydrogensulphate anions would be considered capable of similar specific interactions depending on the metric used to define them. The possible role of the solvent is examined in

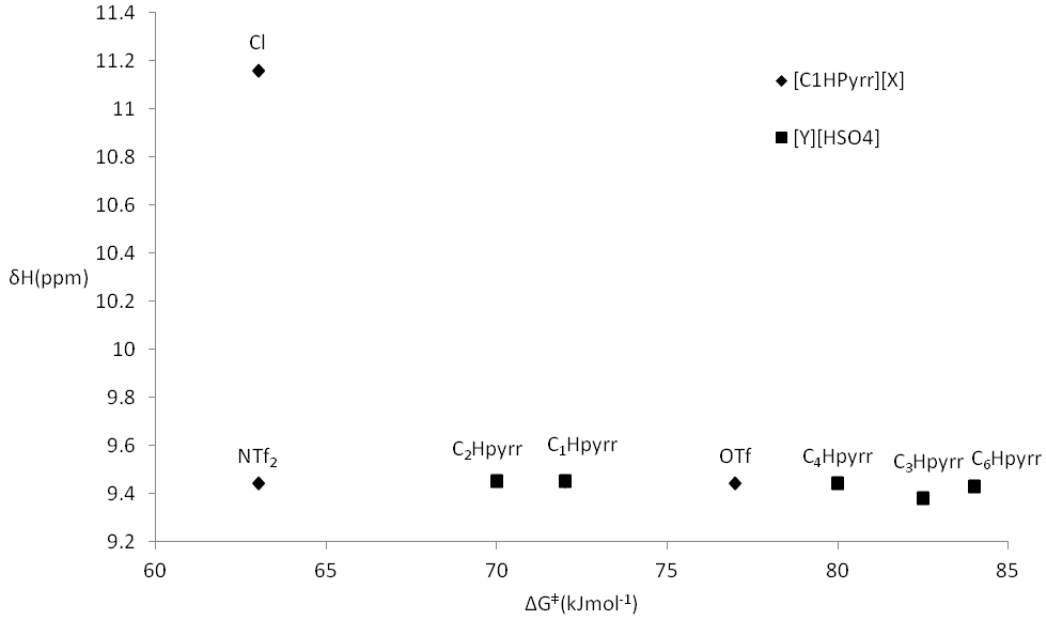


Figure 3.6: Chemical Shift of NH δ(ppm) vs. Activation energy of ring flip $\Delta G^{\ddagger}$

the next section.

A number of other correlations with specific chemical properties of the system were attempted such as the Kamlet-Taft β of the anion, and pKa of the conjugate acid of the anion, however it is apparent that the variation in ring flip activation energy across the series of $[C_xHpyrr][HSO_4]$ ILs precludes a dependence only on a specific property of the anion. Having said that, the largest changes in activation energy of the ring flip occur when the anion is exchanged; the change in activation energy of the ring flip with change in alkyl chain length is less marked. This dependence on both cation and anion means it is necessary for the correlation to be with either a bulk property of the IL, or a combination of specific properties of both the cation and the anion for each IL.

The fact that chemical shift of the NH proton of the $[C_xHpyrr][Y]$ ILs seems to be invariant (with the exception of the Cl^-) makes it necessary to scrutinise the role of the solvent, since it is possible that this chemical shift is being determined by some hydrogen bonding interaction with the solvent. Unfortunately because of the paucity of high temperature NMR solvents, it was not practical to switch solvents entirely; the obvious candidate, DMF, is also a hydrogen bond acceptor, others such

as toluene don't mix with ILs. However it is possible to examine one IL in a range of solvents, as long as the IL used has a low enough coalescence temperature.

3.3.2 The Role of the Solvent

While it was not the intent of this study to examine the role of the solvent, the fact that it was impossible to examine the neat ILs meant that it was necessary to work in solution, which means the solvent choice and effect must be scrutinised. Although the solvent effect was minimised by working at a fixed concentration of IL in DMSO, it was still prudent to examine the role of the solvent to see if there are strong specific effects that are masking the underlying behaviour of the IL.

In order to examine the role of the solvent it was decided to study one IL in a variety of solvents. Since the purpose of this is to examine any specific interactions between the solvent and the IL, it was decided to use $[C_1Hpyrr][NTf_2]$, this is because the $[NTf_2]^-$ anion does not engage in strong specific interactions. Additionally, $[C_1Hpyrr][NTf_2]$ has already been shown to have a low ring proton coalescence temperature in DMSO, which made it a good candidate for having ring proton coalescence temperatures in the liquid range of other solvents. Figure 3.7 shows the ring flip activation energy of $[C_1Hpyrr][NTf_2]$ in various organic solvents plotted against the solvent β.

As the figure shows, there is no correlation between the solvent β value and the ring flip activation energy. The hydrogen bond accepting ability of the solvent is conceptually the most likely to have a strong effect on the ring flip, given the presence of a hydrogen bond donor on the pyrrolidinium cation, however it is unwise to examine solvent properties in isolation; covariance of properties can mask correlations. A full Linear Solvation Energy Relationship (LSER) was calculated and the graph of the result is shown in Fig 3.8, where the x-axis is the experimentally observed ring flip activation energy and the y-axis is the value predicted by the LSER. The LSER here includes the three Kamlet-Taft solvent parameters, α, β and π^* and takes the form shown in Eqn 3.21, where Δ $G_0^{\ddagger}$, a, b and p are parameters of the fitting.

$$\Delta G^{\ddagger} = \Delta G_0^{\ddagger} + a\alpha + b\beta + p\pi^* \tag{3.21}$$

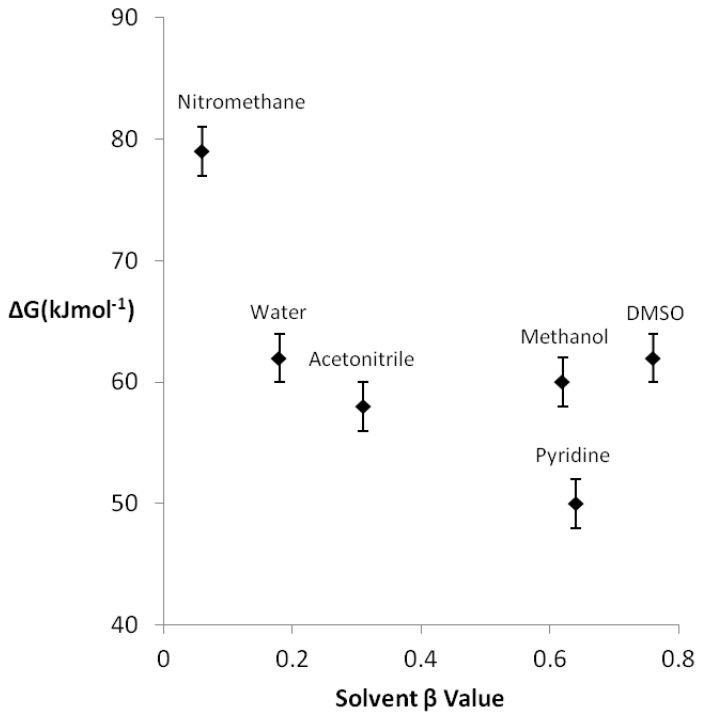


Figure 3.7: β Value of Solvent vs. Ring Flip Activation Energy of $[C_1Hpyrr][NTf_2]$ ($\Delta G^{\ddagger}$)

A correlation test of the regression analysis of the experimental and predicted ring flip activation energies found the probability threshold value (p-value) to be 0.15, thus the correlation fails to pass the 95% confidence interval test ($p \leq 0.05$), which means there is no correlation between the solvent's (Kamlet-Taft) properties and the ring flip activation energy of $[C_1Hpyrr][NTf_2]$. It is typical to analyse the pairs of Kamlet-Taft parameters should the full three parameter relationship fail, because it is possible that correlations can be masked by cancelling effects. The threshold probability values for the paired variables are as follows: α and β, p=0.16, α and π^*, p=0.09, β and π^*, p=0.17. So it can be concluded that there is no correlation between the three Kamlet-Taft parameters and the ring flip activation energy, since all of the paired variables fail to pass a test for significance at the 95% confidence interval.

However if water is excluded from the data set a different picture emerges. The LSER of the experimental and predicted activation energies of $[C_1Hpyrr][NTf_2]$ in molecular solvents excluding water are shown in Fig. 3.9. The quality of the fit is

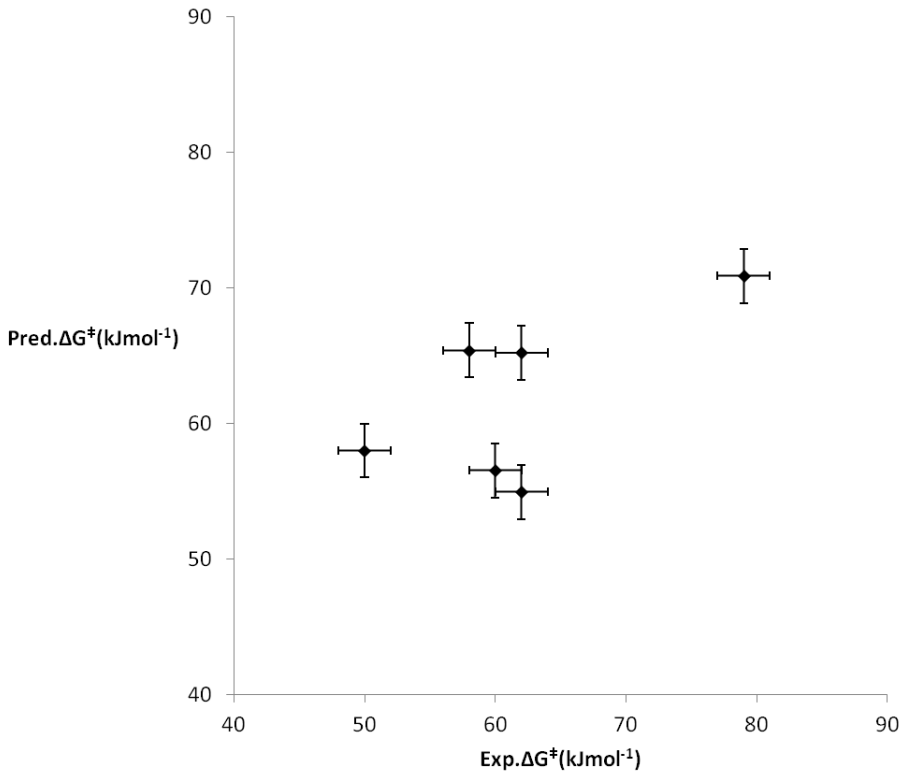


Figure 3.8: LSER showing Experimental (Exp.) and Predicted (Pred.) Ring Flip Activation Energies ($\Delta G^{\ddagger}$)

extremely high and the probability threshold value (p-value) is 0.0001. It is clear that water is behaving in a different manner to the other solvents. It is likely that this is a result of profoundly non-ideal mixing behaviour, given the hydrophobic nature of the $[NTf_2]^-$ anion and the relatively high concentration used in the experiments.

The full LSER for the correlation without water is shown in Equation 3.22.

$$\Delta G^{\ddagger} = -25.6 + 40.4\alpha - 37.7\beta + 115.6\pi^{*} \tag{3.22}$$

With the non-ideal behaviour of water eliminated it is concluded that the molecular solvents are affecting the ring flip activation energy of the reaction in some 'typical' way; additionally the parameters of the fitting show that no single solvent property is drastically affecting the ring flip activation energy. It can be seen that α and β are having approximately equal and opposite effects on the ring flip activation energy; an increase in α leads to an increase in the ring flip activation energy and an increase in β leads to a decrease in ring flip activation energy. Increasing π^{*} increases the ring flip activation energy and is having an effect about three times

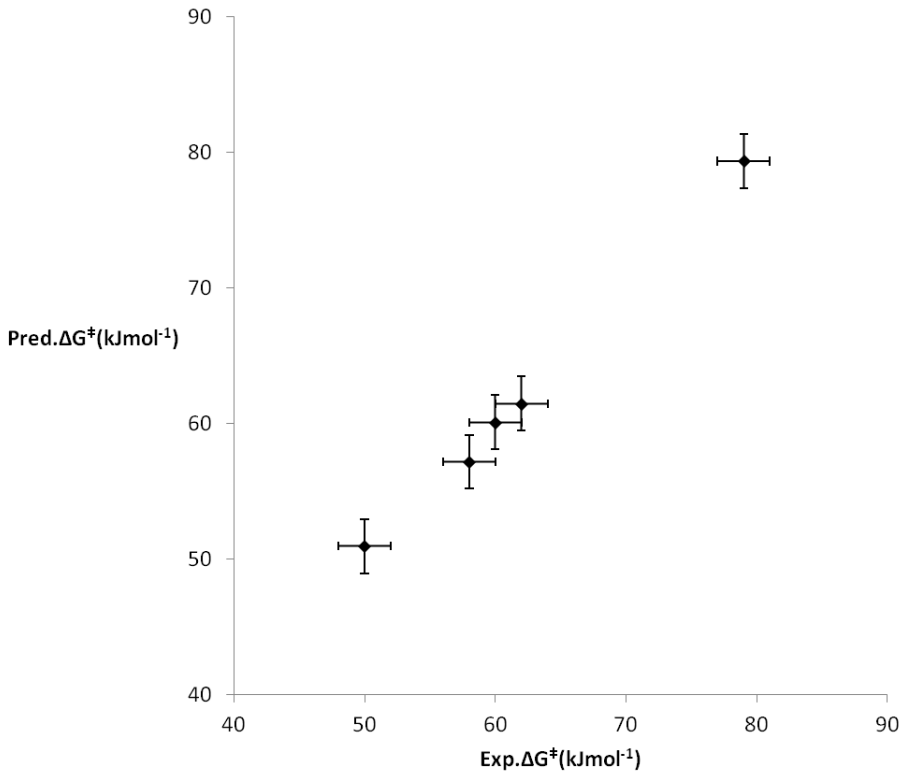


Figure 3.9: LSER showing Experimental (Exp.) and Predicted (Pred.) Ring Flip Activation Energies ($\Delta G^{\ddagger}$) exluding water

stronger than α. While the 'y-intercept' term seems to be large and negative, the intercept of the line of best fit in Fig. 3.9 is 0.2. The Kamlet-Taft parameters of DMSO are α=0, β=0.76, π^*=1, which gives a predicted ring flip activation energy of 61.5kJmol^{-1} which agrees with the experimental value of 62kJmol^{-1}. Therefore it is safe to continue with the analysis of the ILs in DMSO, knowing that while the DMSO is having some effect on the system, it is coming from 'normal' solvation behaviour and not from some specific effect unique to DMSO.

Unfortunately the Kamlet-Taft parameters of the ILs in this study are not known, nor were they determined experimentally because of the acidity of the $[HSO_4]^-$ ILs and that $[C_1Hpyrr]Cl$, $[C_1Hpyrr][OTf]$ and $[C_1Hpyrr][NTf_2]$ are all solids at room temperature.

3.3.3 Density Measurements

In order to determine the proportion of free volume in solution it was necessary to perform density measurements on the ILs. While this is relatively straight-forward, even for viscous liquids, the ILs that are solid at room temperature require a different approach. There are several alternatives: solid state density, melt density or solution density. Determining the solid state density can be done from a crystal structure, however one must then assume that there is no change in density upon melting which, although approximately true for ILs, is not very precise. Melt density is suitable if a wide enough temperature range is accessible to account for any temperature dependent changes in liquid density. Unfortunately the available densitometer only operates over a short range above room temperature. Finally a range of solutions of differing concentration can be made. This is suitable as it allows for the calculation of a theoretical liquid phase density at room temperature, however care must be taken to ensure that a relatively ideal solution is used; extremes in excess mixing properties will lead to a non-linear set of data. Acetonitrile was used as the solvent. Figs. 3.10, 3.11 and 3.12 show the density measurements of the three ILs [C_1Hpyrr][OTf], [C_1Hpyrr]Cl and [C_1Hpyrr][NTf_2], respectively.

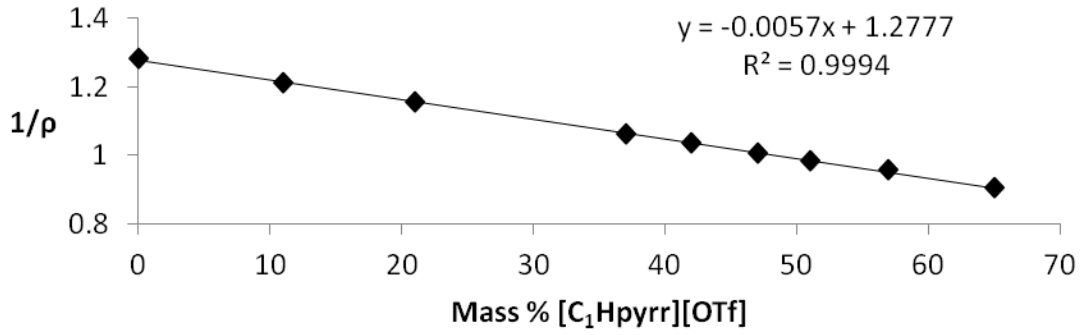


Figure 3.10: Density Measurement Of Mixture Of [C_1Hpyrr][OTf] And Acetonitrile

By extrapolating using the least squares fitting line estimate the density of the pure IL can be calculated. The fit is very good for all three ILs and appears to be completely linear, which, while not proving that the IL and acetonitrile mix ideally, shows that deviations from ideality are small and not compositionally dependent. The densities of the ILs studied are shown in Table 3.2.

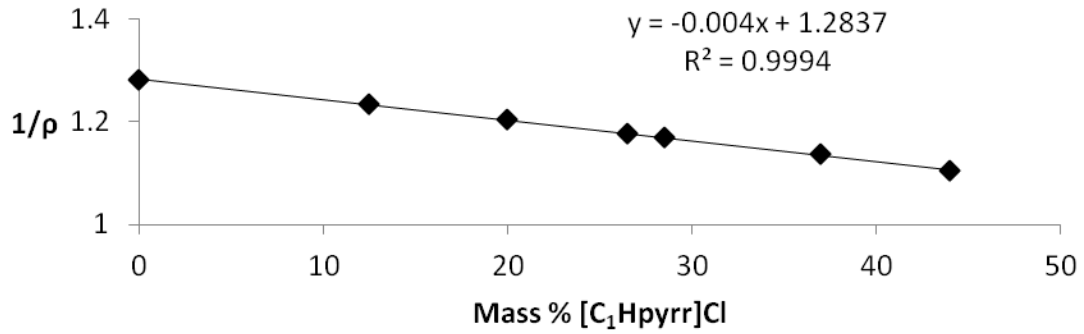


Figure 3.11: Density Measurement Of Mixture Of $[C_1Hpyrr]Cl$ And Acetonitrile

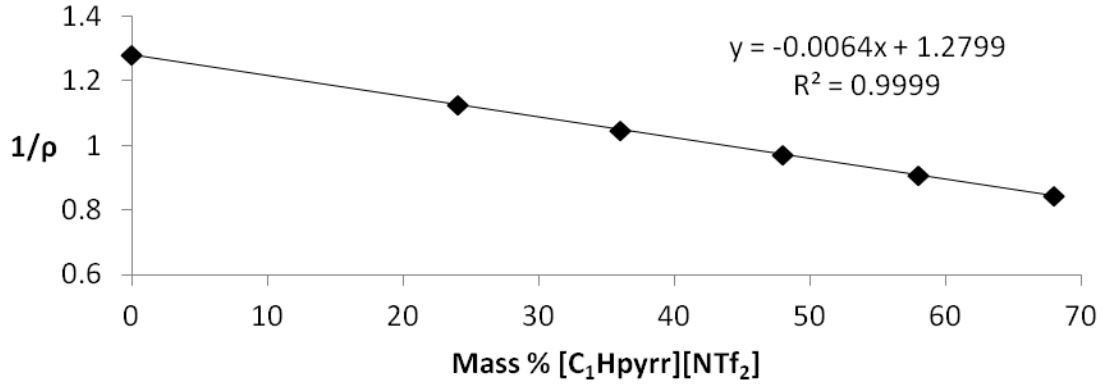


Figure 3.12: Density Measurement Of Mixture Of $[C_1Hpyrr][NTf_2]$ And Acetonitrile

As can be seen in Fig. 3.13 there is no clear trend linking activation energy with density, particularly when considering $[C_1Hpyrr]Cl$ and $[C_1Hpyrr][NTf_2]$, which have the lowest and highest densities, respectively, but identical ring flip activation energies. This agrees with the result of $[C_1Hpyrr][NTf_2]$ in molecular solvents, where no correlation was found between ring flip activation energy and the density of the solvent.

3.3.4 Free Volumes

The free volume of a solution is simply a measure of how much free space there is between ions (or molecules) in the solution and can be calculated by subtracting a theoretical volume from the real volume. Table 3.3 shows the volumes of the ions. The ionic volumes were calculated using the methods outlined in the introduction of

Ionic Liquid	Density(gcm^{-3})	$\Delta G^{\ddagger}$($kJmol^{-1}$)
$[C_1Hpyrr][HSO_4]$	1.36	72
$[C_2Hpyrr][HSO_4]$	1.30	70
$[C_3Hpyrr][HSO_4]$	1.26	82
$[C_4Hpyrr][HSO_4]$	1.22	80
$[C_6Hpyrr][HSO_4]$	1.15	84
$[C_1Hpyrr]Cl$	1.13	62
$[C_1Hpyrr][NTf_2]$	1.56	62
$[C_1Hpyrr][OTf]$	1.41	77

Table 3.2: Table of IL Densities and Ring Flip Activation Energies

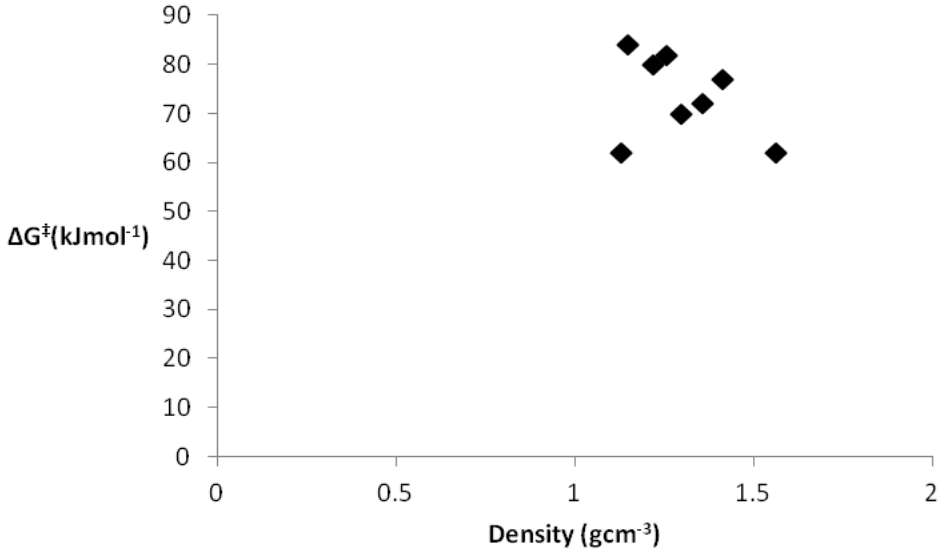


Figure 3.13: Activation energy of ring flip $\Delta G^{\ddagger}$($kJmol^{-1}$) vs. Density(gcm^{-3})

this chapter, with the exception of chloride. The two ionic volumes of the chloride in the table represent the upper and lower limit of the volume of a chloride anion, based on two different ionic radii. The lower limit comes from 'crystal' radius, which is 167pm, the upper limit is from the 'soft sphere' model, radius 218pm. This is a large variation; the contribution of the chloride ion to the total volume of $[C_1Hpyrr]Cl$ is 14% for the crystal radius and 26% for the radius using the soft sphere radius. This has a profound effect on the results and illustrates the difficulties in calculating ionic and molecular volumes. For a single spherical ion it makes a significant difference. For molecules and polyatomic ions much of the volume is internal, which means

deciding where the 'edge' of the molecular orbital is has a less significant effect on the total volume.

Ionic Liquid	Cation(Å^3)	Anion(Å^3)
[C_1Hpyrr][HSO_4]	74.09	53.38
[C_2Hpyrr][HSO_4]	93.14	53.38
[C_3Hpyrr][HSO_4]	101.07	53.38
[C_4Hpyrr][HSO_4]	117.21	53.38
[C_6Hpyrr][HSO_4]	145.48	53.38
[C_1Hpyrr]Cl	74.09	11.74-26.12
[C_1Hpyrr][NTf_2]	74.09	139.7
[C_1Hpyrr][OTf]	74.09	56.92

Table 3.3: Calculated Ionic Volumes

The molecular volumes (the sum of the ionic volumes) and densities (converted into a volume expression) can be combined to calculate the free volumes in solution. Table 3.4 shows the free volumes calculated for each pure IL, where Vol_t is the theoretical volume and Vol_r is the real volume. A similar treatment was applied to DMSO, the NMR solvent, and it was found to have a molecular volume of 66.16cm^{3}mol^{-1} and free volume of 11.66cm^{3}mol^{-1}.

Ionic Liquid	Vol_t(cm^{3}mol^{-1})	Vol_r(cm^{3}mol^{-1})	Free Vol(cm^{3}mol^{-1})
[C_1Hpyrr][HSO_4]	127.67	134.73	7.06
[C_2Hpyrr][HSO_4]	146.58	151.73	5.15
[C_3Hpyrr][HSO_4]	154.65	167.69	13.04
[C_4Hpyrr][HSO_4]	170.78	184.68	13.89
[C_6Hpyrr][HSO_4]	199.06	218.56	19.50
[C_1Hpyrr][NTf_2]	234.09	234.35	21.20
[C_1Hpyrr][OTf]	149.77	166.24	36.10
[C_1Hpyrr]Cl	100.21	107.62	7.41

Table 3.4: Ionic Liquid Volumes, Density, Free Volumes

The free volume of an ideal solution varies linearly as composition changes. Since all of the data was collected at 40mol% in DMSO it is possible to calculate the free

Ionic Liquid	Free Volume(cm^3mol^{-1})	Activation Energy ($kJmol^{-1}$)
$[C_1Hpyrr][HSO_4]$	9.82	72
$[C_2Hpyrr][HSO_4]$	9.06	70
$[C_3Hpyrr][HSO_4]$	12.21	82
$[C_4Hpyrr][HSO_4]$	12.55	80
$[C_6Hpyrr][HSO_4]$	14.80	84
$[C_1Hpyrr][NTf_2]$	15.21	62
$[C_1Hpyrr][OTf]$	21.08	77
$[C_1Hpyrr]Cl$	15.71	62

Table 3.5: Free Volume of Solutions of Ionic Liquds (40% in DMSO), and Ring Flip Activation Energies

volume of the solution. The free volumes and activation energies of the solutions are shown in Table 3.5 and are shown in Figure 3.14.

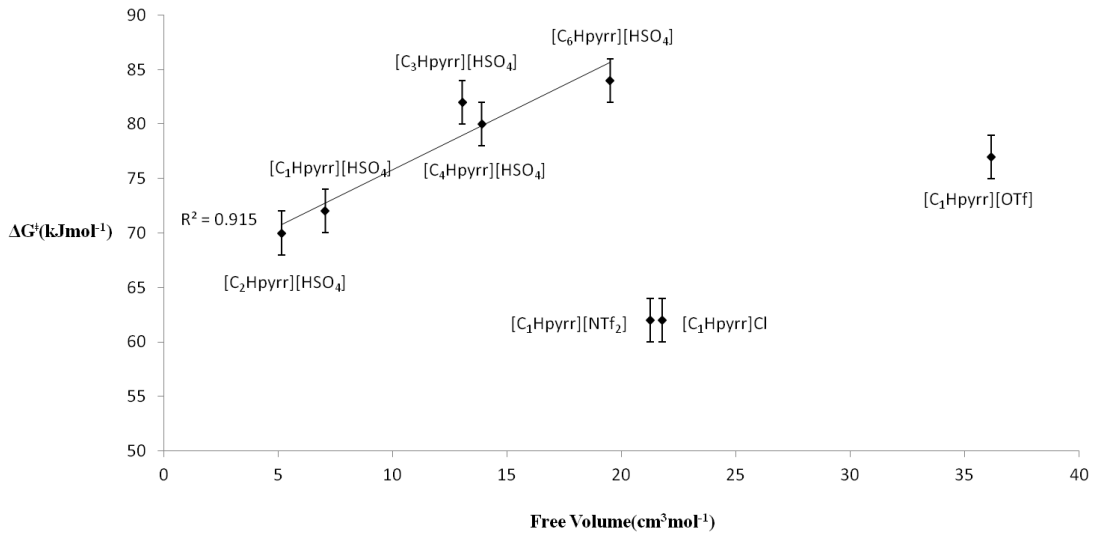


Figure 3.14: Ring Flip Activation Energy vs Free Volume

While there is no correlation for the ring flip activation energy across all the ILs, for the series of $[C_xHpyrr][HSO_4]$ (x= 1, 2, 3, 4, 6) ILs there is a correlation between the ring flip activation energy and the free volume. The coefficient of determination (R^2) of the $[C_xHpyrr][HSO_4]$ (x=1, 2, 3, 4 or 6) series alone is 0.92 and the residual values (predicted ring flip activation energy minus observed ring flip activation energy) are all within the experimental error, with the exception of the $[C_3Hpyrr][HSO_4]$, which

has a residual of 3kJmol^{-1}. The threshold value of the test statistic (p-value) for this data is 0.0108, so it passes the 95% confidence test.

That the ring activation energy of [C$_x$Hpyrr][HSO$_4$] ILs in DMSO increases as the free volume increases is quite unusual; it would be expected conceptually that a larger free volume of solution would reduce the ring flip activation energy, however that is not the case here. While the precise explanation is not known it is likely that there is some underlying entropic effect which is affecting both properties simultaneously.

3.4 Results of study of ring flip activation energy of [C$_1$Hpyrr]$^+$ cation in [C$_1$Hpyrr][HSO$_4$] and [C$_4$C$_1$im][NTf$_2$] mixtures

The ILs studied thus far been examined at a fixed concentration in a solution in order to eliminate any concentration effect. It was decided to examine the way in which the ring flip activation energy changes as the concentration composition of the mixture changes. This was done in a mixture of [C$_1$Hpyrr][HSO$_4$] and [C$_4$C$_1$im][NTf$_2$] as this also provided the opportunity to examine the nature of mixing in ILs from a thermodynamic perspective.

The results of the mixing study are shown in Figures 3.15 and 3.16, plotted against more fraction of [C$_1$Hpyrr][HSO$_4$] and free volume, respectively. What can be seen is a linear change in ring flip activation energy with the free volume of the mixture. The concentration range is from 5 mol% to 45 mol% of [C$_1$Hpyrr][HSO$_4$]; it was not possible to use mixtures with a higher mole percentage of [C$_1$Hpyrr][HSO$_4$] because the coalescence temperature of the ring protons was above the temperature limit of the spectrometer and below 5mol% the temperature dependent peaks become difficult to locate on the baseline.

These results show that as the free volume of the solution increases the activation energy of the [C$_1$Hpyrr][HSO$_4$] decreases. Unfortunately it was not possible to probe

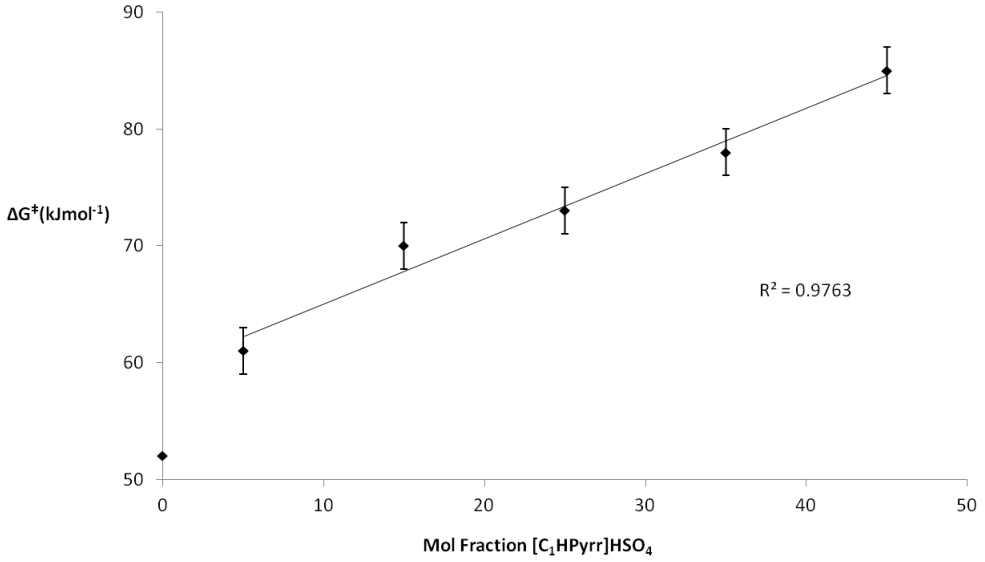


Figure 3.15: Activation Energy of Ring Flip vs Free Volume of mixture of $[C_1Hpyrr][HSO_4]$ and $[C_4C_1im][NTf_2]$

very dilute or very concentrated mixtures, so the limiting behaviour has not been examined, however it is clear that there is a statistically significant correlation; the threshold value of the test statistic (p-value) is 0.0011, so it passes the 99% confidence interval. The trend found here is the opposite of the correlation between free volume and ring flip activation energy of $[C_xHpyrr][HSO_4]$ ILs in DMSO, which is unusual. The result here agrees with the expectation result that the ring flip activation energy of $[C_1Hpyrr]^+$ decreases as the free volume increases.

This result provides support for the conclusions about the correlation between free volume and activation energy and is in agreement with existing literature, stating that ILs mix almost ideally.[46,93] The linear change in ring flip activation energy and mole fraction of $[C_1Hpyrr][HSO_4]$ in the mixture with $[C_4C_1im][NTf_2]$ suggests that the ring flip is dependent on a bulk property; dependence on specific interactions would result in large deviations from linearity.

The results show behaviour that is analogous to the behaviour seen by Lui *et al.*.[44] They found that the molar extinction coefficient of Kosower's complex (a substituted pyrridinium iodide) is linear with its concentration in an IL, where as in a molecular solvent the molar extinction coefficient is essentially constant. Here we

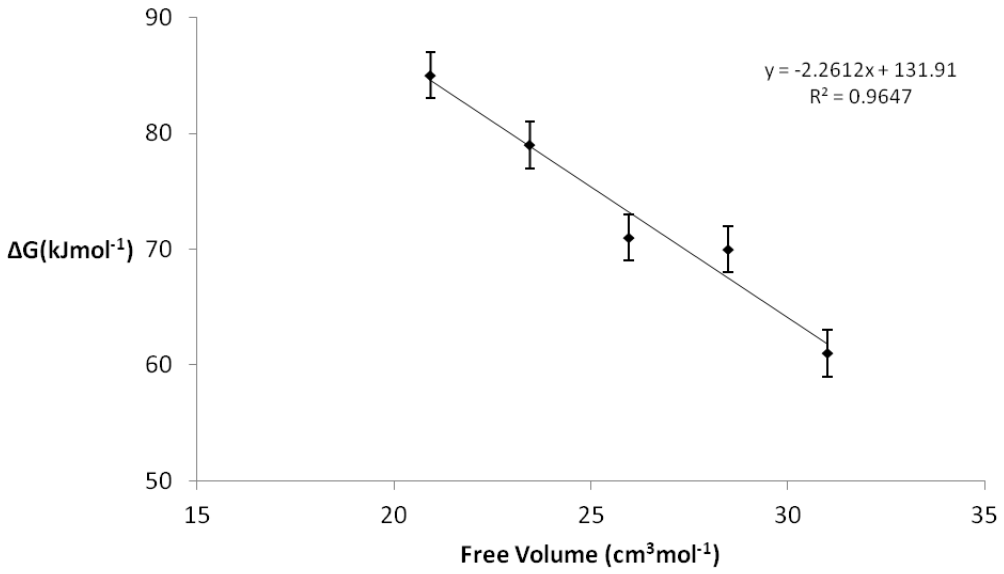


Figure 3.16: Activation Energy of Ring Flip vs Free Volume of mixture of $[C_1Hpyrr][HSO_4]$ and $[C_4C_1im][NTf_2]$

find that the activation energy of the ring flip varies linearly between what should be the activation of energy in pure $[C_1Hpyrr][HSO_4]$ and the activation energy of $[C_1Hpyrr][HSO_4]$ at infinite dilution in $[C_4C_1pyrr][NTf_2]$.

3.5 Conclusions

The efforts to discover the fundamental relationships governing the ring flip behaviour of these pyrrolidinium based ILs has been frustrated at every step by numerous complications and limitations. It would have been preferable to work in the pure melt phase at all times, however the fact that some of the ILs are solid at room temperature and the spectra of the other ILs coalesced outside of the spectrometer's range set the study off on a difficult footing. Working at a fixed concentration in DMSO was a practical solution to this problem, as it effectively removed both of these limitations.

The main results of interest are as follows. There is a LSER that determines the ring flip activation energy of $[C_1Hpyrr][NTf_2]$ in molecular solvents, although this relationship does not predict the behaviour of the aqueous system because of non-

ideal mixing caused by the hydrophobic $[NTf_2]^-$ anion.

There is a correlation between the ring flip activation energy of the $[C_xHpyrr][HSO_4]$ (x= 1, 2, 3, 4, 6) ILs and the free volume of the solution. As the free volume increases the ring flip activation energy increases. This was the only satisfactory correlation found because of the finding that $[C_2Hpyrr][HSO_4]$ has a lower ring flip activation energy than $[C_1Hpyrr][HSO_4]$ and the rest of the series increases according to the alkyl chain length.

There is also a correlation between the ring flip activation energy of $[C_1Hpyrr][HSO_4]$ and the free volume in mixtures of $[C_1Hpyrr][HSO_4]$ and $[C_4C_1im][NTf_2]$. In this case the ring flip activation energy decreases as the free volume of the solution increases.

These two opposite correlations with free volume are remarkable and are not simply explained. It is likely the there is an underlying entropic effect governing the behaviour of the $[C_xHpyrr][HSO_4]$ series of ILs, however that effect is not known. It is likely that in order to elucidate this relationship further complete thermodynamic data would have to be gathered for these ILs.

Other work on this area could take a number of approaches. It would perhaps be prudent to investigate a second anion with a series of different alkyl chain lengths on the cation. Also using other anions derived from acids would be interesting; nitrate or phosphate anions would produce liquids similar to the hydrogensulfate salts. A mixing study of at least $[C_1Hpyrr][HSO_4]$ and DMSO could be undertaken, if only for the sake of completeness.

Another question remains; in the absence of a strong hydrogen bonding interaction involving the N-H bond, what is it about the $[C_1Hpyrr]^+$ systems that hinders the activation energy of the ring flip relative to $[C_4C_1pyrr]^+$ system? This merits close consideration and offers numerous potential avenues of exploration. Further investigation could begin by examining the ring flip activation energy of $[HHpyrr][HSO_4]$, $[C_1C_1pyrr][HSO_4]$ and the $[C_4C_1pyrr][Y]$ (Y=$[HSO_4]$, [OTf] or Cl).

Should further investigation be pursued, it is clear that a plethora of thermodynamic data will be required to elucidate fully the behaviour governing the ring flip of pyrrolidinium based ILs.

Chapter 4

X-Ray Diffractometry of Imidazolium Ionic Liquids

4.1 Aims

Dispersion interactions are weak intermolecular attractions which are prominent in systems with a large number of electrons and systems that are polarisible. There is some unpublished computational data, from within the group, that shows IL anions are capable of dispersion interactions, which can result in a favourable (if relatively weak) interaction with the alkyl chain of the cation.[94] Unfortunately, there is no direct experimental measurement for dispersion interactions, however their presence and absence may be inferred with careful experimental design.

The aim of this chapter is to investigate the role that the anion's dispersion interactions play in the structure of ILs and what types of structuring are present in ILs. In order to do this, a range of ILs with symmetric or asymmetric imidazolium cations with a variety of anions were synthesised. The cations are $[C_xC_1im]^+$ (x=4, 6 or 8), $[C_6C_2im]^+$, and $[C_xC_xim]^+$ (x=4 or 6). The anions are Cl^-, Br^-, $[NTf_2]^-$, $[NO_3]^-$ or $[SCN]^-$.

These dispersion interactions will be examined using small angle X-Ray diffractometry. The peak positions and intensities provide information about the liquid state

structure. In particular inspection of the scattering peak caused by alkyl chain-alkyl chain interactions (which will be introduced fully in the following sections)will enable dispersion interactions between the alkyl chains and anions to be inferred if they are present.

The X-Ray diffractometry was performed at Imperial College London on a laboratory X-Ray beamline and also at the Diamond Light Source, the UK synchotron X-Ray Source. The details of the laboratory beamline are given in Section 4.3.

The scattering patterns will be treated mathematically, using Gaussian fitting methods to determine the peak positions and intensities, details of which can be found in Section 4.3.6

4.2 Introduction

There are two broad categories of liquid systems that have profound structural anisotropy. The first is lyotropic liquid crystals, which are multicomponent systems. A lyotropic crystal is a chemical compound that will form liquid crystal phases upon the addition of (certain) solvents. The second is thermotropic liquid crystals. A thermotropic liquid crystal is a compound that will for liquid crystal phases in its pure molten state over some temperature range. Lyotropic liquid crystals can, in the context of ILs, be further split into systems in which the IL is the amphiphile and systems in which the IL is the medium. The behaviour of ILs as the amphiphile will not be discussed here, as it does little to inform discussion of the pure IL state. The behaviour of ILs as self-assembly media and the thermotropic behaviour of ILs will be reviewed below.

4.2.1 Ionic Liquids as self-assembly media

Self-assembly of amphiphiles was first reported in ionic media in series of papers by Reinsborough and Bloom in the late 1960s. They investigated surfactants in molten pyridinium chloride.[95,96] At a similar time Ray[97] discovered that ethane-1,2-diol

(ethylene glycol) also induces self-assembly of amphiphiles. These two discoveries are believed to be the first reports of self-assembly in non-aqueous media.

The first report of an IL as a medium for self-assembly was ethylammonium nitrate (EAN).[98,99] This puts ILs on a short list of solvents that can promote self-assembly. This list include various glycols, formamides and hydrazine. The inclusion of ILs in this select group of solvents opens up an interesting avenue for exploring the behaviour of lyotropic systems, because normally only the surfactant can be systematically modified (with the exception of the small range of formamides which have been systematically studied in some limited sense[100]). Up until 2005, other than EAN, the only ILs investigated were $[C_4C_1im][PF_6]$ and $[C_4C_1im]Cl$.[101] There are also two short reviews on the use of ILs in the synthesis of inorganic materials, which are of interest because of the way in which amphipilic substances can be used to template nanoparticle growth.[102,103] This application has driven much of the recent interest in ILs as self-assembly media.

Ethylammonium nitrate is the most widely studied of all ILs in this area. Thermodynamic measurements showed that the free energy of transfer of a non-polar gas into EAN is similar, but slightly less, than the free energy of transfer of a non-polar gas into water. The behaviour is dominated by entropic contributions at room temperature.[104] In contrast to this, the transfer of alcohols into EAN was found to be dissimilar to the transfer of alcohols into water but similar to transfer of alcohols into polar aprotic solvents such as DMF, DMSO and ethylene glycol.[105] These data suggest that the alkyl chains of the alcohols are more stable in EAN than in water. This means there is less of an entropic force driving self-assembly in EAN systems than in aqueous systems. This is because self-assembly of the alcohols in EAN requires less structure breaking of the EAN solvation sphere around the alcohol alkyl chains. This may seem counter-intuitive, however alkyl chains in water induce extremely organised structuring in the solvation shell, which must be broken before self-assembly occurs. That the alkyl chains are more stable in EAN means the solvation shell need not be so strictly organised in order to minimise the free energy of the system. This data has been corroborated by measurements on phosphlipids in EAN, which shows they adopt more curved structures than the corresponding

aqueous systems.[106,107]

Another feature of self-assembly in EAN that is different than in similar aqueous systems is the partial molar volumes of each component in the system. In aqueous systems the partial molar volume of water increases upon micelle formation, whereas in EAN there is no significant change in its partial molar volume.[108] Again this can be resolved by the need for water to tightly structure around the alkyl chains of the solute molecule. When the water is tightly bound around the freely solvated alkyl chains of the solute, its partial molar volume decreases. Above the CMC (critical micelle concentration) there is no water-alkyl chain interaction, so the partial molar volume increases. In EAN there is no significant rearrangement around the freely solvated alkyl chains, thus there is no increase of partial molar volume above the CMC.

One of the distinguishing features of self-assembly behaviour is the presence of a CMC. Below the critical micelle concentration the amphiphiles are almost entirely at the solution interfaces (typically the liquid gas interface, as water interacts favorably with glass). This effectively minimises the free energy by minimising the number of unfavourable interactions between the water and the solute alkyl chains. However above a certain concentration of amphiphile the most effective way to minimise the free energy is to form micelles in the solution with the head-groups towards the solvent and the non-polar chains clustered in the interior. This sudden switch from surface activity to micelle formation is characteristic of self-assembly and when it occurs sharp deviations in properties such as surface tension and conductivity are observed.

It has been suggested that in polar aprotic solvents micelle formation is *via* freely solvated monomers, dimers, trimers and small aggregates combining, which explains the lack of a sharp changes in the properties of these systems,[109] in comparison to the sharp changes in the properties of similar aqueous systems. At present this seems to be a hypothetical explanation based only on the absence of a sharp CMC; dynamic light scattering (DLS) experiments would provide valuable data on the polydispersity of aggregates in these systems, as micelles in aqueous media are quite monodisperse.

While there is only a limited data set available thus far, the ILs studied all have a sharp CMC. So far there are data on EAN, $[C_2C_1im][NTf_2]$, $[C_4C_1im]Cl$ and $[C_4C_1im][PF_6]$ with a wide range of surfactants.[42] There is also a more extensive list of Gordon parameters of ILs. The Gordon parameter (G) is the surface tension (γ) divided by molar volume (V) to the power of one third, and is shown in Eqn. 4.1. The Gordon parameter is a predictor of a solvent's ability to induce self-assembly in amphiphiles, with higher values indicating an greater ability to induce self-assembly in amphiphiles. The Gordon parameters of ILs predict that many of them will be capable of inducing self-assembly behaviour.

$$G = \frac{\gamma}{V^{\frac{1}{3}}} \tag{4.1}$$

While most studies of lyotropic behaviour focus on relatively dilute solutions, there are a few investigations that discuss the whole concentration range of an amphiphile in an IL. Hexadecyltrimethylammonium bromide (CTAB) and 3,7,11,15-tetramethylhexadecane-1,2,3-triol (phytantriol) were investigated as the amphiphiles in a number of ILs.[110,111] Two amphiphiles were needed in order to examine all of the lyotropic phases, because of the effect of the surfactant shape on the liquid crystal phases which can be formed. This is quantified by the critical packing parameter. The critical packing parameter (CPP) is shown in Eqn. 4.2 is the ratio of the amphiphile volume (v) and the product of the head group cross section area and the amphiphile length. The CPP is a predictor of the type of lyotropic phase an amphiphile will form.

$$CCP = \frac{v}{a.l} \tag{4.2}$$

CTAB has a low critical packing parameter and tends to form normally curved surfaces (micelles and hexagonal phases). Phytantriol has a higher critical packing parameter and tends to form negatively curved surfaces (inverse micelles and inverse hexagonal phases). Using these two amphiphiles it was found that all of the liquid crystalline phases can be formed in ILs.[110,111]

There has been a small investigation into aggregation of the amphiphilic ILs

$[C_{16}C_1im][BF_4]$ and $[C_{16}C_1im]Cl$ in EAN,[112] which found that critical aggregate concentrations* were similar to other amphiphiles in EAN and about a factor of 100 greater than the CMC in water.

These data all show that ILs act as highly polar environments, in which aliphatic molecules are unstable and tend towards segregation. Many ILs have an aliphatic segment that is destabilised and will tend to segregate or separate where possible. This effect is discussed in the next section, which is divided into 'long chain' and 'short chain' sections. For the purposes of this thesis 'long chain' refers to systems where the longest alkyl chain (or chains) is dodecyl or longer. This cut-off has been chosen because it is the chain length of the shortest birefringent ILs reported to date in the literature; $[C_{12}C_1im]Cl$[113] and $[C_{12}C_1im][PF_6]$[53] are both birefringent.

4.2.2 Structuring in neat long chain Ionic Liquids: Thermotropic Liquid Crystals

4.2.2.1 Thermotropic Liquid Crystal Phases

A thermotropic compound is a liquid that has some form of anisotropy in its liquid state over some temperature range; that is, it forms a liquid crystal. This leads to many properties, such as refractive index, electrical permitivity and some mechanical properties, being dependent on the direction in which they are measured. All liquid crystals have an upper temperature limit, beyond which structuring is lost and the liquid becomes isotropic; this effect is entropically driven. In lyotropic systems (that is, multi-component systems) the ordered component is typically referred to as an amphiphile; in thermotropic systems (that is, single component systems) it is called a mesogen. While many molecules that are amphiphiles will also be mesogens, the most common moieties of each class of compound are different. Lyotropic amphiphiles most commonly consist of a charged head group with an alkyl tail. Mesogens share the alkyl tail, although the head group is typically a rigid

*In this paper the exact nature of the aggregate was not confirmed; only DLS measurements of aggregate sizes and distributions were collected; hence the use of critical aggregate concentration rather than a more specific term, like CMC

substituted biaryl structure, for example *N*-(4-methoxybenzylidene)-4-butylaniline, shown in Fig. 4.1.

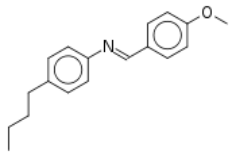


Figure 4.1: *N*-(4-methoxybenzylidene)-4-butylaniline

Liquid crystals are generally conceptualised as pipes or as being pill shaped, however they can also be disks and there are a few interesting examples of banana shaped molecules exhibiting liquid crystallinity.[114–117]

Thermotropic liquid crystals exist in one of a number of phases which have varying degrees of local and long range order. Since most ILs are rod-like, discussion here will be limited to the liquid crystal phases of rod-like molecules. There are two broad categories of liquid crystalline phases for rod-like molecules, these are the nematic phase and the smectic phase, sketches of which are shown in Figs. 4.2 & 4.3.[118]



Figure 4.2: Sketch of the nematic phase[118]

The nematic phase is the least ordered of the liquid crystal phases. In the nematic phase the mesogens are aligned along the long axis of the molecule, which is called the director. The nematic phase is fluid in all directions, however the rates of diffusion parallel and perpendicular to the director are not necessarily equal. In an isotropic liquid diffusion is equal in any direction.

The smectic phases have an additional degree of ordering. The simplest of which is the smectic A phase, in which the mesogens are aligned with the director and

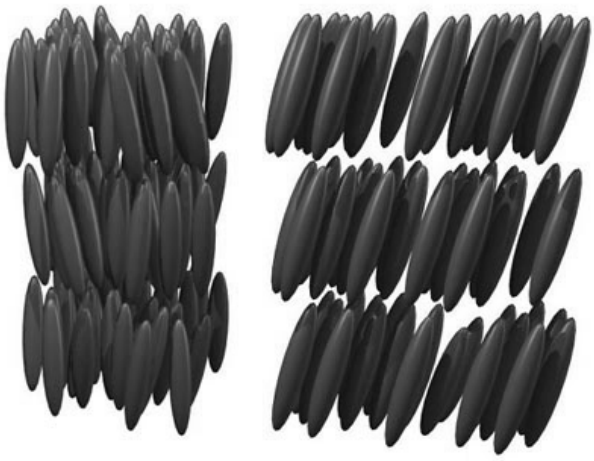


Figure 4.3: Sketch of the smectic A and smectic C phases[118]

are organised into layers in the plane perpendicular to the director, as shown in Fig. 4.3. Smectic phases are completely fluid in the plane, however the exchange of mesogens between layers is slow (although not zero). There are a wide variety of smectic phases, and both nematic and smectic phases can exist in chiral forms.

The use of ionic components in liquid crystals is not unusual; their use is particularly relevant in areas where anisotropic electrical properties are required, for example liquid crystalline displays.

The use of ionic compounds as liquid crystals has been reviewed comprehensively up until 2005 by Binnemans.[119] What follows is an overview of the literature in which ILs or similar compounds are the subject; while there are fascinating examples of biphenyl substituted imidazolium compounds showing thermotropic behaviour,[120] they do not inform our discussion of the structure in RTILs.

4.2.2.2 Thermotropic Behaviour of long chain Ammonium compounds

Alkylammonium chlorides have been investigated with alkyl chains from hexyl to octadecyl[121] and upon heating all undergo a plastic transition (where the alkyl chains melt but the head group remains fixed), then transition into the liquid crystalline smectic A phase, followed by a 'clearing' transition when the liquid becomes isotropic.

Primary amines have also been combined with various acids,[122,123] while mesophases were seen in decylammonium phenylsulfonate, the mesophases were stabilised by using pyridine-3-sulfonate and various napthalene sulfonates, instead of the simple phenylsulfonate. In this context stabilised means the temperature range over which the liquid crystal phase is observed is increased.

There are also some examples of alkylammonium salts with more complex anions that exhibit mesomorphic behaviour, including carboxylic acid derivatives of guadanine and cytosine,[124] and tetrachlorometalates[125–129] which exhibit some unusual anion structures.

Tetraalkylammonium compounds are more widely studied than *N*-alkylammonium compounds, however alkyltrimethylammonium halides are thermally unstable, which limits their thermal range and longevity. Alkyldimethylpropylammonium halides have improved thermal stability (the addition of a single propyl group hinders the approach of a nucleophile to σ^* of the alkyl group, which prevents dealkylation).

Mesophases have been observed for dodecyldimethylpropylammonium bromide and various similar compounds substituted at the 3-propyl position.[130–133] The thermotropic behaviour of alkyldimethylpropylammonium alkane- and benzene-sulfonates have been investigated and all samples exhibited liquid crystalline behaviour.[122,134]

A new type of smectic phase, the smectic T phase, was discovered following investigation into dialkyldimethylammonium bromides,[135] where the T phase has Bragg peaks at integer ratios (in reciprocal space) in the small angle X-ray diffraction (SAXS) region, which indicate a lamellar phase, and peaks in the wide angle X-ray diffraction (WAXS) region with relative spacings of $\sqrt{2}$:$\sqrt{4}$:$\sqrt{5}$, which indicate a tetragonal lattice. A smectic T phase was also found in dialkyldi-(2-hydroxy)-ethylammonium bromide. Some more complex systems incorporating diazobicyclooctane also exhibit a smectic T phase.[136]

Similar to the alkylammonium tetrachlorometallates, tetraalkylammonium tetrachlorometallates show thermotropic behaviour;[137] the addition of the metal centre in these examples induces mesomorphic behaviour in tetraalkylammonium halides that otherwise don't exhibit liquid crystallinity. As both alkylammonium halides

and tetraalkylammonium halides can have mesomorphism induced by the addition of metal halides, it is clear that the formation of hydrogen bonds between the cations an anions is not the driving force for the mesophase formation. The ability of the anions to form extended stable structures with themselves is what induces the mesomorphism.

A vast range of variations of tetraalkylammonium compounds have been synthesised and categorised, such as using cholestanyl groups (very similar to cholesterol) on the ammonium centre.[138] There are also examples of bis-(2-hydroxyethyl)-ω-(biphenyl)alkylammonium chlorides,[139] $\alpha-\omega-$diquaternary ammonium salts[140] and complexes of benzenehexacarbolxylic acid and (6 equivalents of) didodecyldimethylammonium bromide, all of which have exhibited thermotropic behaviour, although the last example surprisingly existed in a lamellar phase rather than a discotic phase.[141]

Phosphonium based mesogens have been examined in detail elsewhere[119] and generally have a wider mesophase range and higher clearing point than the corresponding ammonium salts. They also tend to spontaneously form a non-centrosymmetric bilayer system from which arises spontaneous polarisation caused by displacement of the smectic layers.[142,143] This is different to ammonium based systems, which may not exhibit spontaneous birefringence under a polarising microscope because they form extended homeotropic domains; they often only exhibit birefringence under mechanical strain.

4.2.2.3 Thermotropic Behaviour of long chain Pyridinium compounds

Thermotropic mesomorphism in pyridinium halides was observed as early as 1938, when pyridiniums bearing 12, 14, 16 and 18 carbon length N-alkyl groups were synthesised and investigated.[144] The chloride mesophases were found to be more stable than the bromide and iodide mesophases. The mesophase of $[C_{16}py]Cl$ was later identified as a smectic A phase by Somashekar *et al.*[145] and, in the opinion of the author, it would be reasonable to expect the others to be similar.

There is no requirement for the long chain to be on the nitrogen; indeed Fürst

and Dietz found liquid crystallinity in a variety of 1-methyl-3-alkylpyridinium methosulfates (7-Methoxy-1-methyl-isoquinolin-6-olate) and tosylates, 1-methyl-3-alkoxypyridinium methosulfates and tosylates, and 1-methyl-3-thioalkylpyridinium methosulfates and tosylates.[146]

The chloride salts of 1-protonated 2-alkylpyridines are mesomorphic, however the picrate and picrolinate salts are not.[144] 1-protonated 4-alkylpridinium halides are not mesomorphic, however 1-methylated equivalents are mesomorphic.[147] Interestingly a study of 4-dodecyl-1-alkylpyridinium iodide showed that when the 1 position is methylated thermotropic mesomorphism occurs, however it is absent when the 1 position is either hydrogen, ethyl, *n*-propyl, *i*-propyl, *n*-butyl, *n*-hexyl, 3-hydroxypropyl or 2-methoxyethyl.[148] This is particularly curious in comparison to quaternary ammonium salts, in which 3-hydroxypropyl groups stabilise the liquid crystal phase.

Another interesting feature of the phase behaviour of alkylpyridinium compounds is the stark difference in liquid crystal phase ranges of salts with only small changes in alkyl chain length; 4-dodecyl-1-methylpyridinium iodide has a melting point of 113^{o}C and clearing point of 148^{o}C (a stable liquid crystal range of 35^{o}C), while 4-tetradecyl-1-methylpyridinium iodide has a melting point of 115^{o}C and clearing point of 208^{o}C (a liquid crystal range of 93^{o}C).[148] 1-alkyl-4-methylpyridinium bromides show a similar trend with slight increases in melting point but significant increases in clearing point.[149] Pyridinium compounds of this category have a strong tendency to form large homeotropic regions.[150] Homeotropic regions occur when the director of the mesogen is perpendicular to the substrate or interface, which means they are not birefringent. If the 4-position is replaced with a cyano-group the melting point is increased with no significant change in clearing point, so the mesophase is destabilsed.[151] The structure of the mesophase is also different; while 1-(n-hexadecyl)-4-methylpyridinium iodide has a smectic A phase, 1-(*n*-hexadecyl)-4-cyanopyridinium iodide exists in a smectic B phase.[152] 1-(*n*-hexadecyl)-4-cyanopyridinium iodide also exhibits a distinct thermochromic shift. It is yellow in its crystalline form and red in its liquid crystal state.

4.2.2.4 Thermotropic Behaviour of long chain Imidazolium compounds

For the homologous series of 1-alkyl-3-methylimidazolium halides the melting point minimum is around the *n*-octyl chain length, and the chain length above which Van der Waals interactions become significant is about 12 carbons long (dodecyl). Further complexity is evident because the imidazolium compounds which are liquid at or near to room temperature also have a propensity to super-cool and to form glasses when cooled below their freezing point. Although the melting point is said to be a minimum around $[C_8C_1im]^+$ the melting points are not known; $[C_6C_1im]Cl$ is reported to have a glass transition temperature of 198.1K and $[C_8C_1im]Cl$ a glass transition at 186.1K[56] and neither have a reported freezing point.

Bowlas *et al.*[113] reported the DSC behaviour of the $[C_xC_1im]Cl$ (x=12, 14, 16 or 18) and showed that they exhibit a smectic mesophase which is quite thermally stable. The stability increases with alkyl chain length from about 90^{o}C above the MP to about 150^{o}C above the MP for x=12 and x=18 respectively.

$[C_xC_1im][PF_6]$ salts have been investigated,[153] and it was found that when x =14, 16 or 18 thermotropic behaviour was observed, however for $[C_xC_1im][BF_4]$ ILs thermotropic behaviour was also seen for x=12.[53] This is consistent with larger, more spherical, ions disrupting thermotropic behaviour; while size is not explicitly structure forming or breaking, high symmetry tends to be structure breaking given the requirement for anisotropy. It was again noted in this study that the ILs were prone to form single homeotropic regions which were poorly visualised under a polarising microscope. Also relevant here is a study of $[C_{14}C_1im][PF_6]$ and $[C_{16}C_1im][PF_6]$ which discovered an additional solid-solid transition in these compounds using quasi-elastic neutron scattering.[154] This transition had previously been unobserved using DSC and is attributed to an increase in structural freedom of the alkyl chains without corresponding melting of the imidazolium rings. There are also some SAXS and conductivity data that suggest there exist 'ionic aggregates' or regions of lamellar sheets above the clearing temperature of $[C_{16}C_1im][PF_6]$.[113]

A range of ILs were investigated by Bradley *et al.*,[155] who examined the behaviour of $[C_xC_1im]Y$ ILs, where x=12, 14, 16 or 18 and Y= Cl^-, Br^-, $[BF_4]^-$, $[OTf]^-$ or

$[NTf_2]^-$. No mesosphases were seen for any of the $[NTf_2]^-$ ILs and small mesophase ranges were seen for $[C_{16}C_1im][OTf]$ and $[C_{18}C_1im][OTf]$, but not $[C_{12}C_1im][OTf]$ and $[C_{12}C_1im][OTf]$. The $[BF_4]^-$, Cl^- and Br^- salts showed mesomorphic behaviour for all chain lengths studied and, in agreement with Bowlas *et al.*,[113] the mesophase range became wider as the chain length increased. The phase was identified as a smectic A_2 phase, which is an interdigitated bilayer, the spacing of which correlates with the size of the anion, although the authors attribute the same trend to the ability of the anions to form a three dimensional hydrogen-bonding lattice. While this is also true, there is no evidence presented to suggest an extensive hydrogen bond network is formed and in crystal structures (where available), the $[BF_4]^-$, $[PF_6]^-$, $[OTf]^-$ and $[NTf_2]^-$ salts do not have any interactions that indicate a strong hydrogen bond. That there may be some directional alignment with a C-H bond is normal in minising total energy and does not necessarily indicate a hydrogen bond.

There is also a small amount of work on symmetric 1,3-dialkylimidazolium salts,[156,157] where mesophases were observed in the chloride and bromide salts and described as bilayered lamellar (L_α) phases, but no mesophases were seen in the iodide or hexafluorophosphates.

There is also some work concerning 1-alkyl-3-H-imidazolium salts of chloride, nitrate and tetrafluoroborate.[158] While $[C_{12}C_1im][BF_4]$ and $[C_{12}C_1im]Cl$ are the shortest chains at which a mesophase in seen in dialkylimidazolium salts, both $[C_{10}Him][BF_4]$ and $[C_{10}Him]Cl$ exhibit a smectic A phase. The authors do not speculate as to why 1-alkyl-3-H-imidazolium salts are mesomorphic and 1-alkyl-3-methylimidazolium salts are not. An MD investigation into this would provide valuable information about what governs the formation of stable mesophases in these systems.

As with other cation classes there is a range of more elaborate examples of mesogens incorporating imidazolium moieties, however they bear little resemblance to ILs and are thus excluded here.[159,160]

4.2.3 Structuring in neat short chain Ionic Liquids

The question of what, if any, structuring exists in short chain ILs is one of the main questions this thesis seeks to answer. There is some data already available,[53,57,58,161–165] although there is no consensus on the nature or degree of structuring in ILs.

The techniques used to investigate structuring in ILs are the same as those used to investigate longer chain ILs. The most important measure of whether something is in a liquid crystalline state is the presence of an additional phase transition in the liquid range. This is called the clearing point, when the liquid transitions from being a liquid crystal to an isotropic liquid. Below the clearing point it is also expected that the liquid crystal state be birefringent, although, as has been stated earlier, the formation of continuous homeotropic domains in a liquid crystal suppresses birefringence. Additionally, liquid crystal phases have peaks in the SAXS regime that correspond to the repeat spacing parallel to the director; the precise position and distribution of these vary with the type of mesophase generated. While little emphasis was placed on the results and methods in the previous section, they will be discussed in greater detail in this section.

A complete study of $[C_xC_1im][BF_4]$ ILs (x=0-16, or 18) was undertaken by Seddon and Holbrey,[53] who examined the samples using DSC and polarising microscopy. All of the ILs showed some propensity to super-cool; the difference in solid-(isotropic) liquid transition for $[C_1C_1im][BF_4]$ when heated or cooled was 30.2^oC. The difference between solid-liquid transition temperature when measured under heating and cooling decreases from 20^oC for $[C_{10}C_1im][BF_4]$ to only a 2.3^oC for $[C_{18}C_1im][BF_4]$. This shows a decreasing tendency to supercool as alkyl chain length is increased. The $[C_xC_1im][BF_4]$ ILs with alkyl chains of 2-9 carbons in length all formed glasses rather than crystals and exhibit relatively small differences between heating and cooling transitions. The temperature of the liquid crystal to isotropic liquid transitions for x=12-16 or 18 are approximately equal upon heating and cooling.

The energy of the transitions is also interesting; the solid-liquid transition energy of $[C_1C_1im][BF_4]$ and $[C_2C_1im][BF_4]$ is about $10kJmol^{-1}$ as is that of $[C_{10}C_1im][BF_4]$;

however $[C_{11}C_1im][BF_4]$ has a solid-(isotropic)liquid transition energy of around $24kJ^{-1}mol$, which is much closer to the solid-liquid crystal transition energy of the ILs with longer alkyl chains in the study (that is x=12-16 or 18). The solid-liquid crystal transition energies of these ILs range from $18kJmol^{-1}$ to $27kJmol^{-1}$; the liquid crystal-isotropic liquid transitions are all around $1kJmol^{-1}$.

The first studies into the structure of the liquid state of 'short chain' ILs were MD studies. Early studies examined the spatial distribution of anions around cations which subsequently developed into computationally larger studies, which provide evidence of polar and apolar domains or structures.

Urahata and Ribiero examined the ILs composed of $[C_2C_1im]^+$, $[C_4C_1im]^+$, $[C_6C_1im]^+$ and $[C_8C_1im]^+$ cations and F^-, Cl^-, Br^- and $[PF_6]^-$ anions.[161] They found that as the radius of the anion increases, the favoured position of the anion relative to the imidazolium ring shifts. In ILs with fluoride and chloride as the anion, the favoured position is 'forward' of the C2 carbon, with an offset towards the 3-methyl group. In bromides and hexafluorophosphates the anion is centred over the N-C2-N charged centre of the imidazolim ring. This shift is rationalised by a decrease in the anions tendency towards specific and directional interactions and an increase in the anions tendency towards non-specific interactions (particularly dispersion interactions) as the radius and electron count increases. Increasing the anion size was also associated with an increase in the size of the preferred occupancy regions.

The study also examined the role of the alkyl chain and how it effects the position of the chloride in $[C_xC_1im]Cl$, for x=2, 4, 6 or 8. As the chain increases in length the position of the chloride moves towards the methyl group; interestingly increasing the chain length also appears to push the chloride towards the front of the ring and away from the top position. Also included are radial distribution functions of the cations and anions in $[C_1C_1im]Cl$, $[C_1C_1im][PF_6]$ and $[C_4C_1im][PF_6]$. The radial distributions of the geometric centres of the ions show peaks in cation-anion separation at 4.5Å and 6Å for all three ILs, a cation-cation peak separation at 6Å for all three ILs, and an anion-anion peak at 6Å for $[C_1C_1im]Cl$ and 7Å for $[C_1C_1im][PF_6]$ and $[C_4C_1im][PF_6]$.[161]

Wang and Voth[162,163] used a coarse grain MD method to show the existence of

distinct tail-tail, head-head and anion-anion distances in $[C_xC_1im][NO_3]$ x=3, 4, 6 or 8, while $[C_1C_1im][NO_3]$ and $[C_2C_1im][NO_3]$ showed no evidence of organisation. The alkyl chain-alkyl chain spacing peak is the strongest peak in all cases and becomes more intense as the chain length increases. This alkyl chain-alkyl chain spacing occurs at about 4Å, which is extremely close to the 4.3Å spacing in fluid alkanes. The head groups of the cations also have a small peak in separation of about 4.5Å, which is a described as a 'planar' interaction. The 'planar' interaction refers to two coplanar imidazolium rings, rather than two imidazolium rings stacked above one another. This 'planar' interaction is weaker than the head group separation, which occurs at about 9Å, and less than a quarter of the intensity of the alkyl chain-alkyl chain peak. The authors also note that the alkyl chain-alkyl chain regions remain stable over a range of temperatures and first become diffusive as a collective through solution, before passing a transition above which such apolar domains form only transiently.

Canongia-Lopes *et al.*[164] undertook a similar study (using a more complex computational model) on $[C_xC_1im][PF_6]$ x=2, 4, 6 or 8, as well as $[C_2C_1im][NTf_2]$ and $[C_4C_1im][NTf_2]$. The data are similar to that of Wang and Voth, in that they show a three dimensional network of polar and apolar domains. In this case the study included a comparison of internuclear separations for the carbons along the alkyl chain of $[C_{12}C_1im][PF_6]$, which showed the terminal carbons (C12-'C12) of two neighbouring cations are spaced at about 4Å with a strong shoulder at 5Å. The C11-'C11 and C8-'C8 internuclear separations occur at about 5Å, as well as the C4-'C4 internuclear separation, although this peak is very low intensity. An examination of the cross peaks, such as C12-'C11, would be of interest with reference to the crystal structure of $[C_4C_1im][NO_3]$, which is presented in Section 4.3.1 of this chapter and will be discussed later. The anion-anion separations of the $[C_xC_1im][PF_6]$ salts are around 6Å for all cations in the study (x=2, 4, 6, or 8), which is the same as in the $[C_xC_1im][NO_3]$ ILs modeled by Wang and Voth.[162,163] This is also approximately the same as the separations calculated by Urahata and Ribiero.[161] This indicates that the anion separation is a function of anion size and their spatial distribution around the cation; the chlorides appear closer because they sit 'forward' rather than over the ring which shortens the separation.

Subsequently a number of experimental studies have begun to explore the nature of these local and extended structures. Russina *et al.*[58] undertook a study of $[C_xC_1im][NTf_2]$ (x=2-10) ILs and examined them using energy dispersive X-Ray diffraction (EDXD) and SWAXS. Their results in both SWAXS and EDXD showed good agreement of the main spectral features. For all cation sizes there was a peak corresponding to a structure spacing of 4.5Å, the intensity and position of which is independent of cation size. Another peak occurs corresponding to a spacing of about 7Å, which decreases in intensity and increases in spacing as the chain length increases. The authors are not specific about the origin of the peaks but state that they "essentially related to first neighbor interactions or to intramolecular structural correlations". The final peak, which is often called the pre-peak, occurs at a spacing of 16Å (for $[C_6C_1im][NTf_2]$) and both the spacing and intensity increase as the chain length increases up to a spacing of 21Å for $[C_{10}C_1im][NTf_2]$. However in $[C_2C_1im][NTf_2]$, $[C_3C_1im][NTf_2]$ and $[C_4C_1im][NTf_2]$ the peak is absent and is little more than a strong shoulder in $[C_5C_1im][NTf_2]$. The increase in spacing is explained by the increasing length of the cation. The increase in intensity is a result of an increased amount of 'structuring' in these systems as the structural anisotropy becomes more pronounced. The peaks become somewhat sharper too, which implies that the structure being formed is more stable relative to the disordered state.

Similar behaviour was observed in symmetric $[C_xC_xim][NTf_2]$ ILs (x=2, 3, 4 or 5).[57] Only for $[C_5C_5im][NTf_2]$ is there evidence of pre-peak formation, although the peak position was not accurately determined because the pre-peak appears as a weak peak on the shoulder of the strong, broad 7Å peak. It appears that the symmetric $[C_5C_5im][NTf_2]$ has a shorter pre-peak spacing than $[C_5C_1im][NTf_2]$, at 12Å and 16Å respectively. This is interesting but would require the $[C_5C_5im][NTf_2]$ pre-peak position to be determined *via* mathematical fitting in order to ensure the maximum is correct. For reference the $[C_5C_1im]^+$ cation is about 11.2Å long.

The appearance of $[C_xC_1im][NTf_2]$ (x=2, 4, 6, 8, 10 or 12) ILs were examined by Fujii *et al.*[165] using MD and small angle neutron scattering (SANS). They calculated that the radial distribution functions of the ILs do not change significantly as the alkyl chain length increases; in all cases there are peaks in radial distribution functions at

about 5Å, 10Å and 15Å, which are attributed to inter-ionic spacings. The vector or vectors along which the radial distribution function were calculated were not specified. It would be interesting to contrast the radial distribution functions collected along three perpendicular vectors. Fujii *et al.* also found from their calculations a cation-anion correlation peak at 9Å and an anion-anion correlation at about 8Å, both of which match well with the conclusions of Wang[162] and Canongia-Lopes[164] where anion-anion spacings were about 6Å for the smaller $[NO_3]^-$ and $[PF_6]^-$.

Fujii *et al.*[165] also examined the atom correlation functions of the carbons in the alkyl chains and found results differing slightly from the similar study of Canongia-Lopes *et al.*.[164] While Canongia-Lopes *et al.* found a strong terminal carbon-terminal carbon correlation at 4Å and a shoulder at 5Å for $[C_{12}C_1im][PF_6]$. Fujii found the terminal carbon-terminal carbon correlation to be at 5Å with a shoulder at 4Å in $[C_{10}C_1im][NTf_2]$ and at 4Å in $[C_4C_1im][NTf_2]$.

While the majority of work has focused on imidazolium based ILs there are a number of studies of other ILs that are informative. Kashyap *et al.*[166] studied $[C_xC_1pyrr][NTf_2]$ ILs (x=4, 6, 8 or 10) and examined their structures using SAXS data supported by MD calculations. They found that all the ILs studied had peaks corresponding to real spacings of 7.4Å and 4.6Å. Additionally $[C_{10}C_1pyrr][NTf_2]$ and $[C_8C_1pyrr][NTf_2]$ have a pre-peak corresponding to a real spacing of 17.9Å. The real peaks were partitioned into their subcomponents using MD and it was found they are made up of peaks and anti-peaks[†]. The peak at 17.9Å is found to be the result of a strong anion-anion correlation peak, with a smaller anti-peak of cation-anion correlations. The cation-anion correlation was examined in further detail and found to itself be a combination of a cation(head)-anion peak and a cation(tail)-anion anti-peak. The peak at 7.4Å is also the result of a strong peak and anti-peak cancellation, in this case the extremely strong anion-anion correlation peak is canceled out by an almost equally intense cation-anion correlation anti-peak. There is

[†]The terms peak and anti-peak can be misleading in this context. The terms are used as a tool to describe the phase difference of the diffracted X-Rays, which arises because of path length differences within the sample. Generally the 'peak' is the phase which has the strongest diffraction and in therefore detected and the 'anti-peak' is the out of phase contribution which cancels out some of the 'peak' diffraction. For a detailed explanation see Section 4.3.0.4

a small peak contribution from cation-cation correlations. The peak at 4.6Å has a cation-anion correlation contribution, although it is mostly a cation-cation correlation contribution that increases as the alkyl chain length increases. Kashyap *et al.* did not break the cation-cation correlation down further but is reasonable to assume the correlation is caused by the alkyl chains. There is little anti-peak behaviour in this area of the spectrum. It is worth noting here that the fact that anion-anion correlations dominate the spectrum is not indicative of the anions driving structure formation or being relatively more ordered in the liquid. The dominance of anion correlations in the resultant spectrum is simply a result of the fact that X-Rays are scattered by electrons and anions are electron-rich.

The SAXS diffraction pattern of $[N_{xxx1}][NTf_2]$ ILs has been examined by Santos *et al.*[167] and Pott and Méléard[168] and found results similar to those of imidazolium and pyrrolidinium based ILs; that is cations with butyl chains have two SAXS peaks and longer chains have an additional pre-peak. In all the $[N_{xxx1}][NTf_2]$ ILs there are two peaks, one at 8.0Å and another at 4.6Å. While some authors have attributed the 4.6Å peak to a parallel plane-to-plane distance in imidazolium cations, this was done using crystal structures as a guide. Others have suggested that the 4.6Å spacing is a combination of cation-anion spacings and some interaction of alkyl chains in non-polar domains. The appearance of the same peak in the tetraalkylammonium ILs strongly suggests that this peak is a result of an alkyl chain-alkyl chain spatial correlation. This agrees with MD simulations by Bhargava *et al.*,[169] who found the partial structure factor of the peak corresponding to a 4.6Å spacing in $[C_{10}C_1im][PF_6]$ to be predominantly composed of alkyl chain-alkyl chain interactions with small contribution from an alkyl chain-anion spacing and a ring-ring spacing similar to that seen by Wang and Voth.[162,163] The ring-ring spacing in this case was very broad and flat, so it gives a negligible contribution to the peak shape.

The peak at 8Å spacing in $[N_{xxx1}][NTf_2]$ ILs is attributed by Pott and Méléard to an anion-anion correlation, but the work on the subcomponent contributions by Kashyup *et al.*[166] suggests that there are many 'nearest-neighbour' correlations that cause (and indeed cancel) diffraction signal at this spacing in pyrrolidinium ILs and it is likely that this is true in all ILs, although the relative contributions may

vary according to the particular system being studied. The pre-peak is present in $[N_{6661}][NTf_2]$ and $[N_{8881}][NTf_2]$ at 14Å and 16Å respectively. By mixing the cations the authors found a linear change in pre-peak position; the pre-peak shifts to a larger spacing as the chain length increases. The line of best fit equation is shown in Eqn. 4.3, where d_1 is the pre-peak real spacing and n is the number of carbons in the alkyl chains.

$$d_1(\text{Å}) \;=\; 4.65 + 1.30n \tag{4.3}$$

The figure of 1.30Å per methylene unit is reasonably close to the standard 1.27Å per methylene unit. Kashyup *et al.* go on to state that they believe the system exists in a smectic A phase, despite the lack of birefringence of the samples. The author believes there is insufficient evidence to substantiate this claim.

Hettige *et al.*[170] did a study on $[N_{5555}]I$, $[N_{5555}][PF_6]$ and $[N_{5555}][N(CN)_2]$ using MD. The predicted SAXS spectra of the three compounds interestingly only show two peaks; one around 12.6Å, the pre-peak, and a wider peak at 4.3Å. The absence of a peak in the 8Å region for the symmetric cations is interesting here. By analysing the subcomponent effects they found that in all cases the positive contributions by the cation-cation and anion-anion correlations are canceled out by the cation-anion correlations. This is true of all of the anions, particularly the $[N(CN)_2]^-$ which was chosen because of its relatively low contribution to the correlations. It is worth recalling at this point that the 8Å peak in imidazolium ILs is the result of a peak where the cation-cation and anion-anion correlations are not quite canceled out by the cation-anion correlations.

The general features of the XRD patterns of imidazolium ILs can now be effectively summarised. A peak occurs that corresponds to a real spacing of 4.3Å, which is caused by the alkyl chains interacting. There is MD evidence suggesting this is principally a function of the terminal methyl groups of the long alkyl chain on the cation. A peak corresponding to a real spacing of around 7Å is effectively a measure of the spacing of the first 'solvation' sphere. This peak position is anion dependent. The 7Å peak also shifts to larger spacings and becomes weaker as the alkyl chain

length increases in length. A peak, called the pre-peak, appears in the XRD patterns of ILs where there is significant structural anisotropy. This peak is on the length scale of the cation. The anisotropy of the cations causes them to line up along the longest axis.

4.3 Introduction to X-Ray Diffraction

The first study of X-Rays, at least in which their nature was truly realised, was by Röntgen. Soon after this it was noticed that in some circumstances crystalline samples, when irradiated by X-Rays, transmitted X-Rays that produced patterns of spots, where other materials produced a simple shadow.

The foundation of this behaviour was elucidated by W. and W. Bragg, which earned them the Nobel Prize in Physics in 1915. The mathematical proof was developed with particular reference to X-Rays, however the law applies to all wave diffraction in principle. The simplest statement of Braggs Law is shown in Equation 4.1 where λ is the wavelength of the the light and 'd' is the spacing between regularly spaced lattice planes in the material being irradiated. In the case of X-Rays the lattice points are atoms.

$$n\lambda = 2dsin\theta \tag{4.4}$$

In this form the law states that two parrallel incident X-Rays that reflect off two parallel planes, will have a difference in path length that depends on the distance between the reflecting planes and the angle of incidence relative to the reflecting plane. If this path difference is some integer multiple of the wavelength of the X-Rays, the two X-Rays will emerge in phase. If the path difference is a half number of wavelengths, the waves will emerge out of phase.

The beauty of the Bragg relationship is that simply put, it means that light waves will be diffracted if their wavelength is approximately the same size as the spacing of some repeating structure. The Braggs' work opened up an entirely new avenue

of structure determination, because X-Rays have wavelengths similar to the spacing between atoms in crystals. This means X-Rays can be used to determine the spacings between atoms in crystals and molecules in molecular assemblies. For atoms in crystals the information gathered over many possible orientations of the crystal relative to the incident X-Ray beam means structures can be determined precisely.

4.3.1 Generating X-Rays

X-Rays were discovered using 'cathode ray tubes' or Crookes tubes. In a cathode ray tube, a cathode ionises the air around it, and the potential difference accelerates the electrons towards the target (which is often also the anode). Above a potential difference of about 5kV the electrons have sufficient energy to cause X-Rays to be emitted from the anode or the target, through two processes. The first mode, bremsstrahlung or breaking radiation, is where an electron is deflected from its path by a close approach to a nucleus in its path. This deflection causes an acceleration, which results in emission of an X-Ray tangential to the acceleration vector. This gives a continuum of X-Ray energies depending on the angle of deflection. The second mode is called characteristic X-Ray emission, where the incident electron knocks out a core electron. This vacancy is filled by a higher orbital electron dropping down and a photon is emitted in this process. When the energy of the incident electron is high enough, and the correct target material is used, the emitted photon is a characteristic X-Ray. A sketch of the X-Ray emission spectrum of copper is shown in Fig 4.1[171] at two voltages. K_α and K_β are called characteristic lines. The rest of the emission profile is caused by bremsstrahlung.

Laboratory based X-Ray generators still produce X-Rays in this way. The instrument used in this study had a fixed copper annode, while molybdenum is also a common target material. This method of X-Ray generation produces X-Rays at a range of energies and divergent from the target surface, which necessitates some collection and treatment of the X-Rays into a monochromatic beam.

While any wavelength can, in principle, be collected from a given target, it is desirable to generate the most intense X-Ray beam possible. In order to do this a

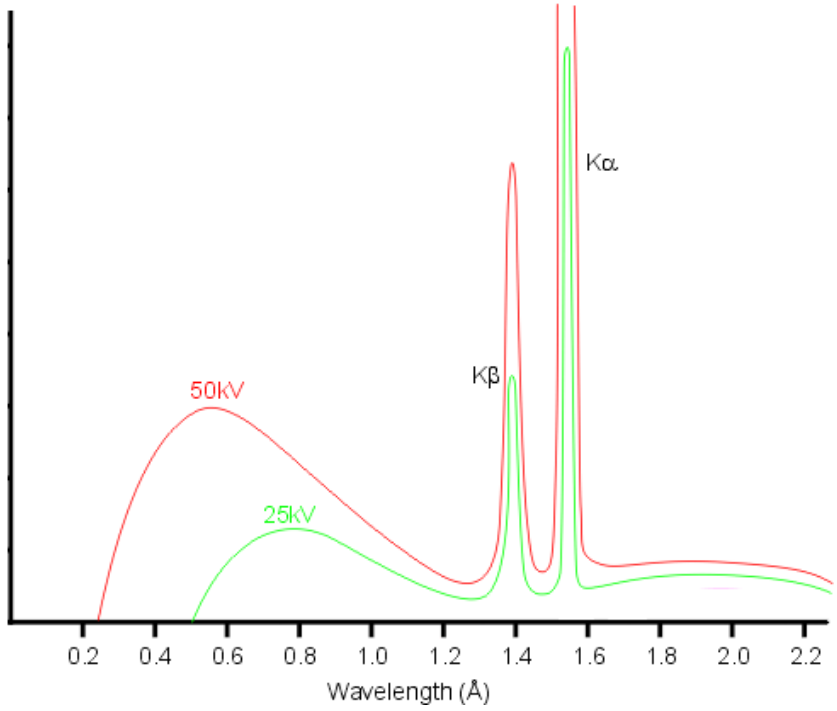


Figure 4.4: Sketch of Copper X-Ray emission profile

characteristic line is isolated to give intense, monochromatic X-Rays. As was already stated, the origin of the characteristic lines is from removal of a core electron followed by a higher level electron dropping in level. The notation used to describe this is as follows: the letters K, L, M and N refer to the principle quantum number (1, 2, 3 and 4 respectively) of the orbital with the vacancy and the suffix refers to the change in principle quantum number ($\alpha = 1$, $\beta = 2$ etc) of the electron which fills the vacancy. So the K_α line represents an electron dropping from the 2 orbital into the 1 orbital, with a change in principle quantum number of 1. While the notation only specifies the principle quantum number, the orbital angular momentum quantum number must change for a transition to be allowed, therefore it should be noted that the K_α is a 2p electron dropping into a 1s orbital and cannot be a 2s electron dropping into a 1s orbital.

For a copper target the K_α line is the most intense characteristic line and is most often used for X-Ray diffraction. In fact the K_α line is further split into $K_{\alpha 1}$ and $K_{\alpha 2}$, which arise because there can also be a change in electron spin quantum number of the electron that is falling into the core orbital vacancy. $K_{\alpha 1}$ represents no change in electron spin quantum number and $K_{\alpha 2}$ represents a change in electron spin quantum

number. $K_{\alpha 1}$ appears at 1.5405Å and $K_{\alpha 2}$ is at 1.5440Å and is about one fifth of the intensity of $K_{\alpha 1}$.

4.3.2 Beam Conditioning

As was stated, the raw X-Rays are not suitable for diffraction measurement, because they are polychromic and are divergent from their generation point.

The first step of conditioning is to monochromate the beam. In the case of copper anodes, the beam is passed through a nickel filter. Nickel strongly absorbs X-Rays with wavelengths below 1.45Å. This filters out the K_{β} line and the high energy bremsstrahlung X-Rays seen in Figure 4.1. This leaves a beam of K_{α} that is still divergent.

There is a second conditioning step to focus or collimate the beam, which in many cases also increases the quality of monochromation.

The instrumentation in this study used polycapillary X-Ray optics to take the divergent beam and produce a collimated beam.[172] The method is conceptually similar to fiber optics, however X-Rays travel faster through glass than the gas interior of the capillary (i.e. for X-Rays the glass has a lower refractive index than the gas), so the X-Rays are in fact totally externally reflected whereas the familiar fiber optics relies on total internal reflection. Because the optical capillaries are flexible, the divergent capillaries can be bent into a parallel bundle, which produces an almost perfectly collimated X-Ray beam. The beam will never perfectly be collimated because the capillaries collect X-Rays over a range of extremely low grazing angles, thus they will exit the optical capillaries with an range of angles. However the grazing angle is very low so the range of angles successfully collected is low. Polycapillary optics also achieve a high beam intensity because the physical configuration of the bundle collects many X-Rays, whereas several other methods can suffer from a loss of beam intensity because they collect X-Rays from one plane or arc.

Other methods for focusing or collimating X-Ray beams include monochromator crystals, Frank optics and toroidal optics. A monochromator crystal is a crystal

(often quartz) that is mechanically bent, which produces a small elliptical section. This can be used to focus the beam (ellipses have two foci) and with fine adjustment can also remove $K_{\alpha 2}$. Frank optics are two glass mirrors bent similarly to the monochromator crystal. At sufficiently shallow incidence angles the X-Rays are reflected rather than absorbed or diffracted, the angle at which reflection occurs is wavelength dependent which allows for further monochromation. Toroidal optics are capable of producing large X-Ray fluxes; they are ring shaped X-Ray mirrors. X-Ray mirrors both focus and monochromate the beam, they also operate over a wider range of incidence angles than crystals or glass mirrors, which helps achieve a higher final flux density.

Two X-Ray sources were used in this study. Some of the samples were examined at the Diamond Light Source, the UK synchotron X-Ray Source. All samples were also examined on a laboratory based beamline using a nickel filtered copper target.

4.3.3 Sample Diffraction

When the conditioned beam is passed through the sample some of the X-Rays will be diffracted by an angle governed fundamentally by Braggs Law. Polydomain samples, like liquids, liquid crystals and powdered crystals do not produce spots in the same way that single crystal samples do.

Powdered crystal are conceptually the most simple polydomain sample. In a powdered crystal sample, the sample is effectively many single crystals oriented randomly relative to the incident X-Ray beam. Many of these crystals will be at the correct angle for Bragg diffraction, but at all radial orientations around the axis of the X-Rays, which produces a ring.

Similarly, in liquid samples a ring is seen, although there is no formal lattice in liquid samples. An example diffraction pattern is shown in Fig. 4.5. This image is a composite of 60 individual images.The rings here are the reciprocals of the real space features. This example shows all 4 bright rings that correspond to real structural spacings, which will be discussed in the following section, although the second and third bright rings are difficult to tell apart and the fourth ring is extremely weak.

With the diffraction patterns collected thus, it is necessary to process them to extract information.

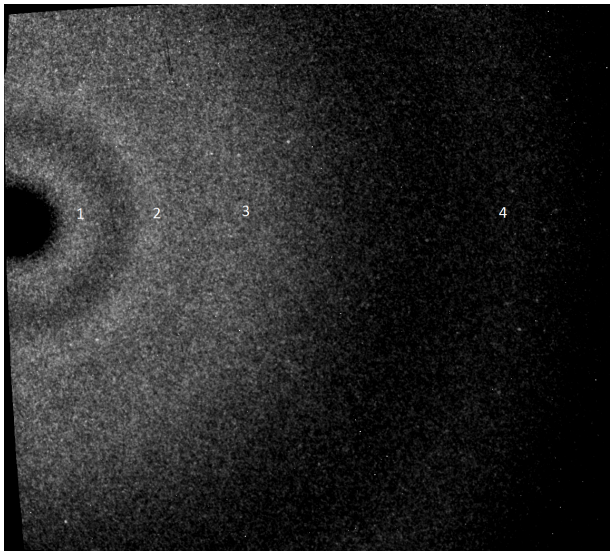


Figure 4.5: Example Diffraction Pattern Image

4.3.4 The Phase Shift

As was mentioned in section 4.2.3 the occurrence of a phase shift can significantly impact the appearance of the collected pattern. If two in phase incident X-Rays are reflected by the same angle, but have slightly different path lengths through the sample, their relative phase will be changed. This phase shift of the diffracted X-Rays is visualised in Fig. 4.6. These waves will now interfere with one another. If the phase shift is zero or nπ for even values of n, the waves remain in phase. Thus the sum of the wave vectors is twice that of a single X-Ray and the effective signal at the detector is 2. If the phase shift is odd values of nπ the two waves are out of phase. Thus the sum of the wave vectors at the detector is 0 and no response is triggered.

The phase shift can cause much information about the sample to be lost, however MD calculations can provide much insight into the relative phase contributions to each peak and how interference affects the observed pattern. This was discussed in Section 4.2.3.

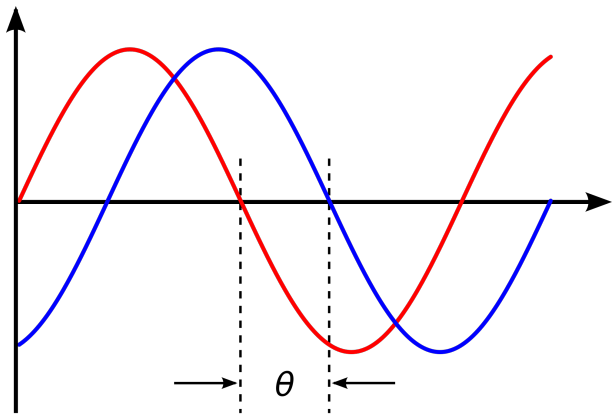


Figure 4.6: Phase Shift of Two Light Waves

4.3.5 Transmission Profile

In the course of collecting X-Ray diffraction data it is normal to collect data concerning how strongly the sample is diffracting. Two of the ways to do this are to use a photo-diode or to attenuate the transmitted X-Rays. A photo diode can be put in the beam stop, which can accurately determine the flux of X-Rays at the beam stop and can be combined with the integration of the X-Rays incident at the detector. Attenuating the transmitted X-Rays usually involves placing a thin metal sheet in front of the detector and then collecting data using a very short exposure time, so that the detector does not become saturated by the main beam. Unfortunately collecting transmission profiles was not possible with the available equipment.

The alternative to using complete transmission data is to collect background data (including an empty glass capillary) under the normal experimental conditions, however this cannot be simply subtracted from the sample data. There are two reasons why the background cannot be simply subtracted. Firstly, when a sample is present there are additional sources of primary diffraction and attenuation, which affect the flux of X-Ray transmission. Secondly, when a sample is present there are additional sources of secondary diffraction and attenuation which affects the flux of primarily diffracted X-Rays at the detector. This is unfortunate, but not prohibitive. The following section contains further information regarding the methods used to account for this, and the affect this has on the results.

Due to an electrical failure, the beamline had to be reconfigured before diffraction

patterns of $[C_8C_1im]Cl$ and Br and $[C_4C_4im][NO_3]$ were recorded. As a result, the diffraction patterns of these ILs are significantly lower in intensity than the rest of the data. These ILs will be marked with asterisks when appropriate to serve as a reminder of this. All the intensity data collected is in arbitrary units, however the reconfiguration affected the transmitted beam intensity, hence the caveat.

4.3.6 Data Fitting Methods

The methods used to transform a diffraction pattern into a real spacing will be briefly outlined here. An example diffraction pattern was shown Fig. 4.5. This image is radially integrated which produces a graph of the diffraction intensity plotted against angular displacement from the main beam, initially expressed in pixels. The angular displacement in pixels is converted to reciprocal Ångstroms ($Å^{-1}$) using Silver Behenate as a calibrant, which has a regular layer spacing of 58.38Å. The spacing in reciprocal Ångstroms is the reciprocal of the repeat spacing 'd' in Braggs Law and the angular displacement is twice the angle of diffraction in Braggs Law (2θ).

The radial integration of the diffraction pattern from the background is shown in Fig. 4.7. This includes contributions from scattering from the air in the beamline and an empty capillary in the sample block. As can be seen from integration, the background will result in a non-linear baseline, peaking at 0.044S, which must be taken into account when examining the data. Unfortunately a simple subtraction was not possible because transmission values could not be collected. A number of methods were trialled to account for this.

The first method used was to reduce the blank capillary intensity by an arbitrary fraction, however this was found to be somewhat problematic and no single reduced intensity subtraction was found to be adequate for all the ILs. This is because the ILs diffract differently depending on their composition.

The second method attempted to build on this by allowing the reduction in intensity of the background to be varied as part of the mathematical fitting. This worked well for many of the weakly diffracting samples, however for the strongly diffracting

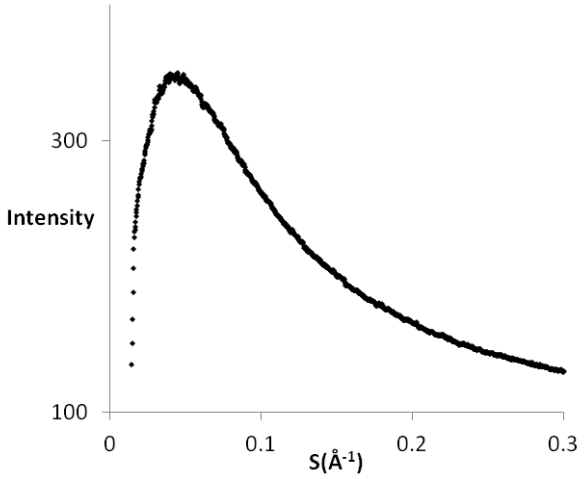


Figure 4.7: Radial Integration of Diffraction Pattern of Blank Capillary

samples this method tended to reduce the contribution of the background to zero. This method proved to be particularly reliable at fitting the peaks that occur around 0.1Å^{-1}.

The third method that was used was to segment the integration plot and fit each peak individually on a sloping baseline, which was allowed to change as part of the fitting. This method produced excellent fitting data for the wide angle peaks around 0.25Å^{-1} where the background contribution is relatively linear. The smaller angle peaks are in an area of the integration where the background contribution is rapidly changing in gradient. Additionally the peaks in the small S region are close together, so they overlap. The sloping baseline method doesn't adequately account for peak overlap and it is preferable to allow the overlap of peaks to occur in the fitting model.

Attempts to fit the whole trace of data onto a single sloped baseline had mixed success. In many cases the optimal solution had a steep positive gradient which skews the peak maxima towards zero.

The final method which arrives consistently at excellent fits constrains the model to small negative gradients, while discarding points in the very small S regime (up to around 0.024^{-1}) to improve the fit. This method eliminates parasitic scatter from around the beamstop.

This method was found to be satisfactory and produces peak maxima that are in

agreement with those in the literature (where available). The peaks in the small angle regime ultimately have small contributions from the blank capillary which affects their intensity and width, however their peak positions are well fitted.

With the exception of the freely sloping baseline which resulted in badly shifted peaks, the methods all caused less than 0.01Å^{-1} variation in the peak around 0.22Å^{-1} (4.5Å) and even less in the two very small angle peaks (around 0.05Å^{-1}). There was more variation in the position of the 0.1Å^{-1} (8Å) peak, particularly in samples where this is the strongest peak, such as the $[NTf_2]^-$ ILs. In these cases the peak position was calculated with the inclusion of the blank capillary. For the strongly diffracting sample, such as the $[NO_3]^-$ ILs, the background subtraction resulted in very little difference in peak positions.

Table 4.1 shows the fitted peak positions for $[C_6C_6im][SCN]$. The variation in the peak positions are very small, as such, while considerations of the methodology are important, they are not hugely significant in determining the peak positions.

Peak No.	Background Removed (Å^{-1})	Sloped Baseline (Å^{-1})	Difference (Å^{-1})
1	0.032236	0.029914	0.002322
2	0.066217	0.061304	0.004913
3	0.101724	0.094437	0.007287
4	0.24204	0.234729	0.007311

Table 4.1: Different Fitted Peak Maxima for $[C_6C_6im][SCN]$

4.4 Results and Discussion

As was discussed in the introduction, ILs have a wide range of behaviours relating to structuring in liquids; particularly self-assembly and liquid crystal behaviour[119]. Both of these phenomena involve structural anisotropy and long range order. There is a body of work suggesting that some ILs are thermodynamically ideal solvents in some systems, which strongly suggests they are isotropic[46]. In this work we seek to resolve these apparently conflicting statements by closely examining when structuring begins to occur in ILs.

In order to examine this a range of imidazolium ILs were synthesised (details of which can be found in Chapter 2). $[C_xC_1im]^+$ ILs were prepared, where x is 4, 6 or 8 and then anion is $[NTf_2]^-$, $[NO_3]^-$, $[SCN]^-$, Cl^- or Br^-. It was also decided to synthesise and analyse $[C_4C_4im]^+$, $[C_6C_6im]^+$ and $[C_6C_2im]^+$ with the same anions in order to see what effects may arise from the additional symmetry of the cations.

These salts were selected because they are RTILs; $[C_{10}C_1im]^+$ and longer chain ILs are generally solids and have a high melting point. Similarly $[C_4C_1im]Cl$ and $[C_4C_1im]Br$ are also excluded.

Water content has an extreme effect on many properties of ILs when the most hygroscopic anions, which include chloride, bromide and nitrate, are present. Thiocyanate ILs are likely to be hygroscopic too, although there is little data available at present because they are relatively rare as ILs. It may be noticed that throughout this section no water contents have been stated; this is because, with the exception of the $[NTf_2]^-$ ILs, it was impossible to get a stable reading of water content. The $[NTf_2]^-$ ILs all had water content below 50ppm before they were considered dry enough to use. The other ILs were too viscous to syringe into the Karl-Fischer titrator with any reliability. The ILs were considered dry when they could be heated to 70 degrees under vacuum without any appearance of bubbles. The nitrates were difficult to dry and proved to be extremely hygroscopic. The $[NO_3]^-$ ILs were all first dried on a lyophiliser before being finally dried on a Schlenk line. Capillaries for the X-Ray diffraction experiments were oven dried and were flame sealed once the sample was enclosed. All syringes used to transfer ILs were oven dried and used while still hot from the oven, while this was done in order to maintain the ILs elevated temperature during handling (to keep viscosity low), it also has the side effect preventing water adsorption onto the syringe surface.

4.4.1 Single Crystal Structures

As part of this investigation two novel crystal structures were determined. The full details of their determination can be found in the Appendix.

It has been found here that $[C_4C_1im][NO_3]$ is solid at room temperature and its

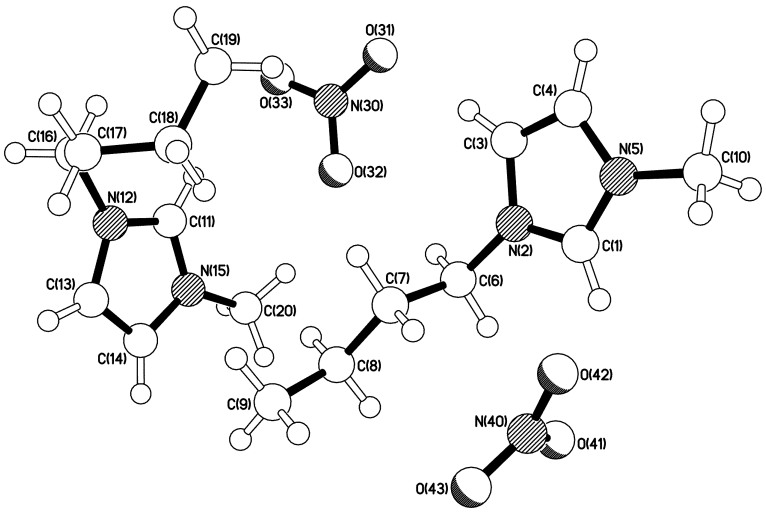


Figure 4.8: Crystal Structure of $[C_4C_1im][NO_3]$

melting point is 30-31^{o}C, which is in agreement with that in the literature.[173] $[C_4C_1im][NO_3]$ has been found to have a triclinic crystal and the reduced symmetry half cell structure is shown in Fig. 4.8 and the packing is shown in Fig 4.9. As $[C_4C_1im][NO_3]$ is deliquescent the optimised resolution of the structure is slightly lower than usual. The nitrate groups are parallel to the imidazolium rings; however not within the same reduced symmetry half cell.

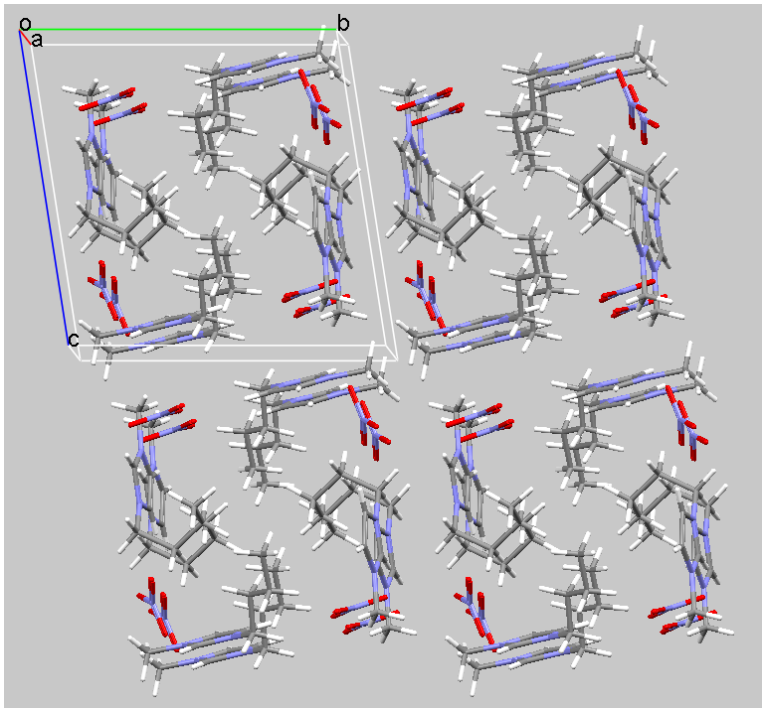


Figure 4.9: Packing Structure of $[C_4C_1im][NO_3]$

The crystal structure here is interesting in that it has two different cation conformers. One cation has the alkyl chain in the all trans conformer (N(2)-C(9)), which the other cation has the alkyl chain in the guache-trans conformer (N(12)-C(19). This is interesting because $[C_4C_1im]Cl$ crystallises in the all trans conformer, while $[C_4C_1im]Br$ crystallises in the gauche-trans conformer.[174]

There is an area of the crystal where there is a 'hydrophobic' pocket; C(9) is 4.3Å from C(8') and similarly C(8) is 4.3Å from C(9') and the bonds C(9)-C(8) and C(9')-C(8') are approximately antiparallel (note the C(x') are in not in the diagram, they are in the full cell). The hydrophobic pocket is readily seen in the packing diagram in Fig. 4.9. The cross distances C(8)-C(8') and C(9)-C(9') are just over 5Å. This is in contrast to $[C_4C_1im]Cl$ where the cations pack into columns aligned in the same direction.

The 'hydrophobic pocket' region of the crystal structure of $[C_4C_1im][NO_3]$ is relevant to literature data discussed in Section 4.1.4, where Canongia-Lopes *et al.*[164] found the terminal carbons in $[C_{12}C_1im][PF_6]$ to show a strong preference to be 4Å apart with a shoulder at 5Å, similarly the C(11)-C(11') showed a strong peak at 5Å with a small shoulder at 6Å. Fujii *et al.*[165] found the terminal carbons in $[C_{10}C_1im][NTf_2]$ to have a relatively broad peak at 5Å and shoulders at 4Å and 6Å. They calculated a similar radial distribution function for $[C_4C_1im][NTf_2]$ and found a strong, surprisingly narrow peak (much more so than the $[C_{10}C_1im][NTf_2]$ case) at 4Å for the terminal carbons of the butyl chains.

$[C_4C_4im]Cl$ is also a solid at room temperature and melts at 48-50^{o}C. The crystal structure of $[C_4C_4im]Cl$ is shown in Fig. 4.10 and the packing structure shown in Fig. 4.11. Note the additional carbon and hydrogen spheres are a result of disorder one alkyl chain. Unusually, the crystal has a chiral orthorhomibic space group and the crystal examined contained only a single pseudo-enantiomer. This pseudo-chirality is a result of an interaction between Cl(1) and H-C(10). This can be seen in the diagram by comparing the alkyl chains; the butyl chain C(6)-C(9) is in the normal all-trans, lowest energy, conformer (the dihedral angle between N(2) and C(8) is 180^o). The alkyl chain C(10)-C(13) is gauche (the dihedral angle between N(5) and C(12) is 60^o). This remarkable crystal structure is likely due to the interaction

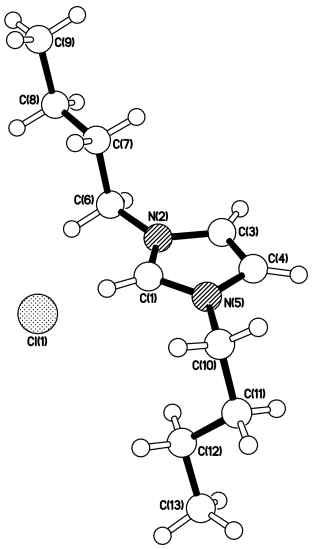


Figure 4.10: Crystal Structure of $[C_4C_4im]Cl$

between the chloride and the H-C(10) lowering the rotational energy barrier around the C(10)-C(11) bond, as was shown computationally by Hunt.[175] This can now be considered as being confirmed experimentally. The lowered rotational barrier of this butyl chain results in disorder in the crystal from C(11) to C(13); the positions of these atoms in Fig. 4.10 is only 87% occupancy, which means the alkyl chains crystallised into a number of conformers. The rest of the atoms are solved to better than 95% occupancy.

The IL $[C_4C_4im]Br$ was rigorously recrystallised from various solvent systems to

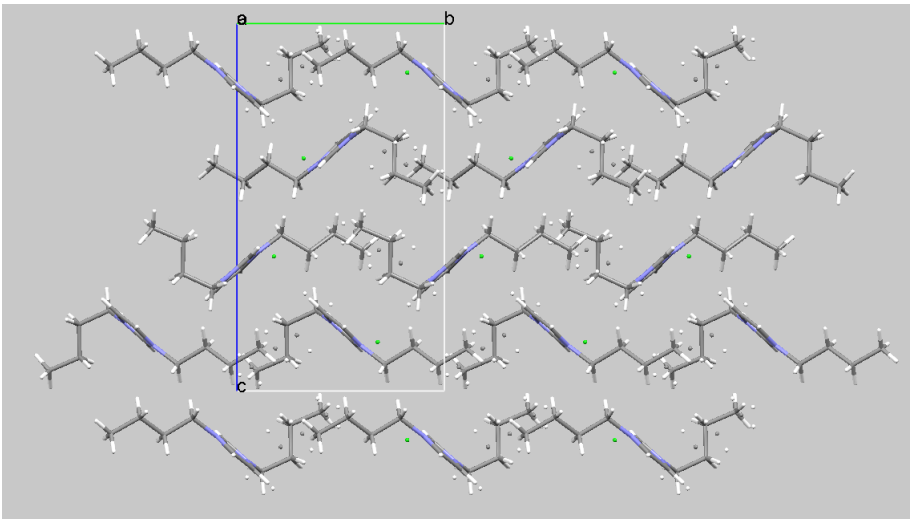


Figure 4.11: Packing Structure of $[C_4C_4im]Cl$

ensure it too was not truly solid at room temperature, however it was not possible to crystallise it (down to -20^{o}C), therefore it is assumed to be a true RTIL rather than a supercooled liquid.

4.4.2 Synchotron X-Ray Diffraction Results

A number of the samples in this study were examined using I22, the small angle scattering beamline at Diamond Light Source, the UK synchotron X-Ray Source. Synchotron sources offer extremely high flux of X-Rays. Figures 4.12 and 4.13[‡]show stack plots of the small angle and wide angle X-Ray (SAXS and WAXS) diffraction patterns at 25^{o}C, intensity is an arbitrary unit. While it is apparent that there is some small peak being formed in many of the examples, which is indicative of some structural feature, the low intensity shows that the structuring is likely to be only local.

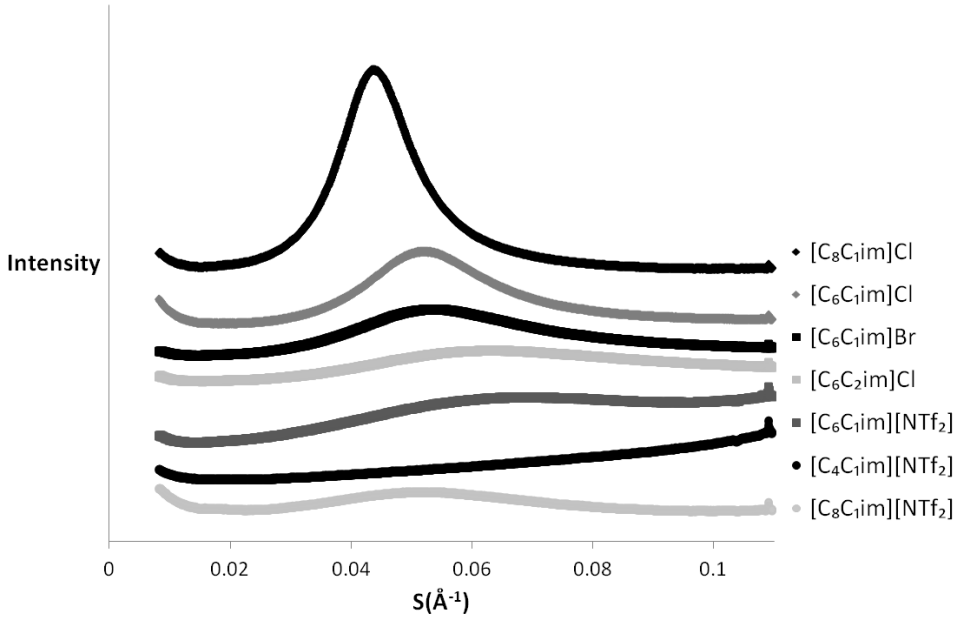


Figure 4.12: SAXS Data Collected on Synchotron

The peak positions were calculated *via* Gaussian fit using a least squares fitting method. The fitted synchotron data showing the repeat spacing of each peak position is shown in Table 4.1 with the repeat spacing peak positions from XRD patterns

[‡]Missing data points are caused by dead pixels in the detector

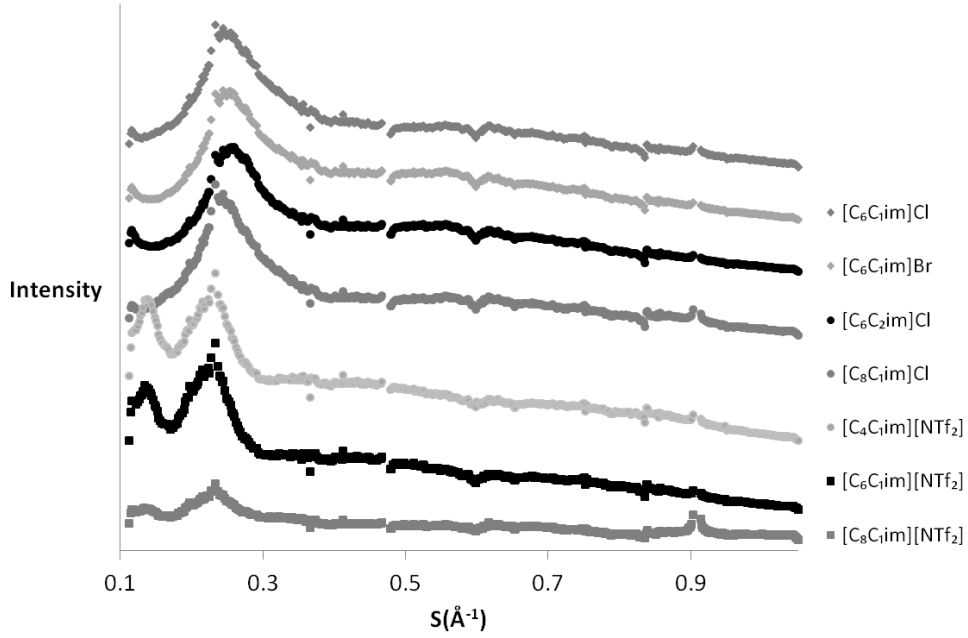


Figure 4.13: WAXS Data Collected on Synchotron

that were collected at Imperial College London on the Bede X-Ray beamline. Note the peaks here are indexed as 2, 3 and 4 in order to have consistent numbering of the peaks; peak 1 was not present in any of the samples examined on the synchotron source. The rationale for the peak numbering is given in the following section (Section 4.4.3).

	Repeat Spacing(Å)					
	2		3		4	
Ionic Liquid	D	B	D	B	D	B
$[C_4C_1im][NTf_2]$	-	-	7.3	7.3	4.4	4.5
$[C_6C_1im][NTf_2]$	14.2	14.1	7.4	7.8	4.5	4.7
$[C_8C_1im][NTf_2]$	19.0	20.5	7.5	7.9	4.3	4.7
$[C_6C_1im]Cl$	19.0	19.8	-	9.5	4.0	3.4
$[C_6C_1im]Br$	18.6	18.3	-	-	3.9	4.7
$[C_6C_2im]Cl$	16.1	24.9	-	10.2	3.9	4.8
$[C_8C_1im]Cl$	22.7	21.7	-	15.6	4.1	4.5

Table 4.2: Table Compaing XRD data from Diamond Advanced Light Source (D) and the laboratory beamline (B)

As can be seen in the table, the agreement between the data collected at the Diamond Light Source and on the Bede beamline at Imperial College London is generally good. In the case of the Cl^- ILs it appears that Peak 3 was in the cross over region of the detectors in the Synchotron data, Peak 3 of the $[NTf_2]^-$ ILs was in the range of the WAXS detector. The peak positions of the $[NTf_2]^-$ ILs agree with those found by Russina *et al.*[58] which is promising, including the absence of a low S peak in $[C_4C_1im][NTf_2]$, which certainly validates the data.

A wider range of ILs were examined using a smaller lab based X-Ray source, which will be presented and the complete data discussed in detail to follow.

4.4.3 SAXS Diffraction Results, grouped by Anion

Figure 4.14 shows the radial integration of the X-Ray diffraction (XRD) pattern of $[C_8C_1im][NO_3]$, which is one of the ILs in this study. This example will be used to introduce the general features of the XRD patterns that will be discussed. There are four peaks of interest on the integrated scattering pattern, three of which have been reported in the literature and one that we belieive to be the first report of its kind. This example pattern was chosen because it shows all four peaks and is displayed here simply to draw attention to the peaks of interest and briefly introduce their origin.

The peak at around $0.25Å^{-1}$, which corresponds to a structure spacing of about 4Å is present in most of XRD patterns of the ILs studied here. This peak is indicative of a close spatial arrangement of the alkyl chains of the cations,[162,169] this will be referred to as Peak 4. Similar peaks occur in gels at 4.2Å and in fluid hydrocarbon chains at 4.6Å.[176] In this region of the pattern there are also small contributions from a cation-cation repeat spacing (of imidazolium rings that are coplanar)[162] and a small contribution from an alkyl chain-anion repeat spacing.[169]

The peak at around $0.12Å^{-1}$, which is a structure spacing of around 9Å, is present in all the ILs studied here and is a complex superposition of peaks and anti-peaks.[170] It is made up of strong anion-anion and cation-cation correlations and has been dubbed in the literature the 'nearest neighbour' peak. This is because it represents

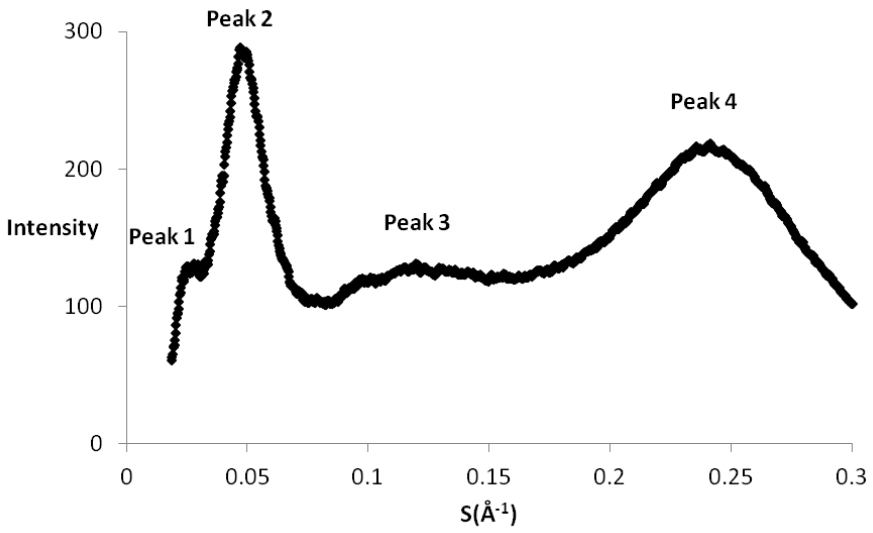


Figure 4.14: Trace of X-Ray Diffraction patterns of $[C_8C_1im][NO_3]$

the distance between neighbouring ions of the same charge, rather than neighbouring ions of opposite charge, which would be closer. This will be referred to as Peak 3.

The relatively sharp strong peak seen at about $0.05Å^{-1}$ (repeat structure spacing of 20Å) in the scattering pattern of $[C_8C_1im][NO_3]$ in Fig. 4.14 is often referred to as the 'pre-peak' and is a result of structuring on a length scale (for $[C_xC_1im]^+$ ILs, at least) somewhat longer than the cation, and often considered to be the repeating length of an 'ion pair'. In a liquid crystal this peak would be extremely strong and quite sharp. This will be referred to as Peak 2 and has been discussed in the introduction to this Chapter as the pre-peak.

The final spectral feature is the small shoulder peak at around $0.03SÅ^{-1}$. We believe this is a real peak and is the first report of its kind (Fig 4.23 in Section 4.4.4.1 shows this peak more clearly). This peak corresponds to a structural feature twice the length of the 'ion pair'. While in depth discussion will follow, the appearance of this sort of peak is unusual; many liquid crystals in smectic phases only exhibit a single layer peak. This will be called Peak 1.

Below is a extensive series of peak tables and stack plots showing all the ILs, grouped by anion. Trends within a group of ILs with the same anion will be discussed here. There are also important trends in the structuring of the ILs when they are grouped by cation; these trends will be discussed in the following section. As a guide to the

eye, the scattering patterns are offset along the Y-axis according to their 0.3Å^{-1} value, which is approximately zero intensity for all the ILs.

The stack plots of integrations displayed below are shown without any background subtraction, this ensures the relative peak intensities are displayed most clearly, while peak positions were determined using the methods outlined earlier (Section 4.3.6)

4.4.3.1 Bis(trifluoromethylsufonyl)imide Ionic Liquids

Table 4.3 shows the peak positions and Figure 4.15 show the stacked diffraction patterns of the $[NTf_2]^-$ ILs. The peak positions agree with those of Russina *et al.*,[57,58] who found Peak 4 at around 0.22Å^{-1} which corresponds to a repeat structure spacing of 4.5Å in all the $[NTf_2]^-$ ILs they examined. Peak 3 is around 0.13Å^{-1} and corresponds to a repeating structure of 7.5Å for all of the $[NTf_2]^-$ ILs, except in $[C_6C_2im][NTf_2]$, $[C_4C_4im][NTf_2]$ and $[C_6C_6im][NTf_2]$. For these three ILs the peak is shifted to a smaller S spacing, which means the repeating structure is slightly larger. This may be a result of having an extended alkyl chain rather than a methyl group; alkyl groups increase the spacing between ions. The pre-peak (Peak 2) is present in all of the ILs including $[C_4C_1im][NTf_2]$, although it is a low intensity shoulder in $[C_4C_4im][NTf_2]$, which may explain why it appears at a shorter S spacing; the Peak 2 maximum lies between the background peak scattering intensity and Peak 3 which are both more intense.

Finally the pattern of $[C_6C_6im][NTf_2]$ has all four peaks present. This is the first example of the 2x pre-peak, which will be discussed in more detail in Section 4.5.1. As can be seen in Table 4.2, Peak 1 corresponds to a real spacing that is almost exactly double that of Peak 2, the exact ratio is 2.03. The work of Xiao *et al.*[57] investigated the SAXS diffraction patterns of the $[C_xC_xim][NTf_2]$ (x= 2, 3, 4 or 5) and found a small pre-peak occurring in $[C_5C_5im][NTf_2]$, although its precise position was not determined. There was no evidence of a peak in the same region of the pattern as Peak 1 in $[C_5C_5im][NTf_2]$. The rest of their results are consistent with the data collected here.

Ionic Liquid	Peak Position (Å)			
	1	2	3	4
$[C_4C_1im][NTf_2]$	-	14.1	7.3	4.6
$[C_6C_1im][NTf_2]$	-	14.1	7.8	4.7
$[C_6C_2im][NTf_2]$	-	16.8	8.4	4.5
$[C_8C_1im][NTf_2]$	-	16.7	7.3	4.3
$[C_4C_4im][NTf_2]$	-	19.3	7.9	4.4
$[C_6C_6im][NTf_2]$	30.1	15.5	8.4	4.5

Table 4.3: Peak Table of $[X][NTf_2]$ ILs

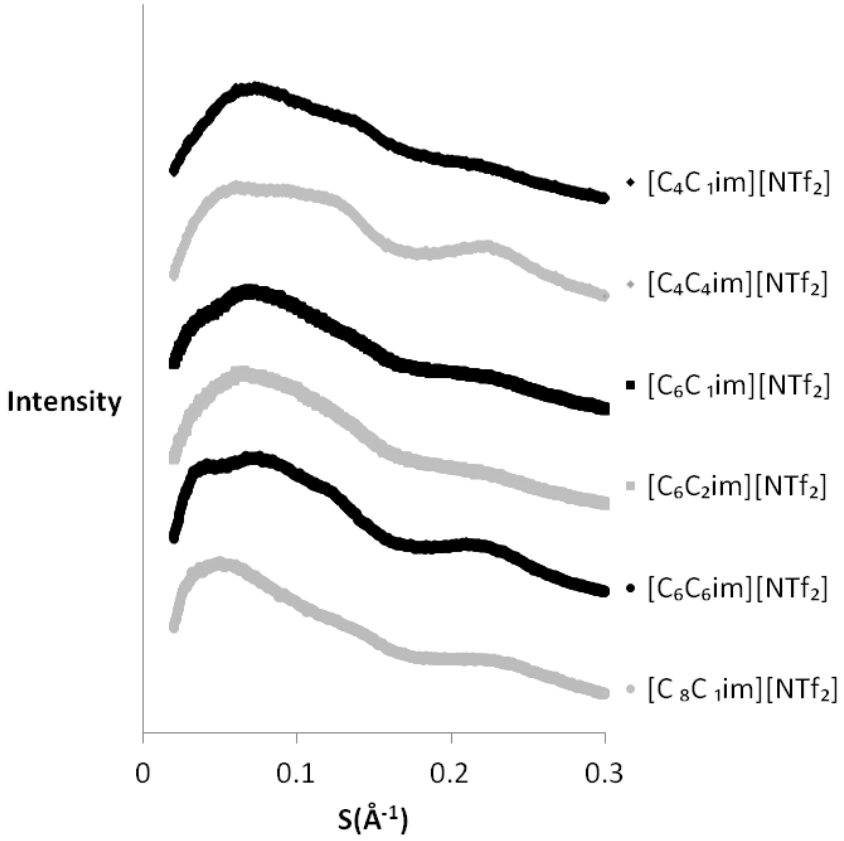


Figure 4.15: Stack plot of Integrations of X-Ray Diffraction patterns of $[X][NTf_2]$ ILs

4.4.3.2 Chloride Ionic Liquids

The peak positions of the chlorides used in this study are shown in Table 4.4 and the patterns are displayed in a stack plot in Fig. 4.16. The chlorides have a very strong Peak 3 around 0.1Å^{-1}, which corresponds to a real spacing of around 10Å. This peak may be stronger and sharper than in other ILs because the small size of the chloride allows it to approach close the imidazolium ring, which gives a narrower distribution to the nearest neighbour interactions. This effect has been seen in MD simulations of 1-alkyl-3-methylimidazolium halides by Urahata *et al.*[161] The position of Peak 2 in [C_8C_1im]Cl is a somewhat lower S spacing than the other chloride ILs, the same is true of Peak 2 in [C_8C_1im]Br, which is lower than the rest of the bromides. This is discussed in the Section 4.4.4.1 and is more noticeable in Figure 4.22. While [C_6C_1im]Cl has a Peak 1 present on the integration of the diffraction pattern, it is not Gaussian which is unusual; even the very sharp Peak 1 of [C_8C_1im][SCN] is Gaussian in form. Nevertheless the Peak 1 is there and corresponds to a structure spacing of 39Å that is double the structure spacing of 19.8Å that gives rise to Peak 2, this suggests that there is additional structuring. The absence of the 2x pre-peak in [C_8C_1im]Cl may be a result of the reduced X-Ray flux during collection of this sample.

Ionic Liquid	Peak Position (Å)			
	1	2	3	4
$[C_6C_1im]Cl$	39.0	19.8	9.5	4.4
$[C_6C_2im]Cl$	-	24.5	10.2	4.8
$[C_8C_1im]Cl$*	-	21.7	15.6	4.5
$[C_6C_6im]Cl$	32.4	15.6	11.2	4.3

Table 4.4: Peak Table of [X]Cl ILs

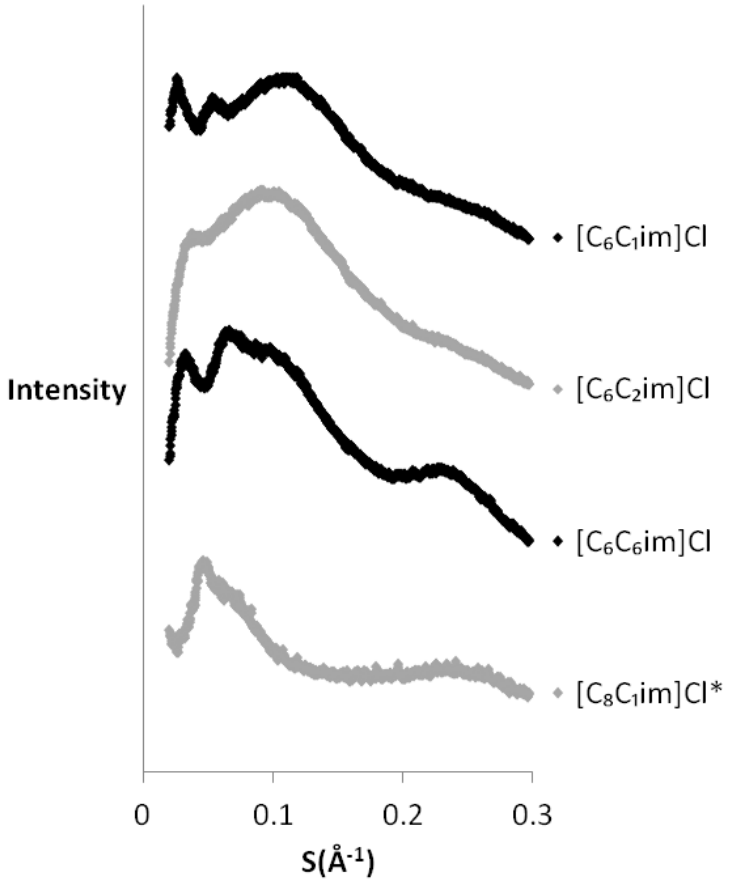


Figure 4.16: Stack plot of 1D scattering patterns of [X]Cl ILs

4.4.3.3 Bromide Ionic Liquids

The bromide ILs in the study showed the least overall structure. This can be seen in Fig 4.17. The peaks that are present, which are shown in Table 4.5 are weak and wide; even $[C_6C_6im]Br$ shows little structure, which is unusual because the other $[C_6C_6im]^+$ ILs are all quite structured. There is a 0.25Å^{-1} peak (Peak 4) all examples, however it is very much broader than the 0.25Å^{-1} peaks in the other ILs. This will be discussed in Section 4.5.1 and is illustrated well by Figure 4.15.

There are no strong trends to discuss within this group. It is clear than the bromide anion is disrupting all structuring in the ILs. There is no strong evidence of nearest neighbour interactions in these ILs. This is consistent with the work of Aoun *et al.*.[177] In the XRD patterns of $[C_2C_1im]Br$, $[C_4C_1im]Br$ and $[C_6C_1im]Br$ they found a peak around 0.26Å^{-1} which was about 1Å^{-1} wide at the full width half max (estimated graphically). They also found a nearest neighbour peak around 8Å for all ILs and a small pre-peak in the XRD pattern of $[C_6C_1im]Br$.

Ionic Liquid	Peak Position (Å)			
	1	2	3	4
$[C_6C_1im]Br$	-	14.4	6.8	4.8
$[C_6C_2im]Br$	-	14.4	7.5	4.5
$[C_8C_1im]Br$*	-	22.2	17.5	4.5
$[C_4C_4im]Br$	-	11.6	7.6	4.2
$[C_6C_6im]Br$	-	18.0	8.7	4.6

Table 4.5: Peak Table of [X]Br ILs

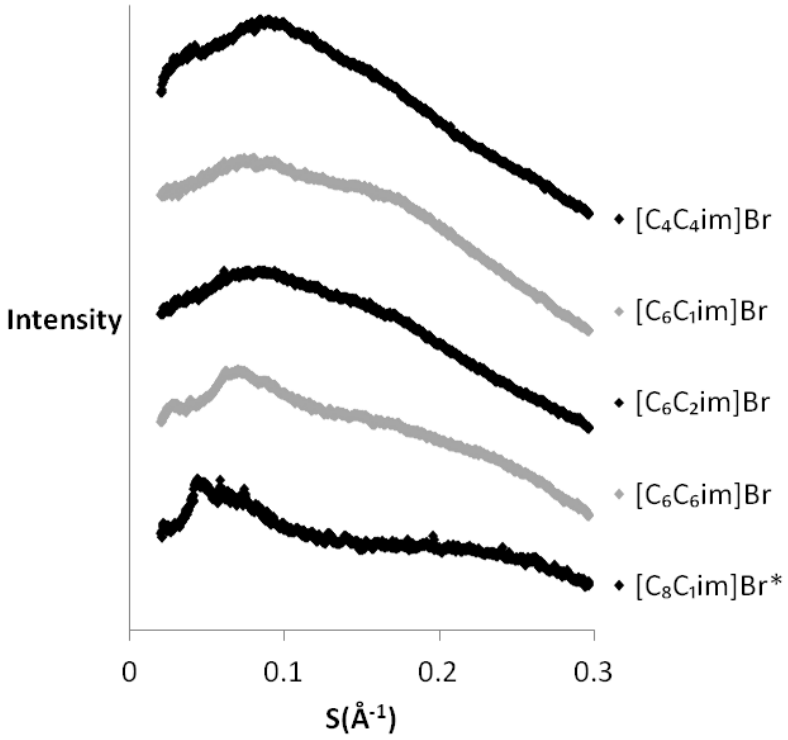


Figure 4.17: Stack plot of 1D scattering patterns of [X]Br ILs

4.4.3.4 Nitrate Ionic Liquids

The results of the nitrate ILs are shown in Table 4.6 and Figure 4.18. The nitrate ILs were the strongest scattering samples studied; this is likely due to an overall increase of structuring, however there may be effects caused by the different correlation abilities of the anions. All of the nitrate ILs have a peak at 0.25Å^{-1} which corresponds to a spacing of 4Å which is somewhat shorter than that seen in the other ILs. The shortening of the alkyl chain-alkyl chain spacing and the general increase in structuring may be the result of more favourable imidazolium ring-nitrate interaction which forces the alkyl chains closer together. If that were the only reason it would be expected that the chloride ILs would exhibit a similar level of structuring, however the chlorides have only a strong, sharp nearest neighbour peak and rather less structuring overall. The difference in resolution of the nearest neighbour peak may be a function of the anions scattering ability; the electrons of the chloride ion are localised however the nitrate, despite having more electrons, has them spread over 4 atoms.

What is clear is that the nitrates are highly structured; both $[C_8C_1im][NO_3]$ and $[C_6C_6im][NO_3]$ have a strong Peak 2 (pre-peak) which indicates a large amount of structural anisotropy in these systems. The Peak 2 or pre-peak of $[C_8C_1im][NO_3]$ is at 0.047Å^{-1}, which represents a repeat spacing of 21.5Å. The $[C_8C_1im]^+$ cation is 15.1Å in length and the $[NO_3]^-$ is about 5Å across. $[C_8C_1im][NO_3]$ also seems to have a 2x pre-peak (Peak 1), as the inclusion of a peak in the very low S significantly improved the goodness of fit of the model. However the peak seems to be of low intensity and appears very much as a shoulder on Peak 2. It is also the only $[C_8C_1im]^+$ IL which exhibits this 2x pre-peak, which may be a result of the relative increase of structuring in the $[NO_3]^-$ ILs.

The scattering pattern of $[C_6C_6im][NO_3]$ is similar to those of the other $[C_6C_6im]^+$ ILs, and it has all four peaks present.

Ionic Liquid	Peak Position (Å)			
	1	2	3	4
$[C_6C_1im][NO_3]$	-	20.9	10.8	4.1
$[C_6C_2im][NO_3]$	-	-	9.0	4.1
$[C_8C_1im][NO_3]$	38.8	21.0	8.8	4.2
$[C_4C_4im][NO_3]$	-	16.2	9.0	4.0
$[C_6C_6im][NO_3]$	34.0	16.4	10.6	4.2

Table 4.6: Peak Table of $[X][NO_3]$ ILs

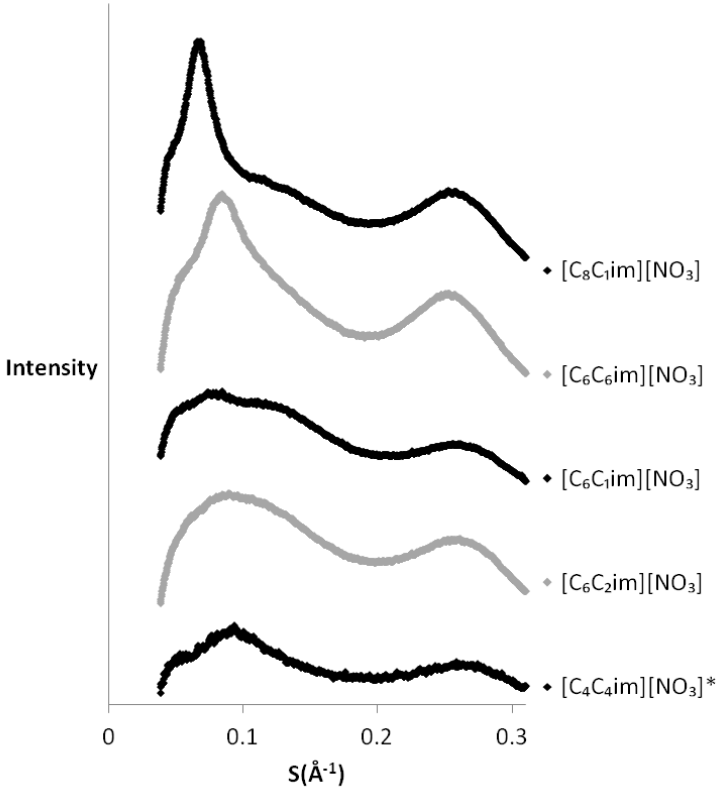


Figure 4.18: Stack plot of 1D scattering patterns of $[X][NO_3]$ ILs

4.4.3.5 Thiocyanate Ionic Liquids

Of all the ILs studied here the ILs with thiocyanate anions have the most surprising scattering patterns. All of the thiocyanate ILs used here have a strong pre-peak in the small S range (Peak 1 in the tables), even the very short $[C_4C_1im][SCN]$. The peaks have been labelled as Peak 1 because of where they appear on the integration, not because of any strict assignment. In most of the ILs Peak 1 corresponds to twice the structure spacing of the pre-peak, or Peak 2, however this is not true of the $[SCN]^-$ ILs, most of which do not have a Peak 2, except $[C_6C_6im][SCN]$ which has both Peak 1 and Peak 2. The peak positions of the thiocyanate ILs are shown in Table 4.7 and the traces of the XRD patterns are shown in a stack plot in Figure 4.19.

	Peak Position (Å)			
Ionic Liquid	1	2	3	4
$[C_4C_1im][SCN]$	31.4	-	10.2	-
$[C_6C_1im][SCN]$	36.7	-	8.8	-
$[C_6C_2im][SCN]$	32.6	-	9.6	4.3
$[C_8C_1im][SCN]$	45.1	-	8.9	-
$[C_4C_4im][SCN]$	32.1	-	9.3	3.8
$[C_6C_6im][SCN]$	31.3	15.6	9.8	4.2

Table 4.7: Peak Table of [X][SCN] ILs

The occurrence of the pre-peak in $[C_4C_1im][SCN]$ is remarkable because all of the literature that has examined $[C_4C_1im]^+$ ILs has shown only peaks around $0.1Å^{-1}$ and $0.25Å^{-1}$ (Peak 3 and 4 here); there has been no evidence of a pre-peak in such short chain ILs. The $0.1Å^{-1}$ and $0.23Å^{-1}$ peaks correspond to the nearest neighbour spacing at 8Å and the alkyl chain-alkyl chain spacing at 4.5Å, respectively. While $[C_4C_1im][SCN]$ has a strong peak corresponding to the nearest neighbour interactions at $0.1Å^{-1}$, there is no evidence of a peak at $0.25Å^{-1}$. The small S peak corresponding to a repeat structure of 31.4Å is very close to being the length of two $[C_4C_1im]^+$ cations and two $[SCN]^-$ anions, which are about 10Å and 6Å long respectively, their sum being 32Å.

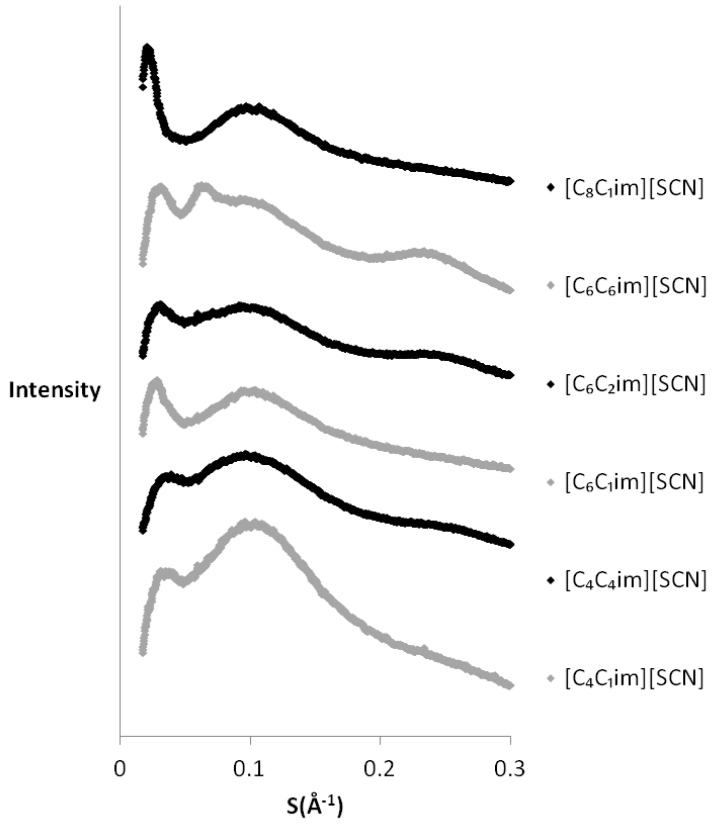


Figure 4.19: Stack plot of 1D scattering patterns of [X][SCN] ILs

The scattering pattern of $[C_8C_1im][SCN]$ shows a very strong peak at $0.022Å^{-1}$, which corresponds to a repeat spacing of 45.1Å. As with the $[C_4C_1im][SCN]$, this low S peak is approximately the length of two cations and two anions. $[C_8C_1im]^+$ is 15.0Å long.

The appearance of a very low S peak (Peak 1) in the $[C_xC_1im][SCN]$ ILs (x=4, 6 or 8) indicates a different type of structure forming in these systems. A pre-peak occurring at a spacing which corresponds to a structure that is approximately the sum of the ion lengths is now well documented for $[C_xC_1im][Y]$ ILs, when the alkyl chain is hexyl- or longer. It is unique in the XRD patterns of $[C_xC_1im][SCN]$ ILs to have a pre-peak which corresponds to a structure spacing of twice the length of the ions. This likely reflects a change in the type of structure being formed. A pre-peak that is the length of an ion pair is indicative of a smectic like structure. A pre-peak that is twice the length of the ion pair is indicative of a lamellar structure. A more detailed discussion of the occurance of Peak 1 and higher order peaks is in section

4.4.4.4, although it is in reference to $[C_6C_6im]^+$ ILs in particular.

The scattering patterns of the two $[SCN]^-$ ILs with symmetric cations, $[C_4C_4im][SCN]$ and $[C_6C_6im][SCN]$ are quite similar to one another. Both have a small S pre-peak which are caused by repeating structures of 32Å and 31Å respectively. It would be expected that the $[C_6C_6im][SCN]$ would have a larger repeat spacing as it has longer alkyl chains. The $[C_6C_6im][SCN]$ has a pre-peak that is slightly shorter than the length of the cation and a peak at twice this spacing.

The peak around $0.25Å^{-1}$, Peak 4, which is indicative of alkyl chain-alkyl chain interactions, is either not present or is very weak in the thiocyanate ILs. The complete absence of Peak 4 in $[C_8C_1im][SCN]$ is interesting because there is a strong sharp Peak 1 in the low S regime. The appearance of a pre-peak on the length scale of the sum of the ion lengths, or twice the sum of the ion lengths in this case, is indicative of a preferential alignment along the long axis of the cation, this is similar to the director of a mesogen. This preference for parallel alignment would be expected to occur with an increase in intensity of Peak 4 as the alkyl chains also begin to align parallel to the neighbouring alkyl chains. The absence of Peak 4 in the thiocyanate ILs will be discussed in Section 4.5.1.

4.4.4 X-Ray Diffraction Results, Grouped by Cation

4.4.4.1 The origin of the pre-peak

Most of the ILs have a pre-peak that corresponds to a repeat structure spacing that is slightly longer than the cation. The repeat structure spacings that give rise to the pre-peak for the $[C_8C_1im]^+$ ILs are shown in Table 4.8. The $[C_8C_1im]^+$ cation is 15Å in length with the alkyl chain extended, although a repeat structure that results in a diffraction peak must include the molecular spacing, so assuming the intermolecular distance is about 3Å, a single 'repeat cation unit' would be around 18Å. This is shown in Figure 4.20. The repeating structures in the $[C_8C_1im]^+$ ILs are all about 21Å, with the exception of $[C_8C_1im][SCN]$, where the repeating structure is around 45Å and is about twice the length of the cation. Considering the extreme differences in size of anions studied, the fact that the pre-peaks are all around 21Å strongly suggests that the anion has little effect on the repeating structure that gives rise to pre-peak. These repeating structure sizes agree with those in the literature for $[C_8C_1im]^+$ salts of Cl^-, $[NTf_2]^-$, $[PF_6]^-$ and $[BF_4]^-$, which are all around 21Å. The appearance of a pre-peak that is a result of a repeating structure on the length scale of the cation is indicative of a smectic like structure, where there is a preference for a structure layered perpendicular to the long axis of the imidazolium cations.

Ionic Liquid	pre-peak position (Å)
$[C_8C_1im][NTf_2]$	20.5
$[C_8C_1im]Cl$	21.7
$[C_8C_1im]Br$	22.2
$[C_8C_1im][NO_3]$	21.0
$[C_8C_1im][SCN]$	45.2

Table 4.8: Table of pre-peak Positions of $[C_8C_1im]^+$ ILs

The position of the pre-peak seems to be determined by the length of one cation in most ILs and exhibits a smectic like spacing, however the pre-peak of $[C_8C_1im][SCN]$, and indeed all $[C_xC_1im][SCN]^-$ ILs studied here, does not follow this trend. Additionally $[C_4C_1im][SCN]$ has a pre-peak which is unique among $[C_4C_1im]^+$ ILs.

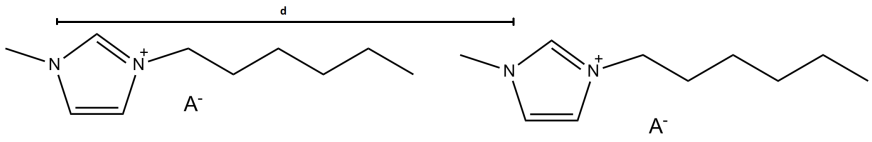


Figure 4.20: Sketch of the molecular structure giving rise to the pre-peak in ILs

Clearly $[C_xC_1im][SCN]$ ILs have a unique repeating structure. The repeat structure spacing in $[C_8C_1im][SCN]$ is double the length of the repeat structure of the other $[C_8C_1im]^+$ ILs, plus 3Å. It is believed that the $[SCN]^-$ ILs form a lamellar like phase, illustrated in Fig. 4.21. The positions of the anions relative to the cations many contribute to the 'extra' 3Å spacing, although this is not reflected in the sketch. The position of the anions in the sketch is to illustrate a possible arrangement that would explain the absence of a Peak 4 in the 1-alkyl-3-methylimidazolium thiocyanate ILs. The thiocyanate is the only linear anion in this study, which may allow it to lie parallel to the alkyl chain to maximise dispersion interactions, this could explain the absence of a Peak 4 at around $0.25Å^{-1}$, which comes from alkyl chain-alkyl chain interactions.

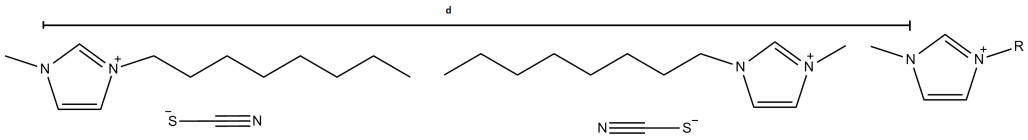


Figure 4.21: Sketch of the molecular structures giving rise to the pre-peak in $[SCN]^-$ ILs

The conclusion to this is that the thiocyanate ILs exhibit a profoundly different liquid state structure than other ILs. This is believed to be a unique result and certainly merits further examination. MD simulations could provide insight into the nature of the structure. The inclusion of thiocyanate ILs could also be used as a powerful test of an MD simulations accuracy; should the simulation accurately predict a change in structural behaviour of thiocyanate ILs relative to other ILs it would validate the model significantly.

Given the unique structural behaviour of the thiocyanate ILs, it would be interesting to examine 1-alkyl-3-methylimidazolium thiocyanates with alkyl chain lengths from dedecyl- to hexadecyl- in length and discover when these salts become liquid crystals.

It is possible the behaviour would be different to that already seen in the literature.

4.4.4.2 The effect of the Anion

One of the aims of this research was to investigate the role of the anion in the appearance of the XRD patterns of ILs. Of particular interest is the role of dispersion interactions between anions and alkyl chains and their influence on other structural features in XRD patterns of ILs. There is unpublished computational evidence from within the group concerning the study of cluster formation in ILs that suggests dispersion interactions between the alkyl chains and anions can occur and this affects the nature of the structuring of the IL. Dispersion interactions involve the interaction of dipoles between molecules, although they exclude the interaction between two permanent dipoles (Keesom forces). Dispersion interactions include the interaction of a permanent dipole with an induced dipole, however the symmetry of most IL anions means they do not have permanent dipole moments, despite often having asymmetric electron distributions. The exception in this case is the thiocyanate anion, which has a dipole moment. What effect the addition of the permanent dipole-induced dipole interactions will have on the total of the dispersion interactions of the thiocyanate ILs is not clear, given that the other anions will have dispersion interactions with the alkyl chains solely composed of instantaneous dipole-instantaneous dipole interactions. The $[NTf_2]^-$ anion has a dipole moment when the trifluoromethyl groups are cis, but no dipole moment when the trifluoromethyl groups are trans. The trans conformer is the lower in energy of the two, so it is likely to be in this conformer.

Dispersion interactions are more prominent in molecules or ions with more electrons; the instantaneous dipoles occur because of spontaneous asymmetry in the distribution of electrons in their orbitals, thus when there are more electrons instantaneous dipoles occur more regularly. However it is not simply a function of the number of electrons; three of the anions in this study, bromide, nitrate and thiocyanate, have similar numbers of electrons (36, 32 and 30 respectively). The size of the orbital also has an effect; larger orbitals have a greater tendency to have instantaneous dipole effects (that is, they are more polarizible). So while the electron counts of the three

anions are similar, the nitrate anion has electrons in 2p orbitals which are small, the thiocyanate has a electrons spread over 2p and 3p orbitals and the bromide has electrons in 4p orbitals, thus nitrate is not particularly prone to dispersion interactions, while thiocyanate is and bromide even more so. The $[NTf_2]^-$ anion is an interesting case; it is large and has many electrons but it is not particularly soft.

It is possible to examine these interactions using X-Ray diffraction because the alkyl chains in an IL tend to be clustered into a non-polar domain[164]. The formation of a non-polar domain gives rise to a peak in the integration of the XRD pattern at around 0.25Å^{-1} caused by correlations between the alkyl chains perpendicular to the chain axis. This has been dubbed Peak 4 in this thesis. This peak occurs because of scattering from alkyl chain-alkyl chain repeat structures. If the anions engage in dispersion interactions with the chains this would be expected to disrupt the non-polar domain.

Figure 4.22 shows a stack plot of $[C_8C_1im]^+$ ILs. Figure 4.23 shows a stack plot of $[C_6C_6im]^+$ ILs. The peaks intensities, with the exception of Cl^- and Br^- are comparable within this data set and give some indication of the extent of structuring.

As can be seen in the figures, $[C_8C_1im][NO_3]$ (Fig. 4.22) and $[C_6C_6im][NO_3]$ (Fig. 4.23) both have very intense diffraction peaks. As Peak 4, around 0.24Å^{-1} (4.2Å), is solely made up of alkyl chain-alkyl chain interactions, differences in the correlation ability of the anions can be ignored.

So it is safe to conclude that the nitrate systems are exhibiting more structuring of the alkyl chain region than other ILs. While the intensity has not been corrected for IL density, which will affect the apparent extent of structuring, this effect will be relatively small as IL densities vary over a relatively small range.

Peak 4 is more intense in $[C_6C_6im][Y]$ than it is in the corresponding $[C_8C_1im][Y]$. It would be premature to immediately conclude that the $[C_6C_6im]^+$ ILs have more structuring, this is because each cation now has two alkyl chains capable of producing a diffraction signal; it would be expected that this would approximately double the total scattering intensity.

The most important result from these data sets is that the anion plays a significant

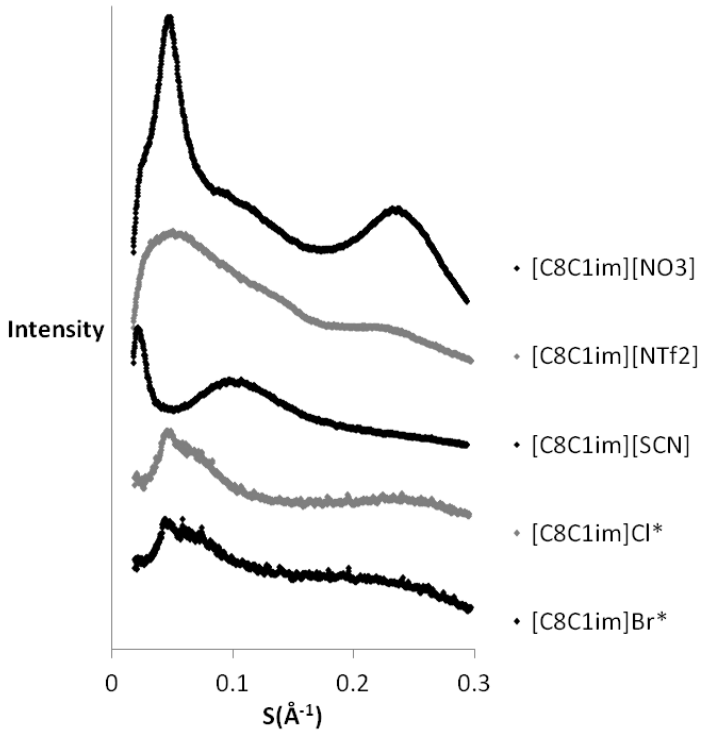


Figure 4.22: Stack of Integrations of X-Ray Diffraction patterns of $[C_8C_1im][Y]$ ILs

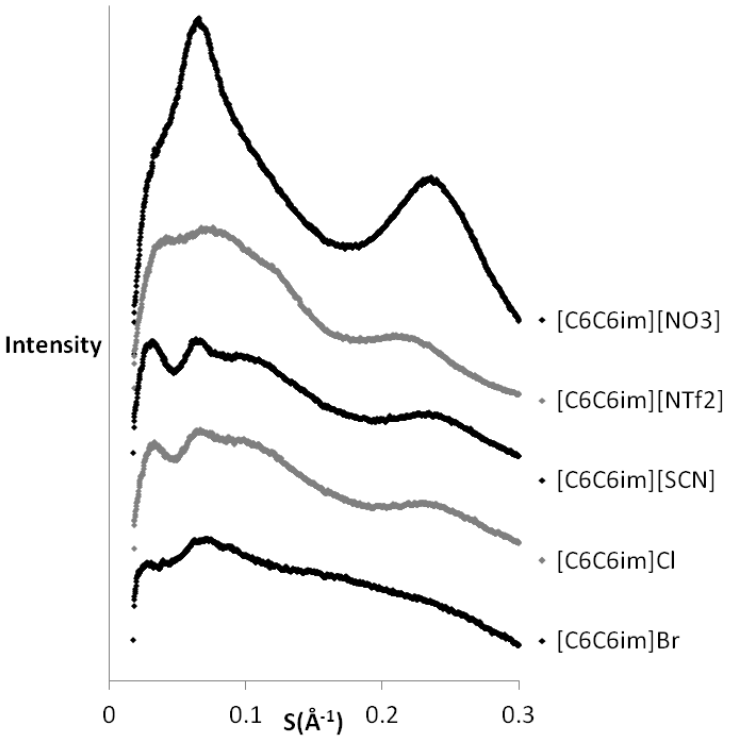


Figure 4.23: Stack of Integrations of X-Ray Diffraction patterns of $[C_6C_6im][Y]$ ILs

Ionic Liquid	Repeating Structure (Å)		Ratio
	Peak 1	Peak 2	
$[C_6C_6im][NO_3]$	34.0	16.4	2.07
$[C_6C_6im][NTf_2]$	28.8	14.2	2.03
$[C_6C_6im][SCN]$	31.3	15.6	2.01
$[C_6C_6im]Cl$	30.3	15.4	1.97
$[C_6C_6im]Br$	45.8	17.2	2.7

Table 4.9: Peak Table of $[C_6C_6im][Y]$ ILs

role in disrupting the non-polar domain. For the $[C_8C_1im]^+$ ILs the extent of alkyl chain-alkyl chain correlation follows the order $[NO_3]^- >> [NTf_2]^- \approx Cl^- > Br^- > [SCN]^-$. For the $[C_6C_6im]^+$ ILs it follows the order $[NO_3]^- >> [NTf_2]^- \approx Cl^- \approx [SCN]^- > Br^-$.

This trend shows that anions capable of dispersion interactions exhibit a significant ability to interrupt the alkyl chain-alkyl chain interactions of the cations. This is a remarkable result given that dispersion interactions are typically believed to be insignificant in short chain systems. MD simulations on the position of the anion relative to the cation typically show longer alkyl chains pushing the anion away[161], this seems to agree with the results of Russina *et al.*[58] who found the intensity of Peak 3, which arises from nearest neighbour spacings, becomes less intense as the alkyl chain length is increased.

The precise mechanism for this interruption is unclear; if the anion was disrupting the non-polar domain by positioning itself between the alkyl chains there would be a significant change in the nearest neighbour peak and it would also affect the position of the pre-peak. In the case of $[C_8C_1im][SCN]$ there is no Peak 4 present, however there is still a strong Peak 2 or pre-peak.

4.4.4.3 Unique Feature in the XRD patterns of $[C_6C_6im]^+$ ILs

Another feature in the diffraction patterns of the $[C_6C_6im]^+$ ILs that can be seen in Fig. 4.23 is the presence of an additional peak in the very low S range. This feature is most clearly seen in the diffraction patterns of $[C_6C_6im][SCN]$ and $[C_6C_6im]Cl$.

The length of the $[C_6C_6im]^+$ cation is about 18.2Å, and the position of the pre-peak is slightly shorter than this, which suggests some amount of inter-digitation between the cations. The occurrence of an additional peak at twice the spacing of the Peak 2 (the pre-peak) is, to the best knowledge of the author, the first report of a peak of this nature in an IL. The position of Peak 1 in $[C_6C_6im]Br$ is extremely close to the beam-stop, as well as being low intensity and broad. As a result of this the peak fitting cuts off very close to the peak maximum, thus its position is not thought to be reliable and this IL will need to be re-examined on a X-Ray beamline that can resolve smaller scattering angles, before meaningful conclusions can be drawn about the appearance of Peak 1 for this IL in particular. In the case of the $[C_6C_6im][NO_3]$ Peak 1 is hidden as a weak shoulder on the extremely strong Peak 2 (pre-peak), however it is believed to be real because including the Peak 1 significantly improved the goodness of fit of the model.

The spacing that Peak 2 (or the pre-peak) corresponds to is somewhat shorter than the length of the cation. The two major conformers of 1,3-dialkylimidazolium cations are the 'V'-Shaped and the linear conformers, shown in Figs. 4.24 and 4.25. The 'V'-Shaped conformer has a terminal group separation of 16.6Å and the linear conformer has a terminal group separation of 18.2Å, so including some intermolecular spacing, a repeat spacing would be expected to occur some 3-4Å longer than this, which would put the repeat spacing at around 20Å and 22Å, for 'V'-shaped and linear conformers respectively. These two lengths are significantly longer than the spacing observed in all the ILs examined here, which are all around 16Å. That being said the cation lengths stated here are rigid, all trans alkyl chain lengths; it is commonly observed in thermotropic systems that there is a small decrease in layer spacing upon melting because molten alkyl chains are effectively shorter than their solid state equivalents. Additionally no account is being made of the anion in this case; in $[C_xC_1im]^+$ systems Peak 2 (pre-peak) is often near the length of a cation plus an anion, the data here suggests that the anion doesn't contribute to the pre-peak spacing in 1,3-dialkylimidazolium ILs. The most likely explanation is some alkyl chain overlap between neighbouring cations, which would reduce the repeat spacing, however it is difficult to provide evidence of this beyond the presence of a strong alkyl chain-alkyl chain interactions.

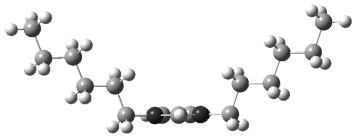


Figure 4.24: 'V'-Shaped conformer of $[C_6C_6im]^+$ Cation

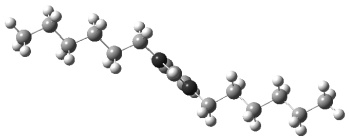


Figure 4.25: Linear conformer of $[C_6C_6im]^+$ Cation

There is another conformer to be considered, which is derived from crystal structures observed of similar, although significantly longer, N,N'-dialkylbenzylimidazolium salts reported by Lee *et al.*[157]. A 'sketch' (that is an unoptimised structure) of the 'L'-shaped conformer of the $[C_6C_6im]^+$ cation is shown in Fig. 4.26 and is around 9Å long. If this were the cation conformer in the liquid state the anion position would play a significant role in determining the repeat spacing. This particular structure seems unlikely as the repeat spacing of the $[C_6C_6im]^+$ ILs varied little considering the range of anion sizes examined.

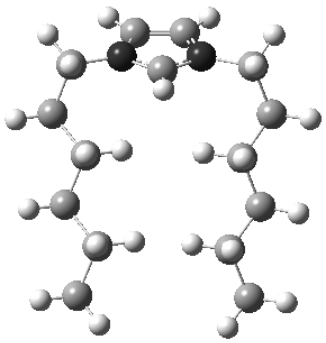


Figure 4.26: 'L'-Shaped conformer of $[C_6C_6im]^+$ Cation

4.4.4.4 The origin of Peak 1

The structural origin of the Peak 1 (2x pre-peak) and its relationship to Peak 2 (the pre-peak) in $[C_6C_6im]^+$ ILs will be discussed here, however first the origin of higher order diffraction peaks in diffraction patterns must be introduced.

In the Bragg Equation (Eqn. 4.5) n is the order of the diffraction peak. Higher order peaks normally only occur in highly structured systems.

$$n\lambda = 2dsin\theta \tag{4.5}$$

For example, in order to produce 6 higher order peaks (that is 7 peaks in total), there must be at least 8 parallel planes in the diffracting structure. Crystals with well defined crystal plane spacings, such as the calibrant used in this study, silver behenate, are capable of producing many higher order peaks. In these cases the first order peak occurs at the smallest diffraction angle, and is (usually) the most intense. Higher order peaks appear at wider diffraction angles with (usually) lower intensities. The higher order peaks are spaced at integer ratios of scattering angle. Structured liquids do not always have higher order peaks, and those that do have higher order peaks rarely have more than one or two. This is because long range order is disrupted by thermal motions in these systems; it is extremely unlikely that there will be many perfectly parallel planes.

The first order peak of a repeating structure is always at the lowest scattering angle (in this case expressed in $Å^{-1}$) and higher order peak appear at wider angles (that is larger S spacings in $Å^{-1}$). This is because the 1D diffraction patterns here have an axis in $Å^{-1}$ which assumes the peak order is one. So if the repeat spacing of a 1,3-dialkylimidazolium IL is $0.061Å^{-1}$ (this is taken from $[C_6C_6im][NO_3]$ as an example), the second order peak, n=2, would appear at $0.122Å^{-1}$. Expressing the axis in degrees or radians avoids including the assumption of n=1 in the axis scale, however the ease of converting the x value into a real spacing is lost.

With this established, the structural origin of Peak 1 and Peak 2, could be a result of two different liquid structures.

The first possible explanation for the origin of Peak 1 is that it is the first order diffraction peak of a repeating structure and Peak 2, is the second order peak of this repeating structure. If Peak 1 and Peak 2 are first and second order peaks, the conformer of the $[C_6C_6im]^+$ cation would be 'V'-Shaped. Table 4.9 showed the peak positions, their ratio agrees with the integer spacing of higher order peaks. As the repeating structure in this case is two cations in length, those cations must be either structurally or symmetrically inequivalent. The linear conformer would not have two different symmetries of cation. However if the cations are 'V'-Shaped and the alkyl chains align to maximize their overlap, an alternating structure such as the one shown in Fig 4.27 explains the repeating structure being (slightly less than) twice the cation length. In this figure 'd' is the repeat spacing in the Bragg equation and 'L' is the length of the cation.

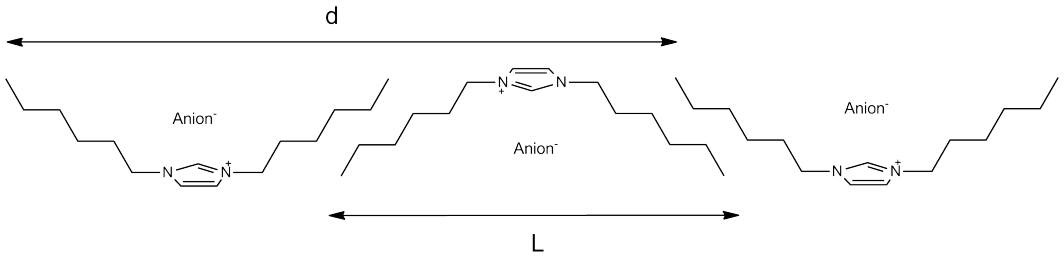


Figure 4.27: Possible repeating Structure of $[C_6C_6im]^+$ ILs in 'V'-Shaped Conformer

This type of structure is supported by evidence from the diffraction patterns of $[C_6C_6im]Cl$ and $[C_6C_6im][SCN]$. Both of these ILs have a Peak 1 that is stronger than the corresponding Peak 2. In the diffraction pattern of $[C_6C_6im]Cl$ the ratio of the peak intensities (P1/P2) is 2.1, in the diffraction pattern of $[C_6C_6im][SCN]$ the ratio of the peak intensities (P1/P2) is 2.2. The fact that both of these ILs have a Peak 1 that is more intense than Peak 2 is consistent with Peak 2 being a second order peak. However, the other three $[C_6C_6im]^+$ ILs do not have the same ratio. The peak ratio (P1/P2) in the diffraction pattern of $[C_6C_6im][NTf_2]$ is close to 1, in the diffraction pattern of $[C_6C_6im]Br$ the ratio (P1/P2) is 0.5 and in the diffraction pattern of $[C_6C_6im][NO_3]$ the ratio (P1/P2) is also close to 0.5. The appearance of higher order peaks would imply there are multiple well defined layers of cations in these ILs.

The second possible explanation for the appearance of both Peak 1 and Peak 2 in

these ILs is the formation of two different domains of repeating structures in the IL. Since it appears that ILs are not structured through the entire liquid, it is possible that there are regions of repeating structure arising from the 'V'-Shaped conformer, which would lead to Peak 1 appearing and separate regions of repeating structure arising from the linear-conformer, which would lead to Peak 2 appearing.

A sketch of the repeating structure in $[C_6C_6im]^+$ ILs is shown in Fig 4.28, where 'L' is the length of the cation and 'd' is the repeat structure that gives rise to the diffraction peak. The inter-digitation of the alkyl-chains causes the repeating structure to be shorter than the length of the cations. While it is an assumption that the alkyl chains are inter-digitated, rather than the effective cation size being shorter because of the free rotation of the alkyl chains, there is some evidence to suggest this. In the $[C_xC_1im]^+$ based ILs the repeat structure is determined only by the cation length and is always somewhat longer than the cation, this suggests that the alkyl chain is fully extended in the $[C_xC_1im]^+$ ILs, and it is therefore reasonable to expect the same to be true in the $[C_6C_6im]^+$ ILs.

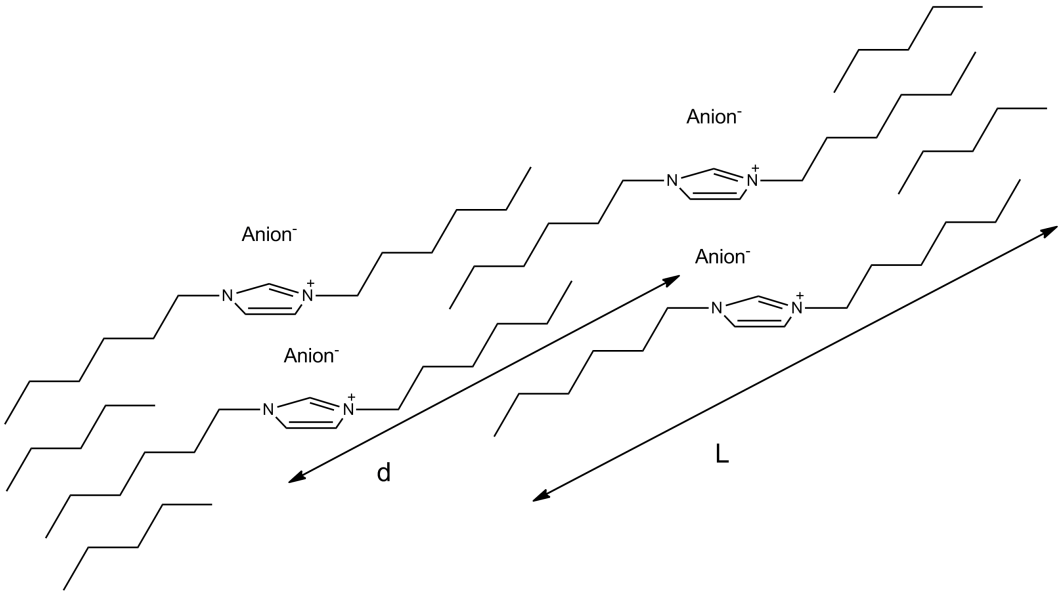


Figure 4.28: Repeating Structure of $[C_6C_6im]^+$ ILs

With the evidence here it is difficult to determine which of the two possible explanations is correct. It is possible that an examination of some asymmetric dialkylimidazolium based ILs would allow for a more certain assignment; examining the diffraction patterns of $[C_7C_5im][Y]$ ILs may provide some insight, given that

they are asymmetric but have the same total number of alkyl carbons in the chains.

4.5 Conclusions and Further Work

4.5.1 Conclusions

A range of ILs were synthesised for X-Ray diffraction studies, several novel ILs were prepared and several synthetic results are of interest. It was found that $[C_4C_1im][NO_3]$ is a solid at room temperature, with a melting point of 30-31^{o}C and a triclinic crystal packing group. It was also found that $[C_4C_4im]Cl$ is a solid with a melting point of 48-50^{o}C and had a chiral othorhombic crystal packing group. The formation of a pseudo-chiral crystal structure is the result of a interaction of the chloride with and one of the alkyl chains; this also reduced the energy barrier of rotation of the alkyl chain, which results in disorder in this chain.

The XRD patterns of many ILs were studied and several unique features were identified.

Most ILs have structural anisotropy which results in repeating structures that cause a pre-peak to occur in the XRD patterns. The pre-peak in most ILs is a result of some smectic phase like arrangement of ions in the liquid state, and is classified by the appearance of the pre-peak at a spacing that corresponds to a repeating structure somewhat longer than the cation.

It was found here that 1-alkyl-3-methylimidazolium thiocyanate ILs, with butyl, hexyl or octyl chains, have a pre-peak that corresponds to a repeating structure that is slightly longer than twice the length of the cation. This result is novel; other 1-alkyl-3-methylimidazolium ILs examined here and in the literature have a pre-peak that corresponds to a repeating structure that is slightly longer than the cation. This shows that thiocyanate ILs have some lamellar like structure in the liquid state. Additionally this is believed to be the first report of the appearance of a pre-peak in a 1-butyl-3-methylimidazolium IL.

The role of dispersion interactions between the anions and alkyl chains has been

examined using SAXS. It has been found that 'soft' anions with many electrons, such as thiocyanate and bromide, show an ability to interact favourably with alkyl-chains. This interrupts the alkyl chain-alkyl chain interaction which gives rise to a peak in the X-Ray diffraction pattern corresponding to a repeat spacing of about 4.5Å. What is interesting is that in the case of the thiocyanate ILs there is a pre-peak which is indicative of liquid state structuring, while in the bromide ILs the diffraction pattern peaks were wide and weak, which is indicative of relatively little liquid state structuring. Clearly interrupting the alkyl chain-alkyl chain interaction does not necessarily interrupt the other repeating structures. This result is unique and merits further investigation using MD simulations and further XRD experiments.

A range of $[C_6C_6im]^+$ ILs were synthesised and were discovered to have an additional diffraction peak (Peak 1) in the very low S range that corresponds to a repeating structure slightly shorter than twice the cation length. There are two possible explanations for the occurrence of this peak and its relationship to Peak 2, which occurs at double the S spacing. The first possibility is that there are two different repeating state structures forming in the liquid, that give rise to two distinct diffraction peaks. In this case one of the structures has a repeating unit that is slightly less than twice the cation length and the other structure has a repeating unit that is slightly less than one cation length. The second possible explanation is that Peak 1 is the first order diffraction peak of a repeating structure that is repeating over two cation lengths, and Peak 2 is the second order diffraction peak of this repeating structure; in this case the result would be indicative that the $[C_6C_6im]^+$ ILs have multiple well defined layers of smectic like sheets. Unfortunately the precise origin of the additional peak cannot be determined without additional data, however it is most likely (in the opinion of the author) that what is being seen is a first and second order diffraction peak.

4.5.2 Further Work

There are numerous potential avenues to explore that would provide useful information to complement what has been found here. The unique result of the structure of the thiocyanate ILs would benefit from additional investigation. It would be inter-

esting to investigate other anions to discover if any of them exhibit such a different, MD simulations would be complementary to this, as they could provide insight into the specific interactions and ionic interactions that determine whether an IL has a smectic like or lamellar like liquid structure.

The nitrate ILs were strongly scattering. This suggests that they have a greater degree of structuring in the liquid state than the other ILs. It would be interesting to extend the study of the nitrate ILs to longer chain lengths and to examine them with DSC and Polarising Microscopy studies over a range of temperatures, to see if liquid crystal states occur, particularly in the symmetric dialkylimidazolium nitrates.

A study examining the SAXS diffraction patterns of $[C_xC_y\text{im}]^+$ ILs, when x=5 and y=7 could provide results that would allow the precise origin of the Peak 1 and its relationship to Peak 2 (often called the pre-peak).

Chapter 5

Conclusion

The pyrrolidinium ring flip activation energy of $[C_xHpyrr]^+$ based ILs was examined using variable temperature NMR spectroscopy. Unfortunately it was not possible to examine the neat liquids, thus the study was undertaken in solution.

It was found that the solvent effect on the pyrrolidinium ring flip activation energy of $[C_1Hpyrr][NTf_2]$ was explained by an LSER using the Kamlet-Taft parameters of the solvent, with the exception of water, which was found to have behaviour not accurately predicted by the LSER. This is likely due to non-ideal effects caused by the 'hydrophobic' $[NTf_2]^-$ anion. DMSO fitted the LSER trend and was used as a solvent for study.

There was no correlation found to explain the pyrrolidinium ring flip activation energy of $[C_1Hpyrr]Y$ ILs, where Y = $[HSO_4]^-$, $[NTf_2]^-$, $[OTf]^-$ or Cl^-.

A positive correlation was found between the pyrrolidinium ring flip activation energy and solution free volume for homologous series of $[C_xHpyrr][HSO_4]$ ILs, where x = 1, 2, 3, 4 or 6. The ring flip activation energy increased proportionally to the free volume of the solution. The correlation was statistically significant and is reinforced by the finding the the ring flip activation energy and free volume of $[C_2Hpyrr][HSO_4]$ in DMSO is lower than that of $[C_1Hpyrr][HSO_4]$ in DMSO, while the rest of the homologous series followed an increasing trend as the alkyl chain length. While the correlation exists there is no intuitive explanation for it; it is most likely that there

is an underlying entropic effect that is being observed *via* the free volume calculation. A full examination of this effect would require a complicated experimental design; separating the Gibb's free activation energy term into enthalpy and entropy terms can be either done using isothermal or isobaric experiments. As the activation energy is calculated using the coalescence temperature, isothermal experiments are not possible, therefore a pressure controlled NMR cell would be required.

A wide range of imidazolium based ILs were synthesised for XRD studies. It was found $[C_4C_1im][NO_3]$ is a solid with a melting point of 30-31^oC and was found in a triclinic crystal. It was also found the $[C_4C_4im]Cl$ is a solid with a melting point of 48-50^oC that crystallised in a chiral orthorhombic packing group. The structure is pseudo-chiral because of an interaction between the chloride and one of the butyl-chains, which also lowers the rotational barrier of the butyl group, resulting in a gauche-trans butyl chain conformer.

It was found that 1-alkyl-3-methylimidazolium thiocyanate ILs have a unique liquid state structure, based on the pre-peak position in these ILs. While the other 1-alkyl-3-methylimidazolium ILs in this study, and those in the literature, have a pre-peak that corresponds to a repeat spacing that is slightly longer than the cation, the thiocyanate ILs have a pre-peak that corresponds to a repeat spacing that is slightly longer than two cations. This indicated that the thiocyanate ILs have liquid state structures that are lamellar like, compared to the smectic like structures of other ILs.

It was also found that 1,3-dihexylimidazolium ILs have two peaks in the low S regime of their XRD patterns. The appearance of the two peaks is either a result of first and second order diffraction peaks or a mixed liquid state structure. Unfortunately it was not possible to determine which explanation is correct with the available data.

It has been shown here that the thiocyanate and bromide anions have the ability to engage in dispersion interactions with the alkyl chains of 1-alkyl-3-methylimidazolium and 1,3-dialkylimidazolium ILs. This has been inferred by the absence in these two ILs of a XRD peak corresponding to a repeat structure spacing of 4.5Å. This peak occurs as a result of forming non-polar domains in the ILs; when dispersion interactions are present this peak is absent. Interestingly in the cases of $[C_4C_1im][SCN]$,

$[C_6C_1im][SCN]$ and $[C_8C_1im][SCN]$ a pre-peak is present and the 4.5Å peak is absent. This suggests that absence of the 4.5Å peak is not necessarily indicative of a lower amount of structuring overall.

Bibliography

[1] P. Walden, *Bulletin of the Academy of Science, St. Petersburg*, 1914, 405.

[2] J. S. Wilkes and M. J. Zaworotko, *J. Chem. Soc., Chem. Comm.*, 1992, 965.

[3] B. Kirchner, *Ionic Liquids*, Springer-Verlag, Berlin Heidelberg, 2009.

[4] P. Wasserscheid and T. Welton, *Ionic Liquids in Synthesis*, Wiley-VCH, Berlin, 2006.

[5] M. Freemantle, *An Introduction To Ionic Liquids*, RSC Publishing, Cambridge, 2010.

[6] M. Tariq, M. G. Freire, B. Saramago, J. P. Coutinho, J. N. C. Lopes and L. P. N. Rebelo, *Chem. Soc. Rev.*, 2012, **41**, 829–68.

[7] H. Tokuda, K. Hayamizu, K. Ishii, M. A. B. H. Susan and M. Watanabe, *J. Phys. Chem. B*, 2004, **108**, 16593–16600.

[8] H. Tokuda, K. Hayamizu, K. Ishii, M. A. B. H. Susan and M. Watanabe, *J. Phys. Chem. B*, 2005, **109**, 6103–10.

[9] H. Tokuda, K. Ishii, M. A. B. H. Susan, S. Tsuzuki, K. Hayamizu and M. Watanabe, *J. Phys. Chem. B*, 2006, **110**, 2833–9.

[10] R. Hagiwara and J. S. Lee, *Electrochem.*, 2007, **75**, 23.

[11] *Ionic Liquid Database*, http://ilthermo.boulder.nist.gov/ILThermo/mainmenu.

[12] J. P. Hallett and T. Welton, *Chem. Rev.*, 2011, **111**, 3508–76.

[13] V. I. Pârvulescu and C. Hardacre, *Chem. Rev.*, 2007, **107**, 2615–65.

[14] F. van Rantwijk and R. A. Sheldon, *Chem. Rev.*, 2007, **107**, 2757–85.

[15] T. L. Greaves, D. F. Kennedy, S. T. Mudie and C. J. Drummond, *J. Phys. Chem. B*, 2010, **114**, 10022–31.

[16] T. L. Greaves and C. J. Drummond, *Chem. Rev.*, 2008, **108**, 206–37.

[17] S.-G. Lee, *Chem. Comm.*, 2006, 1049–63.

[18] N. V. Plechkova and K. R. Seddon, *Chem. Soc. Rev.*, 2008, **37**, 123–50.

[19] W. Arlt, M. Seiler, C. Jork and T. Schneider, *Ionic liquids as selective additives for the separation of close-boiling or azeotropic mixtures, Patent WO 2002 074718*, 2002.

[20] J. D. Holbrey and R. D. Rogers, *Dissolution and processing of cellulose using ionic liquids, cellulose solution, and regenerating cellulose, Patent WO 2003 029329*, 2003.

[21] S. Sowmiah, V. Srinivasadesikan, M.-C. Tseng and Y.-H. Chu, *Molecules*, 2009, **14**, 3780–813.

[22] Y. Chen, Y. Cao, Y. Shi, Z. Xue and T. Mu, *Ind. Eng. Chem. Res.*, 2012, **51**, 7418.

[23] H. L. Ngo, K. LeCompte, L. Hargens and A. B. McEwen, *Thermochimica Acta*, 2000, **357-358**, 97–102.

[24] K. J. Baranyai, G. B. Deacon, D. R. MacFarlane, J. M. Pringle and J. L. Scott, *Aust. J. Chem.*, 2004, **57**, 145.

[25] A. Arce, M. J. Earle, S. P. Katdare, H. Rodríguez and K. R. Seddon, *Fluid Phase Eq.*, 2007, **261**, 427–433.

[26] K. C. Lethesh, K. Van Hecke, L. Van Meervelt, P. Nockemann, B. Kirchner, S. Zahn, T. N. Parac-Vogt, W. Dehaen and K. Binnemans, *J. Phys. Chem. B*, 2011, **115**, 8424–38.

[27] H. Zhao, G. A. Baker, Z. Song, O. Olubajo, T. Crittle and D. Peters, *Green Chem.*, 2008, **10**, 696.

[28] J. R. Harjani, J. Farrell, M. T. Garcia, R. D. Singer and P. J. Scammells, *Green Chem.*, 2009, **11**, 821.

[29] F. Endres, *Physical chemistry chemical physics : PCCP*, 2010, **12**, 1648.

[30] N. Deenadayalu, K. C. Ngcongo, T. M. Letcher and D. Ramjugernath, *J. Chem. Eng. Data*, 2006, **51**, 988–991.

[31] P. Illner, A. Zahl, R. Puchta, N. van Eikema Hommes, P. Wasserscheid and R. van Eldik, *J. Organomet. Chem.*, 2005, **690**, 3567–3576.

[32] C. P. Mehnert, R. A. Cook, N. C. Dispenziere and M. Afeworki, *J. Am. Chem. Soc.*, 2002, **124**, 12932–3.

[33] P. Wang, S. M. Zakeeruddin, J.-E. Moser and M. Gratzel, *J. Phys. Chem. B*, 2003, **107**, 13280–13285.

[34] P. Wang, S. M. Zakeeruddin, R. Humphry-Baker and M. Gratzel, *Chem. Mater..*, 2004, **16**, 2694–2696.

[35] J. P. Hallett, C. L. Liotta, G. Ranieri and T. Welton, *J. Org. Chem.*, 2009, **74**, 1864.

[36] J. M. Crosthwaite, S. N. V. K. Aki, E. J. Maginn and J. F. Brennecke, *J. Phys. Chem. B*, 2004, **108**, 5113–5119.

[37] J. M. Crosthwaite, S. N. V. K. Aki, E. J. Maginn and J. F. Brennecke, *Fluid Phase Eq.*, 2005, **228-229**, 303–309.

[38] A. Makowska, E. Dyoniziak, A. Siporska and J. Szydowski, *J. Phys. Chem. B*, 2010, **114**, 2504–8.

[39] S. S. Shinde, B. S. Lee and D. Y. Chi, *Org. Letts.*, 2008, **10**, 733–5.

[40] A. Heintz, *J. Chem. Therodynam.*, 2005, **37**, 525–535.

[41] A. Brandt, J. Gräsvik and J. P. Hallett, *Green Chem.*, 2013, **15**, 550.

[42] T. L. Greaves and C. J. Drummond, *Chem. Soc. Rev.*, 2008, **37**, 1709–26.

[43] H. Niedermeyer, J. P. Hallett, I. J. Villar-Garcia, P. A. Hunt and T. Welton, *Chem. Soc. Rev.*, 2012, 7780–7802.

[44] M. Y. Lui, L. Crowhurst, J. P. Hallett, P. a. Hunt, H. Niedermeyer and T. Welton, *Chem. Sci.*, 2011, **2**, 1491.

[45] R. M. Lynden-Bell, *Physical chemistry chemical physics : PCCP*, 2010, **12**, 1733.

[46] P. Navia, J. Troncoso and L. Roman, *J. Chem. Eng. Data*, 2007, **52**, 1369–1374.

[47] O. Borodin, G. D. Smith and W. Henderson, *J. Phys. Chem. B*, 2006, **110**, 16879–16886.

[48] R. W. Taft and M. J. Kamlet, *J. Am. Chem. Soc.*, 1976, **98**, 2886–2894.

[49] M. J. Kamlet and R. W. Taft, *J. Am. Chem. Soc.*, 1976, **98**, 377–383.

[50] G. Ranieri, J. P. Hallett and T. Welton, *Ind. Eng. Chem. Res.*, 2008, **47**, 638–644.

[51] N. L. Lancaster, T. Welton and G. B. Young, *J. Chem. Soc., Perkin Trans. 2*, 2001, 2267–2270.

[52] N. L. Lancaster, P. A. Salter, T. Welton and G. B. Young, *J. Org. Chem.*, 2002, **67**, 8855–61.

[53] J. D. Holbrey and K. R. Seddon, *Dalton Trans.*, 1999, 2133–2139.

[54] C. Jork, C. Kristen, D. Pieraccini, A. Stark, C. Chiappe, Y. A. Beste and W. Arlt, *J. Chem. Thermo.*, 2005, **37**, 537–558.

[55] N. W. Smith, S. P. Gourisankar, J.-L. Montchamp and S. V. Dzyuba, *New J. Chem.*, 2011, **35**, 909.

[56] J. G. Huddleston, A. E. Visser, W. M. Reichert, H. D. Willauer, G. A. Broker and R. D. Rogers, *Green Chem.*, 2001, **3**, 156–164.

[57] D. Xiao, L. G. Hines Jr, S. Li, R. A. Bartsch, E. L. Quitevis, O. Russina, A. Triolo and L. G. Hines, *J. Phys. Chem. B*, 2009, **113**, 6426–33.

[58] O. Russina, A. Triolo, L. Gontrani, R. Caminiti, D. Xiao, L. G. Hines Jr, R. A. Bartsch, E. L. Quitevis, N. Pleckhova and K. R. Seddon, *Journal of Physics: Condensed Matter*, 2009, **21**, 424121.

[59] U. Domaska and M. Królikowska, *J. Sol. Chem.*, 2012, **41**, 1422–1445.

[60] J. M. Pringle, J. Golding, C. M. Forsyth, G. B. Deacon, M. Forsyth and D. R. MacFarlane, *J. Mat. Chem.*, 2002, **12**, 3475–3480.

[61] K. R. Seddon, A. Stark and M.-J. Torres, *Pure and Applied Chemistry*, 2000, **72**, 2275–2287.

[62] W. Heitler and E. Teller, *Proc. Roy. Soc. A: Math., Phys. Eng. Sci.*, 1936, **155**, 629–639.

[63] E. M. Purcell, H. C. Torrey and R. V. Pound, *Phys. Revs.*, 1946, **69**, 37.

[64] R. A. Ogg, *J. Chem. Phys.*, 1954, **22**, 560.

[65] A. Steigel and H. W. Speiss, *Dynamic NMR Spectroscopy*, Springer-Verlag, Berlin Heidelberg; New York, 1978.

[66] H. S. Gutowsky and C. H. Holm, *J. Chem. Phys.*, 1956, **25**, 1228–1234.

[67] H. S. Gutowsky and A. Saika, *J. Chem. Phys.*, 1953, **21**, 1688.

[68] H. Eyring, *J. Chem. Phys.*, 1935, **3**, 107.

[69] Y. Umebayashi, T. Mitsugi, K. Fujii, S. Seki, K. Chiba, H. Yamamoto, J. N. Canongia Lopes, A. A. H. Pádua, M. Takeuchi, R. Kanzaki and S.-i. Ishiguro, *J. Phys. Chem. B*, 2009, **113**, 4338–46.

[70] A. Szabo and N. S. Ostlund, *Modern Quantum Chemistry*, McGraw-Hill, New York, 1989.

[71] W. Koch and M. C. Holthausen, *A Chemist's Guide to Density Functional Theory*, Wiley-VCH, Weinheim, 2nd edn., 2001.

[72] S. F. Sousa, P. A. Fernandes and M. J. a. Ramos, *J. Phys. Chem. A*, 2007, **111**, 10439–52.

[73] H. S. Vosko, L. Wilk and M. Nusair, *Can. J. Phys.*, 1980, **58**, 1200.

[74] A. D. Becke, *Phys. Revs. A*, 1988, **38**, 3098–3100.

[75] A. D. Becke, *J. Chem. Phys.*, 1993, **98**, 5648.

[76] C. Moller and M. S. Plesset, *Phys. Revs.*, 1934, **46**, 618.

[77] Y. Zhao, N. E. Schultz and D. G. Truhlar, *J. Chem. Phys.*, 2005, **123**, 161103.

[78] Y. Zhao, N. E. Schultz and D. G. Truhlar, *J. Chem. Theor. Comput.*, 2006, **2**, 364–382.

[79] A. Landé, *Zeitschrift fur Physik*, 1920, 191.

[80] R. J. Collin and B. C. Smith, *Dalton Trans.*, 2005, 702–5.

[81] P. F. Lang and B. C. Smith, *Dalton Trans.*, 2010, **39**, 7786–91.

[82] A. Bondi, *J. Phys. Chem.*, 1964, **68**, 441.

[83] H. Edelsbrunner, M. Facello and J. Liang, *Dis. Appl. Maths.*, 1998, **88**, 83.

[84] L. E. Kavraki, *Molecular Shapes and Surfaces*, 2012, http://cnx.org/content/m11616/1.10/.

[85] R. F. W. Bader, M. T. Carroll, J. R. Cheeseman and C. Chang, *J. Am. Chem. Soc.*, 1987, **109**, 7968–7979.

[86] A. S. Mitchell and M. A. Spackman, *J. Comp. Chem.*, 2000, **21**, 933.

[87] R. Fürth, *Mathematical Proceedings of the Cambridge Philosophical Society*, 1941, **37**, 252.

[88] A. P. Abbott, *Chem. Phys. Chem.*, 2004, **5**, 1242–6.

[89] A. P. Abbott, *Chem. Phys. Chem.*, 2005, **6**, 2502–5.

[90] A. P. Abbott, R. C. Harris and K. S. Ryder, *J. Phys. Chem. B*, 2007, **111**, 4910–3.

[91] C. Larriba, Y. Yoshida and J. Fernández de la Mora, *J. Phys. Chem. B*, 2008, **112**, 12401–7.

[92] J. B. Lambert and W. L. Oliver Jr, *J. Am. Chem. Soc.*, 1969, **91**, 7774.

[93] P. Navia, J. Troncoso and L. Romaní, *J. Sol. Chem.*, 2008, **37**, 677–688.

[94] R. P. Matthews and P. A. Hunt.

[95] H. Bloom and V. C. Reinsborough, *Aust. J. Chem.*, 1967, **20**, 2583.

[96] H. Bloom and V. C. Reinsborough, *Aust. J. Chem.*, 1969, **22**, 519.

[97] A. Ray, *J. Am. Chem. Soc.*, 1969, **91**, 6511.

[98] D. F. Evans, A. Yamauchi, R. Roman and E. Z. Casassa, *J. Coll. Interfac. Sci.*, 1982, **88**, 89.

[99] D. F. Evans, A. Yamauchi, G. J. Wei and V. A. Bloomfield, *J. Phys. Chem.*, 1983, **89**, 3537–3541.

[100] M. Akhter and S. M. Alawi, *Colloids and Surfaces A: Physicochemical and Engineering Aspects*, 2003, **219**, 281–290.

[101] G. A. Baker and S. Pandey, in *Ionic Liquids III A: Fundamentals, Progress, Challenges and Opportunities*, American Chemical Society, 2005, ch. Amphiphili, pp. 234–243.

[102] Y. Zhou, *Curr. Nanosci.*, 2005, **1**, 35–42.

[103] M. Antonietti, D. Kuang, B. Smarsly and Y. Zhou, *Angew. Chem. Int. Ed.*, 2004, **43**, 4988–92.

[104] D. F. Evans, *Langmuir*, 1988, 3–12.

[105] D. Mirejovsky and E. M. Arnett, *J. Am. Chem. Soc.*, 1983, **105**, 1112–1117.

[106] T. J. O. Leary and I. W. Levin, *J. Phys. Chem.*, 1984, **88**, 4074–4078.

[107] W. Tamura-Lis, L. J. Lis and P. J. Quinn, *J. Coll. Interfac. Sci.*, 1992, **150**, 200–207.

[108] S. Bordel Velasco, M. Turmine, D. Di Caprio and P. Letellier, *Colloids and Surfaces A: Physicochemical and Engineering Aspects*, 2006, **275**, 50–54.

[109] A. J. Ward and C. du Reau, in *Surface and Colloid Science*, ed. E. Matijevic and M. Borkovec, Plenum Press, New York, 2nd edn., 1993, ch. 4.

[110] T. L. Greaves, A. Weerawardena, C. Fong and C. J. Drummond, *Langmuir*, 2007, **23**, 402–4.

[111] T. L. Greaves, A. Weerawardena, C. Fong and C. J. Drummond, *J. Phys. Chem. B*, 2007, **111**, 4082–8.

[112] S. Thomaier and W. Kunz, *J. Mol. Liq.*, 2007, **130**, 104–107.

[113] C. J. Bowlas, D. W. Bruceb and K. R. Seddon, *Chem. Comm.*, 1996, 1625–1626.

[114] T. Niori, T. Sekine, J. Watanabe, T. Furukawa and H. Takezoe, *Mats. Chem. Comms.*, 1996, **6**, 1231–1233.

[115] Y. Matsunaga and S. Miyamoto, *Mol. Crys. Liq. Crys. Sci. Tech. Sec. A: Mol. Crys. Liq. Crys.*, 1993, **237**, 311–317.

[116] T. Akutagawa, Y. Matsunaga and K. Yasuhara, *Liq. Crys.*, 1994, **17**, 659–666.

[117] A. Jakli, S. Rauch, D. Lotzsch and G. Heppke, *Phys. Revs. E*, 1998, **57**, 6737.

[118] C. J. Barrett, *Introduction to Liquid Crystals*, 2012, http://barrett–group.mcgill.ca/tutorials/liquid_cr.

[119] K. Binnemans, *Chem. Rev.*, 2005, **105**, 4148–204.

[120] B.-P. Wu, M.-L. Pang, T.-F. Tan and J.-B. Meng, *Liq. Crys.*, 2012, **39**, 579.

[121] V. Busico, P. Cernicchiaro, P. Corradini and M. Vacatello, *J. Phys. Chem.*, 1983, **87**, 1631–1635.

[122] M. Ito, Y. Matsunaga, H. Matsuzaki and S. Shimojima, *Bullet. Chem. Soc. Jap.*, 1989, **62**, 3919.

[123] Y. Matsunaga and T. Tsujimura, *Mol. Crys. Liq. Crys.*, 1991, **200**, 103–108.

[124] D. Tsiourvas, A. P. Mihou, E. A. Couladouros and C. M. Paleos, *Mol. Crys. Liq. Crys. Sci. Tech. Sec. A: Mol. Crys. Liq. Crys.*, 2001, **362**, 177–184.

[125] E. R. Peterson and R. D. Willett, *J. Chem. Phys.*, 1972, **56**, 1879.

[126] M. Vacatello, M. de Girolamo and V. Busico, *J. Chem. Soc., Faraday Trans.*, 1981, **77**, 2367.

[127] D. G. Billing and A. Lemmerer, *New J. Chem.*, 2008, **32**, 1736.

[128] E. Landi and M. Vacatello, *Thermochimica Acta*, 1975, **12**, 141.

[129] E. Landi and M. Vacatello, *Thermochimica Acta*, 1975, **13**, 441.

[130] G. Margomenou-Leonidopoulou, A. Malliaris and C. M. Paleos, *Thermochimica Acta*, 1985, **85**, 147–150.

[131] C. M. Paleos, M. Arkas, R. Seghrouchni and A. Skoulios, *Mol. Crys. Liq. Crys. Sci. Tech. Sec. A: Mol. Crys. Liq. Crys.*, 1995, **268**, 179–182.

[132] M. Arkas, K. Yannakopoulou, C. M. Paleos, P. Weber and A. Skoulios, *Liq. Crys.*, 1995, **18**, 563–569.

[133] C. M. Paleos, M. Arkas and A. Skoulios, *Mol. Crys. Liq. Crys. Sci. Tech.*, 1998, **309**, 237.

[134] Y. Matsunaga and K. Nishida, *Bullet. Chem. Soc. Jap.*, 1988, **61**, 3435.

[135] E. Alami, H. Levy, R. Zana, P. Weber and A. Skoulios, *Liq. Crys.*, 1993, **13**, 201–212.

[136] K. Ohta, T. Sugiyama and T. Nogami, *J. Mat. Chem.*, 2000, **10**, 613.

[137] A. Kanazawa, T. Ikeda and Y. Nagase, *Chem. Mater.*, 2000, **12**, 3776–3782.

[138] L. Lu and R. G. Weiss, *Langmuir*, 1995, **11**, 3630.

[139] M. Huskić and M. Zigon, *Liq. Crys.*, 2002, **29**, 1217–1222.

[140] P. Dais, Kokkinia and M. Paleos, *Molecular Crystals and Liquid Crystals Incorporating Nonlinear Optics*, 1990, **186**, 239–250.

[141] Y. Zakrevskyy, B. Smarsly, J. Stumpe and C. Faul, *Phys. Revs. E*, 2005, **71**, 021701.

[142] A. Kanazawa, T. Ikeda and J. Abe, *Angew. Chem. Int. Ed.*, 2000, **39**, 612–615.

[143] A. Kanazawa, T. Ikeda and J. Abe, *J. Am. Chem. Soc.*, 2001, **123**, 1748–54.

[144] G. A. Knight and B. D. Shaw, *J. Chem Soc.*, 1938, 682.

[145] R. Somashekar, *Mol. Crys. Liq. Crys.*, 1987, **146**, 225–233.

[146] H. Fürst and H. J. Dietz, *Journal für Praktische Chemie*, 1956, **4**, 147–160.

[147] E. J. R. Sudholter, J. B. F. N. Engberts and W. H. de Jeu, *J. Phys. Chem.*, 1982, 1908–1913.

[148] J. J. H. Nusselder, J. B. F. N. Engberts and H. A. Van Doren, *Liq. Crys.*, 1993, **13**, 213–225.

[149] M. Tabrizian, A. Soldera, M. Couturier and C. G. Bazuin, *Liq. Crys.*, 1995, **18**, 475–482.

[150] C. G. Bazuin, D. Guillon, A. Skoulios and J.-F. Nicoud, *Liq. Crys.*, 1986, **1**, 181–188.

[151] D. P. Jackson and B. M. Fung, *Mol. Crys. Liq. Crys.*, 1997, **303**, 73.

[152] C. G. Bazuin, D. Guillon, A. Skoulios and R. Zana, *J. Phys. France*, 1986, **47**, 927–930.

[153] C. M. Gordon, J. D. Holbrey, A. R. Kennedy and K. R. Seddon, *J. Mat. Chem.*, 1998, **8**, 2627–2636.

[154] J. de Roche, C. M. Gordon, C. T. Imrie, M. D. Ingram, A. R. Kennedy, F. L. Celso and A. Triolo, *Chem. Mater.*, 2003, **15**, 3089–3097.

[155] A. E. Bradley, C. Hardacre, J. D. Holbrey, S. Johnston, S. E. J. Mcmath and M. Nieuwenhuyzen, *Chem. Mater.*, 2002, **14**, 629–635.

[156] S. V. Dzyuba and R. A. Bartsch, *Chem. Comm.*, 2001, 1466–1467.

[157] K. M. Lee, C. K. Lee and I. J. B. Lin, *Chem. Comm.*, 1997, **1**, 899–900.

[158] C. K. Lee, H. W. Huang and I. J. B. Lin, *Chem. Comm.*, 2000, 1911–1912.

[159] M. Yoshio, T. Mukai, H. Ohno and T. Kato, *Journal of the American Chemical Society*, 2004, **126**, 994–5.

[160] J. Motoyanagi, T. Fukushima and T. Aida, *Chemical communications (Cambridge, England)*, 2005, 101–3.

[161] S. M. Urahata and M. C. C. Ribeiro, *J. Chem. Phys.*, 2004, **120**, 1855–63.

[162] Y. Wang and G. A. Voth, *J. Am. Chem. Soc.*, 2005, **127**, 12192–3.

[163] Y. Wang and G. A. Voth, *J. Phys. Chem. A*, 2006, **110**, 18601–8.

[164] J. N. A. Canongia Lopes and A. A. H. Pádua, *J. Phys. Chem. B*, 2006, **110**, 3330–5.

[165] K. Fujii, R. Kanzaki, T. Takamuku, Y. Kameda, S. Kohara, M. Kanakubo, M. Shibayama, S.-i. Ishiguro and Y. Umebayashi, *J. Chem. Phys.*, 2011, **135**, 244502.

[166] H. K. Kashyap, J. J. Hettige, H. V. R. Annapureddy and C. J. Margulis, *Chem. Comm.*, 2012, **48**, 5103–5.

[167] C. S. Santos, H. V. R. Annapureddy, N. S. Murthy, H. K. Kashyap, E. W. Castner and C. J. Margulis, *J. Chem. Phys.*, 2011, **134**, 064501.

[168] T. Pott and P. Méléard, *Physical chemistry chemical physics : PCCP*, 2009, **11**, 5469–75.

[169] B. L. Bhargava, R. Devane, M. L. Klein and S. Balasubramanian, *Soft Matter*, 2007, **3**, 1395.

[170] J. J. Hettige, H. K. Kashyap, H. V. R. Annapureddy and C. J. Margulis, *J. Phys. Chem. Letts.*, 2012, 105–110.

[171] J. Karl, *Generation of X-Rays*, 2006, http://pd.chem.ucl.ac.uk/pdnn/inst1/xrays.htm.

[172] P. J. Schields, D. M. Gibson, W. M. Gibson, N. Gao, H. Huang and I. Y. Ponomarev, *Powder Diffraction*, 2002, **17**, 70.

[173] a.a. Strechan, a.G. Kabo, Y. Paulechka, a.V. Blokhin, G. Kabo, a.S. Shaplov and E. Lozinskaya, *Thermochimica Acta*, 2008, **474**, 25–31.

[174] H.-o. Hamaguchi and R. Ozawa., in *Advances In Chemical Physics Volume 131*, ed. S. A. Rice, Wiley-Interscience, New York, 2005, ch. 3.

[175] P. A. Hunt, *J. Phys. Chem. B*, 2007, **111**, 4844–53.

[176] D. M. Small, *Journal of Lipid Research*, 1984, **25**, 1490–500.

[177] B. Aoun, A. Goldbach, M. a. González, S. Kohara, D. L. Price and M.-L. Saboungi, *J. Chem. Phys.*, 2011, **134**, 104509.

Appendix A

Crystal Structures

As part of this work two crystal structures were determined. Full details of their determination, plus selected bond lengths and angles, are displayed below.

A.1 $[C_4C_4im]Cl$

Formula	C11 H21 N2, Cl
Formula weight	216.75
Temperature	173 K
Diffractometer wavelength	0.71073Å
Crystal system	Orthorhombic
Space group	P2(1)2(1)2(1)
a = 8.28497(13) Å	$\alpha = 90^o$
b = 9.4638(2) Å	$\beta = 90^o$
c = 16.7452(4) Å	$\gamma = 90^o$
Volume	1312.95(5) $Å^3$
Density (calculated)	1.097 Mgm^{-3}
Absorption coefficient	0.261 mm^{-1}
Crystal colour / morphology	Colourless blocks
Crystal size	0.52 x 0.42 x 0.39 mm^3
θ range	3.25 to 32.82^0
Index ranges	-12≤h≤12 -14≤k≤12 -18≤l≤24
Reflections collected / unique	14224 / 4472 [R(int) = 0.0223]
Reflections observed [F>4σ(F)]	4032
Absorption correction	Analytical
Max. and min. transmission	0.932 and 0.905 ZZ
Refinement method	Full-matrix least-squares on F2
Data / restraints / parameters	4472 / 40 / 140
Goodness-of-fit on F2	1.083
Final R indices [F>4σ(F)]	R1 = 0.0360, wR2 = 0.0905
R indices (all data)	R1 = 0.0429, wR2 = 0.0950
Absolute structure parameter	-0.03(5)
Largest diff. peak, hole	0.245, -0.193 $eÅ^{-3}$
Mean and maximum shift/error	0.000 and 0.001

Table A.1: Details of $[C_4C_4im]Cl$ Crystal Structure Determination

Atoms	Length(Å)
C(1)-N(2)	1.3288(14)
C(1)-N(5)	1.3343(15)
N(2)-C(3)	1.3813(16)
N(2)-C(6)	1.4729(15)
C(3)-C(4)	1.3549(18)
C(4)-N(5)	1.3738(15)
N(5)-C(10)	1.4759(16)
C(6)-C(7)	1.5146(17)
C(7)-C(8)	1.5183(18)
C(8)-C(9)	1.515(2)
C(10)-C(11)	1.514(2)
C(10)-C(11')	1.589(8)
C(11)-C(12)	1.522(2)
C(12)-C(13)	1.524(3)
C(11')-C(12')	1.519(11)
C(12')-C(13')	1.490(12)

Table A.2: Selected Bond Lengths of $[C_4C_4im]Cl$ Crystal

Atoms	Angle(^{o})
N(2)-C(1)-N(5)	108.21(10)
C(1)-N(2)-C(3)	108.77(10)
C(1)-N(2)-C(6)	126.34(10)
C(3)-N(2)-C(6)	124.73(10)
C(4)-C(3)-N(2)	107.06(11)
C(3)-C(4)-N(5)	106.80(11)
C(1)-N(5)-C(4)	109.14(10)
C(1)-N(5)-C(10)	125.32(10)
C(4)-N(5)-C(10)	125.54(11)
N(2)-C(6)-C(7)	111.81(10)
C(6)-C(7)-C(8)	112.01(11)
C(9)-C(8)-C(7)	112.85(12)
N(5)-C(10)-C(11)	112.28(11)
N(5)-C(10)-C(11')	112.1(3)
C(10)-C(11)-C(12)	113.88(14)
C(11)-C(12)-C(13)	112.28(18)
C(12')-C(11')-C(10)	110.7(7)
C(13')-C(12')-C(11')	117.2(10)

Table A.3: Selected Bond Angles of $[C_4C_4im]Cl$ Crystal

A.2 $[C_4C_1im][NO_3]$

Formula	C8 H15 N2, N O3
Formula weight	201.23
Temperature	173 K
Diffractometer wavelength	0.71073Å
Crystal system	Triclinic
Space group	P-1
a = 8.121(6) Å	$\alpha = 81.14(6)^o$
b = 11.445(7) Å	$\beta = 85.65(7)^o$
c = 11.556(9) Å	$\gamma = 86.95^o$
Volume	1057.3(13)Å^3
Density (calculated)	1.264 Mgm^{-3}
Absorption coefficient	0.097 mm^{-1}
Crystal colour / morphology	Colourless blocks
Crystal size	0.31 x 0.14 x 0.14 mm^3
θ range	3.16 to 32.82^o
Index ranges	-11≤h≤12 -17≤k≤15 -16≤l≤16
Reflections collected / unique	10080 / 6662 [R(int) = 0.0664]
Reflections observed [F>4σ(F)]	2007
Absorption correction	Analytical
Max. and min. transmission	0.989 and 0.982 ZZ
Refinement method	Full-matrix least-squares on F2
Data / restraints / parameters	6662 / 0 / 255
Goodness-of-fit on F2	0.914
Final R indices [F>4σ(F)]	R1 = 0.1166, wR2 = 0.2885
R indices (all data)	R1 = 0.2671, wR2 = 0.3593
Largest diff. peak, hole	0.358, -0.417 eÅ^{-3}
Mean and maximum shift/error	0.000 and 0.000

Table A.4: Details of $[C_4C_1im][NO_3]$ Crystal Structure Determination

Atoms	Bond LengthÅ
C(1)-N(5)	1.314(5)
C(1)-N(2)	1.314(5)
N(2)-C(3)	1.372(5)
N(2)-C(6)	1.468(5)
C(3)-C(4)	1.339(6)
C(4)-N(5)	1.382(5)
N(5)-C(10)	1.491(6)
C(6)-C(7)	1.509(5)
C(7)-C(8)	1.515(6)
C(8)-C(9)	1.489(6)
C(11)-N(12)	1.319(5)
C(11)-N(15)	1.331(5)
N(12)-C(13)	1.371(5)
N(12)-C(16)	1.497(5)
C(13)-C(14)	1.342(6)
C(14)-N(15)	1.370(5)
N(15)-C(20)	1.449(5)
C(16)-C(17)	1.511(7)
C(17)-C(18)	1.502(8)
C(18)-C(19)	1.475(7)
N(30)-O(32)	1.250(4)
N(30)-O(31)	1.252(5)
N(30)-O(33)	1.254(5)
N(40)-O(43)	1.227(4)
N(40)-O(41)	1.251(4)
N(40)-O(42)	1.259(4)

Table A.5: Selected Bond Lengths of $[C_4C_1im][NO_3]$ Crystal

Atoms	Angle(^{o})
N(5)-C(1)-N(2)	110.6(4)
C(1)-N(2)-C(3)	107.0(4)
C(1)-N(2)-C(6)	125.5(3)
C(3)-N(2)-C(6)	127.4(3)
C(4)-C(3)-N(2)	108.3(4)
C(3)-C(4)-N(5)	106.4(4)
C(1)-N(5)-C(4)	107.7(4)
C(1)-N(5)-C(10)	126.6(3)
C(4)-N(5)-C(10)	125.8(4)
N(2)-C(6)-C(7)	110.8(3)
C(6)-C(7)-C(8)	111.4(3)
C(9)-C(8)-C(7)	112.0(4)
N(12)-C(11)-N(15)	109.6(3)
C(11)-N(12)-C(13)	107.3(3)
C(11)-N(12)-C(16)	125.8(4)
C(13)-N(12)-C(16)	126.7(3)
C(14)-C(13)-N(12)	108.4(4)
C(13)-C(14)-N(15)	106.5(4)
C(11)-N(15)-C(14)	108.2(3)
C(11)-N(15)-C(20)	126.4(3)
C(14)-N(15)-C(20)	125.4(3)
N(12)-C(16)-C(17)	112.4(4)
C(18)-C(17)-C(16)	114.5(4)
C(19)-C(18)-C(17)	115.7(5)
O(32)-N(30)-O(31)	120.6(4)
O(32)-N(30)-O(33)	118.7(4)
O(31)-N(30)-O(33)	120.8(3)
O(43)-N(40)-O(41)	119.8(4)
O(43)-N(40)-O(42)	120.2(4)
O(41)-N(40)-O(42)	119.9(3)

Table A.6: Selected Bond Angles of $[C_4C_1im][NO_3]$ Crystal